Study of the climate variability and the role of volcanism in the North Atlantic-Mediterranean sector during the last millennium

Yang Feng

SORBONNE UNIVERSITÉ

Thèse de doctorat de Sciences de l'Environnement

Spécialité : Océan, atmosphère, climat

École doctorale 129 : « Sciences de l'Environnement d'Île-de-France »

Laboratoire d'Océanographie et du Climat
Expérimentations et Approches Numériques (LOCEAN)
Équipe d'Océan et Variabilité du Climat (VARCLIM)

Laboratoire Météorologie Dynamique (LMD)
Équipe d'Étude et Modélisation du Climat et
du Changement Climatique (EMC3)

Study of the climate variability and the role of volcanism in the North Atlantic-Mediterranean sector during the last millennium

FENG Yang

soutenue publiquement le 01/03/2022

Devant un jury composé de :

Pr. Francis CODRON	LOCEAN Sorbonne U., Paris	*Président*
Pr. Wenmin MAN	IAP, Beijing, Chine	*Rapportrice*
Pr. Hugues GOOSSE	UCL, Louvain-la-Neuve, Belgique	*Rapporteur*
Pr. Matthew TOOHEY	U. Saskatchewan, Saskatoon, Canada	*Examinateur*
Pr. Myriam KHODRI	LOCEAN Sorbonne U., Paris	*Directrice de thèse*
Pr. Laurent LI	LMD Sorbonne U., Paris	*Co-directeur de thèse*

Acknowledgements

It is indeed a long expedition full of adventures during the four years' study of PhD thesis. I have lost, but I have gained three thousand more. I have complained, but the world repaid me with more kindness, love and cheering. I learned hardly and acquired solid knowledge to form myself from urban-environment master student to climate science doctor. I fought with my vulnerabilities, sensibilities and depressions, especially during the last halftime of the thesis since the outbreak of Covid-19 in 2019. And finally I grew up from the « clumsy» girl to an early-career researcher with professional skills and objective judgments. I would say in this long journey, it is impossible to reach the destination without the supports and help from so many people. It is a great pleasure for me to thank all the goodness that I have received during the thesis study in France.

I would like to thank firstly the thesis director Myriam Khodri for her help during these many years. Coming from a background in urban environment, climate and its variability were very vague notions when I arrived at LOCEAN. I sincerely thank her for her patience, pedagogy and guidance towards me as well as for all the time she devoted to me throughout this thesis. Without Myriam I would not be who I am today.

I'm also grateful to the thesis co-director, Laurent Li. I thank him for supporting and encouraging me to not abandon the thesis. I also thank him for his availability and trust throughout this thesis, especially during the final semester before the submission of manuscript.

I'm also grateful to three female researchers who I met before the starting of a thesis. They were the tutors of my master-2 internship and gave me courage to carry on a PhD project. They are Marie-Alexandrine Sicre, Juliette Mignot and Masa Kageyama. They set up awesome examples for me to be a good researcher. Marie-Alexandrine also helped me obtain the CSC scholarship and MISTRAL PaleoMex funding to conduct the thesis.

I would like to thank Ms. Man Wenmin and Mr. Hugues Goosse for agreeing to be reviewers for my thesis and for their constructive comments on my manuscript. I would also like to thank Mr. Francis Codron and Mr. Matthew Toohey for having agreed to be part of the members of my jury, despite somewhat special circumstances.

I also thank the ED 129 doctor school direction, especially Laurence Amsili Touchon and Pascale Bouruet-Aubertot. Thanks for their attention and constructive suggestions to make the thesis submission be on schedule.

Special thanks to Nicolas Lebas, who is the engineer of our team VarClim. I appreciate a lot his prompt responses to my every single tiny technical questions. His participation is indispensable to the fulfilment of the simulations analyzed in the thesis.

In this difficult trip I am so lucky to have a lot of companions. In the ancient « bureau copine-copain » of the corridor 46-00, I had pleasant and unforgettable meetings with Paul Royer, Chen Ruihan, Bai Henyi, Carla Geisen, Joana Cruz, Coraline Lesseure, Damien Cardinal, Sarath Pullyottum-Kavil, Vincent & Fanny couple … They have made the lab such an exceptional place and without them the first year of PhD would not have been so nice.

Then installing in the new corridor 45-55, I met more and more lovely PhD and post-doc colleagues of different characters (Violaine Pellichero, Amélie Simon, Francesco D'Amico, Theophine Lebrun, Clovis Thouvenin-masson, Matthew Menary, Lucie Vignes, Beyrem Jebry, Sara Sergi, Alexandre Supply, Adama Sylla, Julián Villamayor, Victor Estella-Perez, Matthis Auger, Léa Olivier, Antoine Nasser, Yona Silvy, Aissatou Badji, Cassien Ndiaye, Weimin Jiang, Lucile Richard, Miao Zeyu, Wang Han, Brady Ferster, Constantin Bone, Clément Haëck, Pierre Chabert …). It is a formidable reunion around the climate science and the dream by young people from different cultures and languages! Especially, I would like to thank dear Clovis and Matthew for the countless convivial lunch/coffee time we spent together. And also sincere thanks to Beyrem for helping tune my "scatter plot", and to dear Carla, Sara and Antoine for helping me correct the orthography and grammar of the long French resume. I thank also Pr. Marie-Noelle Houssais, Pr. Christophe Herbaut, Dmitry Khvorostyanov and Julien Vincent, for their once cheering and kindness towards me. And please excuse-me if there are some other colleagues I have forgotten to mention.

I want also to thank the combined financial funding coming from China Scholarship Council, Chinese Embassy in France, Laboratoire Météorologie Dynamique and MISTRAL PaleoMex Project.

Lastly, a very big thank you to my families and in particular to my parents and my brother, also to my danse club sisters (Chunfei, Jiayi, Dany, Renke, Zixuan, Yunhan, etc), and intimate friends (Jingjing, Simei, Salma, Yann, Haorui, Miao, etc), for their unconditional supports, love and cheering.

Bonne lecture.

Abstract

Large volcanic eruptions are one of the most important natural external forcings to the Earth climate system, with important social and economic consequences. Volcanic effects from large eruptions on climate manifest for a few years both at earth's surface as a cooling and in the stratosphere as a warming. Such impacts lie in principle among the potential predictable features of climate after a volcanic eruption took place. Previous works based on models and observations also suggest an increased probability for a positive phase of the North Atlantic Oscillation (NAO) during the first winter following stratospheric tropical eruptions. Large gaps remain however in our understanding of the climate's response to volcanic eruptions, related to the paucity of observed volcanic events during instrumental era and the degree to which such response depends on the characteristics of the eruption (i.e., hemispheric loading, strength, season) or initial conditions of the climate system when the eruption occurs. Tackling all these factors is crucial to improve our understanding of the underlying physical mechanisms and eventually assess the potential risks associated with future large volcanic eruptions.

This PhD work aims at exploring the above-mentioned issues with the IPSL-CM6A-LR model as part of framed PMIP4 and VolMIP standardized CMIP6 coupled model experiments designed to systematically deal with specific uncertainty factors. The first part of the thesis is devoted to characterising the simulated NAO signal in winters following stratospheric volcanic eruptions using three long transient simulations of the last millennium (500-1849 CE). The uncertainties related to the season, strength and the latitude of the eruptions were also explored. The results reveal that the model simulates increased warming in the stratosphere, a stronger polar vortex and a surface pattern similar to the positive phase of the NAO in the first winter following a summer or a winter tropical eruption, with polar night jet responses amplitudes that are linearly related to the eruption strength. No linear relationship with the eruption magnitude is identified for extra-tropical Northern Hemisphere events while a tendency towards a positive NAO phase is only significant during the same winter as the eruption occurrence. The results show that IPSL-CM6A-LR simulates a considerable influence from large stratospheric volcanic eruptions the two seasons following the eruption.

The second part of the thesis extends the work into the exploration of physical mechanisms by focusing on the well observed Mt. Pinatubo tropical eruption (Philippines,

June 1991). While volcanic eruptions decrease global mean surface temperature through direct radiative dimming effects, the NAO signal over the North Atlantic-Mediterranean sector is suggested to be a dynamical and interactive process between stratosphere and surface. By decomposing the radiative effects of Pinatubo eruption, three large ensemble experiments (N=25) are respectively designed to represent all interferences of volcanic aerosol with the radiative fluxes (*volc-pinatubo-full*), only the volcanic aerosol perturbations to the total (longwave and near-infrared) radiative heating rates (*volc-pinatubo-strat*), or only perturbations to the surface shortwave flux (*volc-pinatubo-surf*). Ensemble members all start from predefined initial conditions sampling the full ENSO cycle and use the same volcanic forcing dataset following the VolMIP protocol. From the simulation experiments, the significant positive NAO in the first volcanic winter is primarily attributed to stratospheric heating in the lower tropical stratosphere which generates stronger subtropical zonal winds through the thermal wind balance and accelerates the polar vortex. The surface cooling plays a destructive role in amplifying polar jets when it is sole in the stage. However, the nonlinear interaction between the stratosphere and troposphere/surface will make a stronger polar vortex in *volc-pinatubo-full* hence a more significant positive NAO. Besides, an equatorward EP flux deflection in the stratosphere in *volc-pinatubo-full* and *volc-pinatubo-strat* indicates that planetary waves mainly propagate toward tropical areas and weakly influence the polar vortex. The results highlight the dominant role of the stratosphere heating on formation of positive NAO in the North Atlantic-Mediterranean sector after the Pinatubo eruption.

Résumé

Les grandes éruptions volcaniques sont l'un des forçages externes naturels les plus importants du système climatique terrestre, avec des conséquences sociales et économiques importantes. Les effets volcaniques des grandes éruptions sur le climat se manifestent pendant quelques années à la fois à la surface de la terre sous forme de refroidissement et dans la stratosphère sous forme de réchauffement. De tels impacts figurent en principe parmi les caractéristiques potentiellement prévisibles du climat après une éruption volcanique. Des travaux antérieurs basés sur des modèles et des observations suggèrent également une probabilité accrue d'une phase positive de l'oscillation nord-atlantique (ONA) au cours du premier hiver suivant les éruptions stratosphériques tropicales. De grandes lacunes subsistent cependant dans notre compréhension de la réponse du climat aux éruptions volcaniques, liées à la rareté des événements volcaniques observés pendant l'ère instrumentale et à la mesure dans laquelle une telle réponse dépend des caractéristiques de l'éruption (c'est-à-dire la position hémisphérique, la force, la saison) ou les conditions initiales du système climatique au moment de l'éruption. Il est crucial de s'attaquer à tous ces facteurs pour améliorer notre compréhension des mécanismes physiques sous-jacents et éventuellement évaluer les risques potentiels associés aux futures grandes éruptions volcaniques.

Le travail de thèse vise à explorer les problèmes mentionnés ci-dessus avec le modèle IPSL-CM6A-LR dans le cadre d'expériences de modèles couplés CMIP6 standardisées PMIP4 et VolMIP conçues pour traiter systématiquement des facteurs d'incertitude spécifiques. La première partie de la thèse est consacrée à la caractérisation du signal d'ONA simulé lors des hivers consécutifs à des éruptions volcaniques stratosphériques à l'aide de trois longues simulations transitoires du dernier millénaire (500-1849 CE). Les incertitudes liées à la saison, à la force et à la latitude des éruptions ont également été explorées. Les résultats révèlent que le modèle simule un réchauffement accru de la stratosphère, un vortex polaire plus fort et un schéma de surface similaire à la phase positive de l'ONA au cours du premier hiver suivant une éruption tropicale estivale ou hivernale, avec des amplitudes de réponses des jets nocturnes polaires qui sont linéairement lié à la force d'éruption. Aucune relation linéaire avec la magnitude de l'éruption n'est identifiée pour les événements extratropicaux de l'hémisphère Nord, tandis qu'une tendance à une phase ONA positive n'est significative que pendant le même hiver que l'occurrence de l'éruption. Les résultats montrent que l'IPSL-CM6A-LR simule une

influence significative des grandes éruptions volcaniques stratosphériques les deux saisons suivant l'éruption.

La deuxième partie de la thèse étend le travail à l'exploration des mécanismes physiques en se concentrant sur l'éruption tropicale la bien observée du Mt. Pinatubo (Philippines, juin 1991). Alors que les éruptions volcaniques diminuent la température de surface moyenne globale par des effets radiatifs directs, il est suggéré que le comportement de l'ONA dans le secteur Atlantique Nord-Méditerranée est un processus dynamique et interactif entre la stratosphère et la surface. En décomposant les effets radiatifs de l'éruption du Pinatubo, trois expériences de grand ensemble (N=25) sont respectivement conçues pour représenter toutes les interférences des aérosols volcaniques avec les flux radiatifs (« volc-pinatubo-full »), soit, seules les perturbations des aérosols volcaniques au total (ondes longues et proche infrarouge) taux de chauffage radiatif (« volc-pinatubo-strat »), soit seulement des perturbations du flux d'ondes courtes de surface (« volc-pinatubo-surf »). D'après nos expériences de simulation, l'ONA positive significative au cours du premier hiver volcanique est principalement attribuée au réchauffement stratosphérique dans la stratosphère tropicale inférieure qui génère des vents zonaux subtropicaux plus forts à travers le bilan thermique des vents et accélère le vortex polaire. Le refroidissement superficiel joue un rôle destructeur en amplifiant les jets polaires lorsqu'il est seul dans la scène. Cependant, l'interaction non-linéaire entre la stratosphère et la troposphère/surface rendra un vortex polaire plus fort dans le « volc-pinatubo-full » d'où une ONA positive plus significative. De plus, une déviation du flux EP vers l'équateur dans la stratosphère dans « volc-pinatubo-full » et « volc-pinatubo-strat » indique que les ondes planétaires se propagent principalement vers les zones tropicales et influencent faiblement le vortex polaire. Les résultats mettent en évidence le rôle dominant du réchauffement de la stratosphère sur la formation de ONA positive dans le secteur Atlantique Nord-Méditerranée après l'éruption du Pinatubo.

Table of Contents

Abbreviations

AMOC	**A**tlantic **M**eridional **O**verturing **C**irculation
AOD	**A**erosol **O**ptical **D**epth
AOGCM	**A**tmosphere **O**cean **G**eneral **C**irculation **M**odel
AR	**A**ssessment **R**eport
CMIP	**C**oupled **M**odel **I**ntercomparison **P**roject
EOF	**E**mpirical **O**rthogonal **F**unction
IPCC	**I**ntergovernmental **P**anel on **C**limate **C**hange
ITCZ	**I**nter**t**ropical **C**onvergence **Z**one
LIA	**L**ittle **I**ce **A**ge
MCA	**M**edieval **C**limate **A**nomaly
MWP	**M**edieval **W**arm **P**eriod
NAO	**N**orth **A**tlantic **O**scillation
NH	**N**orthern **H**emisphere
PC	**P**rincipal **C**omponent
PDF	**P**robability **D**istribution **F**unction
PDSI	**P**almer **D**rought **S**everity **I**ndex
PHYDA	**P**aleo **Hy**drodynamics **D**ata **A**ssimilation product
PMIP	**P**aleoclimate **M**odelling **I**ntercomparison **P**roject
PNA	**P**acific-**N**orth **A**merican Pattern
PNJ	**P**olar **N**ight **J**et
PV	**P**olar **V**ortex
RF	**R**adiative **F**orcing
SH	**S**outhern **H**emisphere
SIC	**S**ea **I**ce **C**oncentration
SLP	**S**ea **L**evel **P**ressure
SST	**S**ea **S**urface **T**emperature
VolMIP	**Vol**canic Forcing **M**odelling **I**ntercomparison **P**roject

Chapter 1

General Introduction

Contents

1.1 Motivations and background

The atmospheric circulation is driven by various processes including the uneven heating of the Earth's surface by solar radiation, land–sea contrast and orography. North Atlantic Oscillation (NAO), the most prominent and recurrent atmospheric circulation pattern in the North Atlantic region (Hurrell et al., 2003), is of critical importance for regional climate change, especially for Europe and the Mediterranean basin. It could act to reinforce or counteract the effects of external forcings. According to the Fifth Assessment Report of the United Nations Intergovernmental Panel on Climate Change (IPCC AR5), volcanic eruptions that inject substantial amounts of SO_2 gas into the stratosphere are the dominant natural cause of externally forced climate change on the annual and multi-decadal time scales. They can explain much of the pre-industrial climate change of the last millennium (Brovkin et al., 2010; Legras et al., 2010; Miller et al., 2012; Schneider et al., 2009). At interannual time scale, a positive NAO that is observed for two boreal winters after large tropical eruptions (e.g. Mt. Tambora eruption in 1815, Mt. Pinatubo eruption in 1991). At longer time scale, Zanchettin et al. (2013) reported a decadal-scale positive winter NAO accompanied by delayed winter warming over Europe that peaks almost one decade after the eruptions in the last half millennium. It is to noted that they use the European seasonal surface air temperature reconstructions (Luterbacher et al., 2004), the seasonal sea level pressure and 500 hPa geopotential height reconstructions over the Eastern North Atlantic and Europe (Luterbacher et al., 2002).

Even though continuous progress has been made in recent decades to produce an increasingly detailed temporal and spatial description of climate change in the North Atlantic-Mediterranean sector, there is a heterogeneity of its expression at local scale (in significance, intensity and duration) between reanalysis/proxy and numerical simulations. Models generally fail to capture the Northern Hemisphere dynamical responses after stratospheric volcanic eruptions (Barnes et al., 2016; Bittner et al., 2016; Braconnot et al., 2012; Charlton-Perez et al., 2013; Driscoll et al., 2012; Stenchikov et al., 2006). Models do not sufficiently well simulate the observed post-volcanic strengthened polar vortex, positive NAO, or Eurasian warming pattern. They tend to overestimate the cooling in the tropical troposphere (Driscoll et al., 2012). On the one hand, dynamical interactions between volcanic radiative forcing and earth climate system still demand adequate and well-founded analysis in *state-of-the-art* climate models. On the other hand, the observed volcanic events in industrial periods are of limited number and usually of small magnitude

(Hartmann et al., 2014), thereby largest uncertainties remain for periods of strong volcanic activity in terms of their effective radiative forcing (Driscoll et al., 2012; Santer et al., 2014).

Under this context, two model intercomparison projects have grabbed our attention in the expedition exploring the dynamical relations between volcanic eruption and North Atlantic winter climate variability. The first is the "Paleoclimate Modelling Intercomparison Project phase 4" (PMIP4), which allows to test the model robustness in simulating volcanic-forced climate variability during the last millennium through its *past1000* experiment (Jungclaus et al., 2017). It also helps us investigate the interactions between the natural forcing factors and the role of eruption conditions in modulating the climate sensitivity. More precisely, the PMIP4-*past1000* experiment will aid us to better understand the climate response to volcanic radiative forcing in long transient simulations during a period where natural forcings and internal variability are far more important than anthropogenic factors. The second is "The Model Intercomparison Project on the climatic response to Volcanic forcing" (VolMIP), which targets on improving the confidences in the attribution and dynamical interpretation of reconstructed post-eruption features and providing insights into regional climate predictability during periods of strong volcanic eruptions (Zanchettin et al., 2016). Analysis of its core experiment protocol *volc-pinatubo* will ensure a process-based understanding of the post-eruption atmosphere dynamics to an idealized 1991 Pinatubo-like eruption.

By applying the latest coupled climate model IPSL-CM6A-LR, we can realize *past1000* ensemble runs of PMIP4 to test the robustness of climate response to volcanic eruptions under different initial conditions and forcing strength. We are also capable of undertaking *volc-pinatubo* experiment of VolMIP to deduce physical mechanisms that play behind the North Atlantic climate and volcanic forcing. Moreover, carrying out these simulations with the global coupled model at lower resolution is a prerequisite for piloting the regional system over the Euro-Mediterranean sector. These simulations will deepen our interpretation of the volcanic related NAO signal and better understand the role of volcanism in influencing the North Atlantic-Mediterranean climate during the last millennium.

1.2 Objectives and organization of thesis

This thesis aims at testing the robustness of this influence during the preindustrial last millennium period where recurrent volcanic eruptions play an irreplaceable role for explaining the interannual and interdecadal variabilities, and, at developing the expertise on understanding physical mechanisms by which the external natural forcing — volcanism — will interfere in the climate internal variability at the North Atlantic-Mediterranean sector. *Ergo*, different approaches including climate model simulations, comparison with reanalysis/proxy, statistical treatments have been applied in the thesis to answer the questions below:

1. Is IPSL-CM6A-LR model capable of capturing the Northern Hemisphere winter climate variability after stratospheric volcanic eruptions? Whether the volcanic eruption conditions (e.g., latitude, season, strength) will alter the responses?
2. By which physical process the earth system responds to volcanic radiative forcing and how to comprehend the dominant processes that control the variations of leading atmospheric circulation pattern, i.e. NAO, over the North Atlantic sector at interannual time scale? Can we decompose the radiative effects of volcanic forcing?
3. How to understand the role of polar night jet, stratospheric warming, eddy fluxes in modulating the volcanic eruption influences on the Northern Hemisphere winter?
4. How could we combine the model simulation with observations (or/and proxy) to reconstruct the past millennium climate, especially its variability after volcanic eruptions and its regional scale climate changes at the Euro-Mediterranean basin? What are the uncertainties? Can we reduce them?

We strive to answer these questions by combining recent observation datasets (since around 1865), paleo proxy and climate models. Long-term paleoclimate reconstructions are useful to describe and understand climate variability under natural forcings. Indeed, uncertainties on the chronology of paleoclimate records are an obstacle to an objective analysis of climate variability. The use of appropriate statistical tools constitutes a first step in the analysis of the past climate variability, even though it does not allow us to understand the physical mechanisms. Today, the development of modelling tools and numerical computing capacities make it possible to go further in this exploration of climate change and in particular to perform large sets of simulations from coupled models over

several hundred years. These models can be validated in particular by comparing the results of climate simulations with observations or reconstructions. In particular, they provide estimates of the response of the climate system to changes in the various known forcings including the volcanism, the foci of thesis. These models are also regularly used to identify the processes and the spatial signature of the climate response to some of these forcings.

The thesis is organized as follows:

- In **Chapter 1**, there is a general introduction to the context, motivations, objectives and organization of the thesis.
- In **Chapter 2**, firstly the past millennium climate variability under natural/ anthropogenic forcing and the significance of studying volcanic eruptions will be briefly described. Focus will then be on the radiative influences of volcanic forcing and on the relations with NAO. A glimpse of climate variability in response to recent big tropical/extratropical volcanic eruptions is given regarding evidence from observations (20th century volcanoes), in particular over the North Atlantic-Mediterranean sector. A review of progresses and challenges (including limited volcanic events during instrumental era, modelling uncertainties and understanding of the mechanism) is also compiled from relevant literatures. Two CMIP6-endorsed research programs, i.e. PMIP4 and VolMIP, which serve as a framework for the thesis, are then introduced. The presentation of model IPSL-CM6A-LR and its volcanic forcing implementation for both *past1000* and *volc-pinatubo* experiments will be given at the end of this chapter.
- In **Chapter 3**, I concentrate on the last millennium simulation (*past1000*) performed by IPSL-CM6A-LR to explore the climate variability over the North Atlantic-Mediterranean region in pre-industrial era. We will execute composite study and analyse with the help of abundant volcanic samples in *past1000* ensemble runs. We mainly investigate the interannual climate variability and sensitivities to various volcanic eruption conditions (e.g., latitude, eruption season, strength).
- **Chapter 4** concentrates on the detection and attribution of changes of the Northern Hemisphere climate and atmospheric circulation in response to stratospheric volcanic eruptions. We will use the process-oriented *volc-pinatubo*

experiment simulated by IPSL-CM6A-LR. The 1991 Pinatubo volcanic eruption event is investigated through three ensemble experiments with full forcing (*volc-pinatubo-full*), stratosphere-warming-only forcing (*volc-pinatubo-strat*) and surface-cooling-only forcing (*volc-pinatubo-surf*) respectively. The physical mechanism linking volcanism and post-eruption winter NAO is investigated in terms of atmospheric dynamics. This chapter is mainly presented as a to-be-submitted journal paper, completed by an additional work on the possible sea-ice feedback effects.

- In **Chapter 5**, I will resume systematically the main results and perspectives linked to thesis work.

Supplementary figures/tables, related essential meteorology dynamics equations, and a detailed French resume will be attached in **Appendix A**, **B**, **C** separately.

Chapter 2

Volcanism and past millennium climate variability

Contents

2.1 Introduction

The last millennium is a period offering relatively precise information on paleoclimatology proxy or historical records. It witnesses important climate variability on interannual, decadal even secular time scales, allowing us to study the life cycles of extreme climate events and weather hazards during this period (for example massive storms, heat waves or cold waves, volcanic eruptions, earthquakes). Investigations on last millennium can also help us to understand the physical mechanisms of the past climate variations and relevant impacts on human societies, which is useful to future climate change projection and to elaboration of adaptation strategies to reduce adverse effects of anthropogenic global warming.

An essential part of the last millennium climate variation is of « natural » variability, independent from human-being behaviours and anthropogenic activities. Two types of processes are related to this « natural » climate variability. Firstly, the climate system can produce « internal » variability by interaction of its different components (especially interaction between the atmosphere and ocean). Secondly, the climate system also reacts to « external » factors which modify the global radiative flux balance. Three types of external factors (we also call them external forcings) related with natural climate variability will continue to act on upcoming climate: (i) slow variations of solar radiation due to gradual changes of earth orbital characteristics around the sun (forcing which also called « astronomic » or « orbital » factor); (ii) variation of solar activities and related solar radiation characteristics; (iii) injection of sulfate particles into atmosphere due to volcanic activities. In the other hand, human activities also began to affect the last millennium climate by land surface occupation changes (e.g. deforestation, farming, urbanization) and injection of polluted particles (anthropogenic aerosols) and greenhouse gases. These so-called « anthropogenic » forcings were otherwise marginal and regionally limited before the industrial era and become significant since the mid-19th century.

What is the role of the internal variability in the context of climate responses to anthropogenic or natural (herein volcanic) forcing? This question has been frequently asked and explored by the scientific community. The last 150 years constitutes a privileged period, with numerous instrumental observations (meteorological, oceanographic, etc), to investigate issues on the detection and attribution of climate change. The common practice is to use climate models to perform ensemble simulations under different forcings. Beyond the contemporary historical period, the last millennium provides a longer context of natural

climate variability, which is indispensable for detecting climate change and attributing climate variations to known forcings. The current efforts of the international community in modelling the last millennium climate are coordinated in the framework PMIP4/CMIP6.

In this chapter, I will start by briefly introducing relevant external forcings and their estimations for the last millennium (section 2.2) Then I will focus on the volcanic forcing in terms of radiative influences (section 2.4). Relations between volcanic eruptions and NAO are then discussed with instrumental evidence in the 20th century (section 2.5). We will also pursue the review of main challenges in studying volcano-NAO in this section. Materials mainly come from relevant CMIP5 and CMIP6 literatures about reconstruction or simulations. Some rationales introducing PMIP4/CMIP6 and VolMIP are then discussed in section 2.6. Finally, the model presentation of **IPSL-CM6A-LR** and its paleo- and Pinatubo-volcanic forcing implementation will be given (section 2.7).

2.2 External forcing in the last millennium

2.2.1 Natural forcing

The last millennium provides rich climate records with multi-decadal-to-centennial variability arising from external forcings and internal processes. It also provides abundant volcanic eruption samples of different characteristics (e.g., latitude, strength, eruption season) allowing us to explore the volcanic contributions to climate interannual changes as well as interdecadal variations.

a. Orbital forcing

The term "orbital forcing" is to denote the incoming solar radiation changes originating from variations in the Earth's orbital parameters as well as changes in its axial tilt. Orbital forcing is of good precision and well known from astronomical calculations for the past and future (Laskar et al., 2004). Changes in eccentricity, longitude of perihelion (related to precession) and axial tilt (obliquity) (Berger and Loutre, 1991) predominantly affect the seasonal and latitudinal distribution and magnitude of solar energy received at the top of the atmosphere (Jansen et al., 2007), and the durations and intensities of local seasons. Obliquity also modulates the annual mean insolation at any given latitude, with opposite effects at high and low latitudes.

The orbital forcing is usually related to multi-centennial trends of temperature, arctic sea ice and glaciers during the current interglacial period, specially the last two

millennia (Masson-Delmotte et al., 2013). It is found that there is little net effect of changes in Earth's orbit around the Sun over the AD 900 to present interval which indicates a negligible impacts of orbital forcing in the last 1000 years (Otto-Bliesner et al., 2016; Owens et al., 2017).

b. Solar forcing

Solar variation takes place at many time scales that include centennial and millennial scales (Helama et al., 2010), as the radiant energy output of the Sun changes (Krivova et al., 2010). As shown in Fig. 2.1b, the assessment of the range of the solar RF from Total solar irradiance (TSI) is -1.2 to 0.2 W/m^2 during the last millennium which covers several updated constructions (Delaygue and Bard, 2011; Lean et al., 1995; Muscheler et al., 2007; Steinhilber et al., 2009; Vieira et al., 2011; Wang et al., 2005) using the 7-year running mean. All reconstructions rely on indirect proxies that inherently are consistent in their shapes, but differ in their amplitude, especially the TSI forcing based on Lean et al. (1995), blue curve in Fig. 2.1b. The solar contribution to the record of global surface temperature change is dominated by the 11-year solar cycle, which can explain global temperature fluctuations up to approximately 0.1°C between minima and maxima. A long-term increasing trend in solar activity in the early 20th century may have augmented the warming recorded during this interval, together with internal variability, greenhouse gas increases and a hiatus in volcanism.

c. Volcanic forcing

Another natural driver of climate change is the volcanic eruptions. Despite its highly episodic nature, volcanic activity affects global climate through the radiative impacts of atmospheric sulfate aerosols caused by volcanic eruptions (which is discussed in detail in section 2.3.). Quantifying volcanic forcing in the pre-satellite period (before 1978) is capital for historical and last millennium climate simulations, climate sensitivity estimates and detection and attribution studies.

Multiple ice cores from Greenland and Antarctica provide sulfate deposition information to help reconstruct volcanic forcing along with atmospheric modelling of aerosol distribution and optical depth. Figure 2.1a displayed two reconstructions of the volcanic aerosol optical depth using polar ice cores, spanning the last 1500 years (GRA: Gao et al., 2008, 2012) and 1200 years (CEA: Crowley and Unterman, 2013). Being generally consistent in the timing of hundreds of eruptions, they differ a lot in the absolute amplitude of peaks which may become one uncertainty source when applying into model simulations.

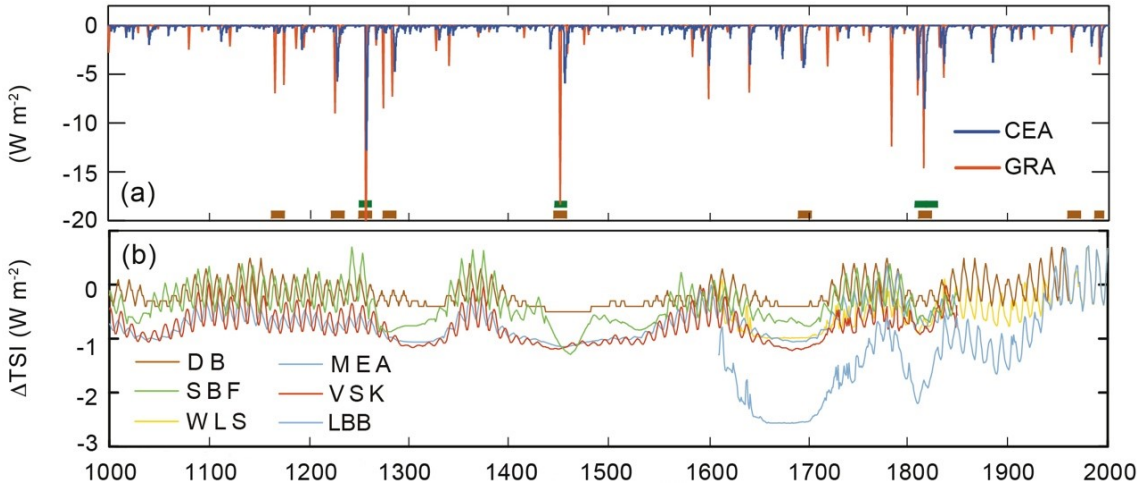

Figure 2.1: **(a)** Two reconstructions of volcanic forcing for the past 1000 years derived from ice core sulfate and used for PMIP3/CMIP5 simulations (Schmidt et al., 2011). GRA: Gao et al. (2008, 2012); CEA: Crowley and Unterman (2013). Volcanic sulfate peaks identified from their isotopic composition as originating from the stratosphere are indicated by squares (green: Greenland; brown: Antarctica)(Baroni et al., 2008; Cole-Dai et al., 2009). **(b)** Reconstructed total solar irradiance (TSI) anomalies back to the year 1000. Proxies of solar activity (e.g., sunspots, 10Be) are used to estimate the parameters of the models or directly TSI. All records except LBB (Lean et al., 1995) have been used for PMIP3/CMIP5 simulations (Schmidt et al., 2011). DB: Delaygue and Bard (2011); MEA: Muscheler et al. (2007); SBF: Steinhilber et al. (2009); WLS: Wang et al. (2005); VSK: Vieira et al. (2011). (source: IPCC AR5, WG1, Chapter 5)

It is true that volcanic forcing reconstruction data used for models are not always consistent. For example, there is debate on the magnitude of stratospheric inputs for the 1783 Laki eruption (Lanciki et al., 2012; Schmidt et al., 2012; Wei et al., 2008). The recurrence time of past large volcanic aerosol injections (eruptions changing the radiative forcing by more than 1 W m^{-2}) varies from 3 to 121 years, with long-term mean value of 35 years (Gao et al., 2012) and 39 years (Crowley and Unterman, 2013), and only two or three periods of 100 years without such eruptions since 850. Hegerl et al. (2006) estimated the uncertainty of the RF for a given volcanic event to be approximately 50%. Differences between reconstructions arise from different proxy data, identification of the type of injection, methodologies to estimate particle distribution and optical depth (Kravitz and Robock, 2011), and parameterization of scavenging for large events (Timmreck et al., 2009). Key limitations are associated with ice core chronology (Plummer et al., 2012; Sigl et al., 2013) and deposition patterns (Moore et al., 2012).

2.2.2 Anthropogenic forcing

Anthropogenic forcings from human activities emerge already since pre-industrial period by injection of greenhouse gases, polluted particles (anthropogenic aerosols) and by the

land use changes (e.g. deforestation, farming, urbanization). Being a marginal forcing as compared to natural forcings to the climate system before 1850 (Masson-Delmotte et al., 2013), the three main categories of anthropogenic forcings (not focus of the thesis) will be shortly presented below.

a. Greenhouse Gases

Greenhouse gases (GHGs) are significant radiative drivers for climate change through absorbing radiation and heating up (Denman et al., 2007; Forster et al., 2007), in which CO_2, CH_4 and N_2O are three gases of most concern during the past millennium. Note, halocarbons used to be a major contributor of 20th century's GHGs before the Montreal Protocol and amendments.

High resolution ice core records reveal that atmospheric CO_2 during the last millennium varied with a drop by 7 to 10 ppm around year 1600, followed by an increase during the 17th century (Ahn et al., 2012; MacFarling Meure et al., 2006; Siegenthaler et al., 2005; Trudinger et al., 2002). Different possible explanations were given for this CO_2 decreasing around 1600, e.g. reduced solar irradiance during the Maunder Minimum, cooling from increases volcanic eruptions, land carbon storage change related with wars (Brovkin et al., 2004, 2010; Frölicher et al., 2011; Gerber et al., 2003; Jones and Cox, 2001; Jungclaus et al., 2010; Kaplan et al., 2011).

Ice core records also confirmed a CH_4 decrease in the late 16th century by about 40 ppb (MacFarling Meure et al., 2006; Mitchell et al., 2011) that scientists related to wetland CH_4 source and changes in biomass burning. No studies are known about mechanisms of N_2O changes for the last millennium.

b. Anthropogenic aerosols

Anthropogenic aerosols that we usually mention include black carbon (BC, formed from the incomplete combustion of fossil and biomass-based fuels), sulfate, nitrate, ammonium and organic aerosol (OA). BC is introduced to atmosphere as primary matter while sulfate, nitrate and ammonium are from secondary aerosol formation processes. OA can originate from either direct emissions or secondary formation by precursor gases.

The anthropogenic aerosols may influence the climate radiative balance through aerosol-radiation interactions (scattering and absorption of radiation), and aerosol-cloud interactions. Studies concentrate mainly on estimating aerosol forcing between 1850 to present (Bellouin et al., 2008; Myhre et al., 2009, 2013; Su et al., 2013).

c. Land use

Anthropogenic land use change has a direct impact on the Earth radiation budget through changes in the surface albedo. Moreover, it can also impact climate via modifying hydrology cycles. According to IPCC AR5 WG1 Chapter 8 (Myhre et al., 2014), it is *very likely* that land use change led to an increase of the Earth albedo with a RF of –0.15 ± 0.10 W m^{-2}, but there is no consensus on the sign of the temperature change induced by anthropogenic land use change.

In a longer time period, Betts et al. (2007) and Goosse et al. (2006) argue that the deforestation in Europe and Asia during the last millennium probably contributed to the "Little Ice Age", together with natural solar and volcanic activity components, before the increase of GHG concentration led to temperatures similar to those experienced in the early part of the last millennium. Gaillard et al. (2010) concluded that there is still significant uncertainty in the anthropogenic land cover change estimations and time evolution.

2.3 Significance of studying volcanic eruptions

First of all, studying volcanic eruptions is an important work concerning disaster prevention and risk management. Several hazards caused by volcanic action can be harmful to life and property. The ash falls and pyroclastic flows after an volcanic eruption are devastating to the surrounding habitats. The destruction of the ancient roman city Pompei after the 79 A.D. Vesuvius eruption is a well-known example. In geological knowledge, most active volcanoes are located around the "Pacific Ring of Fire": an area resulted from plate tectonics. The most recent January 2022 Mt. Tonga eruption at this region has caused horrible tsunami that the whole country has been cut off from the rest of the world for a couple of days. At some monsoon area, severe drought or flood, frost damage, locust and plague outbreaks occurred in the post-eruption years due to significant influence of volcanic eruptions on El Niño–Southern Oscillation variations, which feedback to modulate monsoon climate, and the latter is essential for monsoon region agriculture (e.g., Zhuo et al., 2014). Gao and Gao (2017) also found important European summer hydroclimate responses to volcanic eruptions by using the Old World Drought Atlas (OWDA) developed by Cook et al. (2015).

The sulfuric clouds created by volcanic eruptions can lead to the decreasing of solar radiation and hence the Earth surface temperature. The famous 1815 Tambora eruption in Indonesia Sumbawa Island produced a "year without summer" in 1816 over Europe (Stommel and Stommel, 1979). Such summer cooling is also found after the 1257 Samalas

eruption (Guillet et al., 2017). The last big volcanic eruption Pinatubo in Philippines also caused a global cooling at surface around -0.5℃ (Labitzke and McCormick, 1992).

Scientific studies have also related volcanic eruptions to the political events and civilization collapse (Chen et al., 2020; Gao et al., 2021; Haug et al., 2003; Manning et al., 2017; Zhang et al., 2006). These studies had established links between severe weather after volcanic eruptions and major societal stresses in ancient China, Egypt or Maya civilization. Chen et al. (2020) had even connected the eruption of Mount Parker in the Philippines in 1641 with the collapse of the great Ming dynasty in 1644, though the eruption certainly didn't act alone.

In climate science study, volcanic forcing is of great significance for climate in various aspects, mainly via four main mechanisms (Forster et al., 2007): (1) The aerosol-radiation interaction is the major process for volcanic eruptions to influence climate; (2) Differential (vertical or horizontal) heating can produce thermal gradients in the atmosphere and provokes changes in atmospheric circulation; (3) Volcanic eruptions can also show interactions with other circulation modes and oscillations (see Fig. 2.2), such as El Niño-Southern Oscillation (ENSO), AMO and NAO (foci of this thesis); (4) Volcanic aerosols can modify conditions of atmospheric chemistry and induce ozone depletion with consequences of reduced stratospheric absorption of solar radiation. It is to be noted that the relevant chemical reactions are dependent on anthropogenic chlorine (stratospheric ozone would increase with a volcanic eruption under low-chlorine conditions).

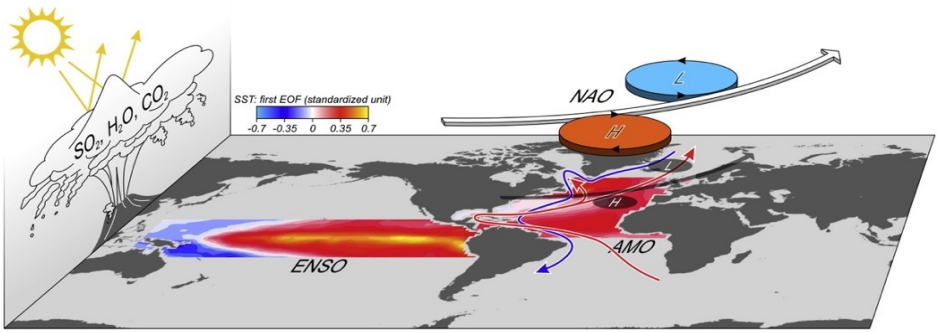

Figure 2.2: Schematic of the main consequences of volcanic eruptions in the atmosphere and their possible interactions with the main climatic modes. The different features are not at scale and just shown to illustrate the key players discussed in Swingedouw et al., (2017). The colours represent the first EOF computed from a principal component analysis using *HadISST* data (Rayner et al., 2003) over the period 1900–2010 for the Tropical Pacific (between 30°S and 30°N) and the North Atlantic (0–60°N) separately, to illustrate the ENSO and AMO modes of variability respectively. The SST data were linearly detrended before performing the principal component analysis. The colour scale represents standardized values over the period 1900–2010. The red and blue arrows in the North Atlantic propose a schematic for the upper warm branch and lower cold branch of the AMOC. The NAO is only represented through a sketch of the anomalous high and low over the North Atlantic, and the anomalous enhanced westerlies associated with it. (source: Swingedouw et al., 2017)

Beyond the direct and short-term impacts of volcanism on climate, evidences also show that there are extended volcanic impacts via long-term memory in the ocean heat content and sea level (Gregory, 2010; Otterå et al., 2010; Stenchikov et al., 2009), although it is clear that the largest impacts are in the two years following stratospheric aerosol injections. For example, Fischer et al. (2007) found the winter effects in the NH has long-term records. Zanchettin et al. (2013) found changes in the North Atlantic Ocean circulation that imply strengthened northward oceanic heat transport a decade after major eruptions, which contributes to the emergence of extensive winter warming over the continental NH along with persistent cooling over Arctic regions on decadal time scales, in agreement with Zhong et al. (2011) and Miller et al. (2012).

Furthermore, volcanism also provides useful hints for better climate projection and better climate change adaptation strategy over the next century. Ammann and Naveau (2003) and Stothers (2007) suggested an ~80 years periodicity in past eruptions, which can provide some climate predictability. But it should be noted that their data record is quite short and imperfect, and there is no mechanism proposed that would cause this periodicity. While the period 1912–1963 was unusual for the past 500 years in having no large volcanic eruptions, and the period 1250–1300 had the most globally climatically significant eruptions in the past 1500 years (C. Gao et al., 2008), current knowledge only allows us to predict such periods on a statistical basis, assuming that the recent past distributions are stationary. Ammann and Naveau (2003), Gusev (2008), and Deligne et al. (2010) studied these statistical properties. Ammann and Naveau (2010) showed how they could be used to produce a statistical distribution for future simulations. Although the future forcing from volcanic eruptions will depend only on the stratospheric aerosol loading for most forcing mechanisms, the future effects on reducing ozone will diminish as ozone depletion substances diminish (Eyring et al., 2010).

Finally, volcanic eruptions provide a natural analogue for geoengineering proposals against ongoing anthropogenic global warming. The stratospheric aerosol cloud can serve to inform us of the impacts of the proposed production of such a cloud as a means to control the climate (Rasch et al., 2008). Plazotta et al. (2018) designed an experiment with solar radiation management by stratospheric aerosol injection (SRM-SAI). They found a mean decrease in land surface temperature by 0.44 K/Wm^2 in the downward solar radiation constrained model, although this cooling depends largely on seasons and geographic areas. Meanwhile it is also important to test long-term impacts of a permanent stratospheric cloud of aerosols by SRM-SAI geoengineering techniques.

It is also to be noted that in the past literature volcanic eruptions were extensively investigated with the objective to create an analogue for the issues of "nuclear winter". Smokes from fires generated by nuclear explosions on cities and industrial areas, which could be lofted into the stratosphere, would cause surface cooling and a reduction of stratospheric ozone (Mills et al., 2008). Volcanic eruptions that produce substantial aerosol clouds in stratosphere also serve as an analogue that supports climate model simulations of the transport and removal of stratospheric aerosols, their impacts on ozone chemistry, their RF, and the climate response. The use of the current global nuclear arsenal still has the potential to produce nuclear winter, with continental temperatures below freezing in summer (Robock, Oman, and Stenchikov, 2007; Toon et al., 2008) and the use of only 100 nuclear weapons could produce climate change unprecedented in recorded human history (Robock, Oman, Stenchikov, et al., 2007), with significant impacts on global agriculture (Ozdogan et al., 2012; Xia and Robock, 2013).

Given all these virtues offered by studies of volcanic eruptions, this thesis is concentrating on analysing the role of volcanism in influencing winter climate variability over the North Atlantic-Mediterranean region at interannual time scale.

2.4 Volcanic radiative influences

The ejections from strong volcanic eruptions to the stratosphere consist of different types of particles (called ash or *tephra*) and gases, in which the sulfate aerosol precursor gases (mainly SO_2) react gradually with the oxidizer OH and H_2O to form H_2SO_4 aerosols (Fig. 2.3) and the resulting sulfate aerosols produce the most significant radiative effects.

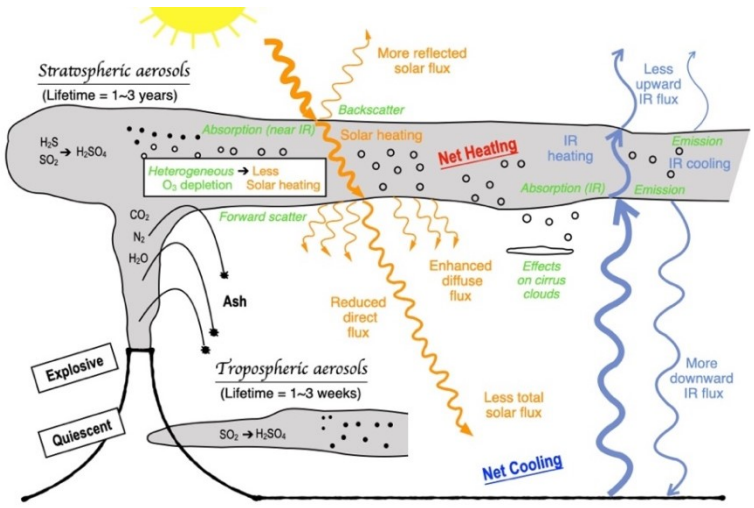

Figure 2.3: Schematic diagram of volcanic inputs to the atmosphere and their effects (source: plate 1 of Robock et al., 2000).

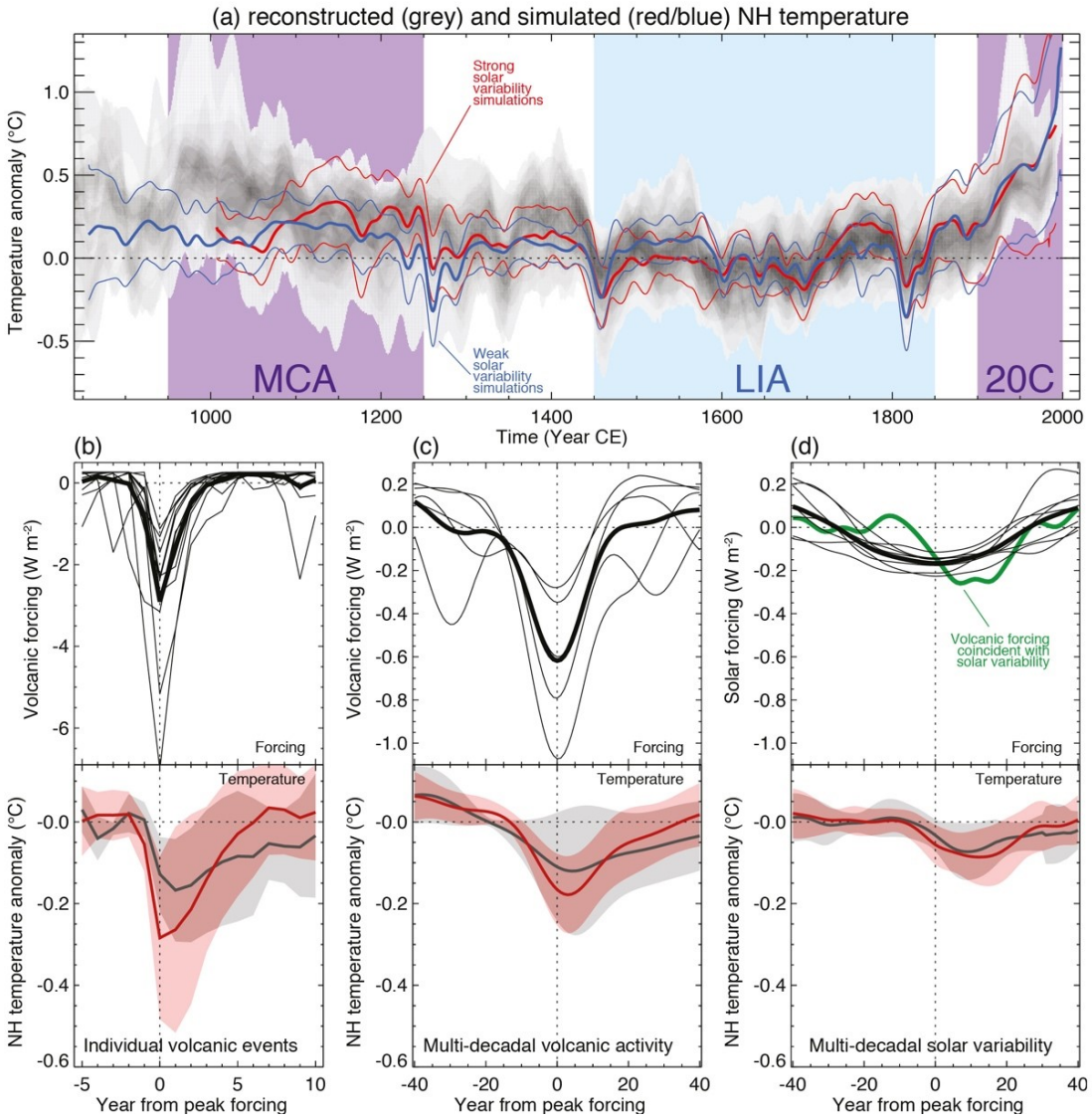

Figure 2.4: Comparisons of simulated and reconstructed Northern Hemisphere (NH) temperature changes. **(a)** Changes over the last millennium (Medieval Climate Anomaly, MCA; Little Ice Age, LIA; 20th century, 20C) **(b)** Response to individual volcanic events. **(c)** Response to multi-decadal periods of volcanic activity. **(d)** Response to multi-decadal variations in solar activity. (a) Simulations shown by coloured lines (thick lines: multi- model-mean; thin lines: multi-model 90% range; red/blue lines: models forced by stronger/weaker solar variability, though other forcings and model sensitivities also differ between the red and blue groups); overlap of reconstructed temperatures shown by grey shading; all data are expressed as anomalies from their 1500–1850 mean and smoothed with a 30-year filter. Superposed composites (time segments from selected periods positioned so that the years with peak negative forcing are aligned) of the forcing and temperature response to: (b) 12 of the strongest individual volcanic forcing events after 1400 (the data shown are not smoothed); (c) multi-decadal changes in volcanic activity; (d) multi-decadal changes in solar irradiance. Upper panels show volcanic or solar forcing for the individual selected periods together with the composite mean (thick line); in (d), the composite mean of volcanic forcing (green) during the solar composite is also shown. Lower panels show the NH temperature composite means and 90% range of spread between simulations (red line, pink shading) or reconstructions (grey line and shading), with overlap indicated by darker shading. Reconstructions, models and further details please refer to Appendix 5.A.1 and 5.A.6 of IPCC AR5, Chapter 5**.** (source: IPCC AR5, WG1, Chapter 5).

The sulfate aerosols have long lifetimes (2 to 3 years) and are effective scatterers of sunlight because of their small size (typical effective radius of 0.5 μm), about the same size as the wavelength of visible light. They interact heavily with solar radiation. Backscattering sunlight to space, the sulfate aerosol increases the planetary albedo and leads to reduction of downward solar energy (mainly shortwave radiation) that reaches the Earth surface (Fig. 2.3). The backscattering effect overcomes the enhanced diffuse radiation and thereby cools the surface (Robock et al., 2000). The famous 1815 Tambora eruption in Indonesia Sumbawa Island produced a "year without summer" in 1816 (Stommel and Stommel, 1979). The last big volcanic eruption Pinatubo in Philippines also caused a global cooling at surface around -0.5℃ (Labitzke and McCormick, 1992). It is resumed by IPCC AR5 that simulated NH temperatures during the last millennium lie mostly within the uncertainty of the available paleo reconstructions (Fig. 2.4a blue and red lines). By further testing the model-reconstruction agreement by compositing NH surface temperature response to 12 largest volcanic eruptions after 1400 CE (Fig. 2.4b-d), IPCC AR5 found that models simulate a significant NH cooling in response to volcanic events (Figure 2.4b; peaks between 0.1°C and 0.5°C depending on model) that lasts 3 to 5 years, overlapping with the signal inferred from reconstructions with annual resolution (0.05°C to 0.3°C). However CMIP5 simulations tend to overestimate cooling following the major 1809 and 1815 eruptions relative to early instrumental data (Brohan et al., 2012). In multi-decadal time scales (Fig. 2.4c), both simulated and reconstructed responses to volcanic forcing are significant and comparable in magnitude, although simulations show a faster recovery (<5 years) than reconstructions. Solar forcing estimated over the last millennium shows weaker variations than volcanic forcing (Fig. 2.4d).

In contrast to the surface cooling, the stratosphere is warmed by absorption of upward terrestrial longwave radiation at the lower aerosol layer and by absorption of solar near-infrared radiation (NIR) at the top (Fig. 2.3). This heating is dominant in the stratosphere, much larger than the cooling effects due to enhanced emissivity (consequently outgoing IR radiation), and due to its O_3 depletion (consequently less solar radiation absorption). Actually aerosols provide surfaces for heterogeneous chemical reactions, favourable for O_3 depletion. Robock (2000), Forster et al. (2007), Timmreck (2012) and Swingedouw et al. (2017) provide summaries of this forcing agent. In one word, surface cooling and stratospheric warming are the two main radiative forcing (RF) influences related to volcanic eruptions. In the next section, we use both observation, paleo

reconstructions and model simulations to bring in the question of how volcanic radiative forcing will influence the North Atlantic-Mediterranean winter climate.

2.5 Volcanic eruption and NAO

One of the most prominent atmospheric circulation modes influencing the North Atlantic-Mediterranean sector winter climate is the North Atlantic Oscillation. Known for its recurrent north-south dipole spatial feature, NAO[1] influences extratropical NH climate by modulating the wind, surface temperature, storminess, precipitation and sea ice over the Atlantic as well as adjacent continents when swinging between its two states, i.e. NAO positive and NAO negative (for a comprehensive review, see Hurrell and Deser, 2009). It was found that after strong stratospheric volcanic eruptions, NAO will vacillate into its positive phase during the first or two winter(s) following the eruption and favour a warmer and wetter winter over North Eurasia. However, emerging studies are showing that this response depends on multiple factors (e.g., eruption latitude, strength, initial climate system state).

In this subsection, we begin with a brief presentation of the NAO climate fingerprints over the North-Atlantic region based mainly on observation/reanalysis datasets. Then we explore relations and uncertainties between volcanism and NAO during post-eruption winters in observation after 5 tropical eruptions and 3 northern high-latitude eruptions during the industrial era (1850-2000 CE). Evidences from paleo reconstruction studies are also discussed to bring up the possible bias. Lastly, a review of progresses and challenges in studying volcano and NAO is introduced in details based on past numerous observation/modelling studies. This section serves as a *state-of-the-art* to the volcanic related NAO in observed, reconstructed and simulated post-eruption winters.

2.5.1 Climate impacts of NAO

The NAO exerts a significant influence on NH wintertime climate. Various indices are possible and relevant to quantify the amplitude of the NAO and to characterize its behaviours. There is no universally accepted index to describe the temporal evolution of NAO (Hurrell and Deser, 2009). In the thesis, to evaluate NAO temporal evolution and to

[1] The dipolar NAO has also been interpreted as the regional manifestation of an annular mode in sea level pressure known as the Arctic Oscillation (AO; Thompson and Wallace, 1998) or the Northern Annular Mode (NAM; Thompson and Wallace, 2000) due to their high correlations over the North Atlantic sector. The AO (NAM) spatial pattern is more zonally symmetric and so differs from the NAO over the North Pacific (Ambaum et al., 2001; Feldstein and Franzke, 2006). In this thesis, the term NAO is used to denote NAO, AO and NAM over the Northern Atlantic-Europe region.

calculate efficiently, the 2-box NAO index method based on Stephenson et al. (2006) has been applied hereafter. In practice, we apply two "boxes" to calculate NAO index. Two large longitude-latitude regions (see black contour boxes in Fig. 2.5b) have been taken from subtropical Mid-Atlantic and southern Europe Region (20°– 55°N, 90°W– 60°E) and from subpolar North Atlantic-Northern Europe region (55°– 90°N, 90°W– 60°E). Then the NAO index is defined as the difference between the December-February mean SLP spatially averaged over these two boxes. This definition firstly has the advantage of being more independent of the NAO centres compared with other methods which use only two sites to calculate the NAO index (e.g., Hurrell, 1995; Jones et al., 1997; Rogers, 1984). Secondly it avoids ambiguity and interpretation problems that occur when using more sophisticated definitions such as those based on principal component analysis (e.g., Deser, 2000) or cluster analysis (e.g, Cassou et al., 2004; Cassou and Terray, 2001; Hurrell and Deser, 2009).

As shown by Fig. 2.5a, we plotted NAO 2-box index time series based on Stephenson et al. (2006) using sea level pressure (SLP) data from 20th Century Reanalysis V2 dataset (*20thRv2*; Compo et al., 2011) dataset over the period 1871-2011 for December to January winter. A regrouping of NAO index calculated by 2-box method, PC1, station-based measurements based on Hurrell (1995) and Jones et al. (1997) over their common period 1865-2019 is also attached in **Appendix A.1** Fig. A.1.1. The 2-box index reveals highest correlation (r=0.97) with the NAO PC1 index calculated from empirical orthogonal function (EOF) analysis.

To present the climate impacts of the NAO, the spatial pattern of the various climate variable differences between high (exceeding one standard deviation) and low NAO index (less than one standard deviation) years are shown in Fig. 2.5b-g. The analysis is carried over the North Atlantic-Mediterranean sector (20°– 90°N, 90°W– 60°E) based mainly on *20thRv2* dataset (Compo et al., 2011) and Hadley Centre Sea Ice and SST dataset (*HasISST*; Rayner et al., 2003).

A clear dipole pattern is observed with negative SLP anomalies in subpolar NH, especially in Greenland and Iceland region, and positive anomalies in the subtropical area (Fig. 2.5b). The pressure vacillation results in the dissimilar heat and moisture transport and distribution over the North Atlantic-Europe area (Hurrell et al., 2003). The clockwise air flow in southern anticyclone combining with the counter-clockwise air flow in the northern cyclone pushes the westerly jet stream carrying warm and humid air to be strong enough to cross the North Atlantic from the east costal of subtropical America to northern part of Europe. The strengthened westerly jets can be clearly seen in Fig. 2.5c which blow through

the North Europe around 60°N. In contrast, the surface wind encounters easterly anomalies which favours dry and cold continental air westward and southward in the south flank of the southern anticyclone resulting in decrease of land temperature (2.5d) and SST (Fig. 2.5f).

As a result, a warmer winter is observed in northern Europe including the Iceland and Scandinavian area during a positive NAO time, while rier and colder conditions occur in southern Europe, the Middle East, and the Mediterranean (2.5d).

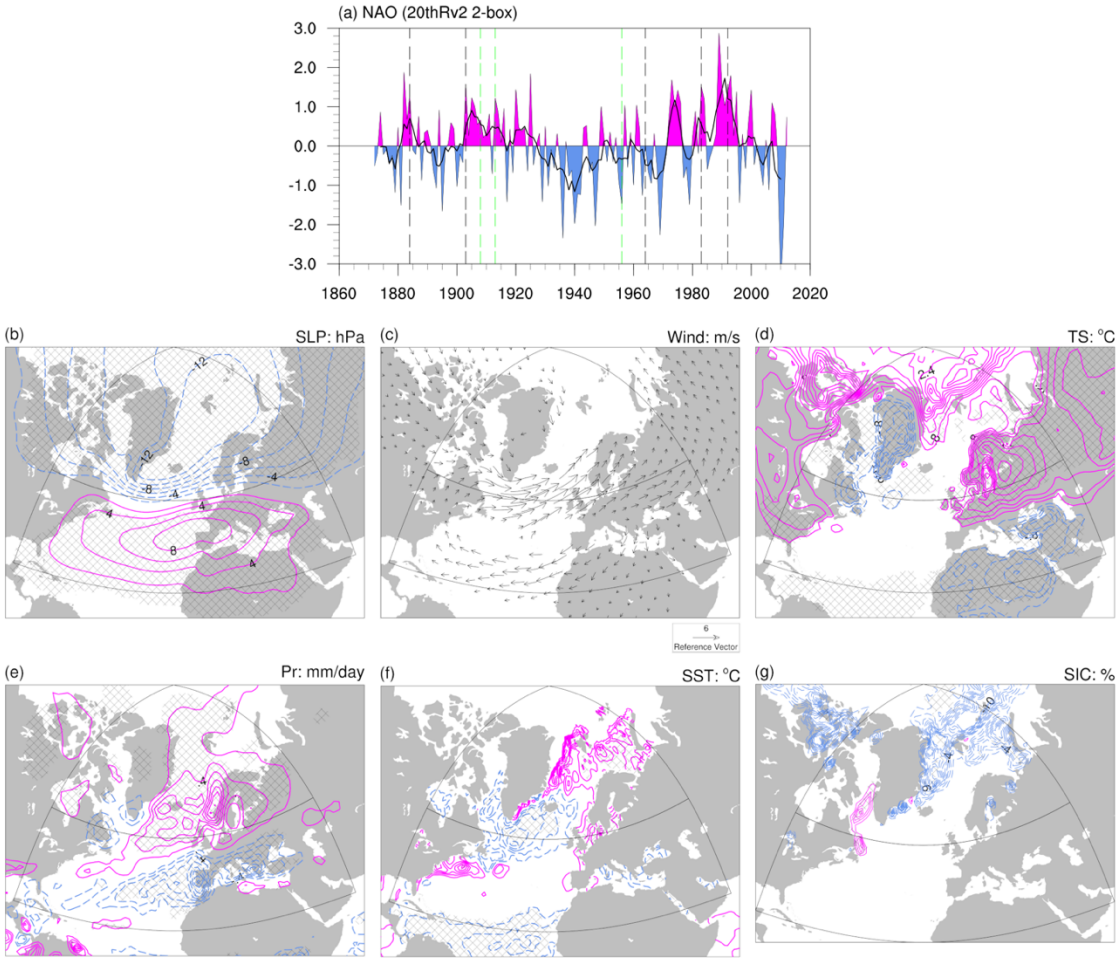

Figure 2.5: NAO index and its climate impacts over the North Atlantic-Mediterranean sector. **(a)** The 2-box NAO index calculated from 30-yrs running anomalies of sea level pressure in *20thRv2* dataset (Compo et al., 2011) over period 1871-2019. Vertical dashed lines indicate the first winter after onset of 5 tropical eruptions (black) and 3 NH eruptions (green). And differences in mean winter (December-February) between years when the NAO index exceeds 1 standard deviation and years when it is less than -1 standard deviation for **(b)** sea level pressure (SLP, hPa), (c) surface wind (Wind, m/s), **(d)** surface temperature (TS, °C), **(f)** precipitation (Pr, mm/day), **(e)** sea surface temperature (SST, °C), **(g)** sea ice concentration (SIC, %) using *20thRv2* dataset (Compo et al., 2011) and *HadISST* dataset (Rayner et al., 2003). Positive (negative) differences are given by the solid (dashed) contours in magenta (blue) colour. Absolute values exceed one derivation are shaded. The contours increments are respectively 2 hPa, 0.4 °C, 0.2 mm/day, 0.1°C and 1% for SLP, TS, Pr, SST and SIC.

Similar to the dipole pattern of SLP, the precipitation also illustrates dipole pattern with wetness in the north whilst dryness in the subtropics in Fig. 2.5e. During high NAO index years, there are north-eastward shift of westerlies which result in more intense and frequent precipitation in the vicinity of Iceland and the Norwegian Sea. The precipitation there hence is much larger than normal especially in orographic areas (such as southern Norway) in the prevailing path of this westerly (Jones et al., 1997).

The leading pattern of SST variability during boreal winter is characterized by a tri-pole pattern with its positive phase occupying a cold anomaly in the subpolar North Atlantic (mainly over Labrador Sea), a warm anomaly in the mid-latitudes centred off Cape Hatteras, and again a cold anomaly in subtropical area between equator and 30°N. It has been reported by Marshall et al. (2001) that changes in the air-sea heat exchanges and surface wind induced Ekman currents associated with NAO variations will contribute to this SST tri-polar structure. As shown in Fig. 2.5f, the SST map based on *HadISST* dataset demonstrates clearly the aforementioned tri-pole pattern when compositing North Atlantic SST between high and low NAO index years. Apart from this pattern, a warmer signature can also be observed in vicinity of the Barents Sea.

As for the winter sea ice anomalies (Fig. 2.5g), we tend to have high sea ice concentrations in Labrador and low sea ice concentrations over the Barents Sea when composting between high and low NAO index years, which is consistent with the NAO's circulation pattern. Deser et al. (2000) suggested that NAO contributes to this seesaw pattern of winter sea ice via wind-driven anomalies of sea ice velocity, surface vertical heat flux and possibly horizontal oceanic heat flux. Moreover, both reanalysis and modelling studies indicate such sea ice variability associated with positive polarity of the NAO tend to generate negative NAO-like atmospheric circulation response, i.e. a negative feedback (Alexander et al., 2004; Deser et al., 2004, 2007; Magnusdottir et al., 2004; Strong et al., 2009).

To conclude, the NAO is the leading pattern of atmospheric circulation variability in the NH and influences significantly the North Atlantic-Mediterranean winter climate. In next subsection, we will see further how volcanic eruptions orchestrate with NAO.

2.5.2 Observation : positive NAO in post-eruption winter?

Although consensus holds that volcanic aerosols produce cooling at the Earth's surface due to reduction of incoming radiation (recalling Fig. 2.3&2.4), the winter following several large tropical eruptions (for example the winter of 1991-92 DJF after Pinatubo eruption) was warmer and wetter than average over North America and North Eurasia both in satellite-

derived lower tropospheric temperature and in synoptic surface observations. Meanwhile negative temperature and rainfall anomalies were observed mainly over the eastern Mediterranean and over the north-eastern part of North America.

This winter anomaly pattern resembles a typical positive NAO phase such that questions arise as to **i)** whether this anomaly is simply internal-variability-driven (Polvani et al., 2019), or produced by a deterministic process after volcanic eruption (due to the reduction of shortwave radiation or other components) ; **ii)** whether this anomaly is privileged response for tropical eruptions, or reproducible (opponent) for extratropical volcanic eruptions. Thereby the dynamical relations between volcanic eruption and atmospheric circulation pattern in boreal winter keep attracting scientists' attention.

In this subsection, we discuss mainly some observed results from reanalysis dataset for 5 tropical eruptions (Krakatau in May 1883, Santa María in October 1902, Agung in February 1963, El Chichón in March 1982 and Pinatubo in June 1991) and 3 NH high-latitude eruptions (Ksudach in March 1907, Katmai also Novarupta in June 1912, Bezymianny in October 1955). Among the eight volcanic eruptions, they all eject scads sulfur into stratosphere (Bluth et al., 1992; Stothers, 1996, 1997, 2001; Zelenski et al., 2015, etc), such as the 1982 El Chichón and 1991 Pinatubo eruptions which ejected around 3.5 Mt (C. Gao et al., 2008) and 9 Mt (Guo et al., 2004) sulfur into the stratosphere respectively. Detailed information of the 8 major eruptions during 1865-2000 is listed in **Appendix A.1** Table A.1.1.

Individual large eruptions produce global or hemispheric cooling for 2 or 3 years. As shown in Fig. 2.6a, global surface air temperature declines after onset of major tropical volcanic eruptions over instrumental era from *HadCRU* (Morice et al., 2012) datasets. The maximum cooling takes place usually at second year after the onset of tropical volcanic eruptions. The extratropical eruptions (Fig. 2.6b) didn't show consistent cooling effects as their tropical counterparts, in part because of the shorter lifetime of their emissions and therefore their impacts. This cooling has indeed different regional signatures. For example, in some regions of the tropics, even for a large eruption like El Chichón, the cooling effects can be superposed and overwhelmed by a large El Niño in the eastern tropical Pacific in summer (Robock, 2000). The Eurasian continent may also have regional winter warming pattern if a positive NAO phase occurs. We wonder if this counterintuitive effect exists in observation and if it is due to any nonlinear response through atmospheric dynamics.

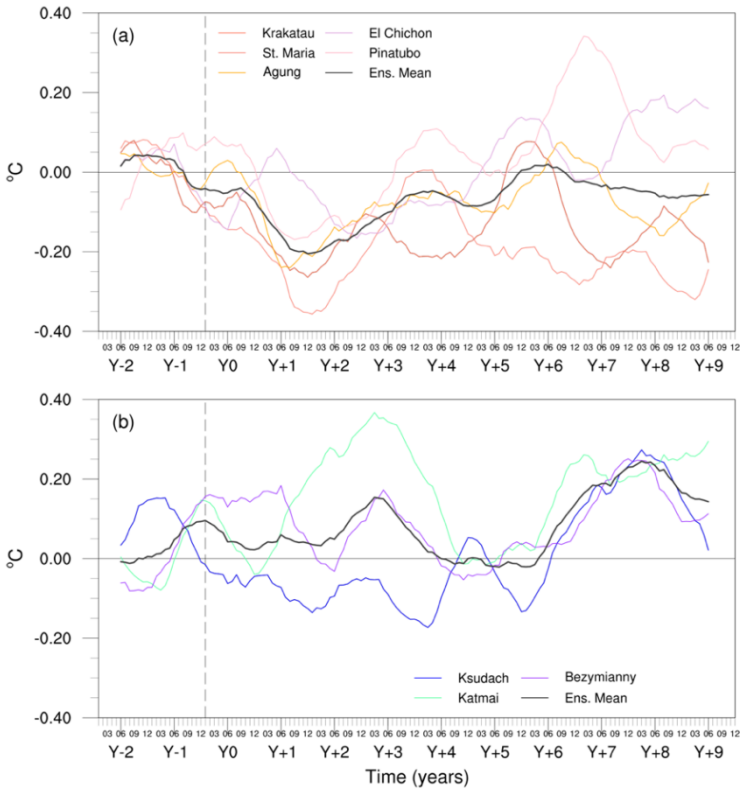

Figure 2.6: Anomalous global atmospheric temperature at the Earth's surface (in °C) in response to **(a)** five major volcanic eruptions (Krakatau in May 1883, Santa María in October 1902, Agung in February 1963, El Chichón in March 1982 and Pinatubo in June 1991) and to **(b)** three major NH high-latitude volcanic eruptions (Ksudach, March 1907; Novarupta/Katmai, June 1912; Bezymianny, October 1955) over the instrumental era from *HadCRU* (Morice et al., 2012) dataset. anomalies refer to the average of the three-year preceding each eruption. The vertical line stands for the onset year of the eruptions. The unit of the x-axis is year. To note, year +1 is defined as the first winter beginning after the onset of the eruption (i.e. 1883–1884, 1902–1903, 1963–1964, 1982–1983, 1991–1992; 1907-1908, 1912-1913, 1955-1956). (adapted from Swingedouw et al., 2017)

In Fig. 2.7, the 2-box NAO index time series are shown from one year before to five years after the same five tropical eruptions and three NH eruptions. Except the 1963 Agung and 1955 Bezymianny eruptions, all other eruptions show a positive NAO index in the first volcanic winter, passing one standard deviation of winter NAO index of the whole period 1871-2011. Their ensemble mean also demonstrates a positive NAO index in the first winter albeit the ensemble signal does not pass one standard deviation. The second winter NAO index signal is less consistent among the eight eruptions. Robock and Mao (1992) already attributed the NAO signal to volcanic eruptions, inspired by the strong positive NAO signal observed in the winters following the Mt. Pinatubo eruption. Nevertheless, we should remind that the actual observation is only "one realization of the true world" and natural variability of NAO is unignorable (as can be seen in Fig. 2.5a) and difficult to be removed.

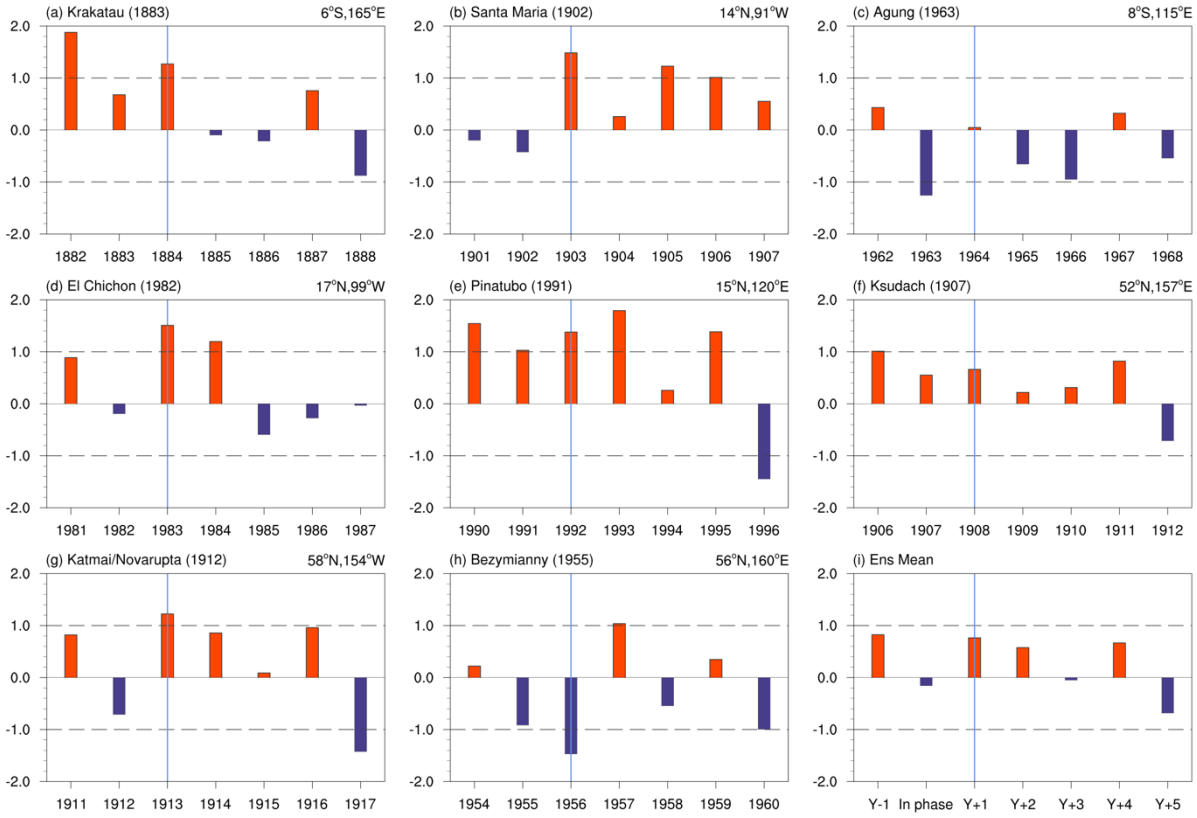

Figure 2.7: The 2-box NAO index calculated from 30-yr running anomalies of sea level pressure in *20thRv2* dataset for same eight major volcanic eruptions as in **Figure 2.6** over the instrumental era and their ensemble mean. The vertical blue line stands for first winter year after the onset of eruptions. The dashed lines indicate ±1 standard derivation of NAO index during period 1871-2011. The unit of the x-axis is year. The indicated year corresponds to the January of the winter season (e.g, 1884 is the winter of 1883/1884).

Continuously Fig. 2.8 and Fig. 2.9 illustrate the anomalies of surface air temperature, surface winds, precipitation and sea level pressure during the first volcanic winter after the five tropical eruptions and the three NH eruptions respectively. Here we recognize that the number of observed events that can be studied is quite limited. In order to account for such small samples, we applied super epoch analysis to test the climate anomalies in post-eruption winter. We build random anomaly distribution from a large number (here 1000) random sequences of winter atmospheric states over the investigated period (i.e. 1871-2011 from *20thRv2* dataset). By estimating the likelihood of the obtained volcanic winter anomalies during these 1000 winter sequences, we arrive to evaluate the confidence level for the attribution of a signal to a chance occurrence. More specifically, signals are considered to be statistically significant (stippled area) if they exceed the 10th–90th percentiles evaluated for the random 1000-sequences anomaly distribution.

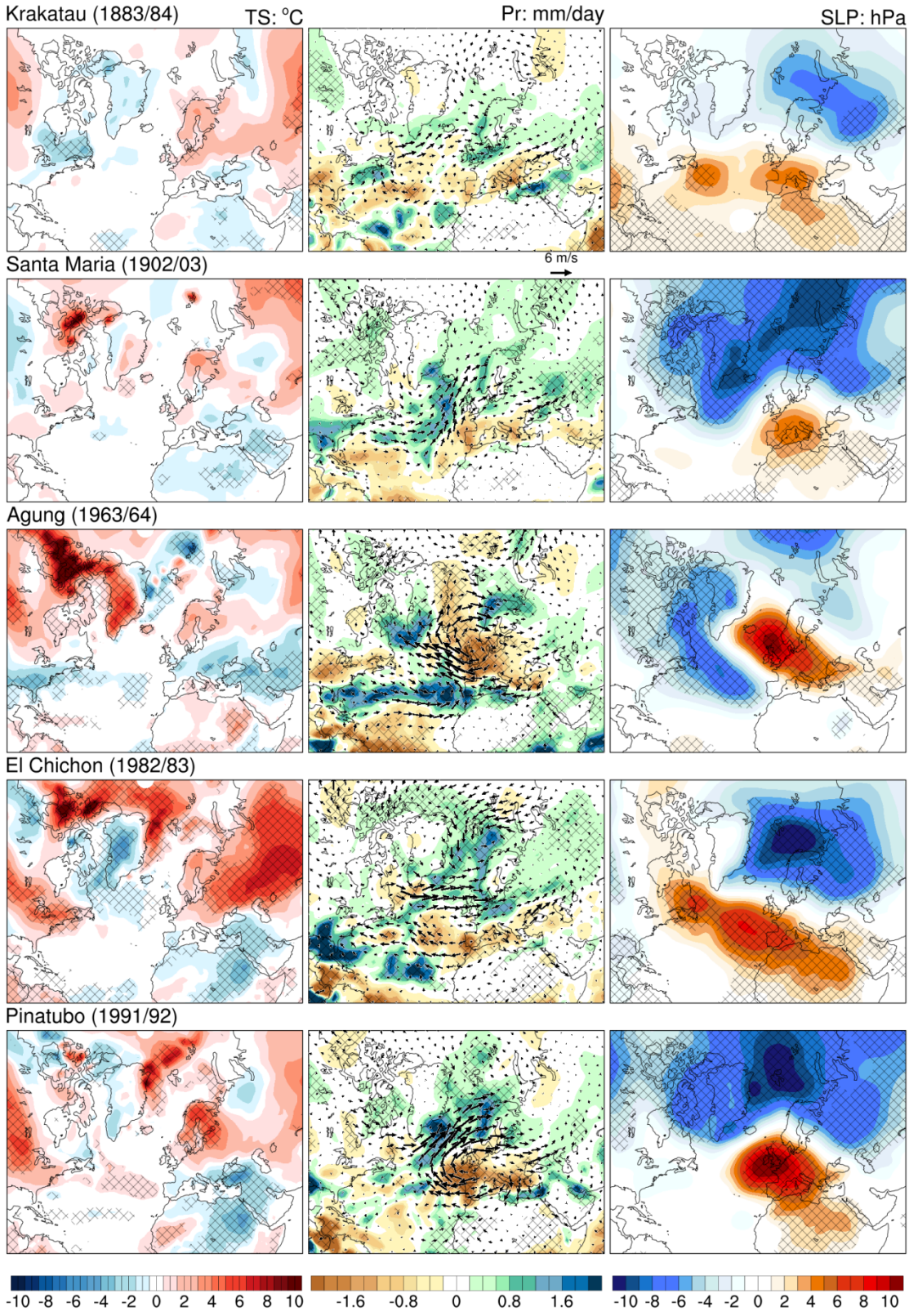

Figure 2.8 : Anomalies of surface air temperature(color; left), precipitation rate (color; middle), surface wind (vector; middle) and SLP anomalies (color; right) over December-February during first winter after onset of five major volcanic eruptions (from top to down, Krakatau, Santa María, Agung, El Chichón and Pinatubo). The anomalies are calculated based on 30-yrs running anomalies. Stippled areas indicate anomalies exceeding 10%~90% confidence interval.

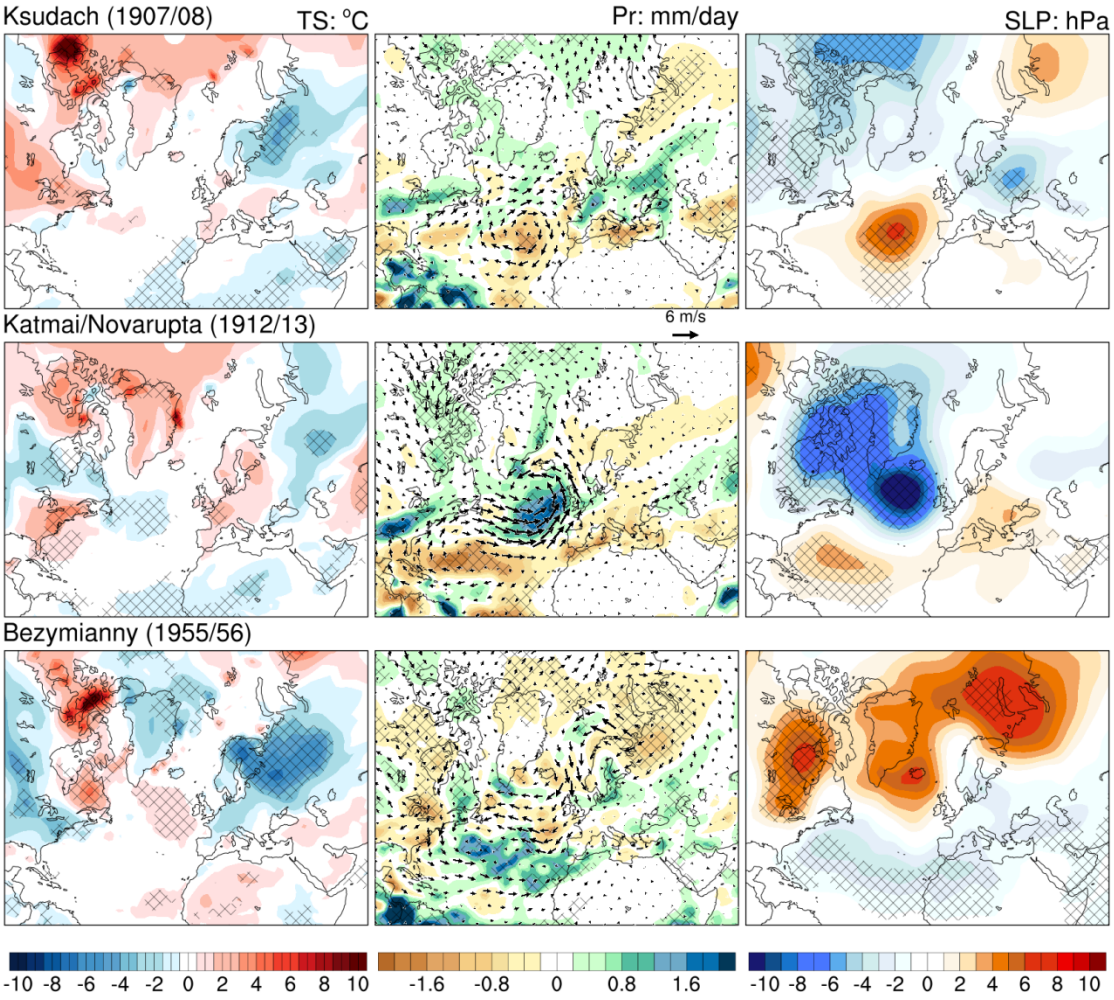

Figure 2.9: Same as **Figure 2.8** but for three major NH high-latitude volcanic eruptions (from top to down, Ksudach, Novarupta/Katmai and Bezymianny). The anomalies are calculated based on 30-yrs running anomalies.

Generally, all tropical eruptions, except 1963 Agung which erupted after a strong negative NAO year (Fig. 2.7c), have shown a positive NAO-like feature with see-saw pattern of SLP anomalies between the subpolar and subtropical North Atlantic, consistent with what has been reported in Christiansen (2008). The North Eurasian continent especially the Scandinavian region encounters a warmer and wetter winter accompanied with a stronger westerlies blowing from south Greenland to North Europe for tropical eruptions. While among the three NH extratropical eruptions, the 1955 Bezymianny also erupted after a strong negative NAO year that followed by a more negative signal after eruption (Fig. 2.7h). For the 1912 Katmai/Novarupta eruption, we observed a strong cyclone south of the Greenland, where counterclockwise wind anomalies appeared. While the winter NAO index for 1907 Ksudach eruption was not significant from Year-1 to Year+5.

In conclusion, limited observational samples prohibit us from drawing plausible conclusions between NAO and volcanic eruptions mainly due to the noisy nature of climate internal variability. Especially when compared to the pronounced winter warming signals from tropical eruptions, the observed signal for extratropical eruptions seems rather ambiguous among only three events. A comprehensive analysis of observation and multi-proxy combined with model simulations are believed to shelter more light on understanding the significance and mechanism for NAO responses after volcanic eruptions.

2.5.3 Review of challenges in studying volcano-NAO

While the previous discussions are based on a relatively small observational sample, scientific studies keep emerging to explore in depth the volcano-NAO relationship with observation/proxy data and model simulations. In this subsection, I present a review of related challenges raised in these studies.

Limited volcanic events during instrumental era

As has been introduced in previous subsection, there is limited observed volcanic events during industrial era, which makes the first challenge in studying volcano-NAO.

Most studies using observations for twentieth century volcanism have inhomogeneous results on the volcanically induced global and regional climate response, partly due to the limited volcanic samples during the industrial era to make robust statistical analysis (Graf et al., 2014; Iles et al., 2013; Maher et al., 2015). Such a small sample size does not completely remove the influences of variability resulting from other forcing terms – for example, the solar cycle was at a maximum at the times of both the El Chichón and Pinatubo eruptions, and El Niño events were observed in the first winters after both eruptions. It is hard to prove whether the NAO signal during volcanic winters is "true" (or statistically significant) with only observational evidence.

To overcome the paucity of volcanic events, two solutions are given by climate scientists. Firstly, last millennium volcanic events that are much larger than those of the twentieth century have been studied using either climate models (e.g., Stevenson et al., 2016, 2017, 2018; Colose et al., 2016; Zanchettin et al., 2013, 2016) or proxy records (e.g., Trouet et al., 2009; D'Arrigo et al., 2009; Schneider et al., 2017; Esper et al., 2015; Cook et al., 2019; Pinto and Raible, 2012; Ortega et al., 2015) with proper statistical methods to analyse the significance of the signal. Secondly, large-ensemble experiments have been designed

based either on some well-observed eruptions (e.g., 1991 Pinatubo eruption) or on idealized volcanic forcing setting in models (e.g., Zhuo et al., 2021; Azoulay et al., 2021).

Regarding proxy study on last millennium volcanic eruptions, Fischer et al. (2007) selected 15 major tropical volcanic eruptions and analysed the winter and summer climate signal following these eruptions by using multi-proxy reconstructions. A significant milder and wetter winter climate was diagnosed in the first and second post-eruption years over northern Europe. They concluded that the warming and humid trends were concurrent with positive phase of NAO for the atmosphere circulation.

As concluded in latest IPCC AR6, new multi-centennial or multi-millennial timescale NAO reconstructions are derived since AR5 from marine and lake sediments, speleothems, tree rings and ice cores (Baker et al., 2015; Cook et al., 2019; Faust et al., 2016; Hernández et al., 2020; Jones et al., 2014; Mellado-Cano et al., 2019; Ortega et al., 2015; Sjolte et al., 2018; Steiger et al., 2018, etc). Tremendous work is still ongoing to use these new reconstructions in volcano-NAO study. In a larger temporal range, Ortega et al. (2015) presented a yearly NAO reconstruction for the whole past millennium on the basis of 48 annually resolved proxy records spreading the Atlantic Ocean. Their reconstruction also reveals a significant positive NAO fingerprint one year after 11 strong volcanic eruptions (listed in **Appendix A.1** Table A.1.2) which is consistent with simulation results and satellite observations for the Mt. Pinatubo eruption. Both studies only considered intense tropical eruptions that we are still not sure of the significance of NAO signal after extratropical eruptions. It is clear that an integrated proxy study for both tropical and extratropical volcanic eruptions on NAO behaviours and NH climate are not adequate for paleo scientific community.

At the same time, estimating the role of explosive volcanism requires large number of climate proxy data with good spatial distribution. While the number of suitable records decreases going back in time, large uncertainty also remains in the estimation of climate variability and forcing factors when using reconstruction data, especially before ~1600 AD (Schneider et al., 2009).

To investigate responses of NAO and global climate to volcanic eruptions, coupled climate system models are particularly useful tools. Certain models have been successfully employed to simulate the major-observed surface cooling effect of large volcanic eruptions, and to compare model outputs to observation/proxy data. Representatively the Paleoclimate Modelling Intercomparison Project (PMIP) is an important effort of the international climate community to understand responses of the climate system to different

climate forcings for different past climatic states beyond the present and historical period. Both PMIP3/CMIP5 and PMIP4/CMIP6 promote the *past1000* experiment focusing on climate variation of the last millennium. One important goal of *past1000* is to investigate climate responses to volcanic forcing with long transient simulations. The challenge of limited well-observed volcanic events can also be largely resolved by studying *past1000* simulations.

Another representative effort of the climate modelling community is the Model Intercomparison Project on the climatic response to Volcanic Forcing (VolMIP), where large ensemble experiments are designed under a common stratospheric aerosol data to study the climate influences and physical processes of volcanic forcing. These two programs (PMIP4 and VolMIP) will be soon introduced in section 2.6.

Modelling uncertainties

While both observations/reconstruction (e.g., Christiansen, 2008; Fischer et al., 2007; Ortega et al., 2015; Robock and Mao, 1992, 1995) of tropical eruptions show positive NAO and pronounced winter warming over the continental Northern Hemisphere after eruption, the modelling studies do not share a universal conclusion. On the one hand, we admit that modelling groups have made huge progress in analysing volcano-NAO. Some models and simulations (e.g., Graf et al., 1993; Kirchner et al., 1999; Shindell et al., 2004; Stenchikov et al., 2002, 2004; Swingedouw et al., 2017) arrive to simulate the post-eruption winter climate related to the positive NAO. On the other hand, it is a fact that there are still simulations indicating a model failure or inefficiency in reproducing the NAO positive phase after largest volcanic eruptions (e.g., Braconnot et al., 2012; Driscoll et al., 2012; Hermanson et al., 2020; Stenchikov et al., 2006; Zambri et al., 2017). Therefore we conclude the second important challenge in studying volcano-NAO is to overcome the modelling uncertainties.

There are multiple factors contributing to the modelling uncertainties. They are related mainly to **i)** structural model differences, **ii)** different volcanic forcing datasets, and **iii)** their implementation within climate models.

(1) Structural model differences

In early times, Stenchikov et al. (2006) have evaluated the volcanic responses in simulations produced by seven of the climate models included in the model intercomparison conducted as part of the preparation of IPCC AR4. As a result, in most of the models (except NCAR PCM), composite SLP there is a similar basic pattern of positive NAO with low pressure over the pole surrounded by a ring of anomalously high pressure.

However, beyond that basic feature, models vary considerably in their SLP anomaly spatial patterns. They concluded that the models in AR4 may simply not have sufficiently fine resolution and sufficiently deep model domains to adequately treat stratospheric dynamics and the stratosphere-troposphere dynamical interactions.

In the recent review work reporting volcanic forcings and influences by Swingedouw et al. (2017), it is shown that among the eight PMIP3/CMIP5 last millennium simulations, only two (CCSM4 and CNRM-CM3) can simulate a positive NAO at 95% confidence level in the first winter after 8 large tropical volcanic eruptions over the period 1000–1900 (Fig. 2.10). We also observe that the precedent version of IPSL's model, IPSL-CM5A-LR, fails to reproduce a statistically significant signal (Fig. 2.10). This lack of winter NAO response in most climate models is certainly a manifestation of their discrepancy, given the evidence of what we found in recent reconstructions (e.g., Ortega et al., 2015).

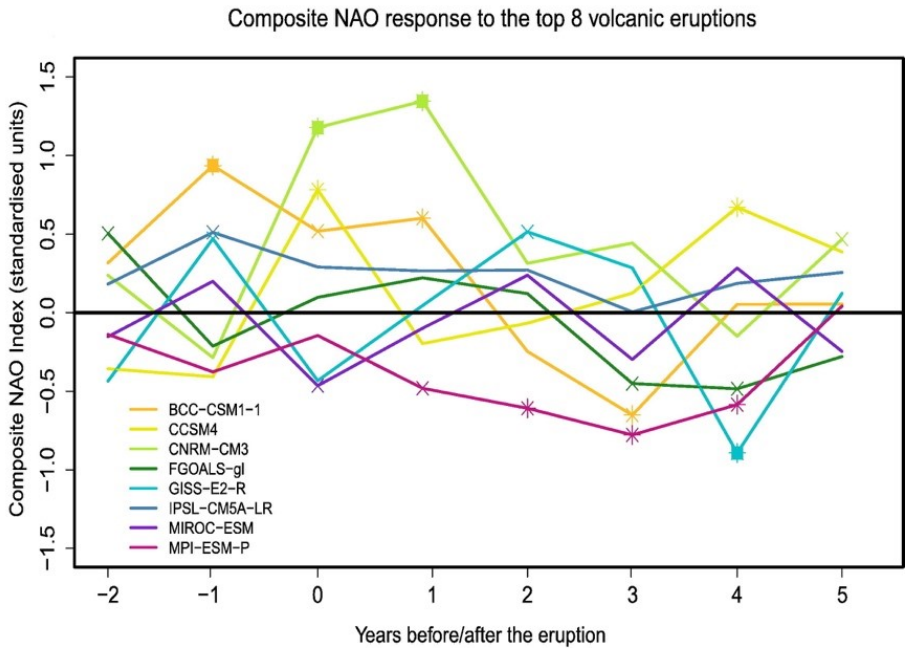

Figure 2.10 : Composite response of winter NAO (in standardized units) to 8 large volcanic eruptions over the period 1000–1900 in a set of 8 PMIP3/CMIP5 last millennium simulations. For the observations, the volcanic eruptions considered took place in 1257, 1600, 1641, 1693, 1809, 1815, 1835 and 1883. To note, for the NAO reconstruction in a), the year 0 here indicates one year later than in Ortega et al. (2015) because that the eruptions have low chance to occur in January–February, which is the winter considered by the reconstruction. For the PMIP3 simulations, the 8 largest volcanic eruptions vary depending on the simulation, and the estimates of volcanic forcing used to produce them. Time series are all standardized with respect to the full reconstructed or simulated period. Significance is assessed following a Monte-Carlo test based on 1000 random selections of 8 years from the corresponding NAO time-series. Significant values at the 90%, 95% and 99% confidence levels are represented by crosses (x), stars (*) and filled squares (■), respectively. (source: Swingedouw et al., 2017)

According to IPCC AR6, influences from major volcanic eruptions appear to be more robust, but some modelling experiments still question the amplitude of the response, which mostly projects on the positive phase of the NAM/NAO (Bittner et al., 2016). By conducting multi-model analysis based mostly on CMIP6 models, Hermanson et al. (2020) has compared the simulated response to three eruptions (Agung, El Chichón and Pinatubo) with observational datasets. They found that there is still a small signal-to-noise ratio in the models, consistent with other studies (Baker et al., 2018; Dunstone et al., 2016; Eade et al., 2014; Scaife and Smith, 2018).

Models vary with each other in resolution, climate component coupling and the representation of physics. It is therefore concluded that internal variability and model differences should be addressed when studying the significance of climate responses to volcanic eruptions.

(2) Different volcanic forcing datasets

Volcanic forcing reconstructions provide essential boundary conditions for climate simulations which aim to reproduce the past climate variability. They have been extensively used to investigate climate variability in instrumental and proxy-based climate records (Ammann et al., 2003; Crowley et al., 2008; Crowley and Unterman, 2013; Gao et al., 2008; Hegerl et al., 2007; Masson-Delmotte et al., 2013; Sato et al., 1993; Sigl et al., 2015; Thomason et al., 2018; Toohey and Sigl, 2017) and have been used to show that volcanism is the dominant natural driver of climate variability in the Earth's recent past (Schurer et al., 2013) and to be implemented in model forcing configuration. The use of different volcanic forcing reconstructions in past PMIP3/CMIP5 last millennium simulations (Schmidt et al., 2011), together with their practical methods of implementation in climate models, constitute an important ingredient for modelling uncertainties.

In the absence of direct observations for the millennium paleo-eruptions, the volcanic forcing recommended within the framework of PMIP3/CMIP5 are obtained with the hypothesis of linear "scaling" between the optical parameters (such as aerosol optical thickness) of sulphated aerosols from the Pinatubo eruption and the amount of sulfuric acid measured in ice cores. As stated before in section 2.2.1, two such reconstructions, described in Gao et al. (2008, 2012) and Crowley and Unterman (2013), have been applied in most PMIP3/CMIP5 models for past millennium simulation (recalling the Fig. 2.1a).

Zambri et al. (2017) analysed the PMIP3 *past1000* simulations from eight models over the world and concluded that climate responses vary greatly between the CEA-forced

(Crowley and Unterman, 2013) and GRA-forced (Gao et al., 2008, 2012) PMIP3 ensembles. Analysis of the individual model results also show that differences among models have a large influence on inter-model spreading, especially on the reflected short wave radiation by volcanic aerosols. And generally, GRA-forced climate models have higher chances in producing a strengthened polar vortex and surface warming in the first boreal winter after large volcanic eruptions.

In a recent research work investigating climate forcings and feedbacks over the last millennium in the PMIP3/CMIP5 models, Atwood et al. (2016) concluded that volcanic forcing accounted for 65% of the total forcing on average but with large inter-model spread (ranging from 50% to 73% or 20.07 to 20.32 W/m^2, across models) based on TOA energy budget analysis.

For individual model, Bittner et al. (2016) showed that the Max Planck Institute Earth System Model (MPI-ESM; Giorgetta et al., 2013) is capable of simulating a strengthened polar vortex in response to a volcanic eruption, and that the response is also strongly dependent on the forcing chosen, and requires a very strong forcing to overcome the high variability of the stratosphere during NH winter. Additionally, Bittner et al. (2016) and Zambri and Robock (2016) showed that most of the CMIP5 models can in fact reproduce this dynamical response in the first winter after an eruption large enough. Both studies used only the two largest tropical eruptions of the historical ensemble period (1850–2005 CE), and both found a significantly weaker signal when including smaller eruptions. Besides, Toohey et al. (2014) suggested that the stratospheric polar vortex responses to past eruptions depend on accurate representation of the space-time structure of the volcanic aerosol forcing.

(3) Volcanic forcing implementation methods in models

The implementation methods of volcanic forcing in models are also responsible for the modelling uncertainties. The implementation process can be divided into two categories (*prognostic* or *prescribed*) to simulate the volcanic aerosol forcing on solar radiation (Fig. 2.11).

Some climate models are coupled with *prognostic aerosol microphysical modules* (e.g., English et al., 2013; Mills et al., 2016; Timmreck, 2012; Toohey et al., 2011; Zambri et al., 2019a, 2019b), which allow for an explicit simulating the full life cycle of the volcanic aerosols, including oxidation from SO_2 to $SO_4^{(2-)}$ aerosol formation and growth via nucleation, condensation, accumulation and coagulation; vertical distribution via sedimentation; and finally the removal processes via wet and dry deposition. For example,

Zambri et al. (2019a, 2019b) used a three-mode prognostic modal aerosol model (MAM3; Liu et al., 2012) to represent aerosols in the atmospheric component of the Community Earth System Model version 1 (CESM1; Hurrell et al., 2013). For such models, simulating the effects of volcanic eruptions on climate requires estimates of the amount of sulfur injected into the stratosphere and the time and location of that injection. Prognostic aerosol modelling, however, comes with an associated large computational expense.

In another commonly applied methodology, climate models take as input reconstructed volcanic forcing datasets, which prescribe certain physical aspects (mostly optical properties) of the volcanic stratospheric sulfate aerosol (e.g. aerosol extinction, aerosol optical depth, single scattering albedo, effective radius, and scattering asymmetry factor). Being relatively less expensive in computational resources, *prescribed aerosol forcing* sets are also widely used in many model simulations for volcanic eruptions, including our model IPSL-CM6A-LR.

Furthermore, volcanic stratospheric sulfate aerosols can affect the solar radiation transfer, and then the climate system, mainly via two pathways:

i. Effective radiative forcing due to aerosol-radiation interactions (*ERFari*);

ii. Effective radiative forcing due to aerosol-cloud interactions (*ERFaci*).

The former consists of backscattering of solar light which decreases the solar energy reaching the Earth surface, and absorption of long wave radiation from the land and near infrared radiation from the Sun (Boucher et al., 2014). The latter accounts for aerosol-related

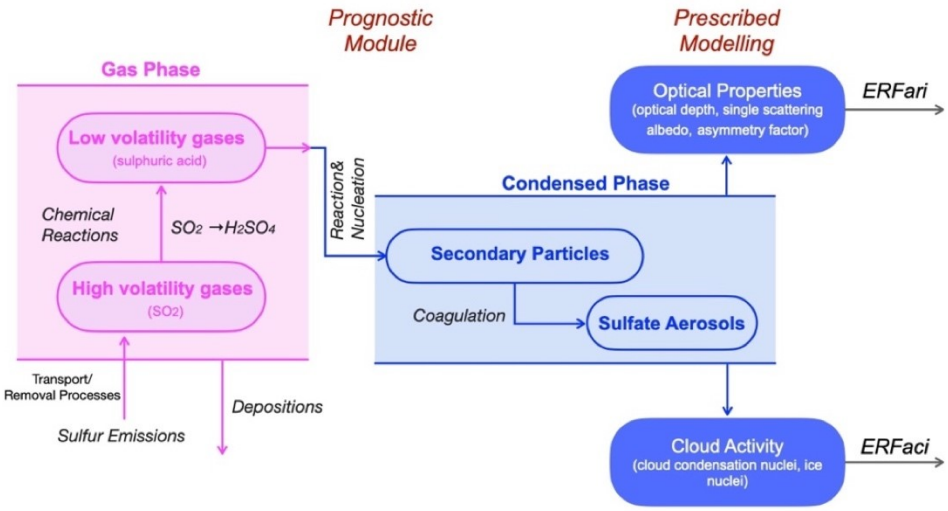

Figure 2.11 : Overview of volcanic sulfate aerosol variables and processes influencing aerosol-radiation and aerosol-cloud interactions. This figure also shows a chain of processes from aerosols to forcing (*ERFari* and *ERFaci*) and corresponding two types of volcanic modelling methods (*Prognostic* and *Prescribed*). (adapted from Fig. 7.12 in IPCC AR5 Chapter 7, Boucher et al., 2014)

microphysical modifications of cloudiness (Twomey, 1977), as well as any secondary effects that result from clouds adjusting their lifetime (i.e., "lifetime effects"; Albrecht, 1989; Liou and Ou, 1989; Pincus and Baker, 1994). It is also reported (Zambri et al., 2019 b) that volcanic eruptions cause not only changes in cloud optical properties but also changes in cloud cover in time and space.

It is reasonably inferred that the different application of ERFari and ERFaci will also become one source of uncertain from volcanic forcing. Despite that the volcanic sulfate aerosols can exert effect on climate through their interactions with clouds, the magnitude of this effect is highly uncertain (Malavelle et al., 2017). In the latest IPCC AR6, it is also stated that due to *limited agreement*, the contribution to volcanic ERF due to sulphate aerosol effects on ice clouds is not included in the overall assessment. In our study we will only concentrate on ERFari of volcanic forcing radiative effects.

To decrease modelling uncertainties evolved from different volcanic forcing datasets or implementation methods, more stringer experimental set-ups (e.g. an identical forcing data set) are implemented in the CMIP6 process, provided an improved basis for multi-model studies. This solution is strictly applied in PMIP4 and VolMIP, so does in our model IPSL-CM6A-LR (section 2.6 and 2.7).

Besides, large modelling uncertainties also come from initial conditions, strength of additional forcing, and ultimately whether a model takes into account sufficient relevant physical processes that will influence the NAO response to volcanic eruptions (Joshi and Jones, 2009; Jungclaus et al., 2010; Schurer et al., 2013). For example, aerosol-radiation interaction, aerosol-cloud interaction, the Quasi Biennial Oscillation (QBO) phase, the Atlantic Multidecadal Oscillation (AMO), teleconnection effects from El Niño Southern Oscillation (ENSO), the stratospheric polar vortex barrier… These aspects will be addressed by modelling teams with an improved knowledge of related climate dynamics (i.e., understanding of the mechanism).

Understanding of the mechanism

The most important challenge in studying volcano-NAO is to understand the physical mechanism behind the phenomenon, which is also a conundrum at continuous study in CMIP6. The mechanisms encompass analyzing not only the effects of two components of volcanic radiative forcing (surface cooling and stratospheric warming), but also the teleconnections between NAO and other climate modes (such as QBO, ENSO).

(1) Stratospheric or tropospheric gradient mechanism

From the past literatures, we can deduce three main theories to explain the mechanism relating tropical volcanic eruptions and NAO:

i) « Stratospheric gradient mechanism type I » refers to the excitation of inherent zonal mean variability modes such as the Polar Vortex or NAO, enhanced by volcanic stratosphere heating. It was mainly explained in Robock et al. (2000) and Raible et al. (2016).

ii) « Stratospheric gradient mechanism type II » refers to the strengthened planetary wave reflection that possibly affects the NAO, which does not resemble the inherent circulation variability, as shown in Graf et al. (2007, 2014) and Bittner et al. (2016).

iii) « Tropospheric gradient mechanism » implies the decrease of zonal mean energy and amplitude of tropospheric waves, as demonstrated in Stenchikov et al. (2002).

Basically, for « Stratospheric gradient mechanism type I », the differential heating between low and high latitudes in the sulphate aerosol laden stratospheric layer would lead to strengthened westerlies in subpolar and midlatitudes in winter, i.e. a strengthened polar vortex. These strong westerlies prevent planetary waves from penetrating into the higher stratosphere and their reflection back to the troposphere creates a circulation pattern responsible for warm air advection over the continents of the Northern Hemisphere. This corresponds to the positive phase of NAO, excited by the volcanic aerosol layer in the stratosphere.

While for « Stratospheric gradient mechanism type II », it is believed that under the differential heating (increased stratospheric meridional temperature gradient), the strengthened polar vortex is not the same as it is during normal winters with a strong polar vortex. Furthermore, instead of being effectively blocked and prevented from upward travelling, planetary waves are facilitated to propagate into the upper stratosphere, as described in Graf et al. (2007). The former two mechanisms are considered as a « Top-Down » process.

Lastly the « Tropospheric gradient mechanism » refers to the dominant role of surface cooling effect in simulating positive NAO during volcanic winters. According to Stenchikov et al. (2002), their surface cooling-only experiments reduce the meridional differential heating and lead to weaker vertical planetary wave energy flux. The diminished wave friction in the lower stratosphere allows the polar vortex to accelerate, and thus activated the wave feedback and positive NAO. Stenchikov et al. (2002) also suggests the tropospheric effect can simultaneously operate with the « Stratospheric gradient

mechanism » and they may reinforce each other, which can lead to a stable and strong climate signal. This mechanism is considered as a « Bottom-Up » process.

It is clear that the above-mentioned processes are key physical mechanisms to understand the mysterious dynamics and interactions between NAO and volcanic radiative forcing. They are also important for numerical models to behave correctly in simulating climatic effect of volcanism.

For example, a recent study (Bittner, Schmidt, et al., 2016) used CMIP5 models to check if the polar vortex propagates to the surface under Pinatubo or Krakatau-like eruptions. It is found that models generally fail to do it, although their polar vortex does show an enhancement signal. Such deficiencies are also revealed by Driscoll et al. (2012). They found models in CMIP5 generally failed to capture the NH atmospheric circulation changes after volcanic eruptions. In comparison, another study by Barnes et al. (2016) showed more optimist results. They found that the Mt. Pinatubo eruption triggered robust changes in both the stratosphere and troposphere, but with deformed NAO modes. Zambri et al. (2017) also show that, in contrast to a good simulation of strengthened polar vortex in most PMIP3 models, only one of the four CEA-forced PMIP3 models (MPI-ESM-P) simulates a pattern of sea level pressure anomalies in line with a positive NAO, and only two of GRA-forced PMIP3 models (CCSM4 and MRI-CGCM3) simulate statistically significant NAO signal. The SLP anomalies are not statistically significant, and therefore do not indicate a robust tendency toward a positive AO in these models. They suggest that individual model difference exist in responses at the stratosphere and at the surface.

Hence efforts should be continued to understand and to improve the model prediction ability in extra-tropics and the dynamics between troposphere and stratosphere to explain the relevant dynamics. This is also one objective of the thesis to check whether the latest IPSL-CM6A-LR model is capable of reproducing the volcanic-related climate variations in post-eruption winters and to elucidate the underlying physical mechanism.

It is to be noted that most mechanism studies have dealt with the effect of recent large tropical eruptions. Impacts of high-latitude volcanic eruptions are far less studied than their low-latitude counterparts. Only a few observational studies have examined the impact of strong volcanic eruptions outside the tropics. Aerosols of extratropical volcanoes have distinct impacts compared to equatorial volcanoes on climate system because of their different meridional distributions (Liu et al., 2016). Some contradictory results are found for extratropical volcanic eruptions compared to tropical ones.

For example, using the Goddard Institute for Space Studies ModelE, Oman et al. (2005) found anomalies resembling a negative phase of NAO in simulations of the 1912 Katmai eruption in Alaska, due in theory to stratospheric heating by volcanic aerosols and a subsequent weakening of the stratospheric polar vortex. By designing experiments based on analogs of the June 1783 Laki eruption using CSEM1 model (Hurrell et al., 2013) with WACCM model (Marsh et al., 2013), Zambri et al. (2019a) found there was no dynamic circulation response to the eruption that indicates Laki caused a negative NAO in the traditionally defined "DJF" winter. However, the monthly snapshots do indicate a robust negative NAO pattern in later winter and early spring, specifically in February to April 1784. On the other hand, D'Arrigo et al. (2011) argued that internal variability in the form of a concurrent El Niño and negative phase of the North Atlantic Oscillation (NAO), and not the Laki eruption, was responsible for the extremely cold winter of 1783-1784.

(2) Other physical processes

From CMIP5 to CMIP6, there is mounting evidence that a correct representation of the Quasi Biennial Oscillation, extratropical stratospheric dynamics (the polar vortex and sudden stratospheric warmings), and related troposphere-stratosphere coupling, as well as their interplay with ENSO, are important for NAO/NAM timing (Domeisen, 2019; Pausata et al., 2020; Predybaylo et al., 2020; Scaife et al., 2016; Zuo et al., 2021) in spite of underestimated troposphere-stratosphere coupling found in models compared to observations (O'Reilly et al., 2019). The forced response from volcanic eruptions is also dependent on the strength, seasonal timing and location of the eruption but may also depend on the mean climate background state (Zanchettin et al., 2013) and/or the phases of the main modes of decadal variability such as the AMV (Ménégoz et al., 2018). Nevertheless, due to the time limit of the thesis study, we will only briefly discuss these "teleconnection" effects in the relevant discussion part of the thesis.

To summary, it is suggested that a correct understanding and representation of physical mechanism is cardinal in modelling study to gain comprehensive knowledge on climate variability to both tropical and extratropical volcanoes.

2.6 Two volcanism-related CMIP6 sub-projects

To address the above challenges, two model intercomparison projects have grabbed our attention during the thesis preparation. They are PMIP4 and VolMIP. A brief introduction to these two programs is given below.

2.6.1 PMIP4

Table 2.1 summarizes the boundary conditions for the PMIP4[2] Tier 1 *past1000* experiment. Compared to the precedent exercise PMIP3, main progress of PMIP4/CMIP6 consists of the following points:

- Newly added model components, e.g. interactive chemistry and aerosol microphysics, allow more explicit representation of forcing-related processes;
- Models generally achieve higher spatial resolutions to run long-term paleo simulations, which makes it possible to improve the representation of mechanisms controlling regional variability and to alleviate biases in the mean state;

Table 2.1: Summary of boundary conditions for the PMIP4/CMIP6 Tier 1 *past1000* experiment.

Feature	PMIP4 recommendation	Source
Orbital	Time-varying	Berger (1978), Schmidt et al. (2011) : https://wiki.lsce.ipsl.fr/pmip3/doku.php/pmip3:design:lm:final#orbital_forcing
Greenhouse gases CO_2, N_2O, CH_4	Time-varying, Same data set as historical	Meinshausen et al. (2017): http://www.climatecollege.unimelb.edu.au/cmip6 https://esgf- node.llnl.gov/search/input4mips/
Volcanic forcing	Time-varying sulfur injections	Sigl et al. (2015), Toohey and Sigl (2017): https://cera-www.dkrz.de/WDCC/ui/cerasearch/entry?acronym=eVolv2k_v1
Volcanic aerosol optical properties*	EVA module	Toohey et al. (2016): https://pmip4.lsce.ipsl.fr/doku.php/exp_design:lm
Solar irradiance	TSI and SSI time-varying	https://pmip4.lsce.ipsl.fr/doku.php/data:solar_satire
Ozone	Parameterization of solar related variations	
Tropospheric aerosols	Methodology same as PiControl	
Vegetation	Methodology same as PiControl	
Land cover changes	Same data set as historical	Lawrence et al. (2016); Hurtt et al. (2020) LUH2: http://luh.umd.edu/ https://esgf- node.llnl.gov/search/input4mips/

* For models that need aerosols optical depth as forcing. (source: Jungclaus et al., 2017)

[2] For PMIP4, simulations of five different periods have been designed in alinement with CMIP6: the millennium prior to the industrial epoch (CMIP6 name: *past1000*; Jungclaus et al., 2017); the mid-Holocene, 6000 years ago (*midHolocene*; Otto-Bliesner et al., 2017); the Last Glacial Maximum, 21 000 years ago (*lgm*; Kageyama et al., 2017); the Last Interglacial, 127 000 years ago (*lig127k*; Otto-Bliesner et al., 2017); and the mid-Pliocene Warm Period, 3.2 million years ago (*midPliocene-eoi400*; Haywood et al., 2016). The readers are directed to these companion articles for more details.

- Improvements in forcing reconstructions regarding their accuracy and complexity have the potential to improve quality in comparative model-data studies. Especially, the volcanic forcing has evolved based on data of Toohey and Sigl (2017) and reconstruction of Sigl et al. (2015). Models using interactive aerosol module and sulphur dioxide injections in *historical* experiments can directly and consistently use the sulphur dioxide injections in *past1000* experiments. As for models using aerosols radiative properties (for example, our model IPSL-CM6A-LR, see section 2.7), Easy Volcanic Aerosol (EVA) module proposed by Toohey et al. (2016) also allows a better reconstruction of space-time structure of sulfate aerosol evolution.
- More stringer experimental set-ups (e.g. an identical forcing data set) and output data are implemented in the CMIP6 process, provided an improved basis for multi-model studies.
- In addition, the PMIP4 *past1000* experiment is closely related to the process-oriented simulations in another project, VolMIP, which ensure a better interaction and a plate-form to test robustness of volcanic eruption climatic impacts.

With these updates made in PMIP4/CMIP6, we will focus continuously on "*past1000*" experiment (first foci of this thesis, see **Chapter 3**) based on IPSL-CM6A-LR to investigate the model efficiency in simulating the climate impacts of the volcanic eruptions during the last millennium with a clear volcanic stratification. The long transient "*past1000*" experiment helps circumvent the small volcanic samples in observations and serves a good metric to test model robustness of IPSL-CM6A-LR. The uncertainties associated with various aspects of volcanic aerosol forcing (e.g., magnitude, hemispheric symmetry, and eruption season) are also carefully studied using cluster analysis.

2.6.2 VolMIP

As presented before, an important climate response to volcanic eruptions is manifested on NAO. Previous works indicate that the tropical eruptions induce positive NAO during the first volcanic winter. However, debates remain regarding the significance of the response and the relevance of physical mechanisms. In fact, simulating volcanically-forced climate variability is a challenging task for climate models. Uncertainties exist regarding the climatic response to strong volcanic forcing identified in coupled climate simulations of CMIP5 (Driscoll et al., 2012; Santer et al., 2014; Timmreck, 2012; Toohey et al., 2014). Model

differences, forcing inputs, and internal variability can all contribute to the simulation spreading and reduce our confidence on model results.

Under this context, the Model Intercomparison Project on the climatic response to volcanic forcing (VolMIP) – an endorsed contribution to CMIP6 – defines a protocol for idealized volcanic-perturbation experiments to improve comparability of results across different climate models. Among VolMIP's numerous idealized volcanic perturbation experiments, the first set of experiments ("*volc-pinatubo*") focuses on the assessment of uncertainty and inter-model differences in the seasonal-to-interannual climatic response to an idealized 1991 Pinatubo-like eruption, representative of the largest magnitude of volcanic events that occurred during the observational period. The "*volc-pinatubo*" experiment set is another essential part (see **Chapter 4**) of this thesis:

- "*volc-pinatubo*" experiments investigate the role of internal variability for volcanic events which are generally characterized by a rather low signal-to-noise ratio in the terms of global-average surface temperature (Zanchettin, Khodri, et al., 2016). We need to carefully inspect the robustness of the short-term dynamical responses to volcanic forcing, to ensure that good forcing fields are used and that sufficiently large simulation members are performed. It is recommended that "*volc-pinatubo-full*" uses what provided by the CMIP6 stratospheric aerosol dataset (Thomason et al., 2018) for the case of the 1991 Pinatubo eruption, consistent with the CMIP6 historical experiment.
- "*volc-pinatubo-full*" is accompanied with two important sensitivity simulations, i.e. "*volc-pinatubo-strat*" and "*volc-pinatubo-surf*". They don't impose aerosol optical properties as in "*volc-pinatubo-full*". Instead, they use certain outputs from the "*volc-pinatubo-full*" which are purposely designed as external constraints. Specifically, "*volc-pinatubo-surf*" specifies a prescribed perturbation to the shortwave flux to mimic the attenuation of solar radiation by volcanic aerosols, and therefore the cooling of the surface. Similarly, "*volc-pinatubo-strat*" specifies a prescribed perturbation to the total (longwave plus shortwave) radiative heating rates, seeking to mimic the local impact of volcanic aerosol. These experiments can help us elucidate the mechanisms through which volcanic forcing leads to changes in atmospheric dynamics and determine the different contributions to response uncertainties that are due to the direct radiative (i.e., surface cooling) and to the dynamical (i.e., stratospheric warming) response.

It is clear that VolMIP provides us interesting climate simulations for the purpose of this thesis, in particular, to elucidate physical mechanism which operate to transform volcanic radiative forcing to the North Atlantic-Mediterranean sector interannual winter climate variability. This work constitutes the main content of **Chapter 4**.

2.7 Model presentation : IPSL-CM6A-LR

All climate simulations that analyse in this theses were performed with the last version of the Institute Pierre-Simon Laplace (IPSL) coupled model (known as IPSL-CM6A-LR), released by the IPSL Climate Modelling Centre (see https://cmc.ipsl.fr) for CMIP6 (Eyring et al., 2016). The model components and the coupled model itself are described in Boucher et al. (2020) and Hourdin et al. (2020). IPSL-CM6A-LR is a powerful *state-of-the-art* platform for a variety of climate issues, including natural climate variability, past climate and future climate projection. This subsection describes firstly the model configuration and secondly volcanic forcing implementation in IPSL-CM6A-LR for *past1000* experiment and *volc-pinatubo* experiment respectively.

2.7.1 Model configuration

IPSL-CM6A-LR is composed of three components coupled from each other (Fig. 2.12). The atmospheric component is LMDZ version 6 (Hourdin et al., 2020), the oceanic model is NEMO version 3.6 and the land surface model is ORCHIDEE (Krinner et al., 2005) version 2.0. LMDZ is built on 79 layers in the vertical, with its highest level up to 80 km. Its horizontal grid has 144 x 143 points, regularly distributed in longitude and latitude, which makes a nominative resolution of 2.5^{o} x 1.3^{o}. The ocean model is made up of three modules dealing with the ocean physics NEMO-OPA (Madec et al., 2017), the sea-ice dynamics and thermodynamics NEMO-LIM3 (Rousset et al., 2015; Vancoppenolle et al., 2009) and the ocean biogeochemistry NEMO-PISCES (Aumont et al., 2015). It has a good representation of the bathymetry with its 75 levels in the vertical. The land surface component ORCHIDEE was designed to simulate major processes of the land surface physics and terrestrial biophysics relevant for water, energy and carbon fluxes between the land surface and atmosphere. It was directly implemented into LMDZ on the same horizontal grid and at every time step of the physics of the atmospheric model (i.e., 15 minutes). It is however to be noted that the vegetation dynamics and the biogeochemical processes are updated for an interval of 24 hours.

The LMDZ and ORCHIDEE models are coupled at every time step of the physics of the atmospheric model (i.e., 15 minutes) with the exception of the biogeochemical processes and the vegetation dynamics for which the coupling frequency is one day. The coupling between LMDZ and NEMO is now performed with the OASIS3-MCT coupler. Outputs from the IPSL-CM6A-LR model are managed by the XML Input/Output Server (XIOS; Meurdesoif et al., 2016).

Other model components can be activated in IPSL-CM6A-LR. These modules include atmospheric chemistry / aerosol microphysics models such as the INteractions with Chemistry and Aerosols (INCA, Hauglustaine et al., 2014), the REactive Processes Ruling the Ozone BUdget in the Stratosphere (REPROBUS, Marchand et al., 2012), and the Sectional Stratospheric Sulfur Aerosol (S3A, Kleinschmitt et al., 2017) models.

Compared to the IPSL-CM5A-LR, and other CMIP5-class models, IPSL-CM6A-LR is significantly improved in terms of climatology, by reducing overall SST biases and improving the latitudinal position of the subtropical jets. IPSL-CM6A-LR is also slightly more sensitive to CO_2 forcing increase (Boucher et al., 2020) and represents a more robust global temperature response than the previous CMIP5 version consistently with current *state- of-the- art* CMIP6 models (Zelinka et al., 2020). IPSL-CM6A-LR also includes improved conservation of energy and water. Resolutions were increased from 96x96x39 to 144x143x79 for atmosphere and land-surface, and from 2° to 1° for ocean. The tuning phase was longer and more thorough with IPSL-CM6A-LR than with IPSL-CM5B-LR.

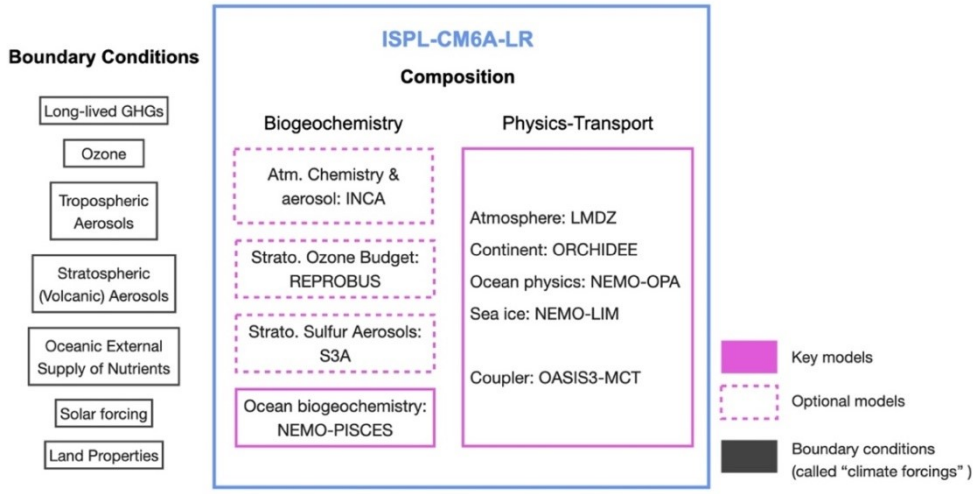

Figure 2.12 : Representation of different components in model IPSL-CM6A-LR (Adapted from Dufresne et al., 2013).

2.7.2 Implementation of volcanic forcing

For the implementation of volcanic forcing in IPSL-CM6A-LR, we use different sources of data provided by the international community from CMIP6 (Eyring et al., 2016). The historical period is from Thomason et al. (2018), including the case of the Pinatubo eruption. The past millennium is from Toohey et al. (2016), Toohey and Sigl (2017). Readers are directed to Lurton et al. (2020) for other forcing implementation in IPSL-CM6A-LR.

Paleo volcanic forcing modelling

After new updates made for PMIP4/CMIP6, the recommended volcanic forcing is the eVolv2k volcanic stratospheric sulfur injection dataset (Toohey and Sigl, 2017) and EVA(2k) stratospheric aerosol optical properties dataset through the use of the EVA forcing generator (Toohey et al., 2016).

Since IPSL-CM6A-LR adopts a *prescribe-aerosol* method for volcanic forcing, the easy volcanic aerosol (EVA) module (Toohey et al., 2016) is applied for paleo volcanic forcing modelling. Through setting the eruption year, month, sulfate injection magnitude and hemispheric ratio in EVA module, stratospheric sulfate mass injected by the volcanic eruption is transferred to mid-visible (550 nm) aerosol optical depth (AOD) and effective radius as volcanic forcing input for model simulations. Volcanic aerosols are represented by monthly mean zonal-mean aerosol optical depths (AOD) that are prescribed with a vertical profile in the stratosphere used in the radiation code of the model. Pinatubo-like eruptions can be also simulated because the construction of EVA relies extensively on observational constraints, especially the observational records of the 1991 Pinatubo eruption. Figure 2.13 demonstrates EVA(2k) volcanic forcing (Toohey et al., 2016) adopted by ISPL-CM6A-LR model for the paleo volcanic forcing modelling during the last millennium (500-1850 CE) in the frame of PMIP4-*past1000*, along with two reconstruction data (Crowley and Unterman, 2013; Gao et al., 2008) as comparisons.

Actually EVA(2k) is closely related to eVolv2k dataset (Toohey and Sigl, 2017), which is reconstructed by linear scaling from the most up-to-date estimates of sulfate deposits in ice published by Sigl et al. (2015). Then EVA module developed by Toohey et al. (2016) arrives to convert the sulfate deposits from eVolv2k to optical property datasets. The resulted optical property dataset is abbreviated as EVA(2k) in the thesis to symbolize the relation between EVA module and eVolv2k. EVA module scaling approach is similar to that of Gao et al. (2008) with the difference that the proportionality links between deposition and AOD peak of Pinatubo vary according to the amplitude of the eruption. Also, a 2/3

exponential scaling between sulfate deposit and AOD have been applies for eruptions larger than Tambora for EVA module. Thus, the AOD remains overestimated for the largest eruptions but to a less extent compared to Gao et al. (2008). In IPSL-CM6, in addition to better horizontal and vertical resolution (144x143x79), there are also improvements in the new radiative code (RRTM) which integrates the flows on the solar spectrum with spectral resolution divided into 6 bands for the shortwave parts and 16 bands for the longwave parts .

The interpolation phase (by streamer) of the optical properties at the spectral resolutions of the model and the various tests (still for Pinatubo) to take into account the interference of aerosols with the solar (visible and near infrared) and the terrestrial infrared radiation made it possible to validate the implementation of volcanic forcing before (EVA) and after 1850 in a coherent way in the model.

Figure 2.14 further illustrates the latitude-time distribution of zonal mean stratospheric aerosol optical depth from EVA(2k) ranging from 500 BCE to 2000 CE. Except those volcanic events with known eruption latitude, the latitudes for Northern, Tropical, Southern volcanic eruptions use default setting of 45°N, 0° and 45°S (Toohey and Sigl, 2017). Since EVA module is based on parameterised 3 boxes, the transport barrier provided by the polar vortex in winter hemisphere is ignored as well as the potential impact of different injection height for sulfate aerosol stratospheric transport. Consistent with Crowley and Unterman (2013), unknown eruptions are assigned an eruption date of 1 January.

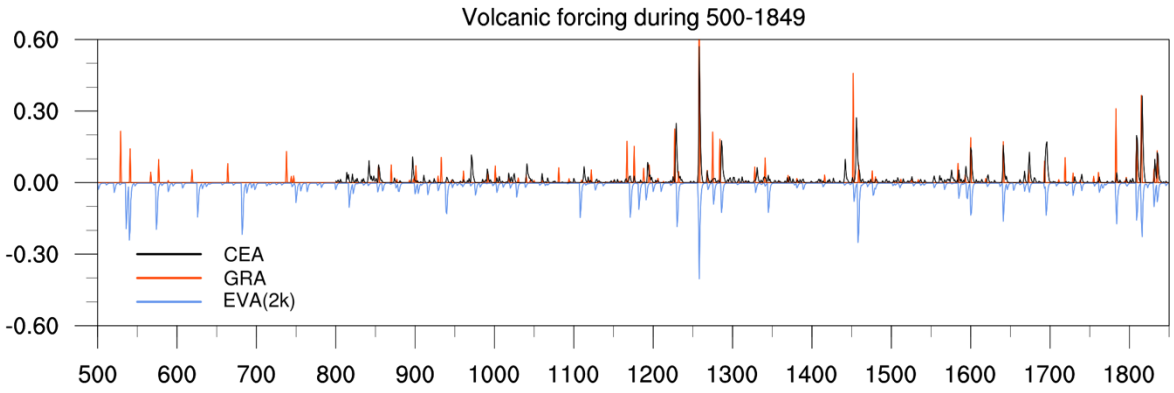

Figure 2.13: Reconstructions of volcanic forcing, 500–1850 CE, shown as global-mean, mid-visible (550 nm) aerosol optical depth (AOD) as annual means time series. Reconstructions include the Gao et al. (2008) (GRA), Crowley and Unterman (2013) (CEA), and PMIP4 recommended forcing, EVA(2k) (Toohey et al., 2016), which is used in IPSL-CM6A-LR model. Note that the AOD in 1258 CE for the GRA reconstruction extends beyond the axis of the plot, with a value of approximately 1.05. AOD for the EVA(2k) reconstruction is shown on the inverted axis in panel for clarity.

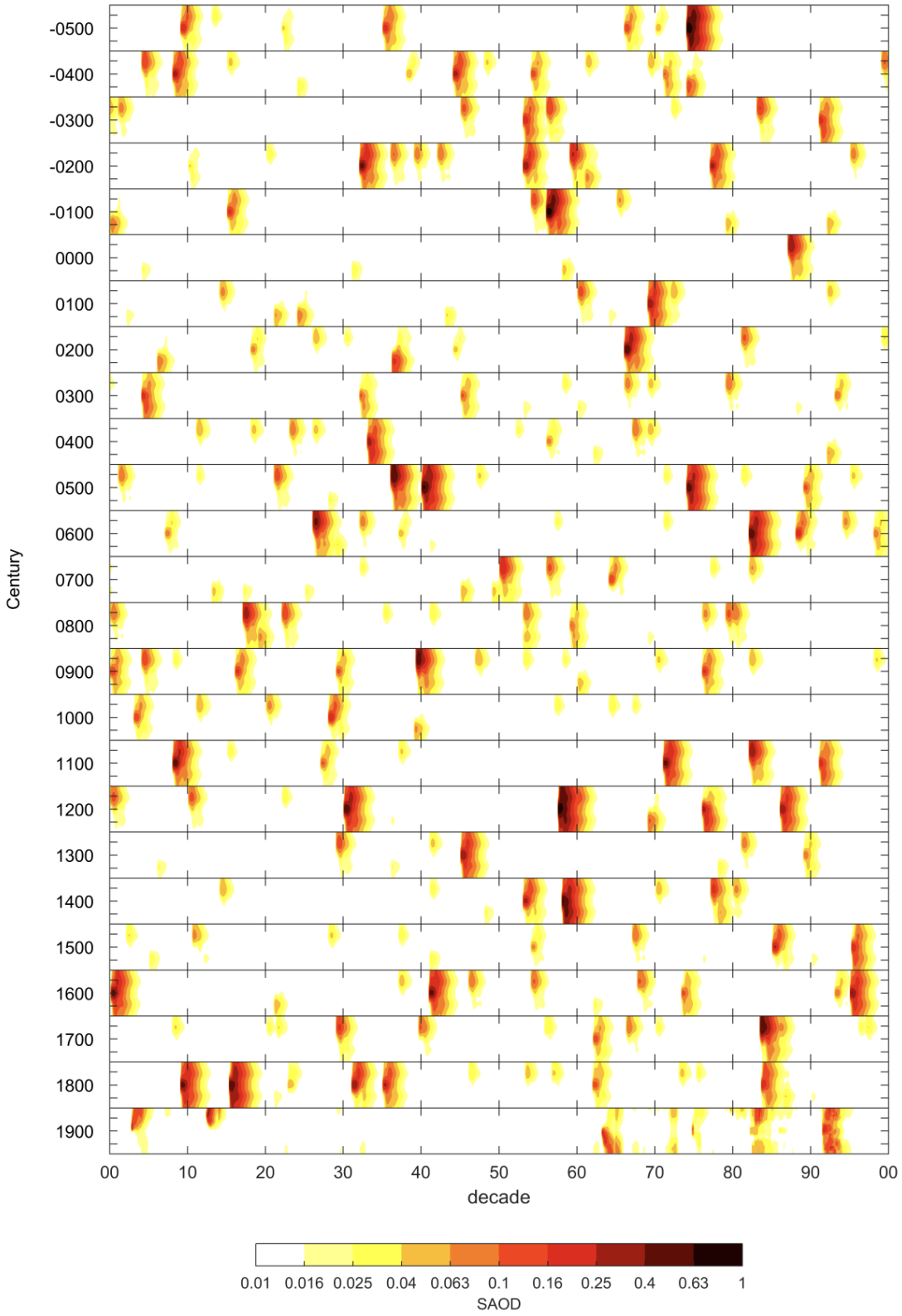

Figure 2.14 : Zonal mean stratospheric aerosol depth as a function of time (x) and latitude (y) for the 500 BCE to 1900 CE period, as reconstructed using the EVA(2k) volcanic stratospheric sulphur injection estimates and the EVA forcing generator. 20th century SAOD values from the CMIP6 historical simulation are appended to extend the SAOD time series to the year 2000. Tick marks on the y-axis of each panel mark 45°S, 0 and 45°N. (source: supplementary information of Toohey and Sigl, 2017)

With these generous volcanic events, I will concentrate on the period 500-1850 CE of *past1000* experiment to study the role of volcanos on climate in the North Atlantic-Mediterranean sector and to carry diagnostics on different sensitivity tests. In particular, the volcanic eruptions will be stratified into different categories based on their eruption latitude (tropical or extratropical), season and strength. By this way, we manage to test the model robustness in simulating a volcanic positive NAO winter and deduce the climate sensitivity to eruptions of different characteristics. The integral study is presented in **Chapter 3**.

Pinatubo volcanic forcing modelling

Having erupted in the Philippines in June 1991, the Pinatubo volcanic eruption represents an ideal historical case to learn mechanism by which volcanism influences the North Atlantic climate.

The eruption injected a considerable amount of sulfur (~ 9Mt, Bluth et al., 1992) into the tropical stratosphere between 22 and 26 km (Read et al., 1993). Like most large volcanic eruptions, Pinatubo certainly injected large dust particles that were quickly removed by gravitational sedimentation. On the other hand, there was no indication in the measurements of an injection of water into the stratosphere. Therefore, only sulfur dioxide (SO_2) injected directly into the stratosphere could globally and permanently disrupt the aerosol layer over several years. SO_2 gas was converted to liquid droplets of sulfuric acid over a period of months, greatly increasing the aerosol load in the stratosphere (McCormick and Veiga, 1992). The volcanic plume remained trapped in the tropics for the first few months after the eruption before spreading across the globe. Sedimentation of volcanic sulfuric acid aerosols to the troposphere has caused a gradual return, over several years, to the background level of stratospheric aerosols (pre-volcanic level) (Russell et al., 1996). The eruption was simulated in IPSL-CM6A-LR by adjusting directly the optical parameters (AOD550, asymmetry factor, single scattering albedo, etc) of atmosphere.

a. Volcanic aerosol optical depth at 550 nm

In order to validate the model, we compared the simulated AOD to instrumental observations during the months following the eruption. The volcanic forcing used for Pinatubo is *Global Space-based Stratospheric Aerosol Climatology* (*GloSSAC*) Version 3 from Thomason et al. (2018). It is a two-dimensional (latitude-height) monthly dataset provided by CMIP6 to be consistent with the volcanic forcing used in the IPSL-CM6A-LR historical CMIP6 experiments (Boucher et al., 2020).

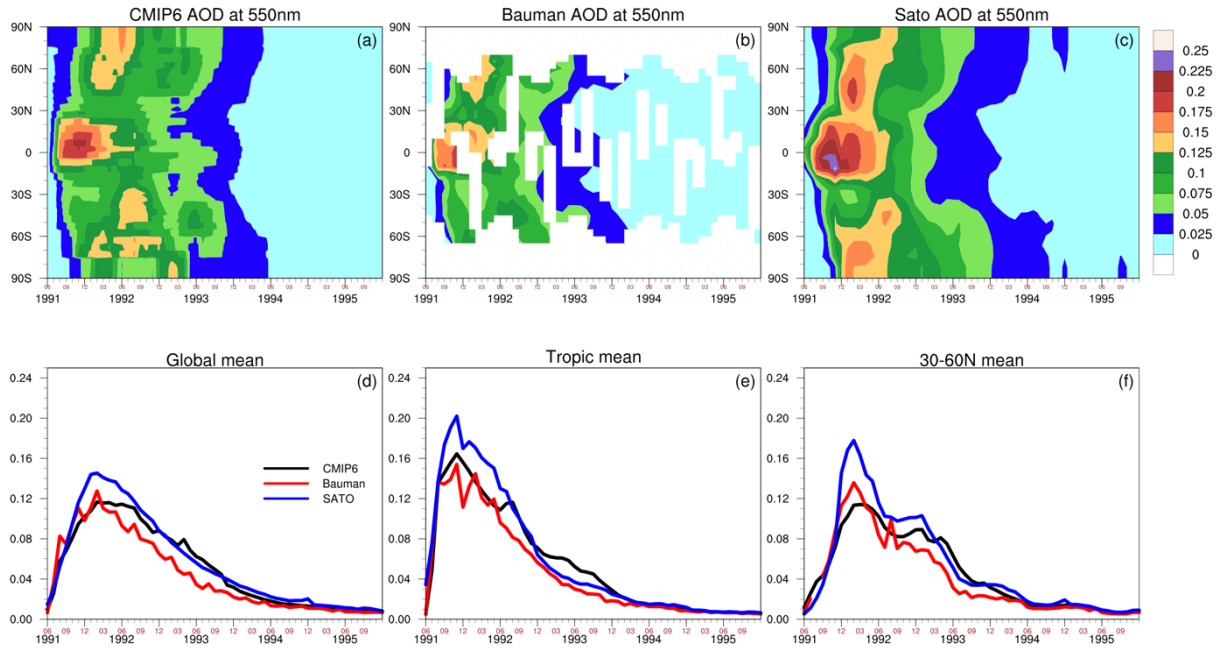

Figure 2.15: Monthly series of the zonal mean (upper panel) and latitudinal band mean (lower panel) of the stratospheric AOD at 0.55 µm observed and simulated over the period 1991-1994 during the Pinatubo eruption. **(a)** Results of the simulation carried out with IPSL-CM6A-lR model using CMIP6 forcing (Thomason et al., 2018). **(b)** AOD derived from the SAGE II-CLAES satellite observation (Bauman et al., 2003) and **(c)** that provided by Sato et al. (1993). And **(d)** global mean, **(e)** tropical mean (15 °S– 15°N), **(f)** Northern Hemisphere middle latitude mean (30 °S– 60°N) for datasets of CMIP6, Bauman et al. (2003) and Sato et al. (1993).

GloSSAC focuses on the Stratospheric Aerosol andGas Experiment (SAGE) series of instruments through 1984 to mid-2005, and on the Optical Spectrograph and InfraRed Imager System (OSIRIS; Rieger et al., 2015) and the Cloud-Aerosol Lidar and Infrared Pathfinder Satellite Observation (CALIPSO; Vernier et al., 2011) data thereafter. They also use data from other space instruments and from ground-based, air, and balloon borne instruments to fill in key gaps in the data set. Combined with statistical methods (e.g. interpolation for empty bins, latitude-equivalent latitude conversion process for higher latitudes), *GloSSAC* ends up to be a global and gap-free datasets on aerosol extinction coefficient at 525 nm and 1020 nm.

Figure 2.15 shows the zonal mean of the stratospheric AOD at 0.55 µm (wavelength important for the impact on the solar radiation in the visible and therefore the radiative forcing) simulated for Pinatubo modelling in IPSL-CM6A-LR model and compared to two observational datasets (SAGE-II-CLAES satellite observation, Bauman et al., 2003; and that provided by Sato et al., 1993). We use the same configuration of the IPSL-CM6A-LR model as used for the historical simulation of CMIP6, except that the anthropogenic emissions are fixed at the 1900 CE level (Lurton et al., 2020). All external forcings are kept to pre-

industrial values except the volcanic aerosol extinction coefficient, single scattering albedo, and asymmetry parameter due to the Pinatubo eruption.

Broadly, the CMIP6 AOD dataset has a good consistence with observational data in spatial distribution and temporal evolution. It also fills the gaps presented in SAGE-II data (Fig. 2.15a&b). Nevertheless, in our simulations, a tropical AOD peak (~0.22) is reached early and overestimated (Fig. 2.15a), when compared with SAGE-II satellite observations. This difference has multiple sources such as for example the failure to take into account feedbacks on the size distribution and life cycle of aerosols. Heated by the surface-emitted infrared radiation, the aerosol layer tends to warm the lower tropical stratosphere by about 3 °K in the first months after the eruption. This heating can potentially amplify the tropical upwelling and horizontal transport, and ultimately promote faster export of freshly formed aerosols to the extra tropics. The maximum simulated AOD nonetheless remains included in the observation error bar. But to notice (Fig. 2.15c), both CMIP6 and SAGE-II datasets have relatively lower AOD values, compared to the data of Sato et al. (1993). Three datasets all peak around the same month for global, tropical (15°S– 15°N) or NH middle latitude (30°S– 60°N) mean (Fig. 2.15d-f). The NH middle latitude (30°S– 60°N) mean peaks at February 1994,
four months later than the peak of tropical mean. This reveals the propagation of volcanic aerosols from tropical areas to high latitudes after the Pinatubo eruption.

b. Radiative forcing

Figure 2.16 shows the spatial and temporal evolution of the zonally averaged volcanic effective radiative forcing (ERF) after the Pinatubo eruption, as implemented in IPSL-CM6A-LR, and calculated through its radiative transfer scheme.

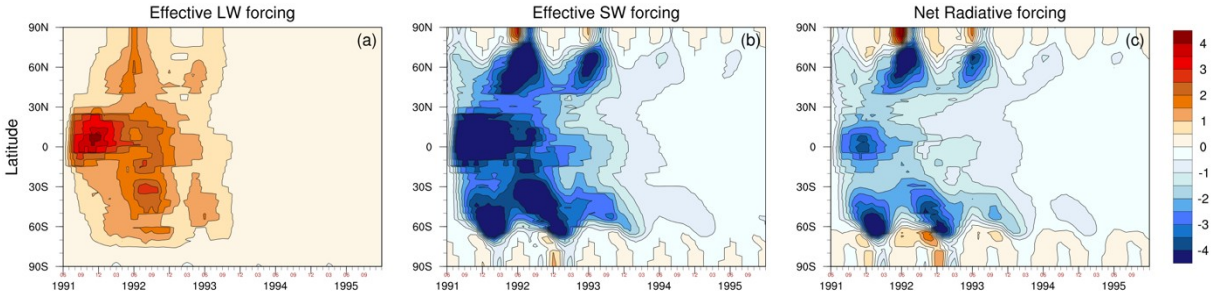

Figure 2.16: All-sky top of atmosphere (TOA) radiative forcings (W/m²) due to Pinatubo volcanic aerosol from June 1991 through December 1995. Shown are **(a)** TOA longwave forcing and **(b)** TOA shortwave forcing, as well as the **(c)** net radiative forcing.

The longwave (LW) forcing from the volcanic aerosols shows a similar spatial and temporal pattern (Figure 2.16a) with the aerosol optical depth in Fig 2.16a. The maximum increase of 4.4 W/m² in the outgoing LW radiation occurs in the tropics in November and persists into December due to the higher temperature in the tropics. Nevertheless, this LW seasonality is far much smaller than that of SW; because of SW's stronger dependence on the seasonality of incoming solar radiation. The LW forcing at high latitudes starts in the winter months. In the north of 60°N, LW anomalies persist into May and June 1992.

The SW radiation anomalies in Fig. 2.16b indicate a maximum reduction of insolation (around 8 W/m²), approximately 5 months after the eruption onset and lasting 2 months in the tropics, while the maximum SW reduction of around 8.7 W/m² occurs in June/July 1992 poleward of 60°N. The spatial location and timing of this maximum are consistent with the latitude of the eruption (5°N) and the timescale (weeks) for conversion of SO_2 to sulfate aerosols, the dominant driver of radiative effects from volcanic eruptions (Kravitz and Robock, 2011; Robock, 2000). In addition, the maximum SW anomaly coincides with the maximum aerosol optical depth perturbation in the simulations (Fig. 2.16a). The radiative effects are strongly dependent on both time and latitude, with the SW anomalies as the major component.

The anomalies near the equator are much stronger than those at high latitudes. At midlatitudes, the decrease in SW forcing is more gradual, and the steepest temporal gradient is seen in the tropics, with anomalies staying below –4 W/m² till September 1992. Since sulfate aerosols can be transported to higher latitudes through the Brewer-Dobson circulation, the SW peaks at high latitudes can be seen several months after the tropics. A weaker amplitude of northern high latitude SW anomaly peak compared to the tropics is due to a lack of insolation at high latitudes during boreal winter months.

Figure 2.16c shows the net ERF due to the volcanic eruption, which is simply the linear combination of Fig. 2.16a and 2.16b. At high latitudes, large negative forcing occurs at later time for the reasons discussed above. Anomalies at midlatitudes follow a similar pattern, but with a more gradual change. Compared to the negative forcing from mid-to-high latitude, a positive anomaly is simulated at the North Pole, which helps exclude the radiative-forced nature of the "cooler pole", and tends to support a more "dynamic" explanation under this context.

In conclusion, the model reproduces relatively well the main characteristics of aerosol distribution, transport and post-eruption radiative forcing of Pinatubo.

To explore and attribute the relative influences of the volcanically-induced solar (shortwave and near-infrared) and longwave fluxes perturbations on climate following Pinatubo, three sets of large ensemble experiments (N=25) are run with a double call to the radiative code with and without volcanic forcing. The *volc-pinatubo-full*, *volc-pinatubo-strat* and *volc-pinatubo-surf* experiments are respectively designed to represent all interferences of volcanic aerosol with the radiative fluxes (*volc-pinatubo-full*), only the volcanic aerosol perturbations to the total (longwave and near-infrared) radiative heating rates (*volc-pinatubo-strat*), or only perturbations to the surface shortwave flux (*volc-pinatubo-surf*).

The integral study is presented in **Chapter 4** in the form of submitting scientific publication.

Chapter 3

Sensitivity of climate variability to volcanic eruption conditions in *past1000*

Contents

3.1 Preamble

Large volcanic eruptions strongly influence the climate, with important social and economic consequences (Robock, 2000; Stommel and Stommel, 1983; Stothers, 2001). At the same time, debate remains regarding the significance of the volcanic related positive NAO winters, as well as the degree to which they depend on the characteristics of the eruption. Understanding these factors is crucial for assessing the potential risks associated with future large eruptions.

The instrumental observations make it possible to document climate variability over a relatively short period. Volcanic events during the instrumental periods are, however, few and of limited magnitude, and their associated dynamical response is very noisy (Hegerl et al., 2011) that modelling analysis is indispensable. In this chapter, I carry out model investigation on the PMIP4 *past1000* simulation experiment using IPSL-CM6A-LR, which in other hand describes the climatic responses to volcanic forcing in long (more than 1000 years) transient pre-industrial simulations.

By tackling the uncertainties evolved from the reconstruction of past volcanic forcing, initial conditions of eruptions (latitude, season), strength of volcanic forcing and comparing eventually the climate response differences, *past1000* experiment will aid us to diagnose the interactions between natural forcing factors (e.g. volcanic forcing) and climate variability during the last millennium. In this chapter, the study is focused on interannual climate influences of different volcanic eruption types (regarding eruption season/latitude/strength) in *past1000* experiment.

One of the approaches used consists in Superposed Epoch Analysis (SEA, Chree, 1913, 1914), or compositing, via carefully and logically sorting eruptions into different categories and comparing mean climate response of each category. Another statistical tool used is the Mont-Carlo Bootstrapping method (Efron and Tibshirani, 1994) by which I resample the original sample data and yield a "pseudo-sample" data. From this "pseudo-sample" data's probability distribution function (PDF) we could estimate the statistical significance of a signal. Current knowledge in the field of climate sciences, statistical methods as well as the increase in computing power make the robustness testing of volcanic signal possible in millennial climate simulation.

This chapter is organised as follows. Section 3.2 gives information about the data and methods. Section 3.3 describes the composite results of volcanic eruptions in *past1000*. Section 3.4 presents the time series of NAO and polar night jet for different eruption types.

Section 3.5 further explores the model sensitivity to eruption types regarding the post-eruption winter climate. Results are discussed in section 3.6 along with concluding.

3.2 Data and methods

3.2.1 Experimental protocol

The *past1000* experiment simulated by IPSL-CM6A-LR consists of three runs which we designate as r1, r2, and r4 respectively. Each run ranges from 500 CE to 1849 CE and contains a tuning period called "pre-mil" from 500 CE to 849 CE, and a millennium part named "pmil" covering 850 CE to 1849 CE.

For simulation r1, its pre-mil departs from a relatively low AMOC state which then increases afterwards. All forcings vary through time except the vegetation is kept constant and fixed at its state of 850 CE. Its pmil also consists of varying forcings except vegetation keep same as year 850 CE. For simulation r2, its AMOC begins from a rather high state and then declines. The other forcing setting is the same as r1, including the same vegetation configuration. Simulation r4, shares the same pre-mil configuration as r1, whilst its pmil part sees all forcings, including vegetation, varying with time.

Since the objective is to study climate variability to volcano eruptions, we will consider r1, r2 and r4 together as members of one ensemble group. Consequently, the volcanic events will be trebled. As has been introduced in section 2.6.2, the EVA module proposed by Toohey et al. (2016b) and the EVA(2k) volcanic forcing reconstruction (Toohey and Sigl, 2017) are used in IPSL-CM6A-LR to simulate the space-time structure of sulfate aerosol evolution at monthly resolution. There is also information in the hemispheric distribution and eruption dates in the EVA(2k), which permits a correct superposed epoch analysis.

Besides the *past1000* experiments, the CMIP6-DECK « piControl » (i.e., preindustrial control, from 1850 to 3049) simulation describing unperturbed preindustrial climate conditions (Eyring et al., 2016) is also used to help estimate the statistical significance.

3.2.2 Anomalies and indices

Anomalies

In this chapter, we are interested in impacts of volcanic eruptions and the associated climate anomalies at interannual time scale. We need firstly to appropriately define the climatology and anomalies. To efficiently eliminate or reduce long-term trend or low-frequency variability, we adopt a strategy of running climatology to deduce the relevant

anomalies. That is, we apply a 30-year (360 months) running window for each individual year to establish its climatology (for instance, the periods 500~529, 501~530, …, 1819~1848). The running window always precedes the actual year, except for the 30 first years at the beginning of the time series where the climatology is just established from these 30 years. Once the climatology is defined, we can obtain anomalies as a deviation from the climatology. We call hereafter such anomalies "30yr running anomalies". This procedure is individually applied to r1, r2, r4 and piControl.

The method of 30yr running anomaly has advantages over another method which deduces the anomaly for each time step with a single climatology defined with the whole

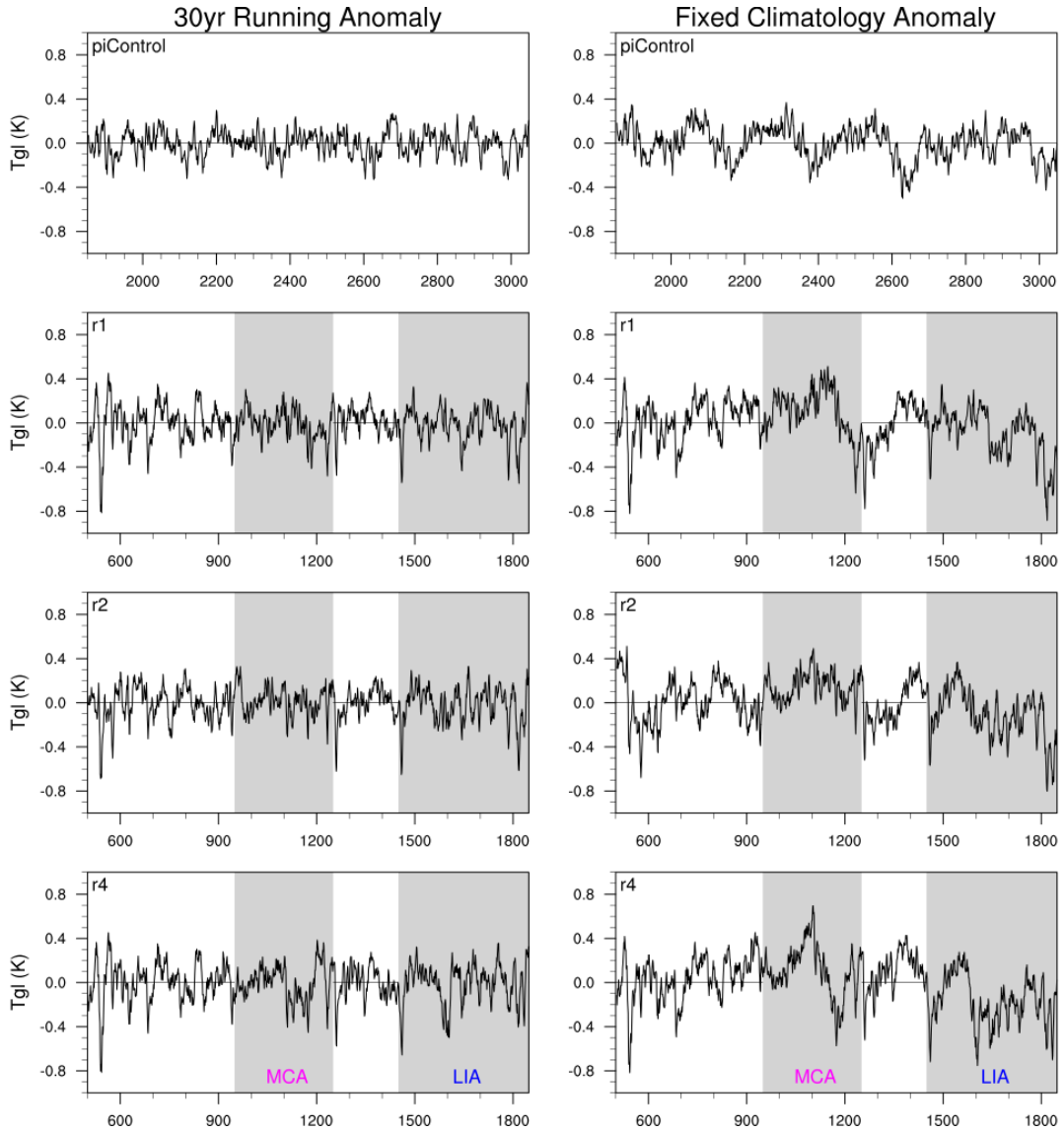

Figure 3.1: Annual global mean temperature time series calculated from 30yr running anomaly method (left panel) and fixed-climatology anomaly method (right panel). From up to bottom is piControl, r1, r2, r4. For display purpose, the time series are showing after taking 5-yr running mean.

period (500~1849). The latter, which we call "fixed climatology anomaly", can hardly separate the volcanic signal from other low-frequency variabilities. For example, Fig. 3.1 illustrates the global average temperature (Tgl) anomalies in piControl and in the three *past1000* runs with the two methods. We can easily observe the "fixed climatology anomaly" in the right panel has a warming tendency during MCA (950~1250 CE) and a cooling trend during LIA (from 1450) for *past1000* runs. While "30yr running anomaly" almost vacillate around 0 which makes a good analogue to study the volcanic factor in interannual climate variability.

For our study, the 30yr running anomalies are calculated for monthly sea level pressure, air temperature, precipitation, wind and geopotential height. And finally we calculate all winter (December-January-February) means and concatenate them together for each run. Consequently, we have anomaly matrix for each climate variable lasting Time=1350 for each *past1000* run. While anomaly matrix has shorter time dimension (Time=1200) for piControl.

AOD550 indices

Locating and classifying volcanic eruptions into proper groups is a core step to study NAO and climate anomalies over the North Atlantic-Mediterranean sector in response to volcanic eruptions which happen in various latitudes and seasons. We adopted the zonal mean of the stratospheric aerosol optical depth at 550 nm (wave-length important for the impact on the solar radiation in the visible and therefore the radiative forcing) to help classify volcanic events. Even though the EVA(2k) provides us AOD550 with monthly resolution, the work is still cumbersome if we directly loop over the latitude-time matrix of AOD550 (which will be in dimension $nlat \times nyr \times nmonth = 143 \times 1350 \times 12$). In order to be more efficient, three indices are calculated based on zonal mean AOD550:

i) AOD550_3060n : average of zonal mean AOD550 on 30°~60°N latitude band;

ii) AOD550_15sn : average of zonal mean AOD550 on 15°S~15°N latitude band;

iii) AOD550_3060s : average of zonal mean AOD550 on 30°~60°S latitude band.

Both monthly and annual mean of these three indices are used in the volcanism categorization.

NAO and PNJ

The two-box NAO index, based on Stephenson et al. (2006), is applied to winter sea level pressure (SLP) of the piControl, r1, r2 and r4 simulations. The NAO index is the difference of mean SLP 30yr-running anomalies between the two boxes covering the

subtropical Mid-Atlantic and southern Europe (90°W-60°E, 20°N-55°N) and the North Atlantic-Northern Europe (90°W-60°E, 55°N-90°N) respectively. It is interesting to note that the NAO variability resembles a white noise in statistical view and it does not show clear periodicity (unlike El Niño phenomena which takes place every a few years). We can have a glimpse at NAO temporal evolution in left panel of Fig. 3.2 showing time series after 5-yr running average filtering.

To indicate the strengthen of polar vortex, we define an index PNJ which is the zonal mean zonal wind anomalies (Polar Night Jet anomalies) at 50 hPa level and 65°N in winters (DJF). The temporal evolution of PNJ is demonstrated in right panel of Fig. 3.2.

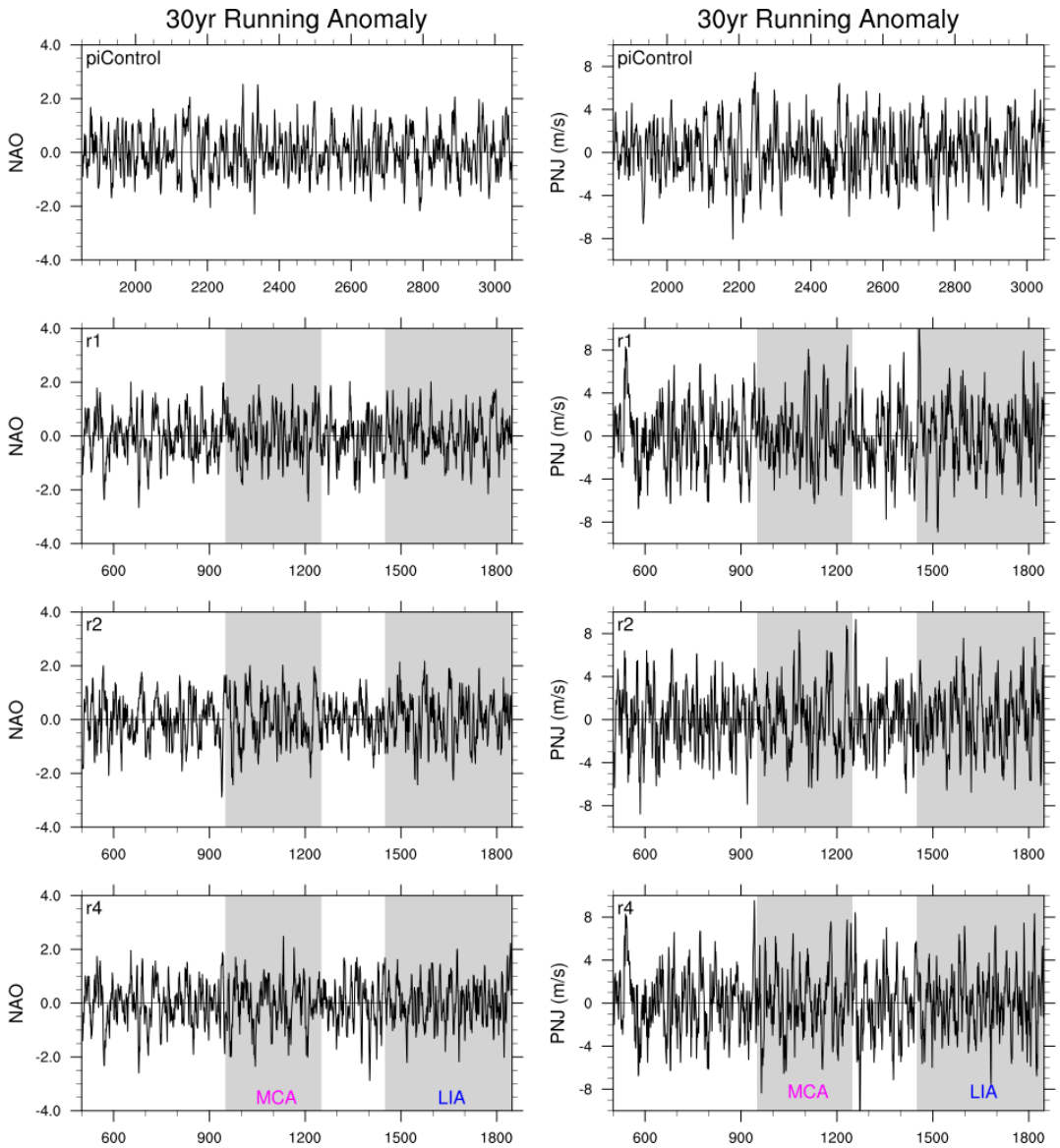

Figure 3.2: Annual NAO (left panel) and PNJ right panel) indices time series calculated from 30yr running anomaly (From up to bottom is piControl, r1, r2, r4. For display purpose, the time series are shown with a 5-yr running mean operation applied.

3.2.3 Composite analysis

Composite analysis is also sometimes called SEA when applied to time series. There are three factors that need to be taken into account in the clustering of volcanic eruptions. The first one is the latitude of eruption. Sulfate aerosols from NH eruptions are mostly constrained in the NH and barely transported to the SH. Similarily SH volcanoes generally do not contribute much to NH aerosol concentration. The equatorial VEs have their aerosols maximum near the equator and decaying poleward quickly. In the EVA(2k) dataset, except volcanic events with precise eruption latitudes, most events are labelled of 45°N, 0° and 45°S. This allows us to easily divide the volcanic eruptions into Northern, Equatorial or Southern events by using the aforementioned three AOD550 indices.

The second factor is the eruption season. The observed AOD550 after Pinatubo shows clear influence of the seasonal cycle of stratospheric transport, with maximum extratropical AOD found in the winter and spring seasons of each hemisphere, qualitatively consistent with the seasonal cycle of the Brewer–Dobson circulation which maximizes in the winter months (Holton et al., 1995). Liu et al. (2016) also reported the aerosol distributions vary significantly between seasonal ensembles for equatorial eruptions. For January and April eruptions, aerosol loading peaks more rapidly in the high northern latitudes relative to the high southern latitudes, whereas the reverse is true for July and October eruptions. The overall radiative forcing is likewise latitudinally dependent based on season, although its behaviour is not identical to the aerosol loading itself, due to modulations of the incident solar radiation during different portions of the seasonal cycle. Considering the fact that aerosol transport is seasonal dependent and that eruptions in EVA(2k) is mostly in January (EVA module default setting for unknown eruptions), we will further put eruption season (winter or other season) into the clustering criteria.

The third factor would be the magnitude of volcanic eruption which we would specify in section 3.3.

After clustering, the volcanic series in same composite are stacked according to Superposed Epoch Analysis (SEA) (Chree, 1912, 1913). This procedure is repeated for each individual ensemble run of *past1000* and the resulted mean signal of each composite will be used in estimating the volcanic impact.

3.2.4 Bootstrapping method

To estimate the statistical significance of the volcanic composite signal, we bootstrap the volcanic-free piControl anomaly (or indices) series (section 3.4&3.5). Bootstrapping is a

method of resampling with replacement, by using the original sample data (Efron and Tibshirani, 1994). This method will produce a pseudo-sample data from which the distribution can be approximated and the statistics of the distribution can be calculated. For example, if the number of volcanic events is N in a certain volcanic cluster, the total period (1200 years) of piControl run is used to select N winter years randomly 10000 times and calculate the N-sample average each time. By using the method of bootstrapping, the probability distribution functions (PDFs) are calculated for anomalies or indices of piControl run. If the volcanic composite average signal lays exceeding 5th–95th percentiles confidence interval (c.i) of the piControl PDFs, we would say the signal is significant at 95% c.i.

3.3 Volcanic eruption categories

3.3.1 Volcanic eruption samples

We firstly classify the volcanoes into three types based on their eruption location, because aerosols from different volcanoes have distinctive meridional distributions. The first type is the NH volcanoes. Aerosols associated with this type have maximum column density in the NH and are barely transported to the SH. As for the SH volcanoes, on the other hand, the aerosols are mostly constrained in the SH and do not contribute much to the NH aerosol concentration. The last type is the equatorial volcanoes and their aerosols have maximum near the equator and decay poleward quickly.

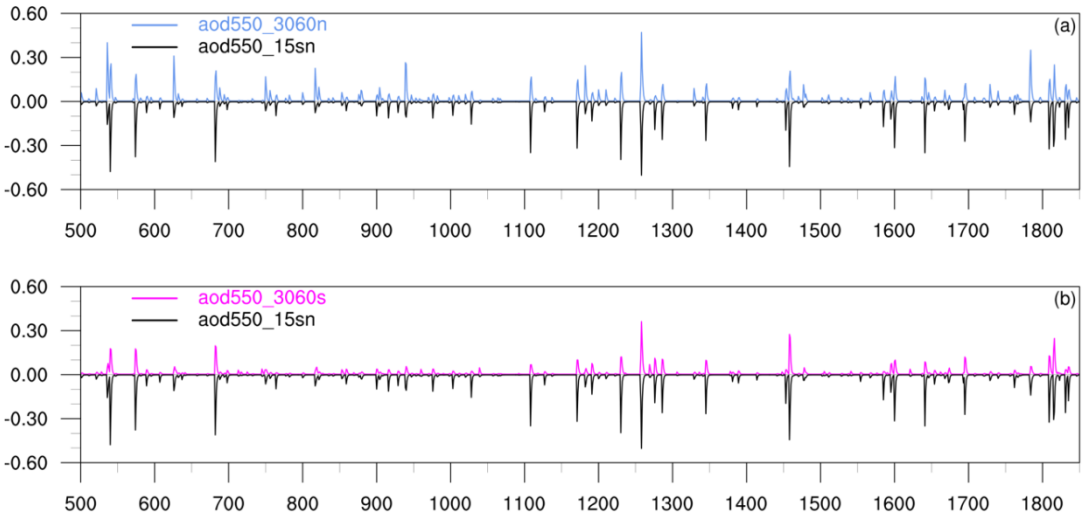

Figure 3.3: Volcanic aerosol forcing for the years 500–1849 CE. **(a)** Annual-mean of AOD550_3060n, blue lines. **(b)** Annual-mean of AOD550_3060s, magenta lines. Index AOD550_15sn is shown in inverted axis in both panels for clarity.

Figure 3.3 shows annual times series of the three AOD550 indices over the period 500-1849. By comparing their strength, we can locate a "NH event" when AOD550_3060n is the biggest among the three indices, a "SH event" when AOD550_3060s is the largest, and an "equatorial event" when ADO55015sn is bigger than both AOD550_3060n and AOD550_3060s. Also only eruptions that have limited or no interference with other eruptions are selected, that's why we will not choose eruption if during five years before or 2 years after its eruption another eruption happens.

Based on this classification, we find 108 eruptions during 500–1849 AD, including 57 NH, 35 equatorial and 16 SH volcanic eruptions with AOD550 value bigger than 0.06. Figure 3.4 left panel checks the aerosol space distribution in the peak year for each AOD550 index, which helps us further validate the eruption hemisphere of volcano. Figure 3.4 right panel displays the volcanic aerosols evolution before and after each eruption in time, which will help us not only figure out eruption month but also delete events too close. By this way two eruptions happened in the same year (853 CE) are excluded (green lines in upper and lower panel of Fig. 3.4), another tropical eruption (in 1693 CE) too close to another eruption is also erased from volcanic samples (green line in middle panel of Fig. 3.4).

Each of the volcanic aerosols injected into the lower stratosphere by large eruptions only lasts 1–2 years and decays quickly thereafter (except July 1257 Samalas, the biggest tropical eruption with its max monthly AOD550_15sn around 0.725). Before the eruptions, the ADO550 is near zero (since a non-zero background stratospheric aerosol forcing is parameterized within EVA by specifying a constant SO_2 injection value ~0.2 Tg/yr). Afterwards, it increases quickly and reaches its maximum at the fourth or fifth month. After the peaks, the aerosol concentration decays quickly, which has only half of the original amplitude in the second year and nearly recovers to the background state without new volcanoes in the third year following each eruption. Although volcanic aerosols are detectable after two years in many cases, in the data set of EVA(2k), the aerosols of each eruption only stay in the stratosphere for about two years.

These 108 volcanic events (57 NH, 35 EQ, 16 SH) will be further divided into winter (DJF) and other season eruptions based on its beginning time. For winter eruptions, we will analyse their in-phase winters, the first and second winters after eruption. While for other season eruptions which do not have in-phase winter, we directly look at their first and second winters. All SH eruptions are very small with AOD550_3060s less than 0.1 that we do not consider SH events into the sample storage. The dividing results are shown in Table 3.1:

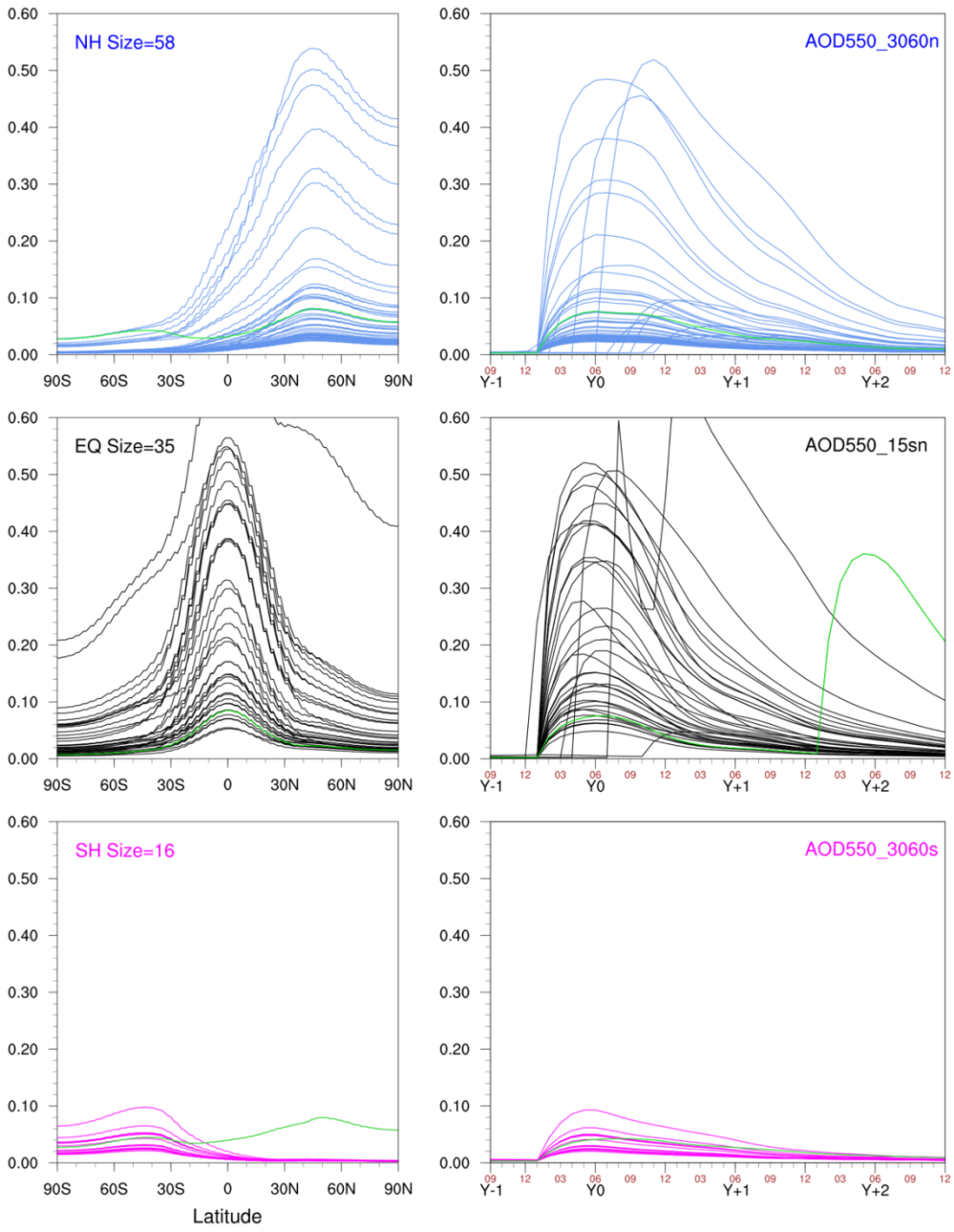

Figure 3.4: Meridional distribution of zonally-averaged, peak month, three AOD550 indices (left panel) and monthly time series of three AOD550 indices and after the eruptions for 108 eruption samples (right panel). The blue, black and magenta curves denote respectively AOD550_3060n for NH eruptions, AOD550_15sn for equatorial eruptions, and AOD550_3060s for SH eruptions. Note that the AOD550_15sn in 1257 CE extends beyond the axis of the plot, with a value of approximately 0.725.

Table 3.1: Summary of volcanic samples after dividing according to eruption season and latitudes.

Latitude	Total Number	Winter Type	Other Season Type
NH	57	52	5
EQ	35	31	4
SH	16	16	-

3.3.2 Scatter plot of PNJ vs eruption strengths

Nevertheless, the 108 volcanic events would not all be used in the cluster analysis.

Firstly we are wondering if there is a "linearity relationship" existing such that stronger eruptions would force a stronger polar night jet and influence NH climate anomalies more easily. Therefore, we take out the PNJ indices for all winter eruptions' in-phase winter and first winter, and for other season eruptions' first winter for r1, r2 and r4. Then the PNJ are plotted versus the eruption strengths (i.e. peak AOD550_3060n for NH events, peak AOD550_15sn for EQ events, and peak AOD550_3060s). The scatter plots (Fig. 3.5) may serve as sensitivity experiments to test the linearity for the PNJ versus the eruption strength.

As shown in Fig. 3.5a, when mixing all events together, it is hard to analyse the linearity between PNJ and AOD550 (R^2=0.21).

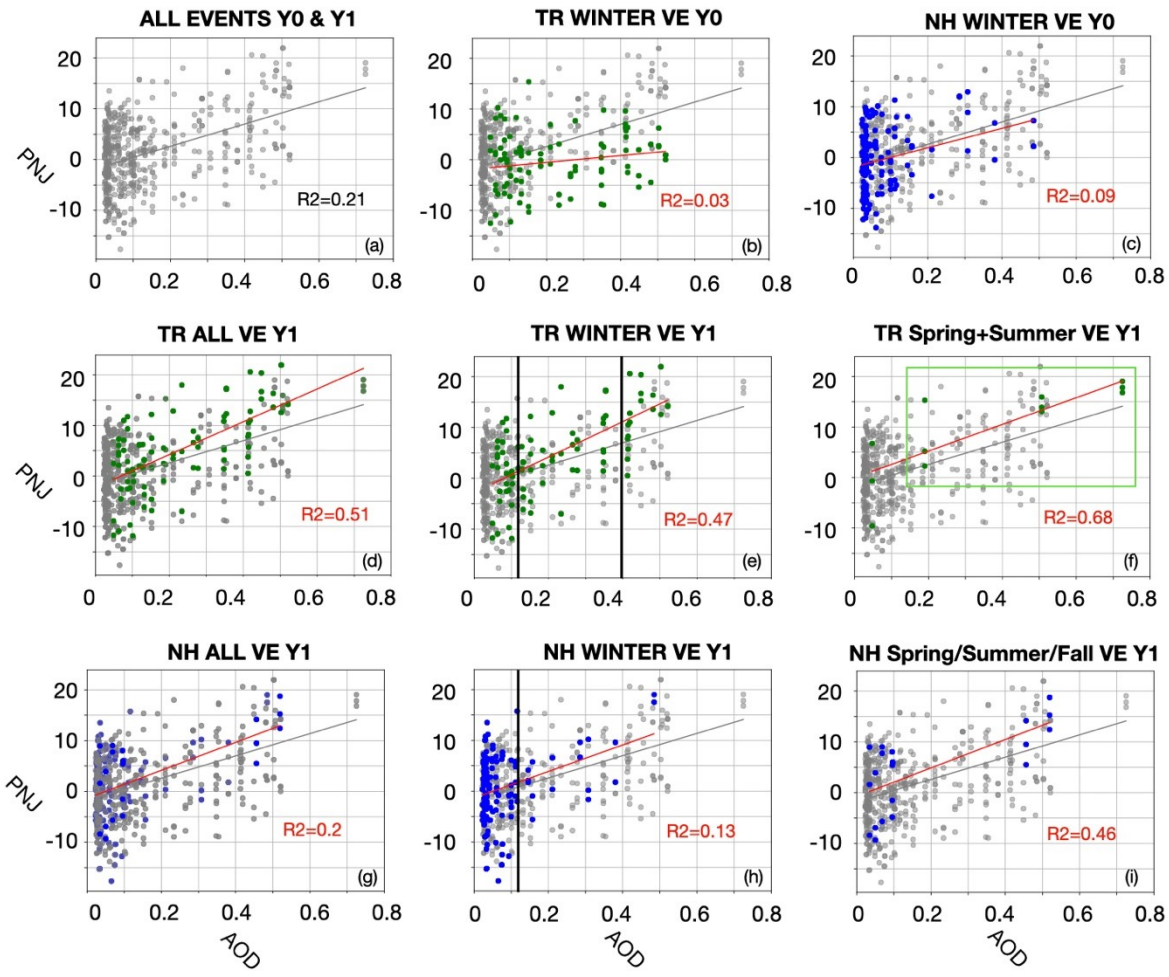

Figure 3.5: Scatter plot of PNJ (unit: m/s) versus max AOD550 for different volcanic eruption type. Blue and green dots designate respectively tropical or NH extra-tropical events. Events not in the specific group are displayed in grey dots as background. Numbers inside each plot indicate the R^2 coefficient of the regression line of each type (in red for specific group, in grey for all events).

When taking out the in-phase winter for tropical and extra-tropical NH events (Fig. 3.5b&c), there is still no linear relationship between PNJ and eruption strength during Y0 (small regression coefficient R^2).

For the total 35 tropical volcanic events, we have 105 PNJ data for the first winter. As shown in Fig. 3.5d, there is a better linearity with R^2=0.51. Even when we split the tropical eruptions into winter ones (Fig. 3.5e) and spring-summer ones (Fig. 3.5f), there are better linear relationships between PNJ and AOD550_15sn max. It is concluded that a stronger polar vortex will be detected in the first winter following a summer or a winter tropical eruption, with polar night jet responses amplitudes that are linearly related to the eruption strength.

For the 57 NH volcanic events, we also have triple size of PNJ data (from r1, r2, r4 together) that can be used to make the scatter plot and regression line. However, non-linear relationship is found for all NH events (Fig. 3.5g) and winter NH events (Fig. 3.5h) during the first winter after eruption. While for the 5 NH other season volcanic events, we have higher linearity (Fig. 3.5i). Nevertheless we do not consider this type due to its sampling issues (either too high or too small).

From what described above, we add a supplementary criteria to select our volcanic events for a better signal-to-noise ratio. It is the strength of eruption. We use 0.11 as the threshold of selection for NH extra-tropical and tropical winter eruptions. The resulted two groups (NHw and EQw) will be used to test the sensitivity to eruption latitude. And we use 0.4 as threshold for massive EQ winter eruptions. The resulted group EQmega will be compared with EQw to test the sensitivity to eruption strength. The 3 large spring-summer EQ volcanic events (inside the green box of Fig. 3.5f) are taken as one category EQe. This group will be used to test the sensitivity to eruption season. As a result, we set up the 4 volcanic categories which are described in next subsection.

3.3.3 Volcanic clusters

Table 3.2 summarizes the final volcanic categories which will be used in clustering analysis and signal significance test. Figure 3.6 and 3.7 display the latitude-time cross section (Hovmöller diagram) of zonal-mean AOD550 for selected NH events and EQ events respectively. Figure 3.8 highlights the selected volcanic events in the whole period (500-1849). We end up with 10 NH winter eruptions with their peak AOD550_3060n bigger than 0.11, 21 EQ winter eruptions with peak AOD550_15sn bigger than 0.11, 7 mega EQ winter eruptions with peak AOD550_15sn bigger than 0.4, and 3 EQ spring-summer eruptions.

Taking three runs of *past1000* experiment as ensemble, we finally will have each cluster size being tripled (i.e., n=Nx3). The tripled size number is parameterized in the bootstrapping process of piControl's 1200 years. That means selecting n=30, 63, 21, 9 winter years randomly a 10000 times for NHw, EQw, EQmega, EQe cluster respectively to create the PDFs of noise.

Table 3.2: Summary of final volcanic categories.

Cluster	Feature			Size N	Volcanic events Begin Year/Month (peak AOD550)		
	Latitude	Season	Strength				
NHw	NH	winter	> 0.11	10	521/1(0.111)	536/1(0.485)	626/1(0.38)
					688/1(0.116)	750/1(0.21)	817/1(0.285)
					1182/1(0.3)	1329/1(0.111)	1477/2(0.157)
					1729/1(0.146)		
EQw	Equator	winter	> 0.11	21	574/1(0.48)	682/1(0.52)	764/1(0.13)
					900/1(0.132)	916/1(0.15)	976/1(0.15)
EQmega *	Equator	winter	> 0.4	7	1003/1(0.13)	1028/1(0.21)	1108/1(0.45)
					1171/1(0.41)	1191/1(0.18)	1230/1(0.50)
					1276/1(0.28)	1286/1(0.35)	1345/1(0.354)
					1453/1(0.265)	1585/1(0.234)	1640/12(0.41)
					1762/2(0.12)	1809/1(0.42)	1831/1(0.35)
EQe	Equator	spring-summer	> 0.11	3	1257/7(0.725)	1595/3(0.19)	1816/4(0.51)

* EQmega volcanic events are listed in blue letters inside the EQw volcanic events box.

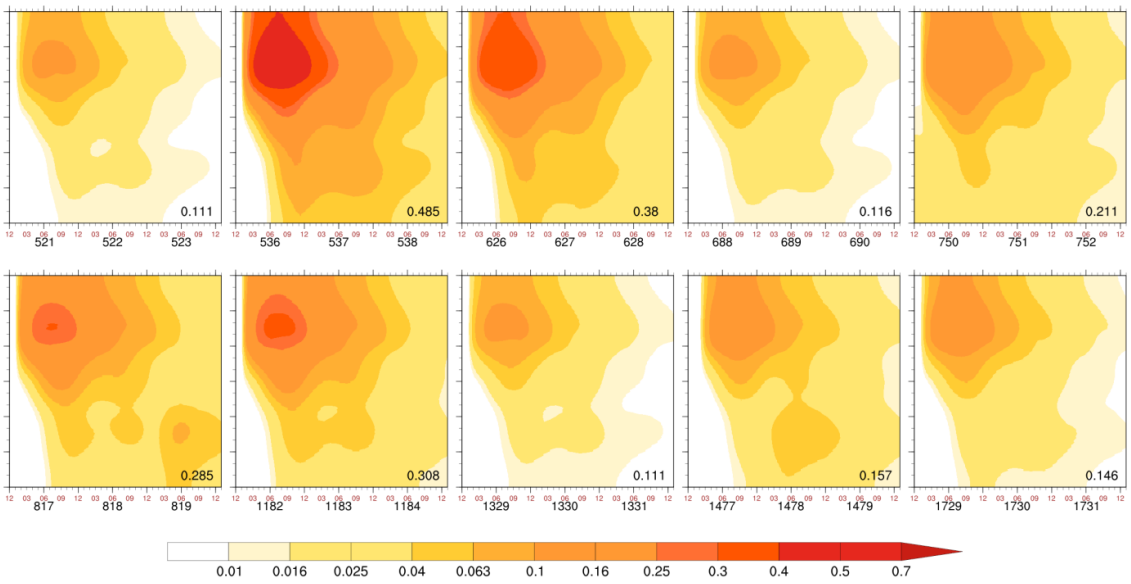

Figure 3.6: AOD550 latitude-time cross section of 10 NHw volcanic events with their peak AOD550_3060n value shown at lower-right corner of each plot. Minor tick marks on the y-axis of each panel are shown in every 10° of latitude.

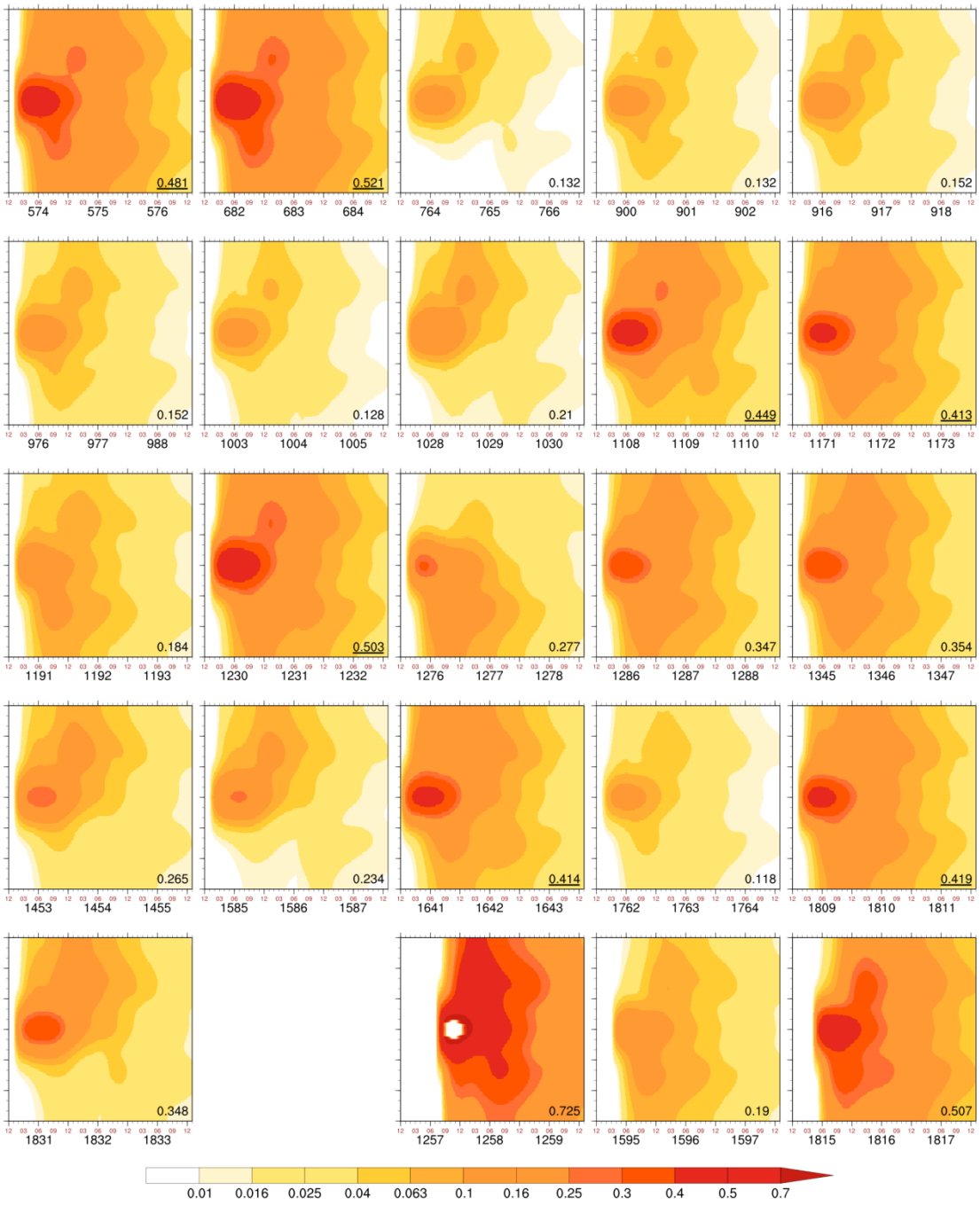

Figure 3.7: AOD550 latitude-time cross section of 21 EQw volcanic events and 3 EQe volcanic events with their peak AOD550_15sn value shown at lower-right corner of each plot. The peak value of AOD550_15sn for 7 EQmega events are underlined. Minor tick marks on the y-axis of each panel are shown in every 10° of latitude.

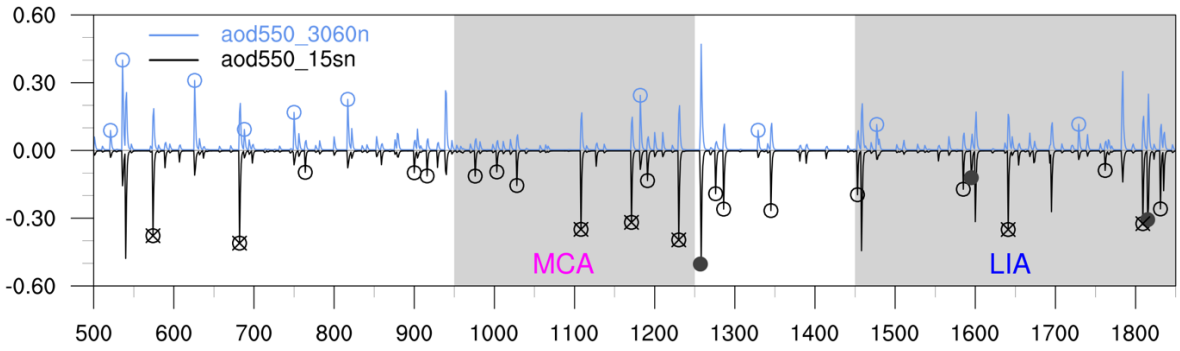

Figure 3.8: Volcanic aerosol forcing for the years 500–1849 CE with annual-mean of AOD550_3060n in blue lines and AOD550_15sn in black in inverted axis. The selected ten NHw and twenty-one EQw events are shown in blue and black hollow circles respectively. The selected seven EQmega events are shown in cross while three EQe events are show in black filled circles.

3.4 NAO and PNJ composite

The average stacked PNJ and NAO responses to the four volcanic clusters calculated from past1000 experiment are shown in Fig. 3.9. The peaks that go over/under the error bars indicate deviation from the piControl climate baseline and are considered to be of volcanic origin. For the NHw cluster (Fig. 3.9a-b), a strong significant (>99% confidence level) increase of PNJ and positive NAO is observed in year 0, which is the in-phase winter. The PNJ is followed with another increase in year 1 (first post-eruption winter year) however the NAO positivity did not cross the significance test in year 1. There is no significant signal in other years.

For the EQw cluster (Fig. 3.9c-d), the high significant peaks (>99% c.i.) for PNJ and NAO did not appear in the eruption winter, but in the first winter year. We assume a different aerosol transportation and radiative effects distribution between NHw and EQw leading to a distinct peak year.

If we select out the mega eruptions out from EQw, we then see another story. For the EQmega cluster (Fig. 3.9e-f), from in-phase winter year to year 2, we can find a significant (>95%) PNJ signal. But the strongest signal for PNJ increase still takes place in first year. The positive NAO is also strong in year 1, although barely crosses the significant line.

For EQe eruptions, the cluster size is nine, including the strongest Samalas eruption. The high significant increase of PNJ and NAO is seen in both first and second year. However, if we recall the aerosol distribution of Samalas (the exceed line in middle panel of Fig. 3.4), which actually endures two peaks during the eruption, it can make the second year PNJ and NAO signal less creditable for EQe cluster.

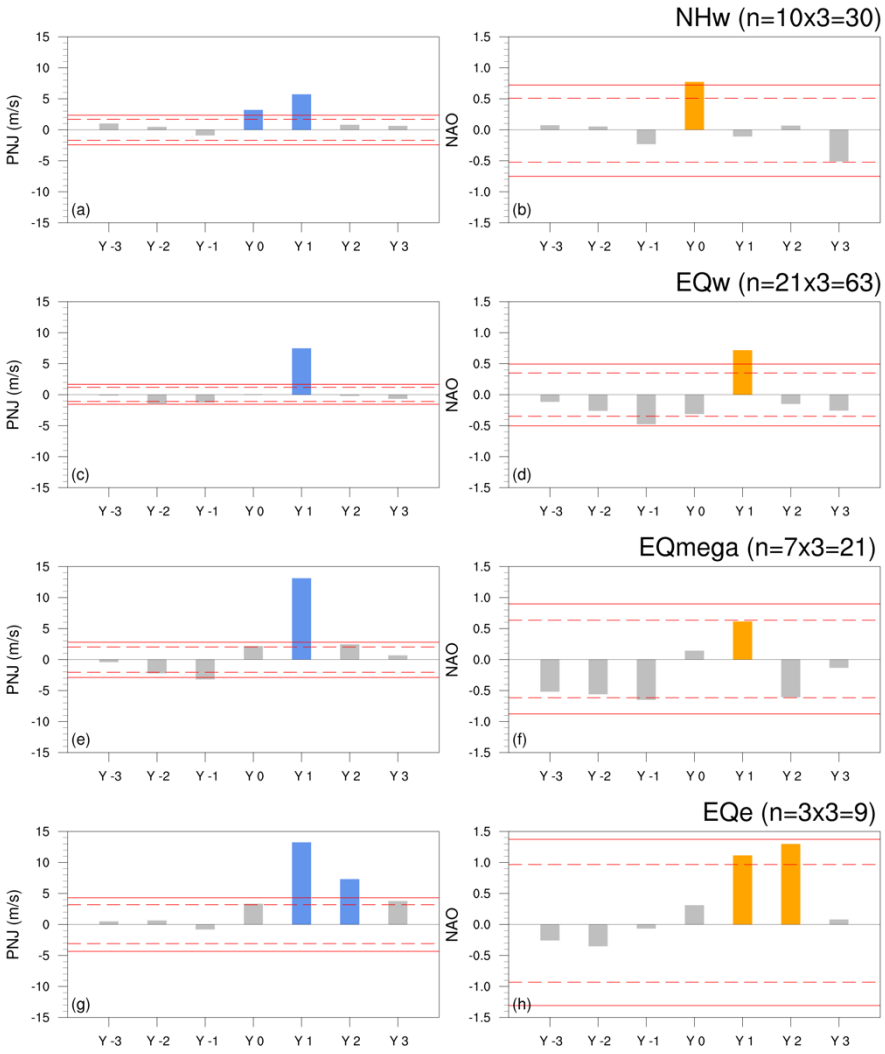

Figure 3.9: Analysis of PNJ and NAO response to **(a)-(b)** NHw, **(c)-(d)** EQw, **(e)-(f)** EQmega and **(g)-(h)** EQmega volcanic cluster. Red solid and dashed lines in each plot indicates from bottom to top, 1st, 5th, 95th and 99th percentile of the n-yr bootstrapping distribution from piControl, where n=30, 63, 21, 9 respectively for different volcanic clusters. To note that year 1 is defined as the first winter beginning after the onset of the eruption.

3.5 Post-eruption interannual winter climate

To further investigate the results from the PNJ and NAO clustering analysis, anomaly composite of surface temperature, precipitation, surface wind, sea level pressure and 50mb geopotential height pattern associated with each volcanic type will be retrieved for in-phase winters, first and second winters. The latitude-height cross section of zonal averaged air temperature, zonal wind and geopotential height will also be analysed. All signals exceeding 5th~95th confidence interval of the n-yrs bootstrapping distribution from piControl will be stippled (n=30, 63, 21, 9 respectively).

3.5.1 In-phase winter

The composite fields of in-phase winter anomalies for three winter volcanic clusters (NHw, EQw, EQmega) are shown in Fig. 3.10. According to Fig. 3.10a-d, a warm and humid pattern is present over North Eurasia, while negative temperature anomalies over North America. The Mediterranean encounters a warmer and wetter winter in the west basin in contrast to a colder and drier winter in the East basin. The temperature and precipitation anomalies can be explained by the anomalous advection of air mass associated to the anomalous atmosphere circulation. We observe strengthened westerlies blowing from the Davis Strait to Scandinavia which is typical circulation anomalies resulted from a dipole of the sea level pressure anomaly over North Atlantic-Europe (i.e., a positive NAO). The strengthened polar vortex is also illustrated in Fig. 3.10d. All clues indicate a positive NAO in-phase winter for NHw volcanic clusters.

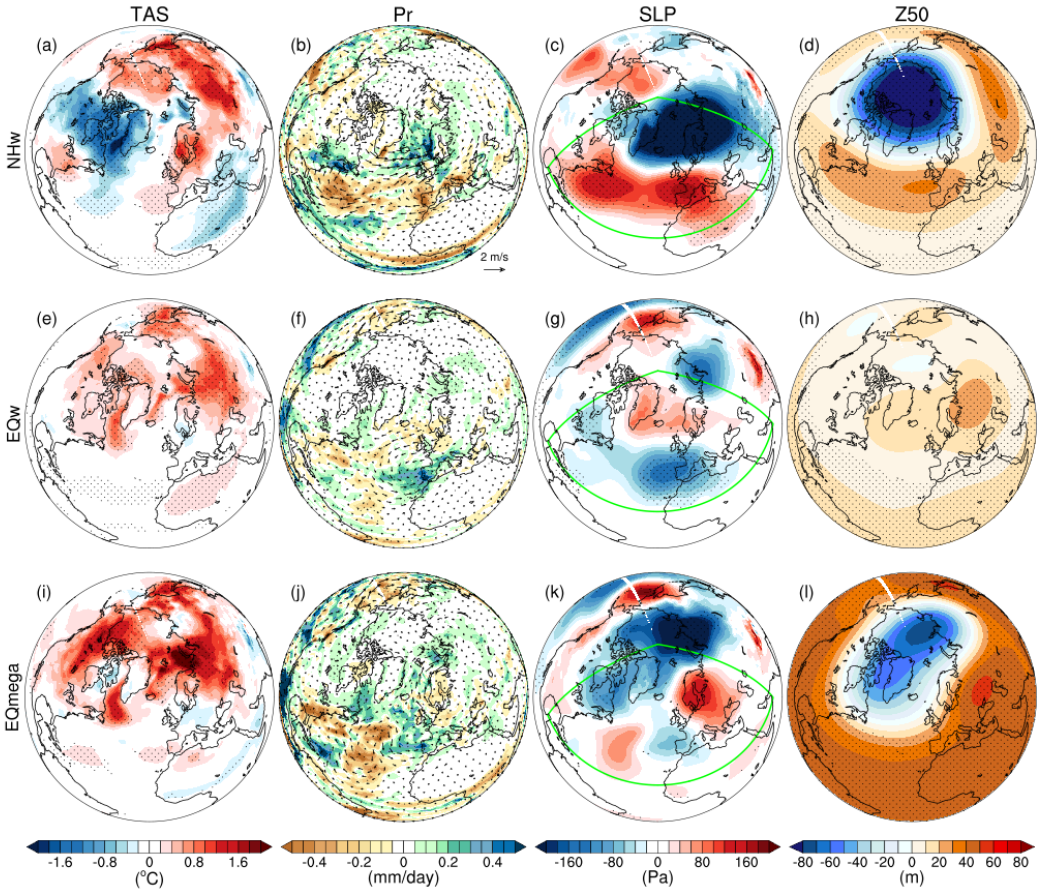

Figure 3.10: The simulated results of the North Hemisphere climate anomalies at surface and stratosphere during in-phase winter for **a-d**: NHw, **e-h**: EQw, **i-l**: EQmega voclaninc cluster, in terms of surface air temperature (TAS), Precipitation (Pr), Sea level pressure (SLP) and geopotential height at 50 hPa (Z50) from left to right column. The dotted area are significant anomalies compared with piControl based on bootstrapping method at 90% confidence level. Green contours outline the area we use to calculate NAO index.

As the for EQw cluster (Fig. 3.10e-h), however, we do not the capture NAO positive phase. Nevertheless, when filtering out massive equatorial winter eruptions, EQmega cluster could reveal a positive NAO-like signals with significant positive temperature anomalies over the Barents Sea and part of north Russia and a deepened polar vortex. Nevertheless distinct traits exist. For example, the sea level pressure anomaly only partly projects on the NAO to the north. Precipitation and surface winds responses are weak and not significant.

In order to investigate the atmosphere structure for in-phase winter, we plot the meridional plane of zonal averaged anomalies of air temperature, zonal wind and geopotential height in Fig. 3.11. The temperature response is consistent with the eruption categories where stratosphere warming concentrates over mid-latitude (30°~60°N) for NHw cluster (Fig. 3.11a), while over tropical region (30°S~30°N) for EQw (Fig. 3.11d) and EQmega(Fig. 3.11g). Moreover, the stratosphere temperature anomaly of EQmega is stronger than that of EQw because higher absorption of solar and terrestrial radiation related with stronger eruptions in EQmega. Under this circumstance, different anomaly patterns of zonal wind and geopotential height are anticipated.

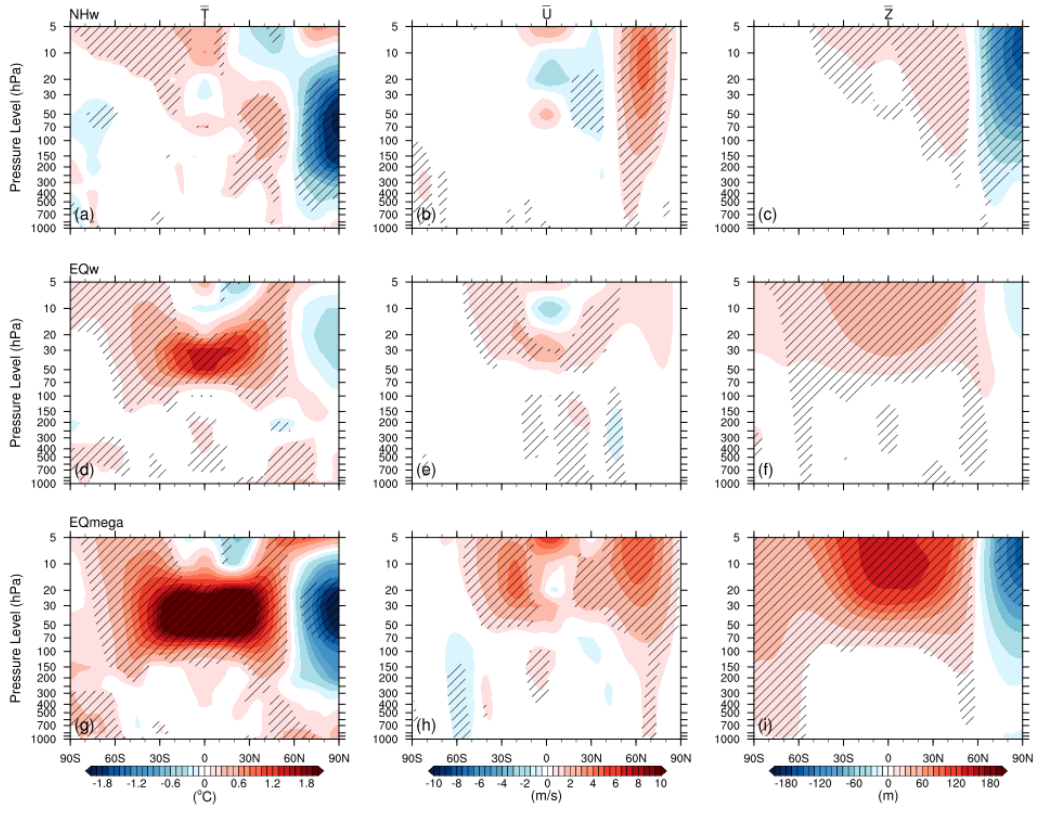

Figure 3.11: Latitude-Pressure cross sections of simulated zonal mean paired anomalies during in-phase winter for **a-d**: NHw, **e-h**: EQw, **i-l**: EQmega voclaninc cluster, in terms of air temperature ($\overline{T}$), zonal wind ($\overline{U}$) and geopotential height ($\overline{Z}$) from left to right column. The area without slashes are significant anomalies compared with piControl based on bootstrapping method at 90% c.i.

The corresponding zonal mean zonal wind and geopotential height for NHw (Fig. 3.11b-c) and EQmega (Fig. 3.11h-i) show that in the NH, the polar night jet is significantly intensified during in-phase winter. In contrary we do not observe such signal in EQw (Fig. 3.11e-f).

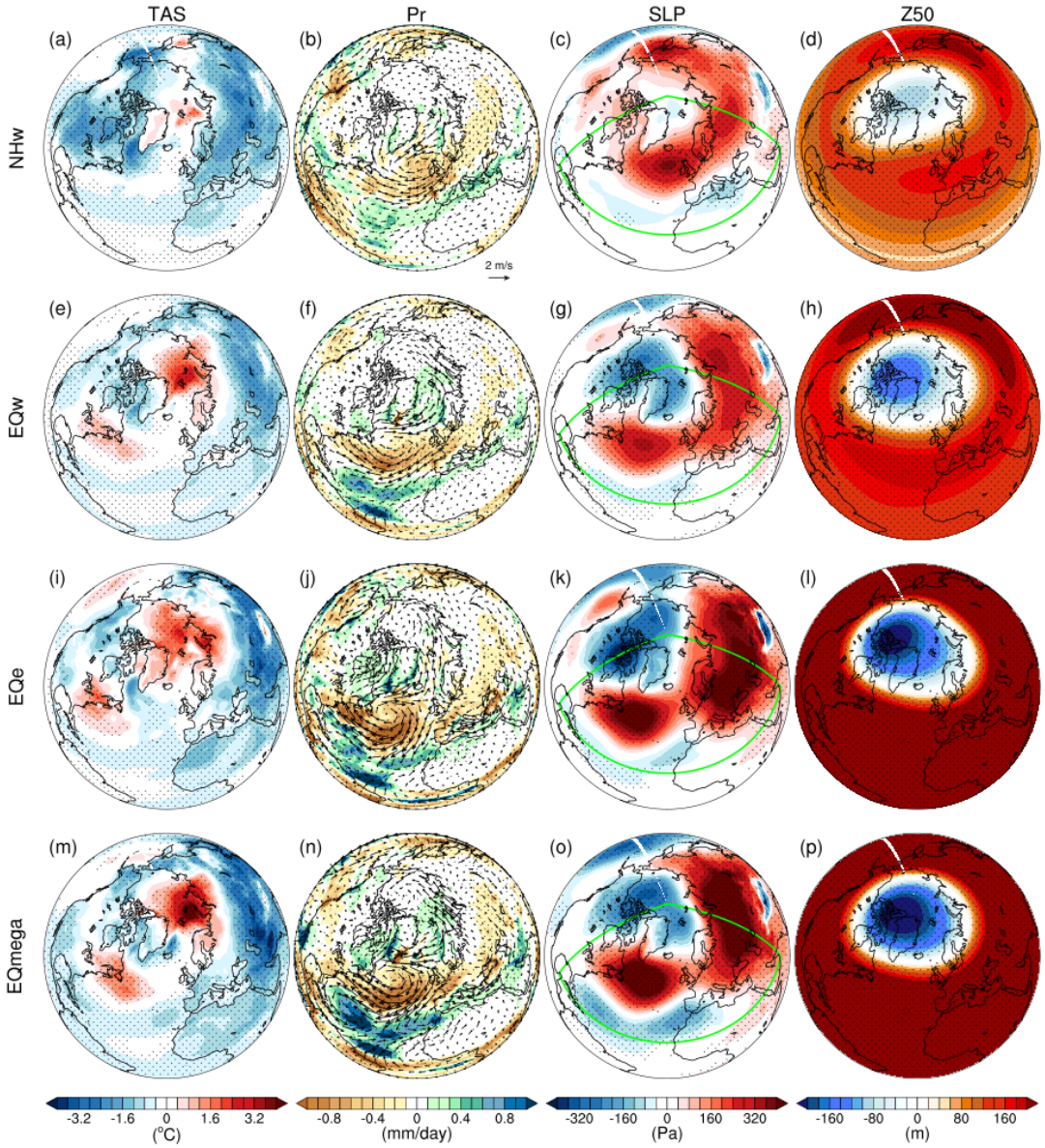

Figure 3.12: The simulated results of the North Hemisphere climate anomalies at surface and stratosphere in the first winter for **a-d**: NHw, **e-h**: EQw, **i-l**: EQe and **m-p**: EQmega voclaninc cluster, in terms of surface air temperature (TAS), Precipitation (Pr), Sea level pressure (SLP) and geopotential height at 50 hPa (Z50) from left to right column. The dotted area are significant anomalies compared with piControl based on bootstrapping method at 90% confidence level. Green contours outline the area we use to calculate NAO index.

3.5.2 Winter 1

Figure 3.12 demonstrates significant temperature, zonal wind and geopotential height during first post-eruption winter for four volcanic clusters (NHw, EQw, EQe and EQmega). All clusters have augmentation of geopotential height at 50 mb pressure level (right panel of Fig. 3.12). However, the surface climate anomalies do not project on positive NAO phase for NHw cluster(Fig. 3.12a-c), only equatorial eruptions encounter a positive NAO-like climate with sea level pressure dipole pattern (Fig. 3.12g, k, o). Surprisingly, the northern center of the Atlantic low displaced rather northward which resulted in stronger westerlies blowing from south Greenland to the Barents Sea (Fig. 3.12f, j, n). As a consequence, the anomalous warming pattern is located over north of Russia and far north of Scandinavia (Fig. 3.12e, i, m).

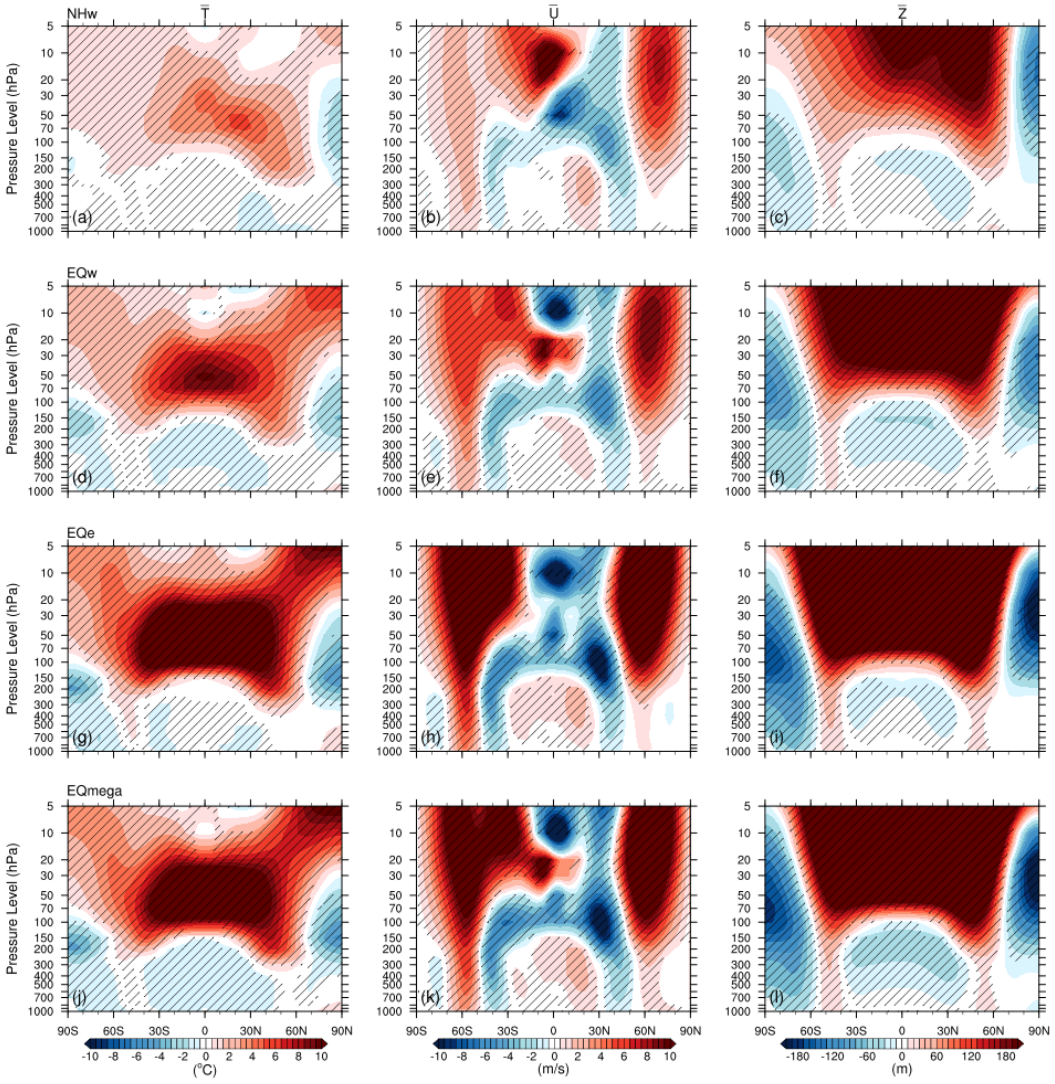

Figure 3.13: Same as **Figure 5.11**, but for the first winter anomalies of **a-c**: NHw, **d-f**: EQw, **g-i**: EQe and **j-l**: EQmega voclaninc cluster.

When comparing the vertical atmosphere structures for each cluster (Fig. 3.13), stratospheric heating coincides with the eruption latitude of corresponding volcanic type (left panel of Fig. 3.13) and all clusters display strengthened polar night jet (middle panel of Fig. 3.13) and deepened polar vortex (right panel of Fig. 3.13) as expected from the temperature anomaly pattern. However, only equatorial events (Fig. 3.13e, h, k) have stratospheric zonal wind anomalies strong enough to reach down the lower troposphere, whilst the zonal wind anomalies for NHw cluster (Fig. 3.13b) occur mostly above the tropopause. This explains the surface climate anomalies of NHw cluster (Fig. 3.12a-c) which do not produce a positive NAO signal. Furthermore, it unveils a question that is to what extent a strengthened polar night jet will correlate with positive NAO. This will be discussed in section 3.5.4.

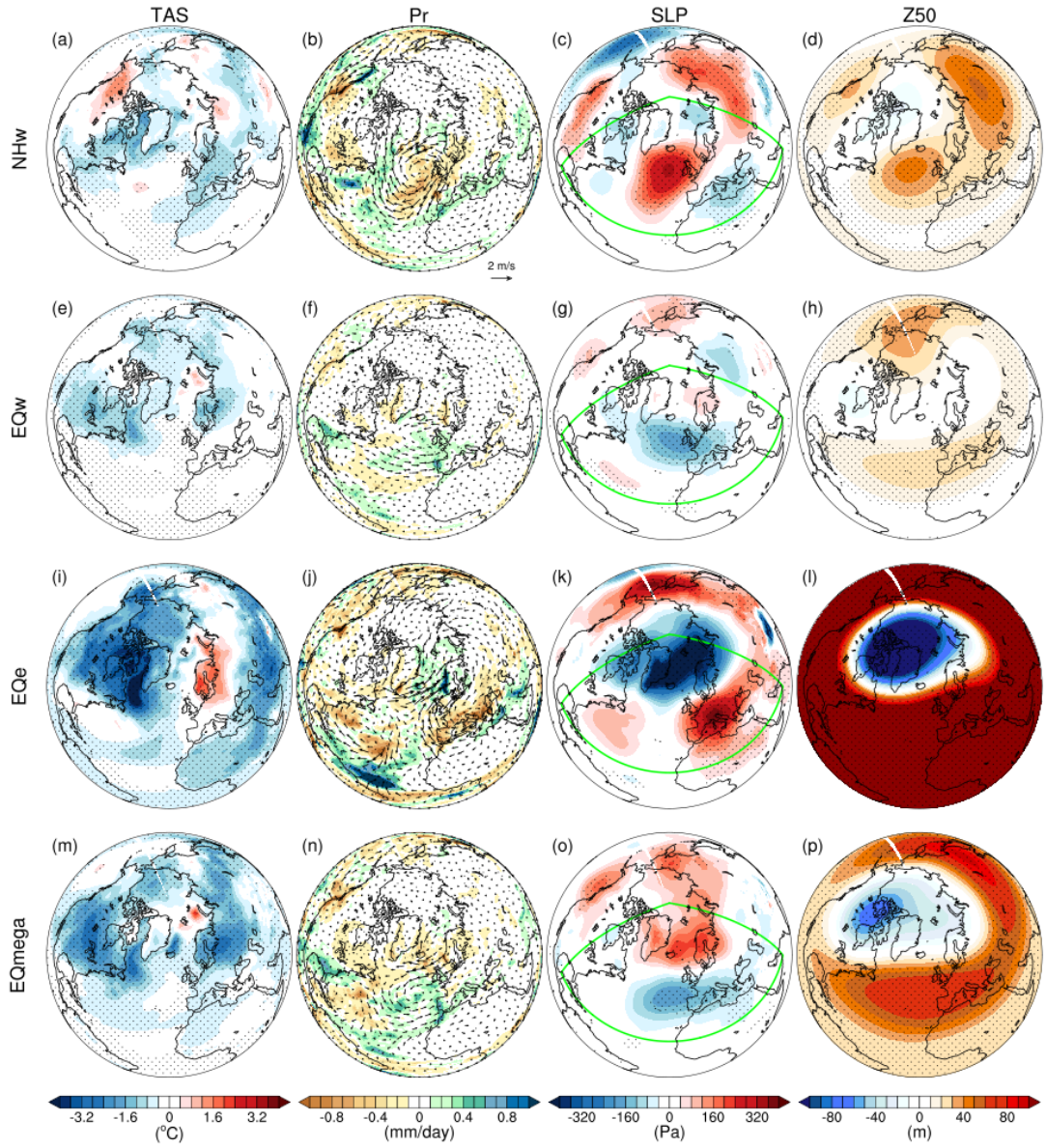

Figure 3.14: Same as **Figure 3.12**, but for the second winter anomalies.

3.5.3 Winter 2

During the second winter, the NAO pattern is not captured for NHw (Fig. 3.14a-d) nor for EQw (Fig. 3.14e-h). Only EQe shows a marginal warming over Scandinavia while cooling everywhere else (Fig. 3.14i). At the same time, the northwest coast side of Scandinavia also shows humid winter caused by anomalous subpolar westerlies bringing moisture under the effect of sea level pressure dipole pattern and strong polar vortex (Fig. 3.14j-l). However, for reasons of smaller sample size (n=9) and aforementioned irregular aerosol distribution of Samalas with two AOD550 peaks, we cannot affirm this positive-NAO like pattern during the second volcanic winter is valid for all spring-summer equatorial events. Large member ensemble experiments are demanded to carry out further diagnostic. Figure 3.14m-p reveal that EQmega cluster is incapable of producing positive NAO signal in the second winter except a weak effect on the polar geopotential height.

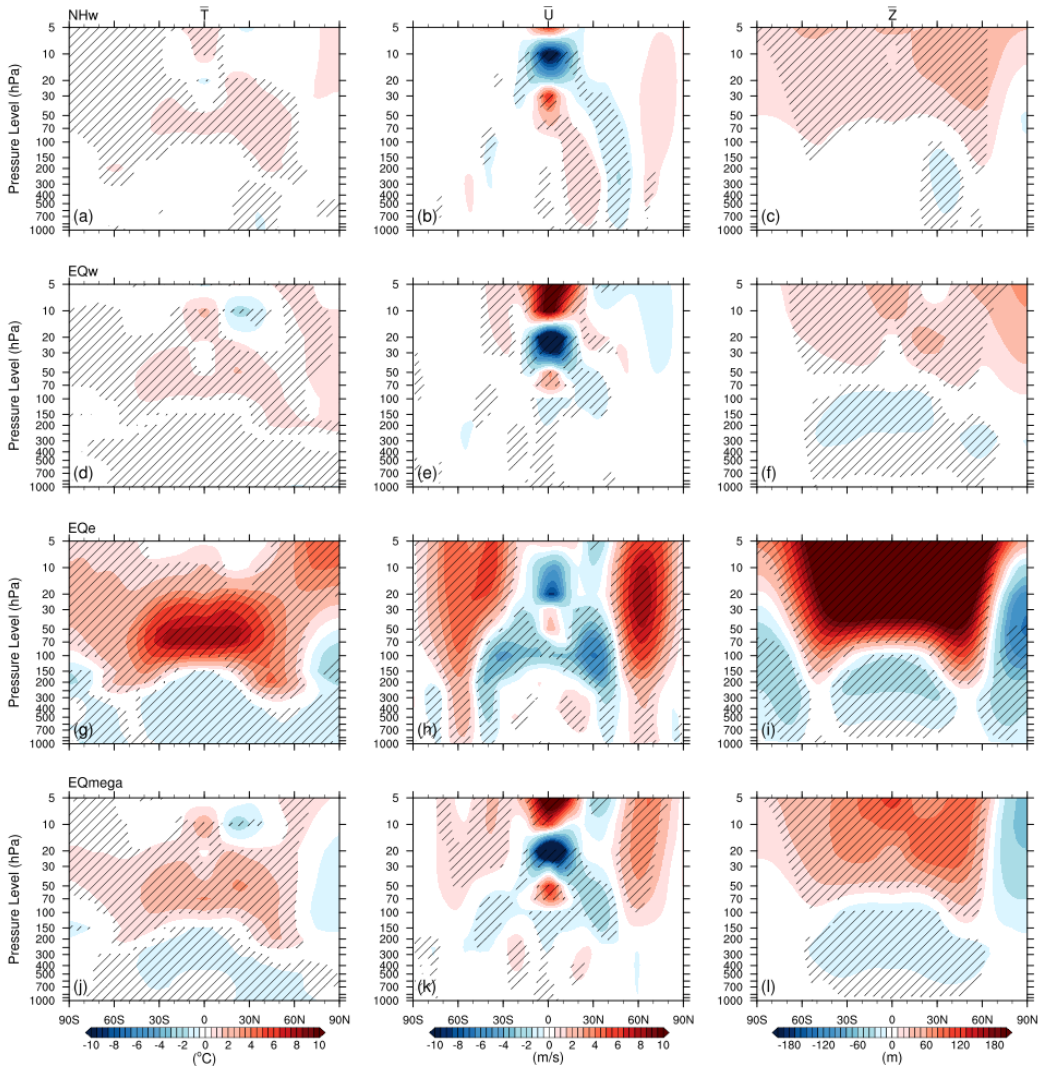

Figure 3.15: Same as **Figure 3.13**, but for the second winter anomalies.

3.5.4 Meridional temperature gradient

As presented before, two "conundrums " could be summarized:

- NHw and EQw volcanic cluster both happened in winter, the forced in-situ polar night jet and positive NAO signals take place at different time (i.e., in-phase winter year for NHw and one year later for EQw). Why?
- Although NHw volcanic events have stronger stratosphere temperature anomalies during the first winter than in-phase winter, only during in-phase winter that the stratospheric polar vortex are positively correlated with positive NAO signal in the lower layer. Why?

In order to elucidate the questions above, we go back to the proposed mechanism for a forced strengthening of stratospheric zonal winds that is the enhanced meridional temperature gradient. We plot the meridional temperature gradients overlayed with zonal wind anomalies for four volcanic clusters in Fig. 3.16. Referring the thermal wind balance introduced in **Appendix B.1** for zonal mean of perturbed zonal wind and perturbed temperature in quasi-geostrophic scaling (small Rossby number), we have: $f\frac{\partial \bar{u}}{\partial z} = -\frac{R}{H}\frac{\partial \bar{T}}{\partial y}$, where overbar indicates zonal mean, u and T are ensemble mean of 30yr running anomalies in each volcanic cluster.

Therefore meridional temperature gradient is crucial in determining the vertical wind shear. For NHw cluster in in-phase winter, we could observe a negative meridional temperature gradient consistent with the positive wind shear from 20 mb to 1000 mb, which indicates the NHw will be able to induce the negative enough temperature gradient once erupted in winter at 45°N. Hence we relate this rapidity to the location of NHw volcanic events, that the sulfate aerosol radiative forcing will act directly over the NH jet.

While for equatorial eruptions, due to the transport lag of aerosols from equator stratosphere to high-latitude area, the meridional temperature gradient remains largely unaffected over mid-to-high latitudes during in-phase winter, which explains EQw cluster's failure in yielding stronger subpolar westerlies that winter. However, if we take out the most strongest eruptions, the massive aerosol loading is supposed to be capable of forcing a strong polar vortex, and concurrently a positive NAO, which is the case of EQmega.

People may wonder now : "so what about the first winter of NHw, why don't they make a strengthened PNJ and NAO? " Actually there is answer from Figure 3.16. The thermal wind balance based on quasi-geostrophic circulation does not apply to tropical atmosphere which may also modulate the polar vortex through Quasi-Biennial Oscillation.

During first post-eruption winter, NHw cluster encounters a rather different Quasi-Biennial Oscillation (an easterly QBO phase) as compared with other winter eruption categories (a westerly QBO phase). Holton and Tan (1980) has proposed an intriguing feature of the Northern Hemi-sphere (NH) that a stronger polar vortex exists when the QBO in the lower stratosphere (50 hPa) is in its westerly phase (QBOw), and, conversely, a weaker polar vortex exists when the QBO is in its easterly phase (QBOe). Such phenomenon, also known as the Holton–Tan effect (THE), is also confirmed by White et al. (2015) that QBOe is associated with increased poleward wave propagation, leading to enhanced wave convergence and in situ wave growth at high latitudes and contributing to the weaker polar vortex. Therefore, we suggest the weakened PNJ signal in the first winter for NHw is a result of QBO phase change, which is eventually related to the different stratospheric diabatic heating pattern of NH eruptions compared to the EQ eruptions. Further work may be predicted in studying dynamics behind QBO modulation effect for eruptions at different latitudes.

Overall, volcanic forced strong PNJ and positive NAO signal depend strongly on the strength, eruption latitude and season of volcanic eruptions, because all these factors are important in deciding the volcanic sulfate aerosol distribution and the resulted meridional atmosphere temperature gradient.

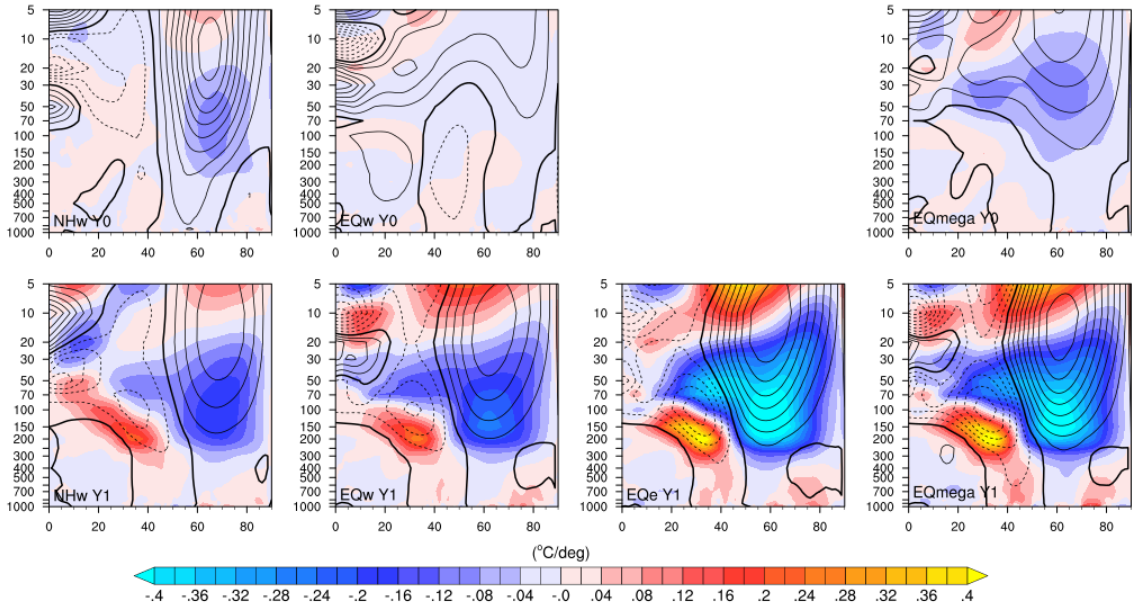

Figure 3.16: NH meridional temperature gradient of zonal mean temperature anomaly ($\partial\overline{T}/\partial y$) during in-phase winter (upper panel), and during 1st winter (lower panel) for NHw, EQw, EQe and EQmega respectively (Units: ℃/deg). The color contours of temperature gradients are overlayed with zonal mean u-wind in black solid lines for positive values and dashed lines for negative values. The incident is 0.5 m/s for wind contours with zero denotes in thicker line.

3.6 Conclusions and discussions

In this chapter, we concentrate on the IPSL-CM6A-LR model performance in its *past1000* simulations to reproduce winter climate anomalies for eruptions in different magnitude, eruption season and latitude at interannual time scale. We evaluate the potential impact of NHw, EQw, EQe and EQmega volcanic events on the North Atlantic Oscillation, North Pole night jet, and consequently the European climate interannual preferential variability. During the study, three runs (r1, r2, r4) from IPSL-CM6A-LR *past1000* experiment involved in CMIP6 database are taken as ensemble members. The significance of composite mean is tested using piControl bootstrapping PDFs. We may conclude the sensitivity of climate response to volcanic conditions as follows:

- The model simulates increased warming in the stratosphere, a stronger polar vortex and a surface pattern similar to the positive phase of the NAO in the first winter following a summer or a winter tropical eruption, with polar night jet responses amplitudes that are linearly related to the eruption strength. No linear relationship with the eruption magnitude is identified for extra-tropical Northern Hemisphere events while a tendency towards a positive NAO phase is only significant during the same winter as the eruption occurrence.
- For the NH high latitude volcanic events, if happened in winter, they can pose effect directly on the meridional temperature gradient near the jet position during in-phase winter, hence leads to positive NAO, which contradicts other literatures (Oman, 2005; Sjolte et al., 2021; Zambri et al., 2019b) suggesting otherwise a negative NAO winter.
- For the EQ volcanic events, it is easier to lead to a positive NAO winter if happened in spring/summer, other than the winter season. The real explanation behind this "seasonal difference" is actually the time needed for sulfate aerosol to propagate to mid-latitude (around 45°N~60°N). The hysteresis between an eruption in tropics and the time of acting on $\partial\bar{T}/\partial y$ through interacting with solar radiation makes a spring/summer EQ eruption easier to produce a positive NAO phase than winter EQ eruptions.
- For the massive winter EQ volcanic events, which we referred as EQmega, albeit they happened in winter season, they are strong enough to influence the $\partial\bar{T}/\partial y$ on mid-latitude (jet position) and hence a strengthened polar night jet.

- Tropical atmosphere can affect the polar vortex through QBO modulation, which is also a possible explanation for that NHw could not force a stronger polar vortex in the first winter due to a easterly QBO phase. Further analysis are anticipated.

It has been reported that high latitude extratropical volcanoes may favour more a negative NAO in the first winter after eruption (Oman, 2005; Sjolte et al., 2021; Zambri et al., 2019b) rather than a positive NAO observed/simulated after tropical volcanic eruptions (Bittner, Schmidt, et al., 2016; Bittner, Timmreck, et al., 2016; Christiansen, 2008; Zambri and Robock, 2016). However, it is unclear whether this is a robust response, and whether there is enough radiation near the pole in the NH wintertime to heat the stratospheric aerosol and overcome the high level of natural variability and elicit such a dynamical response.

In our study, we carefully selected 21 winter Northern extratropical eruptions to carry out statistical tests and make inference. We suggest that winter Northern high latitude are able to produce a forced in-situ positive NAO winter (>99% confidence level) during in-phase winter, which contradicts former studies (Oman, 2005; Sjolte et al., 2021; Zambri et al., 2019b). The RF from high-latitude eruptions is a function of seasonal distribution of insolation and the 3- to 4-month lifetime of high-latitude volcanic aerosols. After ejection, the sulfate aerosols of NHw events interacted with RF around the jet position in the Northern Hemisphere, leading to discernible strengthening of PNJ under the thermal wind balance.

Furthermore, our study suggest that the eruption season has to be considered when studying the climate impact of volcanic eruptions, which is consistent with Stevenson et al. (2017). For equatorial eruptions, a spring/summer event produces a positive NAO phase in the first winter after eruption onset, while a winter event is harder to produce a positive NAO during in-phase winter. This is because volcanic aerosols injected into the stratosphere from a tropical eruption need time to be transported to both hemispheres via Brewer-Dobson circulation and finally reach polar regions. For extratropical eruptions, we only analyse winter Northern high latitude volcanic events. Different from Zambri et al. (2019a, b), we found positive NAO signal during in-phase winter. Nevertheless, this result also hints a possible contribution of eruption season since their Laki volcanic forcing began in June 1783. For the Laki eruption in June 1783, the maximum heating took place at August in the lower stratosphere, in the 50~70° N latitude bin and the location of maximum stratospheric heating anomaly shifts southward as the aerosols are transported

equatorward (Zambri et al., 2019a). This may lead to a rather different heating pattern in the first winter after eruption, which is also responsible for the difference with our NHw eruptions.

In the former researches, Kravitz and Robock (2011) showed that high-latitude eruptions must inject at least 5 Tg (SO_2) into the lower stratosphere in the spring or summer, and much more in fall or winter (15 Tg SO_2 estimated), to have a detectible climatic response. The newly published research by Zhuo et al. (2021) designed Pinatubo-like volcanic ensemble experiments based different latitudes (30° S/ 0°/ 30° N) and different eruption season (June/ December) using MPI-ESM model (Giorgetta et al., 2013). Even though stronger cooling emerges in NH (SH) after NH (SH) eruptions compared to the equatorial ones, their research results didn't reveal heterogeneity of the climate impacts between summer and winter eruptions.

Not only the eruption latitudes/season, but also the volcanic forcing strength can influence the dynamical response of NH climate system to volcanic eruptions in the first boreal winter. Our study points out that when equatorial eruptions are large enough, they are also capable of affecting the polar night jet during in-phase winter after eruption, which confirms in other hand the importance of applying correct volcanic forcing data in numerical simulations. While a large response might be expected due to the large forcing, this result demonstrates that differences between forcing data sets play a large role in the model response to volcanic eruptions, which is consistent with past studies (Bittner et al., 2016; Toohey et al., 2014; Zambri et al., 2017).

In conclusion, IPSL-CM6A-LR *past1000* runs clearly simulates a rather robust positive NAO winter and strengthened polar night jets, which are forced in-situ by volcanic forcing. The timing and strength of this signal are sensitive to the eruption latitude, season and strength. This work is of great importance since explosive stratospheric volcanism represents an essential natural radiative forcing. Understanding how much of the observed climate variability at seasonal and decadal scale is a response to natural and anthropogenic radiative forcing, as opposed to internal variability, is a fundamental challenge and a crucial test for climate models attempting to predict future climate variations (Shindell et al., 2003; Stenchikov, 2002).

Chapter 4

Northern Hemisphere climate and circulation responses to Pinatubo eruption

Contents

4.1 Preamble

Previous chapter has tested the model robustness and climate sensitivity to categorized volcanic eruptions that IPSL-CM6A-LR has demonstrated efficiency in simulating a volcanic positive NAO winter. The objective of this chapter is to study the mechanism by which different radiative components of volcanic forcing can impact the NAO behaviour and Northern Hemisphere climate via volcano induced changes in the atmosphere circulations. This investigation takes the form of a case-study of June 1991 Pinatubo eruption.

The volcanic radiative effects are mainly backscattering short wave solar radiation (causing surface cooling) and absorbing long wave terrestrial radiation from the surface (causing stratosphere heating). We will first assess and discuss the ability of IPSL-CM6A-LR to reproduce climate variability and NAO variation after the 1991 Pinatubo eruption. To do so, we use the VolMIP *volc-pinatubo-full* experiment under full volcanic radiative forcing and compare modes results with reanalysis data. We will pay particular attention to the North Atlantic- Mediterranean geographic sector.

IPSL-CM6A-LR allows the separation of dominant shortwave (surface cooling) and longwave (stratospheric warming) effects of volcanic aerosols. Hence in a second step, we will compare climates among the three experiments *volc-pinatubo-full*, *volc-pinatubo-strat*, *volc-pinatubo-surf*. Unravelling the relative role of surface cooling and stratospheric warming on mean winter climate, NAO, polar vortex and eddy flux in the North Atlantic-Mediterranean basin is of great significance since this will deepen our understanding of the climate sensitivity to different radiative forcing.

Large sets of climate simulations can be performed with the volcanic radiative effects taken collectively or individually, thus making it possible to attribute some of the observed phenomena to specific sources. A dedicated study using this approach with IPSL-CM6A-LR is presented as a publication (to be submitted, section 4.2) at this chapter. This study aims to understand the presence of positive NAO in winter after a tropical volcanic eruption, the most robust basin-wide signal in models and observations. A discussion about the possible negative feedback from surface cooling through sea ice-NAO interaction closes this chapter and allows us to put the results obtained into perspective (section 4.3). In this chapter, two essential theories of atmosphere dynamics are applied. The first is the thermal wind balance, and the second is the Eliassen-Palm flux. Readers are kindly directed to **Appendix B.1** and **B.2** for relevant equations involved.

4.2 Article : Northern Hemisphere winter atmospheric responses to the 1991 Pinatubo eruption : signatures of volcanically-induced stratospheric warming and surface cooling

Title: Northern Hemisphere winter atmospheric responses to the 1991 Pinatubo eruption: signatures of volcanically-induced stratospheric warming and surface cooling

Authors: Yang Feng[1], Myriam Khodri[1], Slimane Bekki[2], Laurent Li[3], Nicolas Lebas[1], …

[1]LOCEAN/IPSL, Sorbonne Université, CNRS, Paris, France (yang.feng@locean.ipsl.fr)
[2]LATMOS/IPSL, Sorbonne Université, CNRS, Paris, France
[3]LMD/IPSL, Sorbonne Université, CNRS, Paris, France

Abstract. This work explores the physical mechanisms between volcanic forcing and climate response in the Northern Hemisphere by focusing on the event of 1991 Pinatubo eruption. While volcanic eruptions decreases global mean surface temperature through direct radiative dimming effects, the NAO signal over the North Atlantic-Mediterranean sector is suggested to be a dynamical and interactive process between stratosphere and surface. By decomposing the radiative effects of Pinatubo eruption, three large ensemble experiments are respectively designed to represent all interferences of volcanic aerosol with the radiative fluxes (*volc-pinatubo-full*), only the volcanic aerosol perturbations to the total (longwave and near-infrared) radiative heating rates (*volc-pinatubo-strat*), or only perturbations to the surface shortwave flux (*volc-pinatubo-surf*). From our simulation experiments, the significant positive NAO in the first volcanic winter is primarily attributed to stratospheric heating by enhancing the meridional temperature gradient and consequently the polar vortex, which is proven to be an up-to-low process. The surface cooling plays a destructive role in amplifying polar jets when it is sole in the stage. However, the nonlinear interaction between the stratosphere and troposphere/surface will make a stronger polar vortex in *volc-pinatubo-full* hence a more significant positive NAO. Besides, an equatorward EP flux deflection in the stratosphere in *volc-pinatubo-full* and *volc-pinatubo-strat* indicates that planetary waves mainly propagate toward tropical areas and weakly influence the polar vortex. As shown by the divergence of EP flux, an acceleration of westerly is also observed at high-troposphere around mid-latitudes for *volc-pinatubo-full* and *volc-pinatubo-strat*. The results highlight the dominant role of the stratosphere heating on formation of positive NAO in the North Atlantic-Mediterranean sector after the Pinatubo eruption.

Keywords: Volcanic forcing - NAO - Polar vortex - Planetary waves - Atmospheric dynamics - VolMIP - Mechanisms

1. Introduction

Strong volcanic eruptions reaching the stratosphere are considered as one of the most important natural external forcings influencing the earth climate system, along with other factors such as anthropogenic actions (Myhre et al., 2013). Large volcanic eruptions can indeed inject into the stratosphere different gases and particles. Among them, sulphur species, mainly in the form of sulphur dioxide (SO_2), are oxidized within a couple of months and converted into sulfate aerosols, thereby enhancing the stratospheric aerosol loading. The lifetime of the aerosol layer typically persists for a few years. During that time, sulfate aerosols formed after tropical eruptions are spread toward the extratropics by the Brewer-Dobson Circulation, and consequently affect the physical and biogeochemical exchanges between the atmosphere, land surface and oceans (Robock, 2000; Raible et al., 2016; Timmreck, 2010; Cole-Dai, 2010). Sulfate volcanic aerosols also interfere with the radiative balance and the global climate by backscattering solar shortwave (SW) radiation and absorbing near-infrared (NIR) and infrared (IR) radiation, which cause a global surface cooling and a warming tendency in the lower stratosphere (Stenchikov et al., 2002; Santer et al., 2014).

The spatially evolving structure of volcanic forcing, largely confined at low latitudes during the first few months after a tropical eruption, induces dynamical effects that can also cause surface warming over large regions of the North Hemisphere (NH) during the first post-eruption winter. Such NH winter warming identified in instrumental observations and proxy reconstructions after several past tropical eruptions, is very similar to observed anomalies during positive phase of the Arctic Oscillation (AO) and North Atlantic Oscillation (NAO) (Graf et al., 1993; Robock, 2000; Shindell et al., 2006; Stenchikov et al., 2002; Fischer et al., 2007; Christiansen, 2008; Zanchettin et al., 2012). The AO positive phase is expressed in winter as a zonally symmetric negative anomaly of sea level pressure (or geopotential height at 500 hPa) in the Arctic and as a positive sea level pressure (or geopotential height at 500 hPa) anomaly in mid-latitudes. It is also associated with a zonally asymmetric warming over North America and Eurasia in high and mid-latitudes, and cooling over Greenland and the eastern Mediterranean. The hypothetic explanation is that AO changes observed after volcanic eruptions are induced by volcanic aerosol heating in the lower tropical stratosphere (Shindell et al., 2001; Stenchikov et al., 2002). According to this mechanism, the lower tropical stratosphere warming strengthens the meridional temperature gradient, which generates stronger subtropical zonal winds through the thermal wind balance and accelerates the polar vortex (Perlwitz and Graf, 1995; Kodera, 1994; Kodera et al., 1996; Shindell et al., 2001; Stenchikov et al., 2002). The strengthened polar vortex can then propagate downward toward the surface, trap the wave energy in the tropospheric circulation (e.g. Baldwin and Dunkerton, 1999) and intensify the westerlies leading to a positive NAO (Graf et al., 1993; Shindell et al., 2004). Stenchikov et al. (2002) have suggested that the resulting stronger polar vortex prevents planetary waves from penetrating into the stratosphere. Stenchikov et al. (2002) further find that the stratospheric aerosol heating is not required to obtain the positive AO response at the surface, and argue that decreased

meridional temperature gradient in the lower troposphere can lead to a decrease of vertical planetary wave activity flux in the lower stratosphere thereby amplifying the polar vortex. The IPCC AR4 models considered in Stenchikov et al. (2006) weakly reproduce the observed tropospheric post-volcano circulation and thermal anomalies. Reasons for this behavior remain speculative and include missing tropospheric and stratospheric processes and stratosphere-troposphere dynamical interactions.

Based on NCEP reanalysis data, Graf et al. (2007) note that wave propagation into the stratosphere is not inhibited but enhanced after volcanic eruptions. They suggest that the planetary waves travel across the stratosphere without interacting with the polar vortex, and are reflected near the stratopause back towards the troposphere, where they impact surface climate. This is a distinct stratosphere-troposphere coupling mechanism, different from that proposed by Stenchikov et al. (2002). According to Graf et al. (2007), most models' failure to represent the right climate response to volcanoes is related to their inability to represent this mechanism of stratosphere-troposphere coupling. CMIP5 models (Driscoll et al., 2012; Ding et al., 2014; Barnes et al., 2016) can partly simulate part of the post-volcanic radiative and dynamical responses, compared to the previous generation of models (Stenchikov et al., 2006). A statistically significant winter warming following the major eruptions of the last 100 years (Driscoll et al., 2012) is simulated but none of the models, regardless of their vertical resolution, are able to simulate a sufficiently strong reduction in the geopotential height at high latitudes that would be consistent with a stronger polar vortex (Charlton-Perez et al., 2013). The hypothesis leading to a preferred enhanced stratospheric polar vortex in post-eruption winters have been questioned by more recent studies suggesting that the mechanism based on the thermal wind balance and outlined above does not always hold (e.g., Bittner et al., 2016), possibly as the zonal wind response to direct aerosol radiative heating may be dominated by other effects, such as the residual circulation response to anomalous wave activity (Toohey et al., 2014).

Accordingly, obvious implications for the polar vortex response stem from the tropical Pacific, a known critical source of tropospheric wave disturbances affecting the stratospheric dynamics (e.g., Graf et al., 2014). Instrumental observations, climate proxy-based reconstructions and CMIP5 models indicate that volcanic eruptions tend to lead to El Niño events (e.g. Khodri et al, 2017; McGregor et al, 2020). There are stratospheric (e.g., Ineson and Scaife, 2009) and tropospheric (e.g., Jiménez-Esteve and Domeisen, 2018) pathways for El Niño Southern Oscillation (ENSO; McPhaden et al. 2006) to affect the atmospheric circulation over the North Atlantic, and project on a negative NAO. This would counteract the NAO+ tendency described above. Brönnimann et al. (2007) suggested, nevertheless, that this ENSO effects does not overwhelm the direct effects of volcanoes on NAO. Sampling issues in simulation ensembles (Lehner et al., 2016) and uncertainty linked to the eruption's season (Stevenson et al., 2017) further add to the complexity of competing influences on the top-down mechanism of volcanic forcing, hence on the post-eruption positive NAO anomaly for moderate or small tropical eruptions.

In this study, the mechanisms for the first post-eruption NH winter response to a Pinatubo-like eruption are revisited using reanalysis and ensemble simulations conducted with the IPSL-CM6A-LR Coupled model (Boucher et al., 2020) as part of the 6th phase of the Coupled Model Intercomparison Project (CMIP6; Eyring et al., 2016). Focus is on assessing (i) the IPSL-CM6A-LR model skills in reproducing key observed features of the first post-eruption NH winter, (ii) the respective role of volcanic forcing and internal climate variability, (iii) the attribution to specific forcing sources related to volcanically-induced surface cooling and stratospheric heating and (iv) the mechanisms underlying the dynamical atmospheric response. We rely on 49 member-ensemble simulations corresponding to the Institut Pierre-Simon Laplace (IPSL) contribution to VolMIP Tier-1 experiments for 1991 Pinatubo volcanic forcing dataset as used in the CMIP6 historical runs (Zanchettin et al., 2016).

The paper is organized as follows: in the next two sections (2 and 3), the data and methods used are introduced, the results obtained are presented in section 4 and discussed in section 5. A summary and the main conclusions are provided in section 6.

2. Data

2.1. Model

We used the CMIP6 version of the Institut Pierre- Simon Laplace (IPSL) coupled atmosphere-ocean general circulation model (AOGCM), called IPSL-CM6A-LR (Boucher et al., 2020). LR stands for low resolution, as the atmospheric grid resolution is 1.25 in latitude, 2.5 139 in longitude and 79 vertical levels (Hourdin et al., 2020). LMDZ6A-LR is coupled to the ORCHIDEE (d'Orgeval et al., 2008) land surface component, version 2.0. In IPSL-CM6A-LR, the oceanic component uses the Nucleus for European Models of the Ocean (NEMO), version 3.6 (Madec et al., 2017), which includes other models to represent sea-ice interactions (NEMO-LIM3; Vancoppenolle et al., 2009; Rousset et al., 2015) and biogeochemistry processes (NEMO-PISCES; Aumont et al., 2015). Compared to the 5A-LR model version and other CMIP5-class models, IPSL-CM6A-LR was significantly improved in terms of the climatology, e.g., by reducing overall SST biases and improving the latitudinal position of subtropical jets. The IPSL-CM6A-LR is also more sensitive to CO_2 forcing increase (Boucher et al., 2020) and represents a more robust global temperature response than the previous CMIP5 version consistently with current state-of-the-art CMIP6 models (Zelinka et al., 2020).

2.2. Experimental protocol

To help analyze the climate response to medium size stratospheric volcanic eruptions, a suite of 49-members short-duration simulations was run with the IPSL-CM6A-LR model over June 1991 to December 2000 for the Mt Pinatubo eruption (June 1991). Ensemble members all start from predefined initial conditions and use the same volcanic forcing dataset following the VolMIP protocol (Table 1).

Table 1. List of simulations with the IPSL-CM6A-LR model analyzed in the paper, the period covered, the size of the ensemble and imposed boundary conditions.

Name	Period	Abbreviation	Ensemble size	Volcanic Forcing	
				Near-infrared and longwave fluxes	Surface shortwave clearsky fluxes
volc-pinatubo-full	06.1991-12.2000	*Full*	25	✔	✔
vol-pinatubo-strat	06.1991-12.2000	*Strat*	25	✔	-
volc-pinatubo-surf	06.1991-12.2000	*Surf*	25	-	✔
piControl	1200 years	-	1	-	-

Initial conditions

Each ensemble member is branched off the IPSL-CM6A-LR CMIP6 piControl run, and starts from May 31th 1991, but with different initial conditions for both ocean and atmosphere. The sampling the for the ocean tries to cover the full cycle of ENSO through the Niño3.4 standardized SST index (cold/neutral/warm), while the sampling for the atmosphere is based on the NAO index (negative/neutral/positive) in the preceding winter. The combination produces a total number of 25 initial states from which our ensemble simulations start, as illustrated in Fig. 1. Among the ensemble simulations, the 25 simulations without volcanic forcing serve as *reference* experiment for Pinatubo ensembles hereafter. It is worthy to note that the NAO index is calculated based on the two-box method (Stephenson et al., 2006) applied to monthly geopotential height anomalies at 500mb.

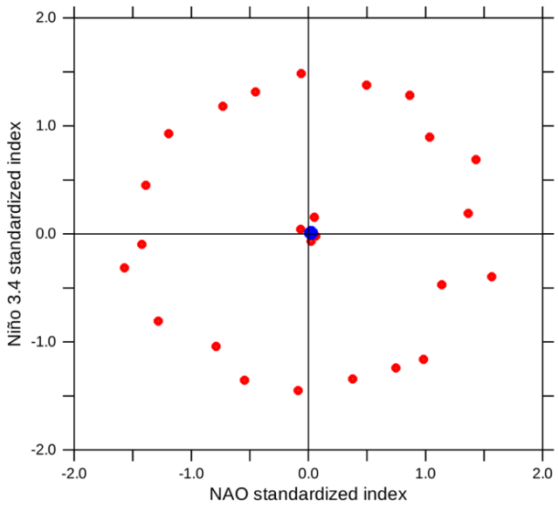

Figure 1. Scatter plot of the NAO and Niño 3.4 December-January-February standardized mean values selected in the piControl simulation as starting dates for the 25-member experiments. The red dots correspond to the values of individual initial conditions and the blue dot to the ensemble mean.

Volcanic forcing implementation

All external forcings in our ensemble simulations were kept to pre-industrial values except the volcanic aerosol extinction coefficient, single scattering albedo, and asymmetry parameter to simulate the Pinatubo eruption. Volcanic forcing data are from the Thomason et al. (2018) Version 3

two-dimensional (latitude-height) monthly dataset (Fig. 2a) provided by CMIP6, consistent with the volcanic forcing used in the IPSL-CM6A-LR historical CMIP6 experiments (Boucher et al., 2020). The original dataset were interpolated offline to the atmospheric model grid, but only in the stratosphere. Values below the model's tropopause were not considered to exclude tropospheric volcanic and non-volcanic aerosols (see Lurton et al., 2020 for the detailed procedure). As shown in Fig. 2a, the stratospheric volcanic aerosols spread from the tropics to the poles from the start of the eruption in June 1991 until late 1992, and then slowly disappears in 1993, being washed out of the stratosphere. Our CMIP6 data are consistent with other available datasets (Fig. 2b).

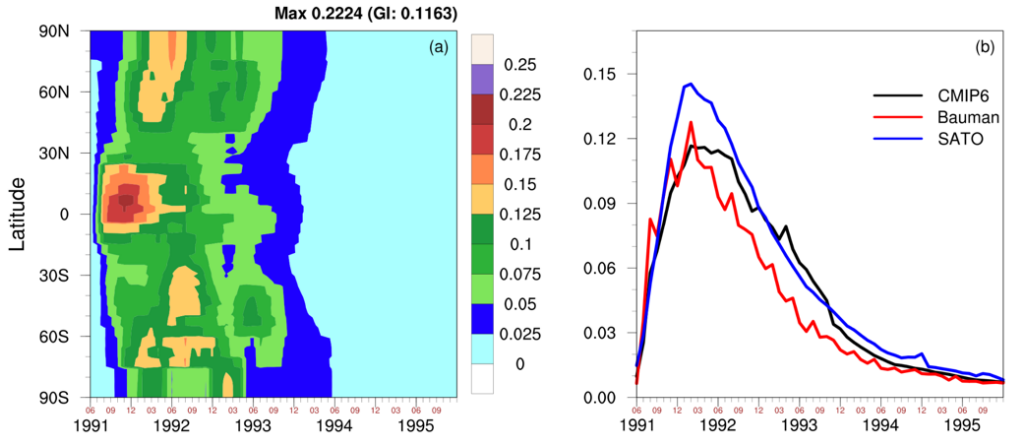

Figure 2. Stratospheric Aerosol Optical Depth at 550 nm (SAOD) over 1991-1995. (a) Latitude-time variations in SAOD as diagnosed in the IPSL-CM6A-LR model after implementation of Thomason et al. (2018) dataset onto the model grid. (b) Monthly time series of global mean SAOD as diagnosed in IPSL-CM6A-LR (back solid curve) compared to datasets derived from satellite instruments (red solid curve; Bauman et al., 2003) and that provided by Sato et al., 1993 (blue curve).

Sensitivity experiments of volcanic effects

Volcanic effects on climate manifest both at earth's surface as a cooling and in the stratosphere as a warming. Our experimental protocol also comprises sensitivity simulations destinated to separate the two effects. To do so, it is enough to call twice the radiative transfer scheme, one with the volcanic aerosols and another without, as illustrated in Fig. 3. The basic simulation, *volc-pinatubo-full*, uses both shortwave and longwave radiative fluxes with volcanic aerosols (representing all interferences of volcanic aerosol) to update the temperature trend. While the *volc-pinatubo-strat* and *volc-pinatubo-surf* sensitivity experiments were respectively designed to represent only the volcanic aerosol perturbations to the total (longwave and near-infrared) radiative heating rates (*volc-pinatubo-strat),* or only perturbations to the surface shortwave flux (*volc-pinatubo-surf*).

In *volc-pinatubo-strat*, the second call to the radiative code is used to diagnose the 3D solar near-infrared (NIR) and terrestrial outgoing longwave (LW) fluxes perturbations, which are then passed on to the model at each radiative transfer time step on top of surface shortwave clear sky (SWcs) fluxes computed during the first call (stratospheric aerosols-free). This procedure allows to take into account the volcanic aerosol radiative heating rates while keeping aerosols-free surface downwelling

SW fluxes (Fig. 3a). In *volc-pinatubo-surf*, the second call to the radiative code is used to diagnose the surface SWcs fluxes which are passed on to the model at each radiative transfer time step along with the first call aerosols-free 3D fluxes (Fig. 3b). This procedure allows to take into account only the reduced surface SW due to increased planetary albedo by volcanic aerosols (and not the climate feedbacks).

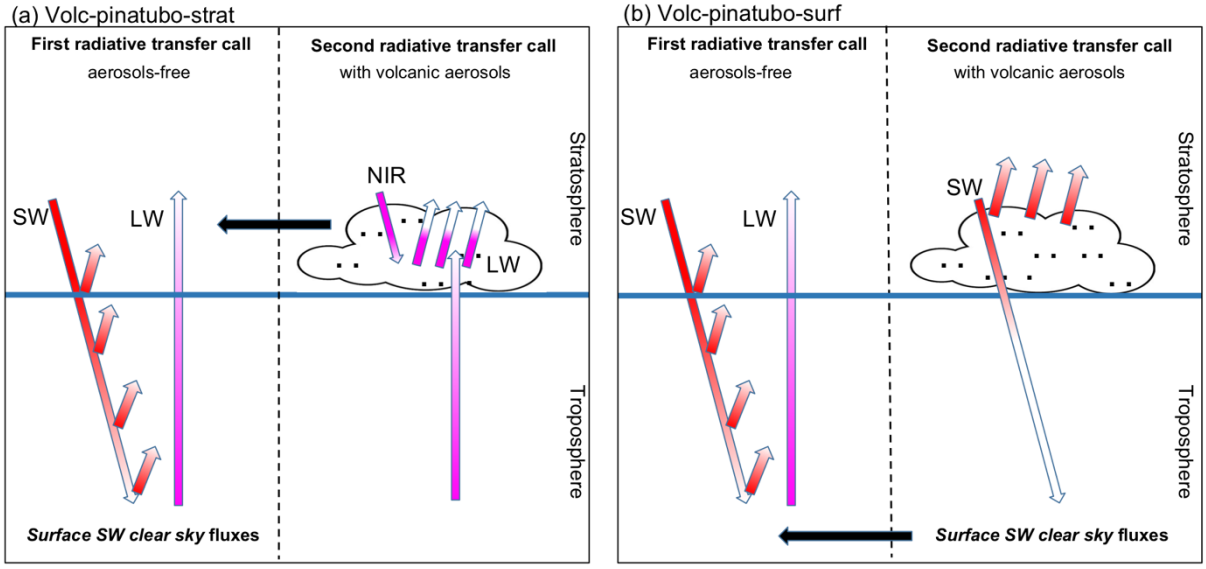

Figure 3. Overview of volcanic radiative forcing implementation of (a) *volc-pinatubo-strat* and (b) *volc-pinatubo-surf* experiments. In both experiments, the first call to the radiative transfer code is aerosol-free and the second call includes volcanic aerosols interference with the radiations. (a) The 3D solar near-infrared (NIR) and terrestrial longwave (LW) fluxes perturbations (purple arrows) diagnosed during the second call to the radiative code are passed on to the model at each radiative transfer time step along with the 3D shortwave (SW) radiative fluxes (red arrows) computed during the first aerosols-free call. (b) The surface SW clear sky fluxes from the second call are passed on to the model at each radiative transfer time step along with the 3D radiative fluxes computed during the first aerosols-free call.

2.3. Reanalysis data

In addition to model outputs including geophysical variables such as air temperature, precipitation rate, wind, sea level pressure and geopotential height, three reanalysis datasets are also used: the NOAA-CIRES 20th Century Reanalysis versions 2 (20th Reanalysis V2, Compo et al., 2011), ERA-Interim reanalysis of the European Centre for Medium-Range Weather Forecasts (Dee et al., 2011) and the National Center for Environmental Prediction (NCEP Reanalysis, Kalnay et al., 1996). Multiple sources of monthly-mean data allow us to cross validate our results.

3. Methods

3.1. Anomalous fields and significance testing

For observational and reanalysis datasets, the anomalies are calculated by removing the 5-year means preceding the Pinatubo eruption, i.e. 1986-1990. For simulations, all anomalies are computed by subtracting the mean seasonal cycle of piControl. This anomaly method does a good job in

identifying and quantifying the most significant volcanically forced response from noisy internal variability, no matter what the initial ocean/atmosphere conditions are.

When the ensemble averages of each volcanic experiment (i.e., *Full*, *Strat*, *Surf*) are compared against the their piControl parent simulation, a two-tailed Student t-test was performed with the number of degrees of freedom corresponding to the total number of members (25+25=50) minus one. This test was applied either at each geographic point or for areal average.

3.2. Climate indices

Two main climate indices are used in our study to monitor climate behaviors of our simulations. They are generally calculated at the level of each individual member, but often expresses as ensemble mean across all members. It is also of general practice to consider the inter-member spread to assess the uncertainty of results with the 90% confidence interval calculated among individual members, according to a two-tailed student t-test. To further evaluate the ensemble-mean trend, we also indicate the cases where at least 2/3 of the members agree and show the same sign.

3.2.1. NAO index

In this study, we calculated the NAO index with the two-box method (Stephenson et al., 2006) applied to monthly sea level pressure (SLP) anomalies. We calculated firstly normalized SLP anomalies in the two boxes covering the subtropical Mid-Atlantic and southern Europe (90°W-60°E, 20°N-55°N) and the North Atlantic-Northern Europe (90°W-60°E, 55°N-90°N) respectively. The NAO index was then simply the difference between these two boxes. The advantage of this methodology is its robustness and low sensitivity to changes of their centers. The results for NAO analysis applying on geopotential height at 500 hPa have also been tested (not shown) and have demonstrated a good resemblance with SLP-based NAO index for both temporal evolution and spatial structure, due to the highly barotropic nature of NAO.

3.2.2. Polar Vortex index

The monthly Polar Vortex Index (PV) is calculated based on the method of Graf et al. (2014) except that we take directly the mean geopotential height anomaly at 50 hPa level over the northern polar cap (north of 65°N). The more negative PV, the stronger polar vortices.

3.3. Meridional temperature gradient

Meridional temperature gradient was calculated for the stratosphere at 50 hPa level from the zonal-mean temperature anomalies for *Full*, *Strat*, *Surf* and *reference* runs. The calculation was done with a simple center finite difference method with respect to every degree of latitude. We name it hereafter dT50. We will concentrate on the Northern Hemisphere for interpreting the meridional temperature gradient.

3.4. Eliassen-Palm flux analysis

To quantify planetary wave propagation under different conditions of external forcing, we calculate the Eliassen-Palm flux (EP flux) based on *Transformed Eulerian Mean* (TEM) equations for quasi-geostrophic eddies (Holton and Hakim, 2013):

$$F_y = -\rho_0 \overline{u'v'}, \qquad F_z = \rho_0 f_0 R \frac{\overline{v'T'}}{N^2 H} \tag{1}$$

where $f_0 = 2\Omega\sin\varphi$ is the Coriolis force, ρ_0 is the air density, N represents the buoyancy frequency, $H = RT_s/g$ is the standard scale height with T_s indicating the global standard average temperature. Primed variables denote *eddies* for zonal wind, meridional wind or temperature. Overbars denote the longitudinally average.

As can be seen in Eq.1, EP flux is a vector in the meridional-vertical (y, z) plane. It involves the eddy fluxes of angular momentum and heat for y and z component respectively: $\mathbf{F} = \{ F_y, F_z \}$. It is believed that the eddy heat and momentum fluxes do not act separately to drive change in the zonal-mean circulation, but only in the combination by the divergence of the EP flux ($\nabla\cdot \mathbf{F}$), which is proportional to the northward meridional fluxes of quasi-geostrophic potential vorticity and expressed by contouring the isolines of the divergence ($\nabla\cdot \mathbf{F}$) (Edmon et al., 1980). Convergent EP flux (negative $\nabla\cdot \mathbf{F}$) is related to intense deceleration of the mean zonal wind and to enhanced poleward residual mean meridional flow in the stratosphere. In contrast, when the EP flux is divergent (positive $\nabla\cdot \mathbf{F}$), the planetary wave propagation is weakened and the mean zonal wind is strengthened.

Monthly fields of temperature and wind were used to calculate the winter EP flux and its divergence of each run to represent the stationary planetary wave activity, which is ultimately important in controlling the eddy heat transport from lower troposphere to upper stratosphere in subtropics (Graf et al., 2007; Li et al., 2011). Figure 4b shows the winter (DJF) climatological EP flux deduced from the piControl run. We also display the counterpart from NCEP data (that can serve as a validation for our simulations, Fig. 4a).

As can be seen in Fig. 4, there are two major branches of EP flux vector for stationary waves and they emerge from the extratropical troposphere. One branch of the vectors starts from the lower troposphere and points upward across the tropopause to the lower and middle stratosphere. This implies the the eddy heat flux dominates the wave activities between the troposphere and the lower and mid-stratosphere, which is also the place prevailed by baroclinic energy (Andrew et al., 1987; Hartmann and Lo, 1998; Holton and Hakim, 2013). Another branch of vectors starts also from the surface but turns equatorward in the upper troposphere. This implies the importance of the eddy momentum flux in the subtropical upper troposphere. During Northern Hemisphere winter, most of the extratropical troposphere shows convergent EP flux, indicating that stationary eddies exert a deceleration effect for the zonal winds.

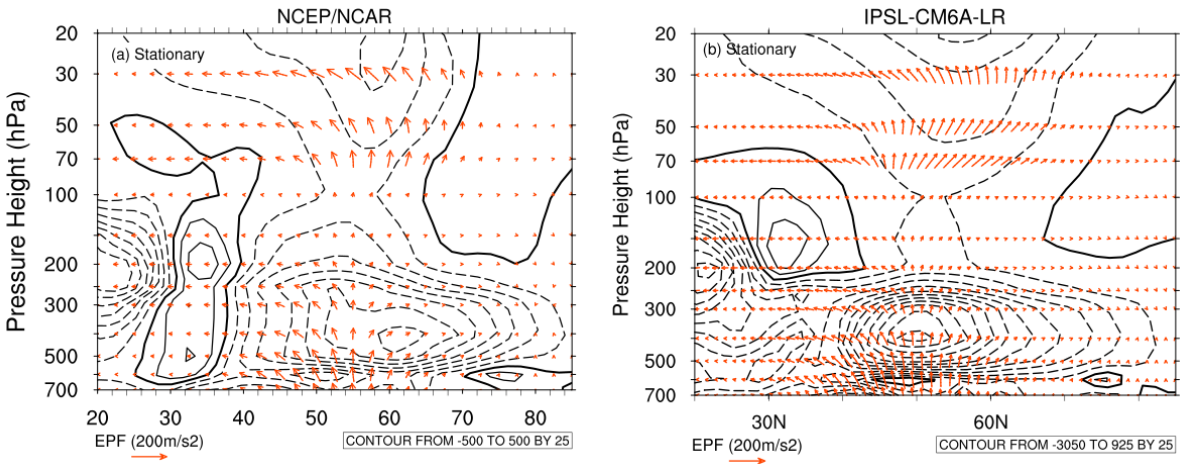

Figure 4: Climatology of Eliassen-Palm flux vector (arrows, units: m/s^2) and its divergence (dashed and solid contours for negative and positive values respectively, units: $m\ s^{-2}$) for Northern Hemisphere winter from **a** NCEP 1986-1990 period, and **b** IPSL-CM6A-LR piControl run.

4. Results

4.1. Time evolution of climate indices after Mt. Pinatubo eruption

In this subsection, we compare the IPSL-CM6A-LR simulation with observational/reanalysis products to evaluate the model's ability in simulating NAO and polar vortex behaviors after the Pinatubo eruption, and also to have a glimpse at the role of the stratosphere warming and surface dimming on modulating the NAO and polar vortex.

All reanalysis data recorded the decrease of global mean surface temperature (Fig. 5a) after Pinatubo eruption, with intensity exceeding -1 standard deviation for more than three years. Strong positive NAO index was observed continuously for the first two winters (DJF 1991/92 and DJF 1992/93, Fig. 5b), which is consistent with a deepened polar vortex during these periods (Fig. 5c) in ERA-Interim and NCEP-reanalysis. The 20th Reanalysis V2 dataset, however, shows larger bias compared to the other two datasets, especially for the polar vortex index. Compo et al. (2011) have reported that there are large uncertainties in 20th Reanalysis V2 dataset for its the upper-layer fields. In the following, we will privilege the NCEP dataset to evaluate our simulations and to assess fingerprints of simulated anomalous climate.

Let's now check whether our climate model is efficient enough to reproduce these emblematic TS/NAO/PV for their time evolution after the Mt. Pinatubo volcanic eruption. Firstly, as expected and displayed in Fig. 5d, the global cooling over land surface is well simulated in *Full* and *Surf*. We observe a slight surface warming in *Strat*, due to certainly the purposely-designed greenhouse effect of the stratospheric aerosols. Our simulations (Fig. 5e-f) successfully capture the strong and significant (90% t-test) positive NAO index along with deepening of the polar vortex for the first winter in *Full*, the experiment including the whole radiative effects of stratospheric volcanic aerosol.

Different from observed NAO time series, the second winter in our simulation shows a significant negative phase of NAO in *Full*, which is consistent with the weakened polar vortex (Fig. 5f, black lines). However, this signal is not robust for following reasons : (1) when we increase the simulation ensemble size from 25 to 49 (not shown), less than 2/3 ensemble members in *Full* produced the weakened polar vortex; (2) when we carry out analysis based on paired ones between each run of *Full* and its corresponding reference run from piControl with same initial states, neither NAO index nor PV signal in the second winter passed the 2/3 member sign consistency test. We suggest a first possible explanation to the weakened to anomalous response of minority members. Other possible explanations will be related to the choice of initial conditions. Albeit we notice both *Surf* and *Full* have a positive NAO tendency in November 1992, they rapidly head to negative NAO phase from December, which hints an influence from surface in the second volcanic winter. The simulation experiment *Strat* reveal positive NAO signals during two winters, but not as significant as *Full*. A similar behaviors applies for the enhanced polar vortex (Fig. 5f, red lines). The NAO index in *Surf* did not show any significant variation in the first two winters (Fig. 5e&f, blue lines). However, it is interesting to notice that during summer 1992 *Surf* tend to deepen the polar vortex (significant positive Z50 anomalies) when *Full* and *Strat* tend to decrease the polar vortex strength, which indicate two different functions in altering the polar vortex from stratospheric warming and surface cooling.

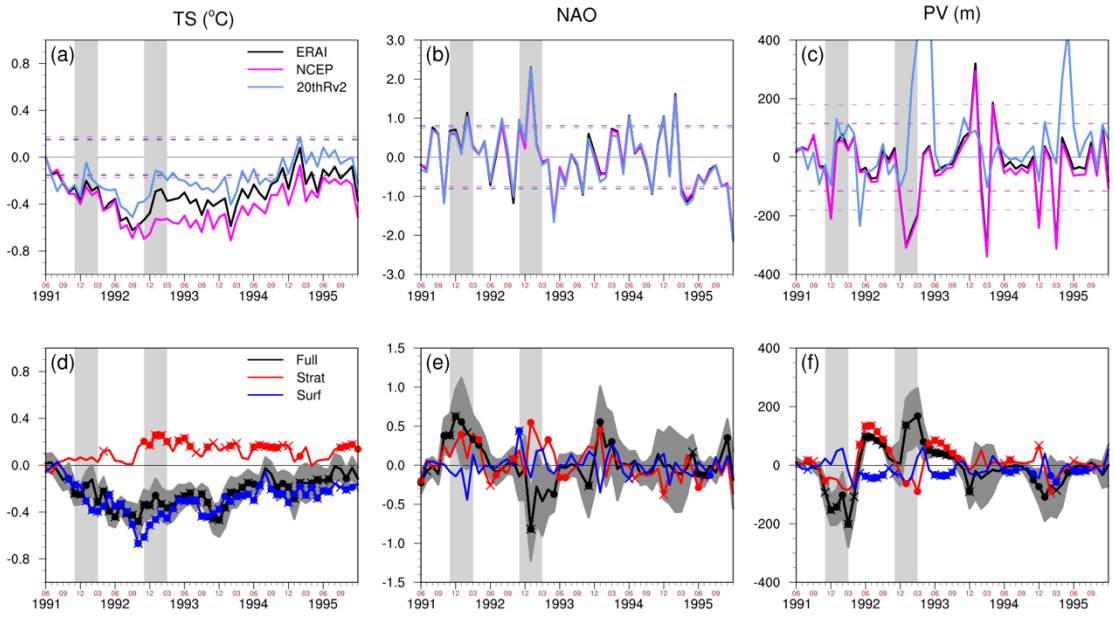

Figure 5: Time series of global mean surface temperature (TS; left panel), NAO index (middle panels) and polar vortex index (right panels) from June 1991 to December 1993 based on sea level pressure from **a- c** Reanalysis data, **d- f** Simulated ensemble runs. Dots indicate respectively that at least 2/3 of ensemble members have anomalies of the same sign. Crosses indicate ensemble mean anomalies are significant compared to piControl at 90% level according to the student t-test.

4.2. Spatial signatures of Northern winter climate

Figure 6 and 7 displays the anomalous fields of SLP, TAS, Pr and Z50 for NCEP reanalysis dataset and *volc-pinatubo* experiment for DJF 1991/1992 and 1992/1993 respectively. The positive NAO phase is clearly shown in sea level pressure with an anomalous dipole of cyclone over Norwegian Sea and anticyclone near the British Isles for both winters in NCEP reanalysis (Fig. 6a and Fig. 7a), the second winter being more remarkable. What comes with a positive NAO is a warmer winter climate over North Europe and the south US in the first winter (Fig. 6b). For the second winter (Fig. 7b), we can observe a wave train structure across North America, while Europe remains very close to the first year. It is also clear that westerly jets around 60°N is enhanced slightly northward shifted. We observe humid winter in North Europe and dryness in the southern flanks of the westerlies, especially in the Mediterranean area (Fig. 6c and Fig. 7c). The significant westerly jet enhancement (compared with 1986-1990 mean state) from the North Atlantic to Scandinavian can carry humid maritime air, which gives good explanation for the precipitation pattern. As for the polar vortex, the first winter (Fig. 6d) see moderate enhancement, with an average of around -80 meters in the Northern cap 65°-90°N in the stratosphere, while there is a firm enhancement for the second winter (an average of more than -200 meters) (Fig. 7d).

Our simulated results reveal strong volcanic influence on main climate and circulation regimes in the North Atlantic-Europe sector in the first winter after Pinatubo eruption. Coherent with reanalysis data, an important cooling is reproduced in South Europe, the Middle-East and Greenland in the experiment *Full*, whilst an important warming is detected in North Europe, the Barents Sea and Siberia (Fig. 6f). The warmer temperature anomalies observed and simulated over Eurasia and Scandinavia after Pinatubo eruption is a typical situation of positive NAO with westerly anomalies around 60°N, responsible for the rainfall augmentation in North Europe and diminution in southeast region of Central Europe. This north shift of the westerlies leaves consequently more places for easterly anomalies occurring in the southern area thereby bring drier continental air to South Europe (Fig. 6g). This atmospheric circulation is directly resulted from the dipole pattern of sea level pressure anomalies with lower pressure center over Svalbard Island and Arctic and higher-pressure center over the North Atlantic (Fig. 6e). Compared with the simulated results from *Strat* and *Surf*, we can see that the positive phase of NAO is principally contributed by the enhancement of the polar vortex (Fig. 6h) in response to the increase of lower stratospheric temperature by aerosols absorbing LW radiation. In fact, the experiment *Strat* (Fig. 6i-l) also simulates similar anomalies which project on the positive NAO phase as in *Full*. In contract, the experiment *Surf* (Fig. 6m-p) projects more likely a negative NAO which suggests a destructive effect in reinforced polar vortex when solely cooling the surface and troposphere. The Northern Hemisphere is more sensitive to radiation reduction in *Surf* due to the fact that land responds more quickly to radiation perturbations (Fig. 6n).

However, the nonlinearity between surface and upper layer interaction seems to reverse the sign of surface-induced contributions and reproduce a stronger positive NAO simulated in *Full*

experiment with combined effects from stratosphere heating and surface cooling than in *Strat* which solely heats the stratosphere. The comparison between the sum of *Strat* and *Surf* (Fig. 6q-t) anomaly responses and that of *Full* experiment further confirms this assumption. It reveals in fact significant differences, especially the addition of *Strat* and *Surf* is weaker compared with the interactive results of volcanic aerosols forcing on radiative effects simulated in *Full*. Further studies will be needed to identify these nonlinear processes. Nevertheless, our results suggest that: (1) the stratospheric heating due to volcanic aerosols infrared absorption dominates the response of winter climate over the North Atlantic-Arctic region in the first winter after the Pinatubo eruption; (2) the only cooling surface effect does not seem to be able to produce a significant positive NAO pattern, which is not totally supportive to Stenchikov et al. (2002); (3) the surface cooling's role in influencing the polar vortex is a destructive effect when it is alone, while a constructive effect when it acts jointly with the stratospheric heating.

In the second winter after the 1991 Pinatubo eruption, cold anomalies are found for almost the whole Northern Hemisphere continent except over Greenland in the experiment *Full* (Fig. 7f). The precipitation endures a decrease over North Europe which can be explained by the easterly anomalies carrying drier air from the continent to the North Atlantic. In contrast, southern Europe is more humid with enhanced westerly anomalies carrying more moisture from the North Atlantic (Fig. 7g). This dipole precipitation anomaly is in agreement with the simulated negative NAO index in Fig. 5e, which can be shown by the sea level pressure anomaly dipole in Fig. 7e. The increased sea level pressure in higher latitudes around the arctic is of barotropic structure accompanied with a weakened polar vortex (Fig. 7h). The polar vortex diminution hints at a breaking of polar night jets and is responsible for the negative NAO we simulated. In comparison, a weak positive NAO is continuously simulated in the experiment *Strat* (Fig. 7i-l), revealing certainly that the different mechanisms operate in *Full* and *Strat* in the second winter after Pinatubo eruption.

During this period, *Surf* still shows a global cooling of surface temperature (Fig. 7n), especially over the Labrador Sea and Barents Sea, along with significant dryness over these two regions and increased northerly anomalies from the Barents Sea through the Denmark Strait to the North Atlantic (Fig. 7o). Furthermore, surface temperature meridional gradient demonstrates in *Surf* an increasing negative trend between the Tropics and the North Pole in the second winter, which should result in an increase of vertical wave activity flux into the troposphere and the lower stratosphere compared with the first winter. Again, the significant anomalies for sea level pressure and geopotential height are mainly located in low- and mid- latitudes (Fig. 7m&p), which implies that it is insufficient to reproduce a positive NAO post-eruption winter by cooling the surface alone. It is worthwhile to note that the addition of *Strat* and *Surf* is far from similar compared with the second winter simulated in *Full*, except the cooling pattern in South Greenland. This distinction stresses again the nonlinear relationship between the stratosphere and surface (Fig. 7q-t).

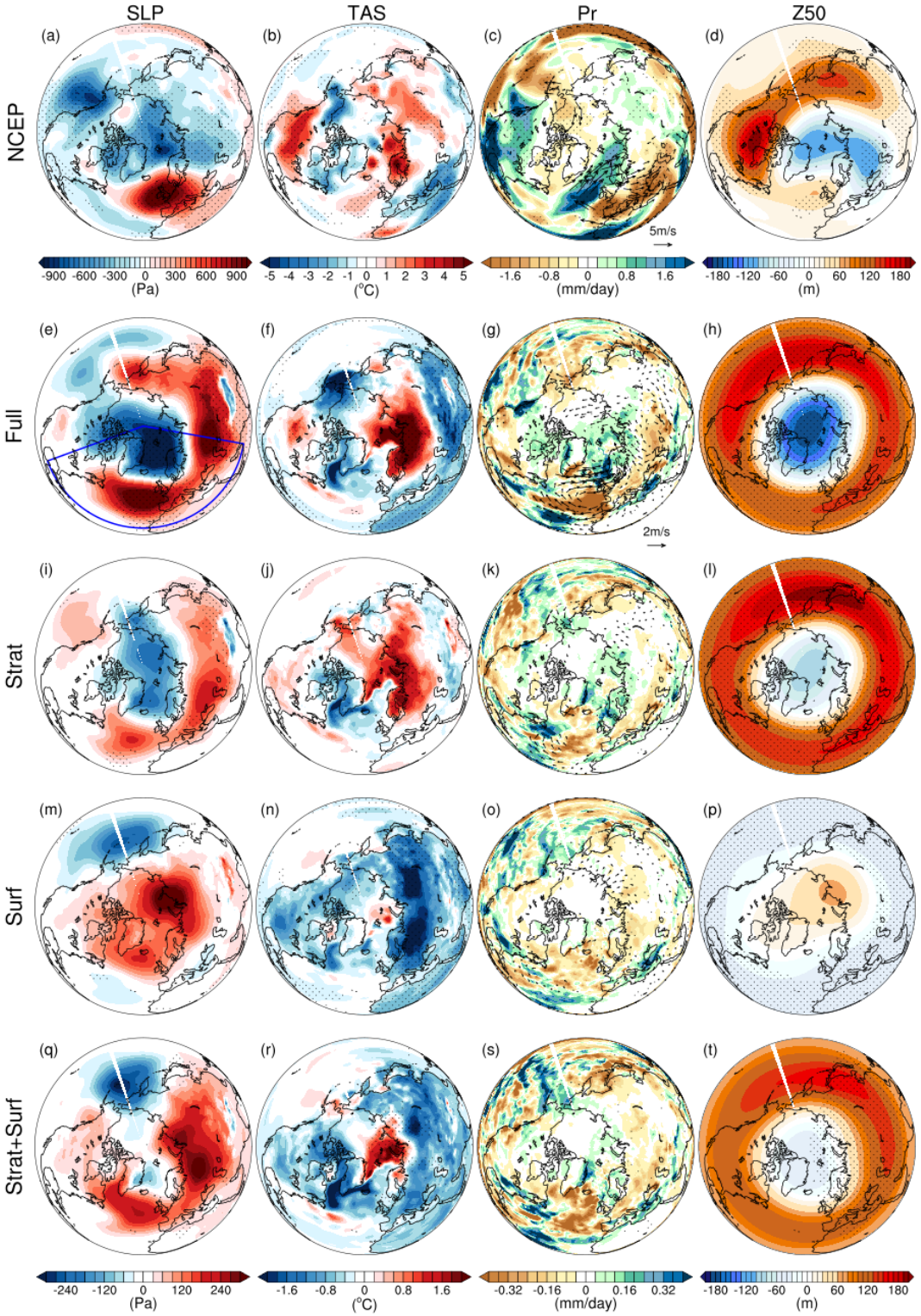

Figure 6: The simulated results of the North Hemisphere climate anomalies at surface and stratosphere in the 1st (DJF 1991/92) winter after 1991 Mt. Pinatubo eruption for **a-d**: NCEP reanalysis, **e-h**: *Full*, **i-l**: *Strat*, **m-p**: *Surf*, and **q-t**: *Strat+Surf* in terms of surface air temperature (TAS), Precipitation (Pr), Sea level pressure (SLP) and geopotential height at 50 hPa (Z50) from left to right column. The dotted area are significant anomalies compared with piControl based on two-tailed t-test at 90% confidence level.

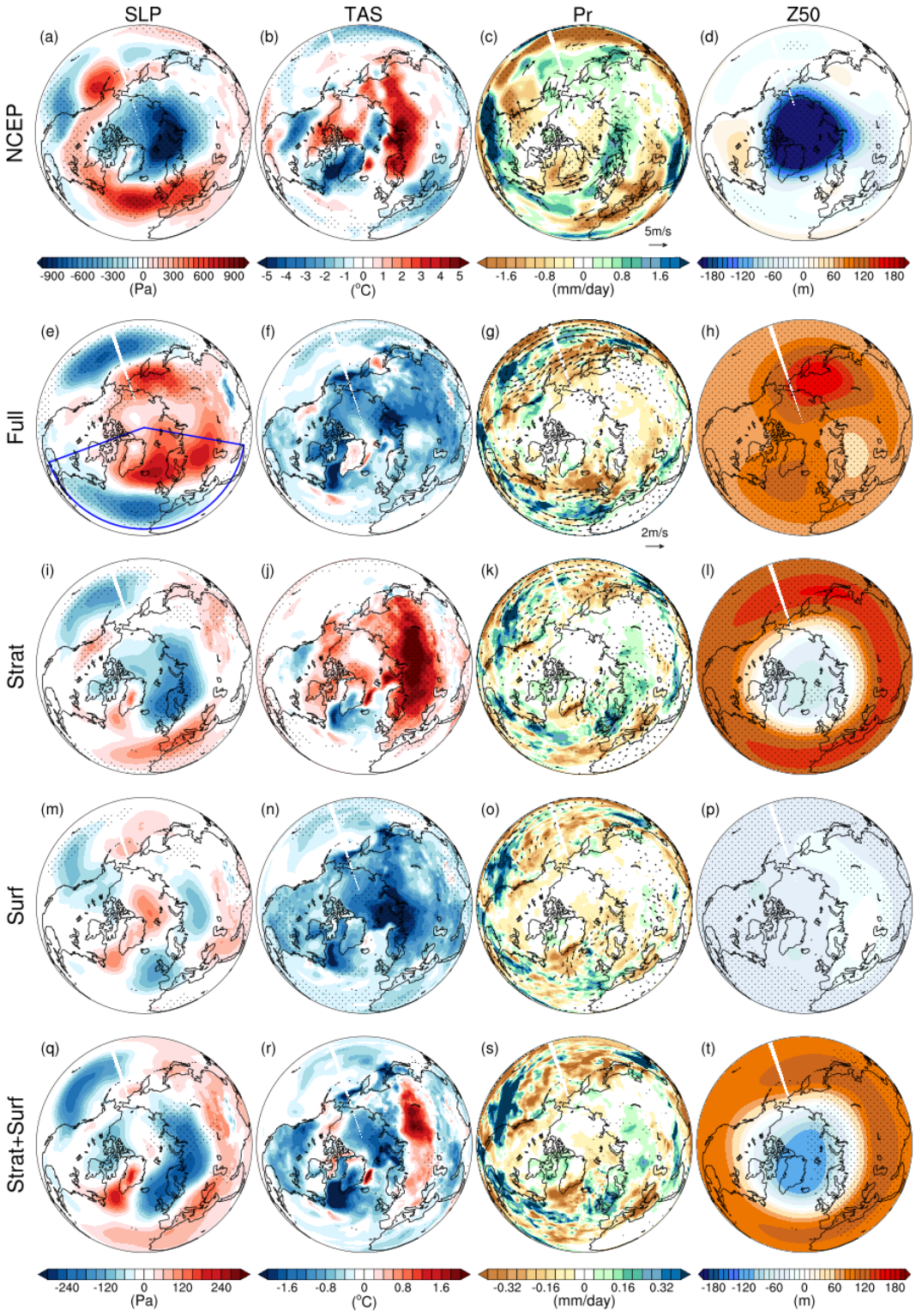

Figure 7: Same as **Figure 6**, but for the 2nd (DJF 1992/93) winter.

4.3. Vertical cross section

Here we investigate the radiative impacts of Pinatubo eruption and atmosphere dynamics.

Firstly we plotted the aerosol-related SW, LW and SW+LW radiation heating rates for the *Full* experiment during two winters when updating the temperature trend of Pinatubo eruption (Fig. 8). As can be seen in, the primary climatic impacts of volcanic aerosols are the reflection of solar SW radiation, which decreases the SW radiative flux at the Earth's surface (Fig. 8a&d), and the absorption of near-IR from solar and IR from the surface, which heats the stratosphere (Fig. 8b&e). The net radiative forcing of aerosol forcing can be seen in SW + LW (Fig. 8c&f) with generally weaker effects in the second winter than in the first winter.

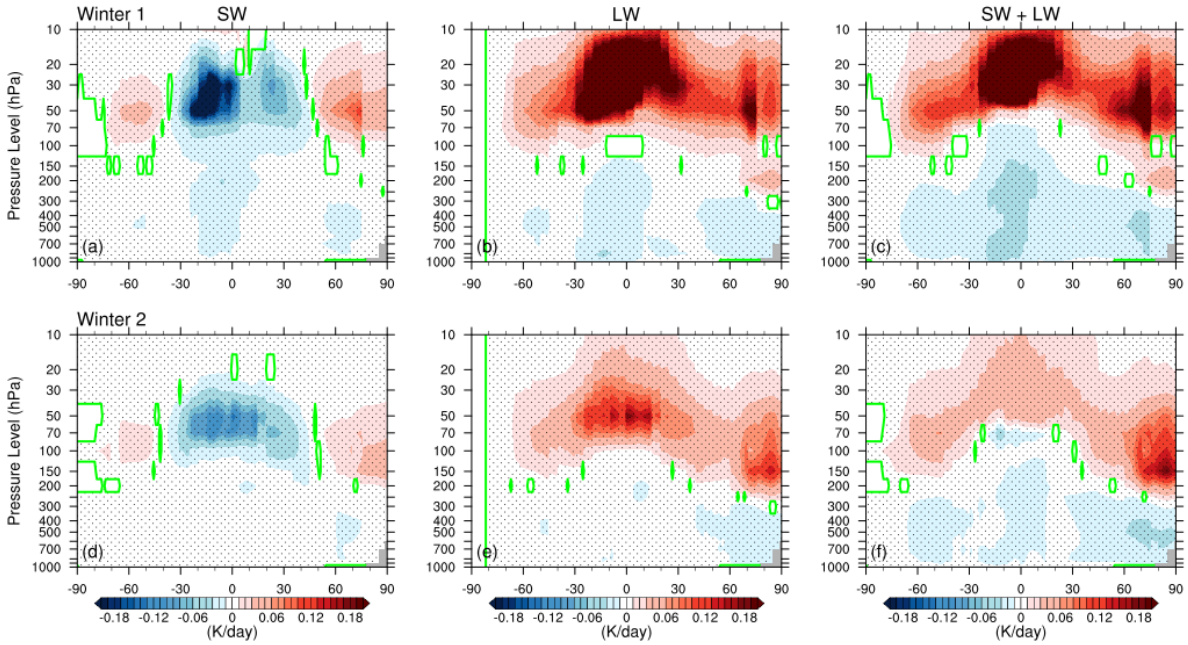

Figure 8: Latitude-Pressure Height cross sections of aerosols radiative heating rates computed within *Full* experiment in the first (upper) and second (lower) winter for **a-d**: SW, **b-e**: LW, **c-f**: SW+LW.

To better explore the atmospheric circulation structure in different experiments, the latitude-pressure height cross sections of temperature, zonal wind and geopotential height anomalies are analyzed in the following section for *Full*, *Strat* and *Surf* (Fig. 9 and 10).

In the first winter for *Full* and *Strat* runs, the radiative effects of volcanic aerosols (Fig. 8) directly lead to positive anomalies of the stratospheric temperature in the tropical and subtropical areas (Fig. 9a&d). In contrast, the northern sub polar demonstrates anomalous cooling which indicates a dynamic process rather than radiative effect is at play in this region. Since injected aerosols reach firstly the tropical stratosphere, they induce strong meridional temperature gradient in the stratosphere between tropical areas and the north pole, which radiatively contributes to the increase of geopotential height (Fig. 9c&f) at low- and mid- latitudes whilst dynamically contributes to the decline of geopotential height over the arctic region. The development of strong polar vortex in turn enhances the westerly jets around 60°N which penetrate from the stratosphere till the surface (Fig.

9b&e), a positive NAO pattern emerges. Consequently, North Europe encounters a relatively warmer and wetter winter due to the northward strengthening of the westerlies in the Northern Hemisphere.

Concurrently, the enhancement of stratospheric westerlies with an anomalous amplitude larger than 10 m/s can efficiently isolate the polar region from the stratospheric warming by sulfate aerosol. Moreover, the westerlies prevents the subpolar and polar stratosphere from influences of tropospheric wave activity flux (which will be discussed in Section 4.4 in Fig. 12).

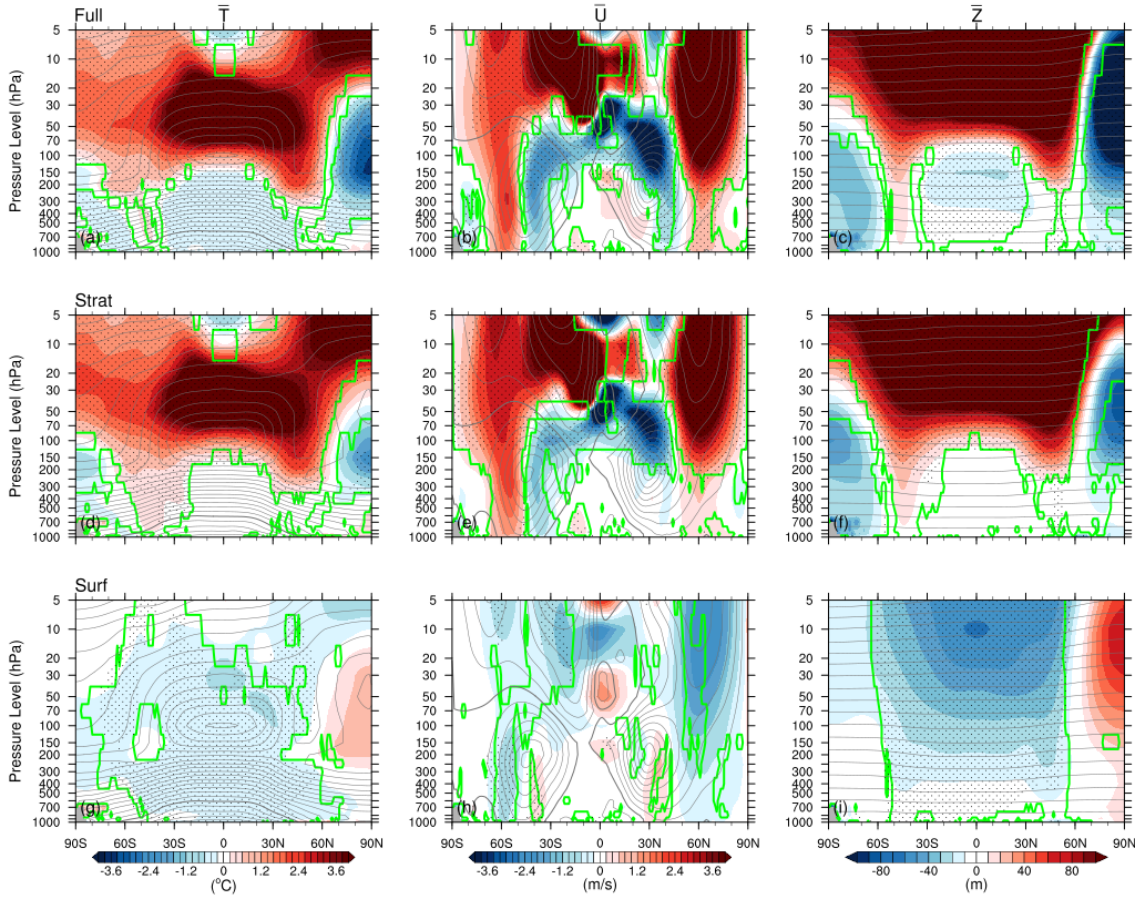

Figure 9: Latitude-Pressure Height cross sections of simulated zonal mean paired anomalies in the 1st winter (DJF 1991/92) for **a-c** *Full*, **d-f** *Strat*, **g-i** *Surf*, in terms of air temperature ($\overline{T}$), zonal wind ($\overline{U}$) and geopotential height ($\overline{Z}$) from left to right column. The stippled area are significant anomalies compared with piControl based on two-tailed t-test at 90% confidence level. Anomalies with more than 2/3 ensemble members agree on sign are enclosed by green contours. The climatology from piControl are plotted in gray contours with incident of 5°C, 5 m/s and 2000 m respectively for air temperature, zonal wind and geopotential height. Thicker lines are Zero contour.

The temperature anomalies in *Surf* runs are marginal in the polar region (Fig. 9g) while significant cooling happens in the tropics and subtropics throughout the whole atmospheric column. The westerlies at 60°N largely decrease (more than 2/3 ensemble runs agree) but are not statistically significant (Fig. 9h), so does the weakening of the polar vortex (Fig. 9i). However from the significant reduction of geopotential height and temperature at low- and mid-latitude areas we can conclude that the surface plays an important destructive role in decreasing the meridional

temperature gradient in the stratosphere, hence a destructive effect to the polar vortex when cooling the surface alone, which is conversely a constructive function when interact with stratosphere heating together in *Full*.

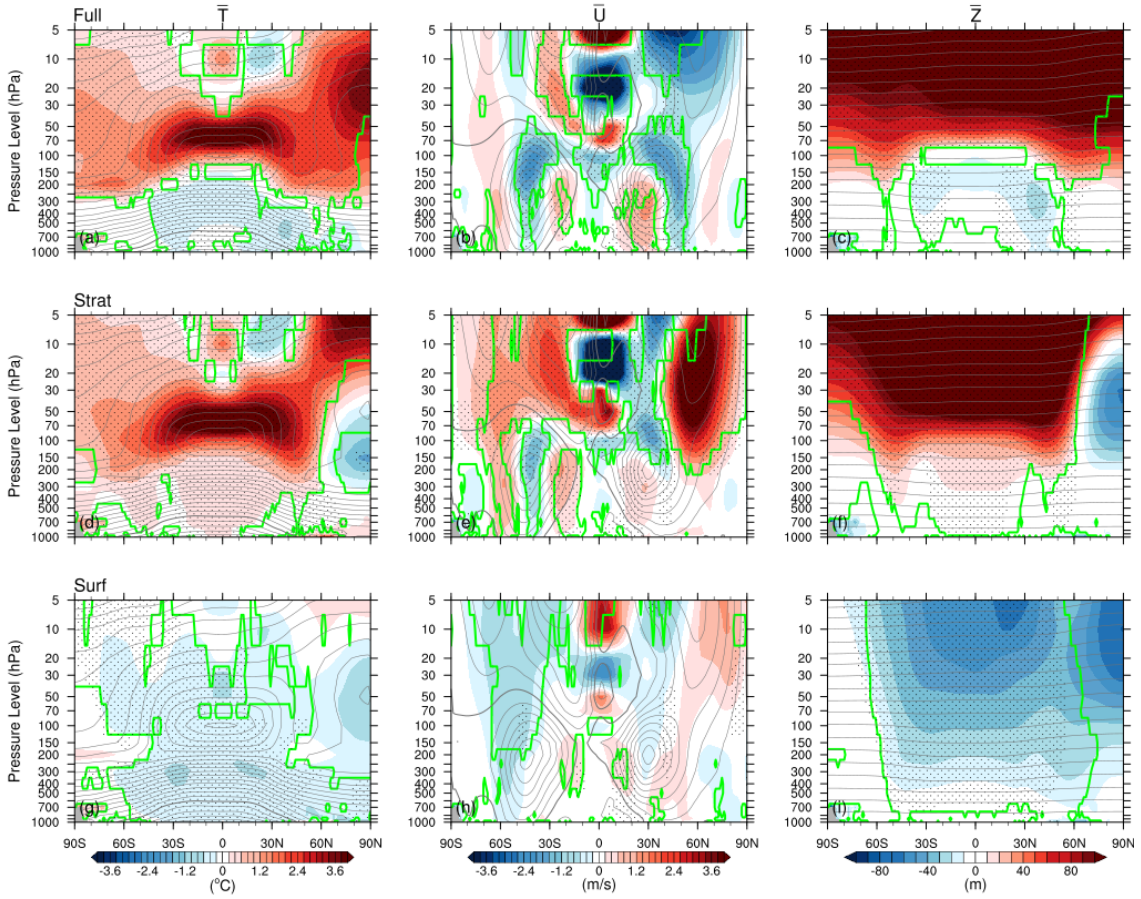

Figure 10: Same as **Figure 9**, but for the 2nd winter (DJF 1992/93).

In the second winter (DJF 1992/93), sudden stratospheric warming (SSW) happened in the arctic and the strong polar vortex disappeared (Fig. 10a&d) for the experiment *Full,* which differed from the continuous cold North Pole and deepening of polar vortex in the *Strat* experiment (Fig. 10b&f). The weakening of polar vortex directly changes the atmosphere circulation in the northern middle and high latitudes in *Full* and entails the southward migration of the westerlies over the North Atlantic, thereby easterly wind anomalies emerge around 60°N (Fig. 10b). A colder and drier winter thus invades North Eurasia. As for the *Strat* experiment, the meridional temperature gradient in the stratosphere (even though weaker than its first winter) is able to maintain the polar jets and the positive phase of NAO in the North Atlantic-Europe sector. The second winter latitude-height fields for *Surf* experiment (Fig. 10g-i) are similar to their counterpart in the first winter except a few insignificant anomalies in the polar area.

We tend to conclude the lack of surface cooling configuration in the experiment *Strat* makes the meridional temperature (anomaly) gradient pattern change, and makes the tropospheric wave drugs weaker than that in *Full,* and consequently the polar vortex does not disappear in *Strat* in the second winter. It is also likely that there is stronger wave propagation for *Surf* in the troposphere in the second winter as compared to the first winter, due to enhanced meridional temperature gradient. Hereafter the respective meridional temperature gradient and planetary wave propagation for each experiment in two winters will be investigated in Section 4.4 and 4.5 respectively to elucidate the mechanisms behind the volcanic forcing induced atmospheric dynamics and climate anomalies.

4.4. Meridional temperature gradient

It has been supported by the thermal wind relation that the meridional temperature gradients at atmopshre are important in explaining the northern polar vortex strengthening after important volcanic eruptions (Perlwitz and Graf, 1995; Kodera, 1994; Kodera et al., 1996; Shindell et al., 2001; Stenchikov et al., 2002). In quasi-geostrophic scaling (small Rossby number), the atmosphere is in good thermal balance and the zonal-mean wind response is given by:

$$f\frac{\partial \bar{u}}{\partial z} = -\frac{R}{H}\frac{\partial \bar{T}}{\partial y} \quad (1)$$

where overbar indicates zonal mean, u and T are perturbations from piControl mean.

It is interesting to notice from equation (1) that the temperature meridional gradient ($\partial\bar{T}/\partial y$) is important in modulating the vertical shear of zonal wind. The more negative $\partial\bar{T}/\partial y$ is at mid-to-high latitudes, the stronger westerly jets will be in the Northern Hemisphere. Hereafter we plotted the latitude-pressure height crosse section of meridional gradient for zonal mean of temperature anomalies to interpretate the results (Figure 11).

The meridional gradient of upper troposphere to stratosphere shows significant negative peak around 60°N in the first winter for both Full and Strat experiments, which are almost overlapping with the significant westerly jet anomalies (Fig. 9b&e). Moreover, the meridional gradient of temperature anomaly (Fig.11a) for these two experiments have undergone continuous amplification in negative direction from 10°N northward, with the strongest ensemble mean anomalous meridional temperature gradient at stratosphere (50 hPa) occurring at 30°N. This indicates a decreasing of temperature anomalies equator northward. Bittner et al. (2016) have suggested the direct response of the zonal wind field to this meridional temperature anomaly gradient pattern (i.e., dT50 peaks at 30°N) is a positive wind anomaly in the subtropical stratosphere, which however, is not observed in our *Full* and *Strat* experiment. Nevertheless this is explicable considering that we have different meridional temperature gradients at 50 hPa (dT50) compared with Bittner et al. (2016). We produced decreased but still positive anomalous temperature gradients from tropical to mid-latitudes (Fig.11b) while they produced a quite negative temperature anomaly gradient at 50 hPa pressure level (their Fig. 5). Therefore based on our simulations, we propose that a decreasing positive meridional

temperature gradient from tropical to mid-latitudes while a more negative gradient at upper troposphere and stratosphere are essential in producing significant westerly anomalies at 60°N in the first winter. If we look at this gradient during the second winter (Fig. 11b), we can observe the *Full* experiment only has significant decreasing positive gradient from the tropics to mid-latitudes while without significant increasing negative temperature gradient, differing from *Strat* which keep in a large degree the first winter pattern. Hence *Full* has produced different zonal wind anomalies in the second winter, while *Strat* occupies similar zonal wind anomalies between two the winters (Fig. 11c&d).

The gradient difference should be treated very carefully by comparing also with the experiment *Surf*. Even though forced by decreased shortwave radiation, basically *Surf* did not pass the ±0.5$\boldsymbol{\sigma}$ interval of piControl reference runs. Only several latitudes have demonstrated significant differences from piControl. Subtle differences can be found for *Surf* at surface between its first winter and second winter with a strengthened cooling at surface in North Hemisphere mid-to-high latitudes in the second winter.

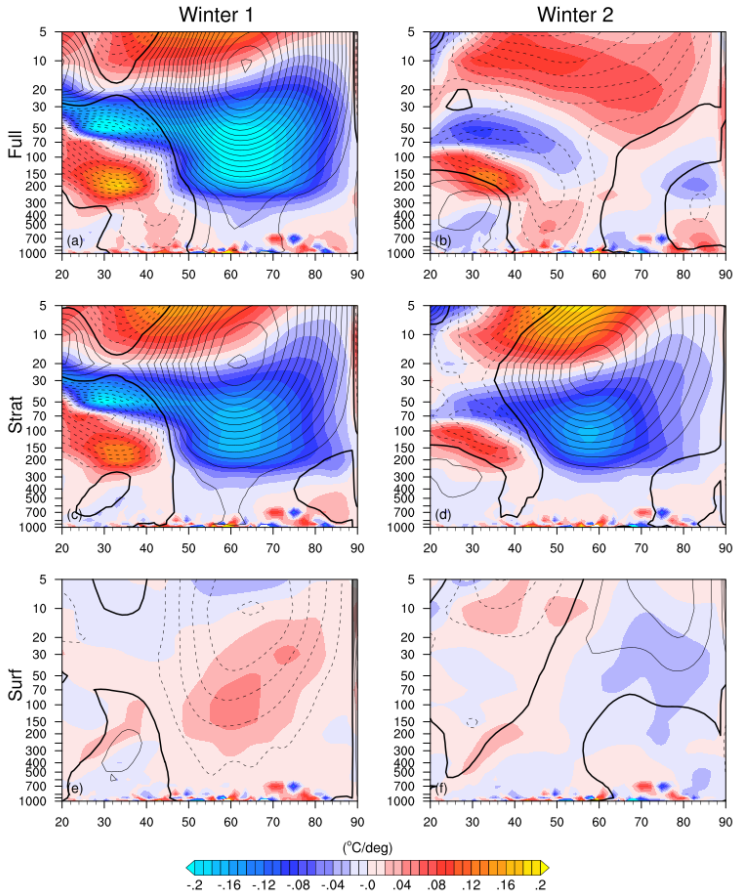

Figure 11: Latitude-Pressure height cross section of zonal mean temperature anomaly gradient averaged over 1st winter (DJF 1991/92) and 2nd winter (DJF 1992/93) respectively for **a-b** *Full*, **c-d** *Strat*, **e-f** *Surf*. The contour lines are corresponding zonal wind anomaly. Units: °C/deg.

At stratosphere (around 50 hP height), the *Surf* also displayed higher positive tendencies in mid-to-high latitudes in the first winter (Fig. 11e) than in the second winter (Fig. 11f). Thereby the *Surf* experiment may have distinct functions in thermal transport and wave propagation from *Full* and *Strat*. This phenomenon in a large degree disagrees with Stenchikov et al. (2002) who stated that winter-season meridional distribution of aerosol radiative cooling in the tropics is favorable to reduce the meridional temperature gradient between tropics and midlatitudes with most significant decrease between 30°N and 60°N.

4.5. EP flux and stationary planetary wave propagation

The wave breaking (or reflection) and weakening polar vortex in Full in the second winter are possibly partly caused by the surface forcing. We will look in detail at the stationary planetary wave propagations for each experiment.

As explained before, the experiment piControl gives a reference of the winter climatology. The main feature in Northern Hemisphere winter is a westerly jet with its maxima of more than 40 m/s in wind speed occurring around 200 hP pressure level (gray contours in Fig. 9&10). This wind can reach down to the troposphere at 30~40°N. At the same time, these polar jets provide wave guidance for the vertical propagation of quasi-stationary planetary waves. A boreal winter shows two branches of EP flux vectors, with one heading upward to transport eddy heat fluxes from troposphere to stratosphere and another heading equatorward in the mid-troposphere to transport eddy momentum fluxes to tropics. While the EP flux convergence (negative values, can be seen in Fig. 4) occasionally can lead to rapid deceleration of the mean zonal flow and at some point may cause a sudden stratospheric warming in the polar region. Normally, if the flow becomes easterly, waves can no longer propagate vertically and radiative cooling processes are able to restore slowly the usual cold North Pole (Holton and Hakim, 2013).

Figure 12a-b reveal the EP flux behaviors in *Full* experiment under full volcanic radiative effects (i.e. stratospheric warming and surface cooling) during the two winters. In the first post-eruption winter, the westerlies are strengthened (increasing more than 5 m/s in the upper stratosphere, see Fig. 9b) and also move around 20° northward in the troposphere, which contributed by a direct influence from the meridional temperature gradient in the stratosphere. The divergent flank of EP divergence (Fig. 12a) is overlapped with only parts of increased polar jets in *Full* and *Strat*. More jets are overlapped with EP convergences which indicate a stronger wave drag. Moreover, the EP flux anomalies (Fig. 12a) bring extra information about the volcanic radiative forcing. While the eddy heat fluxes transport have strengthened from subtropical mid-troposphere to stratosphere (upward red arrows), the eddy momentum flux produce a more equatorward planetary wave propagation (arrows in 20~40°N troposphere and also in the stratosphere from 200 hPa to 10 hPa). This equatorward deflection of wave propagation hence transports more planetary waves to the equator than to the arctic even if we have convergence of EP flux at mid-latitudes and around 55°N from surface to

troposphere (Fig.12a, dashed contours). In the study of Bittner et al. (2016), they suggested that if more equatorward waves are produced, less waves would break at high latitudes where the divergence of the EP flux and the deceleration of the polar vortex are reduced. Hence by applying EP flux, they proposed that strengthening of the polar vortex in late winter (February-March) after volcanic eruption is not solely an effect of the increased temperature gradient acting directly on the polar vortex but also an equatorward deflection of planetary waves propagation. Nevertheless, their findings are more significant for Tambora simulations than their Krakatau-Pinatubo simulations, which qualify in other ways the improvement of our Pinatubo simulation analogs.

In the second winter of *Full* (Fig. 12b), we can observe the convergence of EP flux finally make the wave propagating from surface to subpolar stratosphere with a strong poleward EP flux in the troposphere. This represents an enhanced eddy momentum fluxes propagating poleward. Under this background the zonal westerlies endure a decrease of more than 2 m/s in the stratosphere of mid-high latitudes (40~60°N) (Fig. 10b). Whereas the westerlies get stronger in the sub-tropics troposphere due to the negative NAO phase.

Both winters in *Full* have increased convergence of EP and upward EP flux from troposphere to stratosphere. This is in agreement with Graf et al. (2007) showing that in volcanic winters the vertical EP flux is enhanced compared to normal winters and would reduce the energy that can be reflected downwards from the upper stratosphere. This finding, however, contradicts Stenchikov et al. (2002) who proposed otherwise a slight reduction of vertical EP flux at 400 hPa in the latitude band 30~60°N.

The *Strat* experiment has rather similar pattern of EP flux and divergence with *Full* in the first winter (Fig. 12c). While in the second winter (Fig. 12d), there are also poleward EP flux in the troposphere, but smaller than that observed in *Full*. Divergent zone is also observed in subpolar stratosphere. This represents the planetary wave deceleration effects is much weaker in *Strat* than in *Full*.

While the upward EP flux and its convergence of *Surf* is most visible at lower troposphere during two winters (Fig. 12e, f), significant poleward EP flux and convergence can be found in mid-latitude stratosphere in the first winter (Fig. 12e), indicating a smaller deceleration effect from surface cooling.

Even though the model IPSL-CM6A-LR is able to produce a robust winter warming and enhanced polar jet in the first volcanic winter, our *Full* experiment seems to encounter an easier wave breaking in the second winter, which in other hand, is not the case for the *Strat* experiment. For *Strat*, the first winter (Fig. 12c) is in high resemblance to the *Full* experiment which validates a stratosphere-dominating process in the first winter right after volcanic eruption. However, in the second winter (Fig. 12c) , we can observe the EP convergence is far less extended in *Strat* as compared with *Full*. The EP flux also has less poleward direction in the troposphere than in *Full*. By carrying this comparison, we infer that in the second winter *Full* experiment lose a strong polar jet

because of more planetary wave energy being carried to the troposphere and lower-stratosphere than *Strat* does, which hint at a surface cooling influence (surface cooling is the only difference between *Full* and *Strat* experiment settings).

We can disentangle the surface cooling effects from *Surf* experiment results. Distinct from Stenchikov et al. (2002) who suggested cooling surface would reduce the meridional differential heating at surface and lead to less vertical planetary wave energy flux, we did not observe decrease of EP flux vertical component whereas we witnessed an increased upward EP flux along with anomalous convergence of EP flux confined to the lower troposphere in two winters, indicating an important heat eddy transport from lower troposphere to upper troposphere. As for stratosphere, we only observe a small convergent region with poleward EP flux during the first winter, representing a deceleration effects for westerlies due to enhanced poleward transport of eddy momentum.

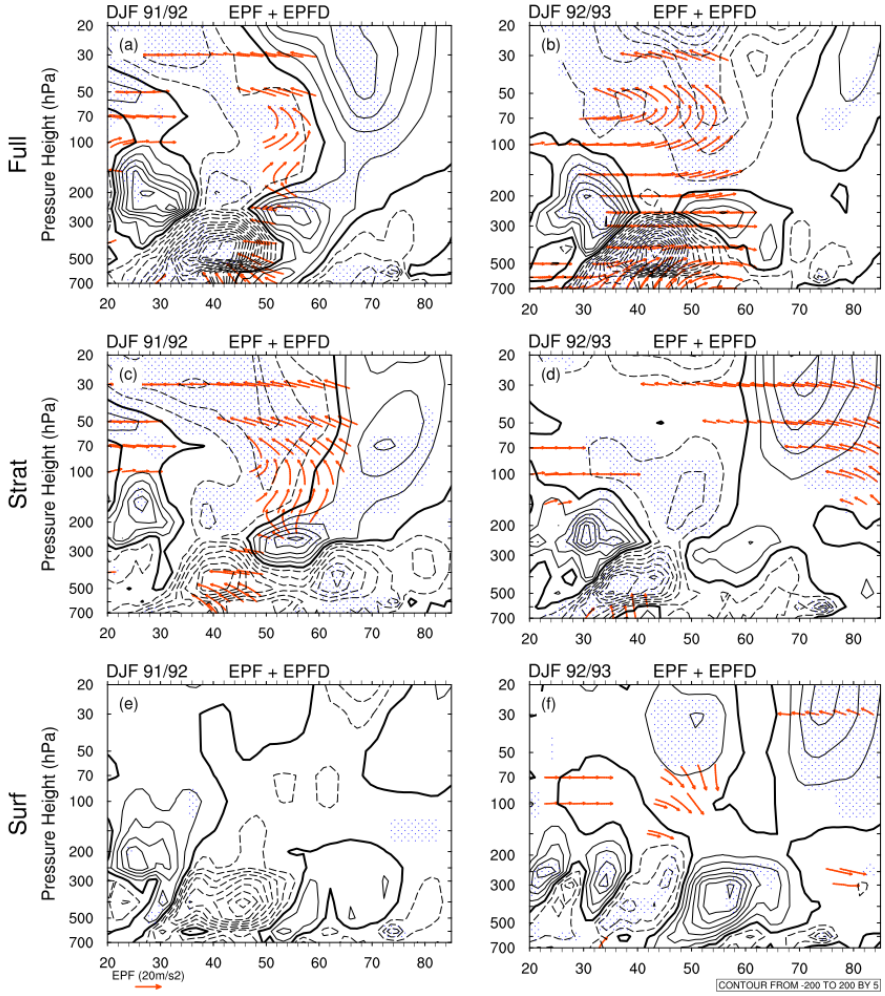

Figure 12: Latitude-Pressure Height cross sections of simulated EP flux anomalies and EP divergence anomalies in the first (left panel) and second (right) winter after 1991 Mt. Pinatubo eruption for **a** and **b** *Full*, **c-d** *Strat*, **e-f** *Surf* experiment. Only significant(90%) anomalies of the EP flux vectors are shown in arrows. Ensemble means of EP divergence are drawn with thin solid (positive) and dashed (negative) contours. Significant (90%) EP flux anomalies are stippled.

The *Surf* experiment actually can serve as a good but reverse climate change configuration compared with present climate warming consensus. By studying *Surf* in more details in the upcoming work, we can explore if cooling the surface can offset specific adverse effects from climate warming, e.g. an easier breaking polar vortex and colder Europe winter. For the moment, it is demonstrated by Fig. 12e&f that: (1) surface cooling effects on planetary wave propagation are different in sign and strength during the two winters in subpolar troposphere and stratosphere; (2) planetary wave transport in the mid-troposphere in *Surf* has dipolar pattern in mid-latitudes in the second winter.

5. Discussions

5.1. Surface cooling effects

With the backscattering effect of stratospheric aerosol loading, volcanic eruptions can directly cause cooling of the Earth surface which may persist for more than two years. The surface cooling is accompanied with changes in surface meridional temperature gradient, which was considered by Stenchikov et al. (2002) as the key factor to provoke the polar vortex acceleration in post-eruption winters. In our study, based on the winter climate (Section 4.2) and meridional temperature gradient (Section 4.4) analysis in our *Surf* experiment, we find by solely imitating the SW decline effects of volcanic eruption cannot reproduce a significantly stronger polar vortex, nor the positive phase of NAO. We attribute this result to the fact that the post-eruption positive NAO winter is more a stratosphere-dominant process. Furthermore, the surface cooling has different roles between when it is alone and when it is interactive with stratosphere thermodynamics. This dynamic interaction between stratosphere and surface is nonlinear therefore we even have stronger positive NAO signal in *Full* than in *Strat*.

When studying the stationary eddies and planetary wave propagation in the *Surf* experiment, we observe significant EP convergence at mid-troposphere in the first winter. Nevertheless, this planetary wave strengthening cannot alter the climate system to modulate the NAO phase except by interacting with stratosphere heating effects.

5.2. Stratospheric warming effects

Our experiments verify the “stratospheric mechanism + wave reflection” (Graf et al., 1993; Graf et al, 2007; Bittner et al., 2016) by model validation for *Full* and *Strat* experiments. The warming of the lower stratosphere indeed strengthens the meridional temperature at the stratosphere and stronger subtropical zonal winds shear are created through the thermal wind balances and the acceleration of the polar vortex. However, a smaller positive NAO amplitude in the *Strat* compared to the *Full* experiment indicates an irreplaceable role of surface cooling effects in post-eruption winters. Moreover, the equatorward deflection of EP flux held explanation for the preservation of polar vortex with less planetary waves transporting poleward (Bittner et al., 2016). And the increased convergence of EP and upward (+ poleward) EP flux are in agreement with Graf et al. (2007) that during volcanic winters the vertical EP flux is enhanced compared to normal winters and would reduce the energy

that can be reflected downwards from the upper stratosphere. It also supports the idea that the variability of polar vortex strength is largely controlled by planetary wave drag, and therefore depends on the upward wave flux from the troposphere into the stratosphere (Newman et al., 2001; Polvani and Waugh, 2004). To complement the stratosphere dynamics analysis, it is suggested to analyze the relation between wave drug and residual circulation anomalies in the future. Since some studies (Shepherd and McLandress, 2011; Toohey et al., 2014; DallaSanta et al., 2019; etc) proposed that polar jet enhancement is controlled primarily by dynamical heating associated with the induced residual circulation rather than the direct aerosol radiative heating.

6. Conclusions and perspectives

The IPSL-CM6A-LR model simulates a robust positive NAO in the first winter whilst a less robust NAO signal in the second winter in response to 1991 Pinatubo eruption in the experiment *Full* which covers full radiative effects from volcanic aerosols forcing, which indicate a rapid wave breaking in the second winter as compared with continuous two positive NAO winters in reanalysis data (Graf et al., 1993; Robock, 2000; Stenchikov et al., 2002; Fischer et al., 2007).

From our simulation experiments, the significant positive NAO in the first volcanic winter is attributed primarily to stratospheric heating by enhancing the meridional temperature gradient and consequently the polar vortex, which is proven to be an up-to-low process. Although during the first volcanic winter stronger convergence of EP flux and more wave drugs happen for *Full* and *Strat* experiments from the surface to the mid-troposphere, consistent with findings of Graf et al. (2007),and Toohey et al. (2014). An equatorward EP flux deflection in Full and Strat will aid planetary waves to propagate more toward tropical areas and influence less the polar vortex (Bittner et al., 2016). The significant divergence of EP flux was confined to the surface and low-troposphere for *Surf*. Figure 13a further demonstrates explicitly the underlying mechanism during the first winter. The surface cooling plays a destructive role in amplifying polar jets when it is alone in the stage. While the nonlinear interaction between stratosphere and troposphere/surface will make a stronger polar vortex in *Full* hence a more visible positive NAO.

During the second volcanic winter, the NAO signal is more noisy with a tendency to negative NAO for *Full*. Such phenomenon is also reported a recent work of Hermanson et al. (2020) for three CMIP6 model. With a tendency to negative NAO, *Full* shows an easier wave breaking. The convergence of EP flux is largely extended in the stratosphere in *Full* than *Strat* indicates a stronger deceleration by stationary planetary waves. Combined with the poleward transport direction, the strong polar vortex regime is easier to break. In a preliminary analysis of the sea ice concentration of the three experiments (not shown), similar sea ice anomaly patterns have been found for Full and Surf. Such pattern resembles a diploe pattern with increased sea ice in the Barents sea while a decline of sea ice in the Labrador sea. It is supposed that surface cooling could also modulate the NAO phase

after volcanic eruption through sea ice negative feedback (Strong et al., 2009). We highly recommend synoptic scale study in the future for a solid founded mechanism behind this interaction.

It is also interesting to supplement that our experiment *Full* has simulated strong El Niño events in winter 1992/93 (not shown). Strong et al. (1986) explained that volcanic aerosols perturbs the Hadley cell circulation in the tropics that reduces the trade winds and triggers an El Niño. It is also suggested by many researchers (Taguchi and Hartmann, 2006; Graf and Zanchettin, 2012; Graf et al., 2015) that El Niño will increase the chance to have a negative NAO by building a subtropical bridge for wave propagation through positive phase of Pacific-North America (PNA) teleconnection pattern. The related results from our Pinatubo simulations will be soon available in the upcoming work of Myriam Khodri (2022). The simulated negative NAO in the second volcanic winter is supposed to be the product of the combined effects from enhanced poleward planetary wave transportation and subtropical teleconnection from El Niño. The supposed mechanism for the second winter is shown in Figure 13b.

Our results highlight the dominant role of the stratosphere heating on formation of positive NAO in the North Atlantic-Eurasia sector after the Pinatubo eruption. The wave reflection also has an important effect in the modulation of polar vortex and NAO. Otherwise, we simulate a noisy negative NAO in *Full* in the second winter, unlike observations/reanalysis. We cannot directly attribute it to a single radiative forcing effect (stratospheric warming or surface cooling). Probably it is attributable to indirect impacts from, e.g. sea-ice feedback on upward planetary wave propagation, which is to be validated in the future work. The influence of stratospheric vortex displacements and splits on surface climate are also an essential subject to study in order to better understand the stratospheric vortex impacts on Earth's surface climate. Furthermore, synoptic scale data analysis is also needed to evaluate the contributions from transient eddies in modulating polar vortex.

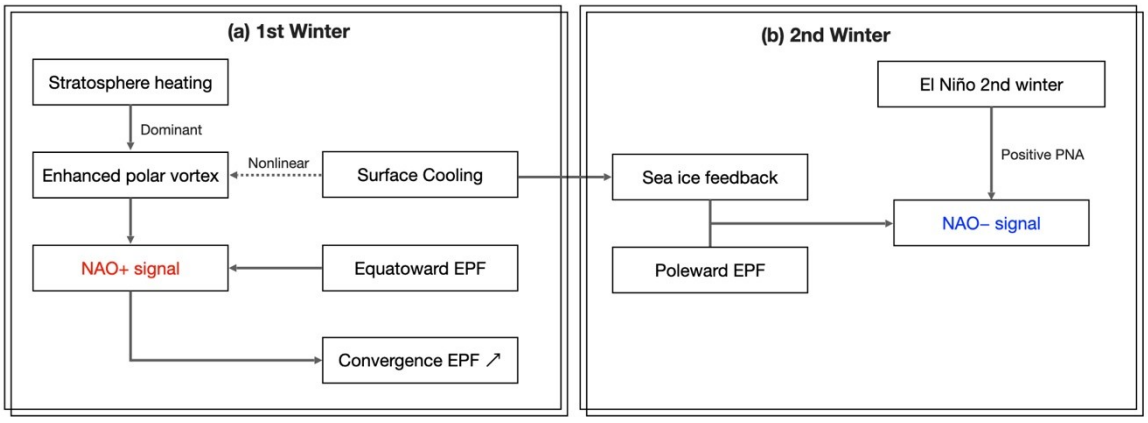

Figure 13: Flow chart demonstration of mechanism for (**a**) positive NAO during the first winter, and (**b**) negative NAO during the second winter after Pinatubo eruption in *Full* experiment.

REFERENCES

Aumont, O., Ethé, C., Tagliabue, A., Bopp, L. and Gehlen, M.: PISCES-v2: an ocean biogeochemical model for carbon and ecosystem studies, Geosci. Model Dev. Discuss., 8(2), 1375–1509, https://doi.org/10.5194/gmdd-8-1375-2015, 2015.

Baldwin, M. P., and Dunkerton, T. J.: Propagation of the Arctic Oscillation from the stratosphere to the troposphere, J. Geophys. Res., 104(D24), 30937– 30946, https://doi.org/10.1029/1999JD900445, 1999.

Barnes, E. A., Solomon, S., & Polvani, L. M.: Robust Wind and Precipitation Responses to the Mount Pinatubo Eruption, as Simulated in the CMIP5 Models, Journal of Climate, 29(13), 4763-4778, https://doi.org/10.1175/JCLI-D-15-0658.1, 2016.

Bauman, J. J., Russell, P. B., Geller, M. A., and Hamill, P.: A stratospheric aerosol climatology from SAGE II and CLAES measurements: 2. Results and comparisons, 1984–1999, J. Geophys. Res., 108, 4383, https://doi.org/10.1029/2002JD002993, 2003.

Bittner, M., Timmreck, C., Schmidt, H., Toohey, M. and Krüger, K.: The impact of wave-mean flow interaction on the Northern Hemisphere polar vortex after tropical volcanic eruptions, Journal of Geophysical Research, 17, https://doi.org/10.1002/2015JD024603 , 2016.

Boucher, O., Servonnat, J., Albright, A. L., Aumont, O., Balkanski, Y., Bastrikov, V., et al: Presentation and evaluation of the IPSL-CM6A-LR climate model, Journal of Advances in Modeling Earth Systems, 12, e2019MS002010, https://doi.org/10.1029/2019MS002010, 2020.

Brönnimann, S.: Impact of El Niño–Southern Oscillation on European climate, Reviews of Geophysics, 45, RG2003, https://doi.org/10.1029/2006RG000199 , 2007.

Charlton-Perez, A. J., et al.: On the lack of stratospheric dynamical variability in low-top versions of the CMIP5 models, J. Geophys. Res. Atmos., 118, 2494– 2505, https://doi.org/10.1002/jgrd.50125, 2013.

Christiansen, B.: Volcanic Eruptions, Large-Scale Modes in the Northern Hemisphere, and the El Niño–Southern Oscillation, Journal of Climate, 21(5), 910-922, https://doi.org/10.1175/2007JCLI1657.1, 2008.

Cole-Dai, J.: Volcanoes and climate. WIREs Clim Change, 1: 824-839. https://doi.org/10.1002/wcc.76, 2010.

Compo, G.P., Whitaker, J.S., Sardeshmukh, P.D., Matsui, N., Allan, R.J., Yin, X., Gleason, B.E., Vose, R.S., Rutledge, G., Bessemoulin, P., Brönnimann, S., Brunet, M., Crouthamel, R.I., Grant, A.N., Groisman, P.Y., Jones, P.D., Kruk, M.C., Kruger, A.C., Marshall, G.J., Maugeri, M., Mok, H.Y., Nordli, Ø., Ross, T.F., Trigo, R.M., Wang, X.L., Woodruff, S.D. and Worley, S.J. : The Twentieth Century Reanalysis Project. Q.J.R. Meteorol. Soc., 137: 1-28. https://doi.org/10.1002/qj.776, 2011.

Dee, D.P., Uppala, S.M., Simmons, A.J., Berrisford, P., Poli, P., Kobayashi, S., Andrae, U., Balmaseda, M.A., Balsamo, G., Bauer, P., Bechtold, P., Beljaars, A.C.M., van de Berg, L., Bidlot, J., Bormann, N., Delsol, C., Dragani, R., Fuentes, M., Geer, A.J., Haimberger, L., Healy, S.B., Hersbach, H., Hólm, E.V., Isaksen, L., Kållberg, P., Köhler, M., Matricardi, M., McNally, A.P., Monge-Sanz, B.M., Morcrette, J.-J., Park, B.-K., Peubey, C., de Rosnay, P., Tavolato, C., Thépaut, J.-N. and Vitart, F.: The ERA-Interim reanalysis: configuration and performance of the data assimilation system. Q.J.R. Meteorol. Soc., 137: 553-597. https://doi.org/10.1002/qj.828, 2011.

Ding, Y., Carton, J. A., Chepurin, G. A., Stenchikov, G., Robock, A., Sentman, L. T. and Krasting, J. P.: Ocean response to volcanic eruptions in Coupled Model Intercomparison Project 5 simulations, J. Geophys. Res. Oceans, 119(9), 5622–5637, https://doi.org/10.1002/2013JC009780, 2014.

D'Orgeval, T., Polcher, J., & de Rosnay, P., Sensitivity of the west African hydrological cycle in ORCHIDEE to infiltration processes, Hydrology and Earth System Sciences, 12(6), 1387–1401, https://doi.org/10.5194/hess-12-1387-2008, 2008.

Driscoll, S., Bozzo, A., Gray, L. J., Robock, A. and Stenchikov, G.: Coupled Model Intercomparison Project 5 (CMIP5) simulations of climate following volcanic eruptions: VOLCANIC IMPACTS IN THE CMIP5 MODELS, J. Geophys. Res., 117(D17), n/a-n/a, https://doi.org/10.1029/2012JD017607, 2012.

Edmon, H..J., B. J. Hoskins, and M. E. McIntyre: Eliassen-Palm crosssections for the troposphere. Journal of the Atmospheric Sciences, 37: 2600- 2616, https://doi.org/10.1175/1520-0469(1980)037<2600:EPCSFT>2.0.CO;2, 1980.

Eyring, V., Bony, S., Meehl, G. A., Senior, C. A., Stevens, B., Stouffer, R. J. and Taylor, K. E.: Overview of the Coupled Model Intercomparison Project Phase 6 (CMIP6) experimental design and organization, Geosci. Model Dev., 9(5), 1937–1958, https://doi.org/10.5194/gmd-9-1937-2016, 2016.

Fischer, E. M., Luterbacher, J., Zorita, E., Tett, S. F. B., Casty, C. and Wanner, H.: European climate response to tropical volcanic eruptions over the last half millennium: CLIMATE RESPONSE TO VOLCANIC ERUPTIONS, Geophys. Res. Lett., 34(5), https://doi.org/10.1029/2006GL027992, 2007.

Graf, H.-F., Kirchner, I., Robock, A. and Schult, I.: Pinatubo eruption winter climate effects: model versus observations, Climate Dynamics, 9(2), 81–93, https://doi.org/10.1007/BF00210011, 1993.

Graf, H.-F., Li, Q., and Giorgetta, M. A.: Volcanic effects on climate: revisiting the mechanisms, Atmos. Chem. Phys., 7, 4503–4511, https://doi.org/10.5194/acp-7-4503-2007, 2007.

Graf, H.-F. and Zanchettin, D.: Central Pacific El Niño, the "subtropical bridge," and Eurasian climate: TWO EL NIÑO TYPES AND EURASIAN CLIMATE, J. Geophys. Res., 117(D01102), https://doi.org/10.1029/2011JD016493, 2012.

Graf, H.-F., Zanchettin, D., Timmreck, C. and Bittner, M.: Observational constraints on the tropospheric and near-surface winter signature of the Northern Hemisphere stratospheric polar vortex, Clim Dyn, 43(12), 3245–3266, https://doi.org/10.1007/s00382-014-2101-0, 2014.

Hermanson, L., Bilbao, R., Dunstone, N., Ménégoz, M., Ortega, P., Pohlmann, H., Robson, J. I., Smith, D. M., Strand, G., Timmreck, C., Yeager, S., and Danabasoglu, G.: Robust Multiyear Climate Impacts of Volcanic Eruptions in Decadal Prediction Systems, J. Geophys. Res. Atmos., 125, https://doi.org/10.1029/2019JD031739, 2020.

Holton, J. R., Hakim, G. J, An Introduction to Dynamic Meteorology (Fifth Edition), Academic Press, Chapter 12, Pages 67-93, ISBN 9780123848666, https://doi.org/10.1016/B978-0-12-384866-6.00003-9, 2013.

Hourdin, F., Rio, C., Grandpeix, J.-Y., Madeleine, J.-B., Cheruy, F., Rochetin, N., et al: LMDZ6A: the atmospheric component of the IPSL climate model with improved and better tuned physics, Journal of Advances in Modeling Earth Systems, 12, e2019MS001892, https://doi.org/10.1029/2019MS001892, 2020.

Ineson, S., Scaife, A.: The role of the stratosphere in the European climate response to El Niño. Nature Geosci 2, 32–36, https://doi.org/10.1038/ngeo381 , 2009.

Jiménez-Esteve, B., & Domeisen, D. I. V.:The Tropospheric Pathway of the ENSO–North Atlantic Teleconnection, Journal of Climate, 31(11), 4563-4584, https://doi.org/10.1175/JCLI-D-17-0716.1, 2018.

Kalnay, E., M. Kanamitsu, R. Kistler, W. Collins, D. Deaven, L. Gandin, M. Iredell, S. Saha, G. White, J. Woollen, Y. Zhu, M. Chelliah, W. Ebisuzaki, W. Higgins, J. Janowiak, K. C. Mo, C. Ropelewski, J. Wang, A. Leetmaa, R. Reynolds, Roy Jenne, and Dennis Joseph: The NCEP/NCAR 40-Year Reanalysis Project", *Bulletin of the AMS,* 77(3) ,437-472, https://doi.org/10.1175/1520-0477(1996)077<0437:TNYRP>2.0.CO;2, 1996.

Khodri, M., Izumo, T., Vialard, J., Janicot, S., Cassou, C., Lengaigne, M., Mignot, J., Gastineau, G., Guilyardi, E., Lebas, N., Robock, A. and McPhaden, M. J.: Tropical explosive volcanic eruptions can trigger El Niño by cooling tropical Africa, Nature Communications, 8(1), https://doi.org/10.1038/s41467-017-00755-6, 2017.

Kodera, K.: Influence of volcanic eruptions on the troposphere through stratospheric dynamical processes in the northern hemisphere winter, J. Geophys. Res., 99(D1), 1273– 1282, https://doi.org/10.1029/93JD02731, 1994.

Krinner, G., Viovy, N., de Noblet-Ducoudré, N., Ogée, J., Polcher, J., Friedlingstein, P., Ciais, P., Sitch, S. and Prentice, I. C.: A dynamic global vegetation model for studies of the coupled atmosphere-biosphere system: DVGM FOR COUPLED CLIMATE STUDIES, Global Biogeochem. Cycles, 19(1), https://doi.org/10.1029/2003GB002199, 2005.

Lehner, F., Schurer, A. P., Hegerl, G. C., Deser, C., and Frölicher, T. L.: The importance of ENSO phase during volcanic eruptions for detection and attribution, Geophys. Res. Lett., 43, 2851– 2858, https://doi.org/10.1002/2016GL067935, 2016.

Li, Q., Graf, H.-F., and Cui, X.: The role of stationary and transient planetary waves in the maintenance of stratospheric polar vortex regimes in Northern Hemisphere winter, Adv. Atmos. Sci., 28, 187–194, https://doi.org/10.1007/s00376-010-9163-7, 2011.

McPhaden, MJ, Zebiak, SE, Glantz, MH : ENSO as an integrating concept in earth science, Science, 314(5806):1740-5. https://doi.org/10.1126/science.1132588, 2006.

Madec, G.: NEMO ocean engine, Notes du Pôle de modélisation de l'Institut Pierre-Simon Laplace (IPSL), 27, 1288-1619, https://doi.org/10.5281/zenodo.3248739, 2017.

McGregor, S., Khodri, M., Maher, N., Ohba, M., Pausata, F.S.R. and Stevenson, S.: The Effect of Strong Volcanic Eruptions on ENSO. In El Niño Southern Oscillation in a Changing Climate (eds M.J. McPhaden, A. Santoso and W. Cai). https://doi.org/10.1002/9781119548164.ch12, 2020.

Myhre, G., Samset, B. H., Schulz, M., Balkanski, Y., Bauer, S., Berntsen, T. K., Bian, H., Bellouin, N., Chin, M., Diehl, T., Easter, R. C., Feichter, J., Ghan, S. J., Hauglustaine, D., Iversen, T., Kinne, S., Kirkevåg, A., Lamarque, J.-F., Lin, G., Liu, X., Lund, M. T., Luo, G., Ma, X., van Noije, T., Penner, J. E., Rasch, P. J., Ruiz, A., Seland, Ø., Skeie, R. B., Stier, P., Takemura, T., Tsigaridis, K., Wang, P., Wang, Z., Xu, L., Yu, H., Yu, F., Yoon, J.-H., Zhang, K., Zhang, H., and Zhou, C.: Radiative forcing of the direct aerosol effect from AeroCom Phase II simulations, Atmos. Chem. Phys., 13, 1853–1877, https://doi.org/10.5194/acp-13-1853-2013, 2013.

Newman, P. A., Nash, E. R., and Rosenfield, J. E.: What controls the temperature of the Arctic stratosphere during the spring?, J. Geophys. Res., 106(D17), 19999– 20010, https://doi.org/10.1029/2000JD000061, 2001.

Pausata, F. S. R., Chafik, L., Caballero, R., David, S. Battisti, D. S.: High-latitude eruptions impacts on ENSO and AMOC, PNAS, 112 (45), 13784-13788; https://doi.org/10.1073/pnas.1509153112, 2015.

Perlwitz, J., & Graf, H.: The Statistical Connection between Tropospheric and Stratospheric Circulation of the Northern Hemisphere in Winter, Journal of Climate, 8(10), 2281-2295, https://doi.org/10.1175/1520-0442(1995)008<2281:TSCBTA>2.0.CO;2, 1995.

Polvani, L. M., & Waugh, D. W.: Upward Wave Activity Flux as a Precursor to Extreme Stratospheric Events and Subsequent Anomalous Surface Weather Regimes, Journal of Climate, 17(18), 3548-3554, https://doi.org/10.1175/1520-0442(2004)017<3548:UWAFAA>2.0.CO;2, 2004.

Raible, C. C., Brönnimann, S., Auchmann, R., Brohan, P., Frölicher, T. L., Graf, H.-F., Jones, P., Luterbacher, J., Muthers, S., Neukom, R., Robock, A., Self, S., Sudrajat, A., Timmreck, C. and Wegmann, M.: Tambora 1815 as a test case for high impact volcanic eruptions: Earth system effects: Tambora 1815 as a test case for high impact volcanic eruptions, WIREs Clim Change, 7(4), 569–589, https://doi.org/10.1002/wcc.407, 2016.

Robock, A.: Volcanic Eruptions and Climate, REVIEWSOF GEOPHYSICS, 29, https://doi.org/10.1029/1998RG000054 , 2000.

Rousset, C., Vancoppenolle, M., Madec, G., Fichefet, T., Flavoni, S., Barthélemy, A., Benshila, R., Chanut, J., Levy, C., Masson, S. and Vivier, F.: The Louvain-La-Neuve sea ice model LIM3.6: global and regional capabilities, Geosci. Model Dev., 8(10), 2991–3005, https://doi.org/10.5194/gmd-8-2991-2015, 2015.

Santer, B. D., Bonfils, C., Painter, J. F., Zelinka, M. D., Mears, C., Solomon, S., Schmidt, G. A., Fyfe, J. C., Cole, J. N. S., Nazarenko, L., Taylor, K. E. and Wentz, F. J.: Volcanic contribution to decadal changes in tropospheric temperature, Nature Geosci, 7(3), 185–189, https://doi.org/10.1038/ngeo2098, 2014.

Sato, M., Hansen, J. E., McCormick, M. P., and Pollack, J. B.: Stratospheric aerosol optical depths, 1850–1990, J. Geophys. Res., 98, 22987, https://doi.org/10.1029/93JD02553, 1993.

Shepherd, T. G., & McLandress, C.: A Robust Mechanism for Strengthening of the Brewer–Dobson Circulation in Response to Climate Change: Critical-Layer Control of Subtropical Wave Breaking, Journal of the Atmospheric Sciences, 68(4), 784-797, https://doi.org/10.1175/2010JAS3608.1, 2011.

Shindell, D. T., Schmidt, G. A., Miller, R. L., and Rind, D.: Northern hemisphere winter climate response to greenhouse gas, ozone, solar, and volcanic forcing, J. Geophys. Res., 106(D7), 7193– 7210, https://doi.org/10.1029/2000JD900547, 2001.

Stenchikov, G.: Arctic Oscillation response to the 1991 Mount Pinatubo eruption: Effects of volcanic aerosols and ozone depletion, J. Geophys. Res., 107(D24), 4803, https://doi.org/10.1029/2002JD002090, 2002.

Stenchikov, G., Hamilton, K., Stouffer, R. J., Robock, A., Ramaswamy, V., Santer, B. and Graf, H.-F.: Arctic Oscillation response to volcanic eruptions in the IPCC AR4 climate models, J. Geophys. Res., 111(D7), D07107, https://doi.org/10.1029/2005JD006286, 2006.

Stephenson, D. B., Pavan, V., Collins, M., Junge, M. M., Quadrelli, R., and Participating CMIP2 Modelling Groups: North Atlantic Oscillation response to transient greenhouse gas forcing and the impact on European winter climate: a CMIP2 multi-model assessment, Climate Dynamics, 27(4), 401–420, https://doi.org/10.1007/s00382-006-0140-x, 2006.

Stevenson, S., Fasullo, J. T., Otto-Bliesner, B. L., Tomas, R. A. and Gao, C.: Role of eruption season in reconciling model and proxy responses to tropical volcanism, Proceedings of the National Academy of Sciences, 114(8), 1822–1826, https://doi.org/10.1073/pnas.1612505114, 2017.

Strong, A. E.: The effect of El Chihcón on the 82/83 El Niño (abstract), Eos Trans, AGU, 67(44), 880, 1986.

Taguchi, M. and Hartmann, D. L.: Increased Occurrence of Stratospheric Sudden Warmings during El Niño as Simulated by WACCM, Journal of Climate, 19(3), 324–332, https://doi.org/10.1175/JCLI3655.1, 2006.

Thomason, L. W., Ernest, N., Millán, L., Rieger, L., Bourassa, A., Vernier, J.-P., Manney, G., Luo, B., Arfeuille, F. and Peter, T.: A global space-based stratospheric aerosol climatology: 1979–2016, Earth Syst. Sci. Data, 10(1), 469–492, https://doi.org/10.5194/essd-10-469-2018, 2018.

Timmreck, C., Graf, H.-F., Lorenz, S. J., Niemeier, U., Zanchettin, D., Matei, D., Jungclaus, J. H., and Crowley, T. J.: Aerosol size confines climate response to volcanic super-eruptions, Geophys. Res. Lett., 37, L24705, https://doi.org/10.1029/2010GL045464, 2010.

Toohey, M., Krüger, K., Bittner, M., Timmreck, C. and Schmidt, H.: The impact of volcanic aerosol on the Northern Hemisphere stratospheric polar vortex: mechanisms and sensitivity to forcing structure, Atmos. Chem. Phys., 14(23), 13063–13079, https://doi.org/10.5194/acp-14-13063-2014, 2014.

Vancoppenolle, M., Thierry Fichefet, Hugues Goosse, Sylvain Bouillon, Gurvan Madec, Miguel Angel Morales Maqueda, Simulating the mass balance and salinity of Arctic and Antarctic sea ice. 1. Model description and validation, Ocean Modelling, 27(1–2), 33-53, ISSN 1463-5003, https://doi.org/10.1016/j.ocemod.2008.10.005, 2009.

Zanchettin, D., Khodri, M., Timmreck, C., Toohey, M., Schmidt, A., Gerber, E. P., Hegerl, G., Robock, A., Pausata, F. S. R., Ball, W. T., Bauer, S. E., Bekki, S., Dhomse, S. S., LeGrande, A. N., Mann, G. W., Marshall, L., Mills, M., Marchand, M., Niemeier, U., Poulain, V., Rozanov, E., Rubino, A., Stenke, A., Tsigaridis, K. and Tummon, F.: The Model Intercomparison Project on the climatic response toVolcanic forcing (VolMIP): experimental design and forcing input data for CMIP6, Geosci. Model Dev., 9(8), 2701–2719, https://doi.org/10.5194/gmd-9-2701-2016, 2016.

Zelinka, M. D., Myers, T. A., McCoy, D. T., Po-Chedley, S., Caldwell, P. M., Ceppi, P., et al. : Causes of higher climate sensitivity in CMIP6 models, Geophysical Research Letters, 47, e2019GL085782. https://doi.org/10.1029/2019GL085782, 2020.

Acknowledgements

This work benefits from the VolMIP project directed by Zanchettin, Khodri et al. (2016) to provide abundant and latest information on Mt. Pinatubo modeling. Simulations are fulfilled with IPSL-CM6A-LR model designed by Institute Pierre Simon Laplace. The authors acknowledge CMIP6, the participating modelling groups, and the ESGF centers (see details on the CMIP Panel website at http://www.wcrp-climate.org/index.php/wgcm-cmip/about-cmip). The authors would like to thank two anonymous reviewers for helpful comments. This work was supported by the Chinese Scholarship Council, Laboratoire Meteorologie Dynamique and MISTRAL PaleoMex program as part of PhD work.

4.3 Surface influences from sea-ice feedbacks

Interactions between winter sea ice variability and North Atlantic Oscillation have been detected and quantified by many researchers based on observations and numerical modelling at different time scales. As the leading mode of climate variability, NAO is expected to exert an influence on the spatial distribution of winter sea ice via wind-driven anomalies of sea ice velocity, surface vertical heat flux and possibly horizontal oceanic heat flux (Strong et al., 2009). As introduced in section 2.4.1 , a dipole pattern of sea ice concentrations with anomalous high over the Labrador Sea and anomalous low over the Barents Sea is observed for positive NAO years (Deser, 2000). While reanalysis and modelling studies suggest that such NAO-induced positive sea-ice dipole pattern will in turn drive NAO into its negative phase (Alexander et al., 2004; Deser et al., 2004, 2007; Magnusdottir et al., 2004; Strong et al., 2009). Deser et al. (2007) examined the transient response of an AOGCM forced by a positive NAO-driven sea ice anomaly pattern. Their results showed that a negative feedback process begins with a localized baroclinic response that reaches peak intensity in 5~10 days, and lasts for 2~3 weeks. While by building up a vector autoregressive model (VAR) for synoptic observation datasets, Strong et al. (2009) solved the relations between sea ice dipole pattern and NAO in an analytical way. They found sea ice dipole pattern generate a localized baroclinic response that persists several weeks, after which wave-mean flow interactions maintains a pattern resembling the negative polarity of the NAO.

In this context, our *volc-pinatubo* experiments provide us a good opportunity to the analyse surface influences from sea-ice feedbacks in different ensemble groups (i.e., *Full*, *Strat*, *Surf*). Since IPSL-CM6A-LR model piControl outputs have not planned for such synoptic scale sea ice analysis at very beginning, we will use directly monthly output of sea ice concentration, sea ice extent, and sea ice velocity from piControl and *volc-pinatubo* runs to get a preview. The monthly output of sea level pressure and surface wind are also incorporated in this subsection.

4.3.1 Sea ice pattern

To better identify the sea ice pattern and its relations with NAO, we apply empirical orthogonal function (EOF) analysis. The winter months (here range from November to March) data of sea ice concentration and sea level pressure anomalies (after minus piControl mean) are concatenated together for period June 1991- December 1993.

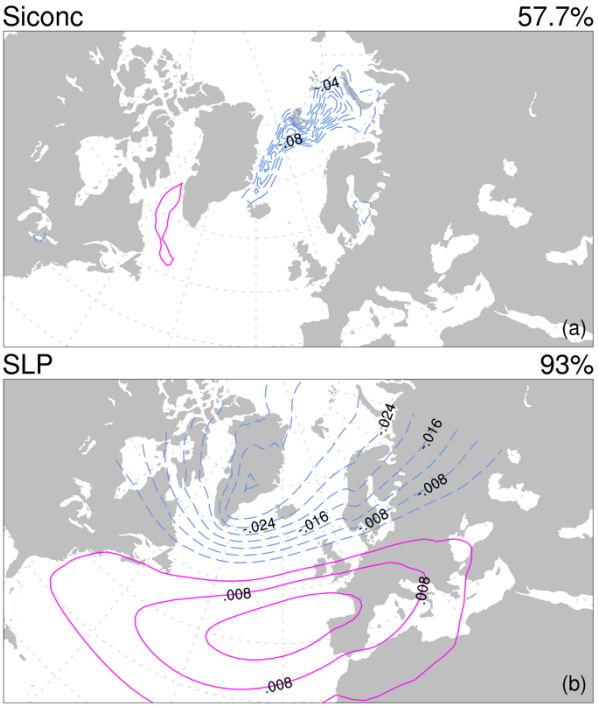

Figure 4.1: **(a)** The leading EOF associated with winter (NDJFM) sea ice concentration contoured at 0.01 with negative values in dashed blue lines and positive values in solid magenta lines, the zero contour suppressed; **(b)** The leading EOF associated with sea level pressure contoured at 0.004. The percentage of the total variance each leading EOF explains is shown on top right of each plot.

Figure 4.1 demonstrates the resulted leading EOF for sea ice concentration and sea level pressure during first two winters after Pinatubo eruptions, which corresponds respectively aforementioned positive phase of sea ice dipole pattern and NAO. We can observe a positive center of action to the south-west of Greenland, and a negative center extending from Greenland Sea to Barents Sea in Fig. 4.1a for sea ice concentration leading EOF (i.e. EOF1).

4.3.2 Negative feedback from sea ice

The spatial pattern of the leading EOFs related with sea ice dipole pattern and positive NAO suggested a physical link between the two underlying phenomena. While Fig. 4.2 displayed the leading principal component (PC) time series obtained by projection of sea ice concentration and sea level pressure onto their leading EOF. Here we define the NAO index (NAO) as the standardized leading PC over the same domain used in Stephenson et al. (2006): 20~90°N, 90°W~60°E; while sea ice dipole pattern index (SIC) as standardized leading PC over the same domain used in Strong et al. (2009): 40~90°N, 90°W~90°E. We notice that NAO and SIC time series are positively corelated in the first winter with similar trend towards positive direction for *Full* experiment (Fig. 4.2a). While in the second winter, we observe a rapid decrease of NAO index in January 1993, accompanied with a positive

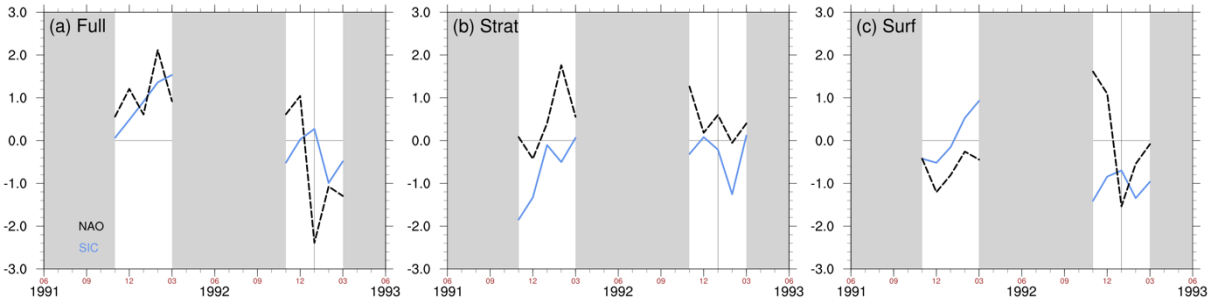

Figure 4.2: Standardized leading PC of sea ice concentration dipole pattern (SIC) in blue solid line and of sea level pressure (NAO) in black dashed lines for experiment **(a)** volc-pinatubo-full, **(b)** volc-pinatubo-strat and (c) volc-pinatubo-surf.

SIC index, which is not observed in *Strat* (Fig. 4.2b). As for second winter in *Surf* experiment, negative NAO index is also captured in January 1993 nevertheless the SIC index remains negative during whole second winter (Fig. 4.2c).

As explained before, the monthly data could not guarantee a precise analysis into the sea ice feedback. Nevertheless, we may still take a glimpse at January 1993 (indicated by vertical grey line in Fig. 4.2) as regards sea ice concentration, ice drift speed and thickness (Fig. 4.3).

Similar to the statistical method applies in section 4.2, ensemble averages of each experiment (i.e. *Full*, *Strat*, *Surf*) are statistically tested with piControl average by a two-tailed Student t-test with the number of degrees of freedom corresponding to the total number of members (25x2=50) minus one. Dots markers have been used in Fig. 4.3 to demonstrate the significance (>90%) of sea ice concentration and sea ice thickness. And we mask the wind if neither zonal wind or meridional wind pass the significant test. So does the sea ice drift velocity vector.

As a result, *Full* experiment reveals typical positive dipole pattern with anomalous high sea ice concentration over Labrador Sea and anomalous low sea ice over Barents Sea (Fig. 4.3a). However the most significant signal is the increase of sea ice over Labrador Sea. Meanwhile the anomalous surface easterlies are very strong, consistent with a negative NAO in January 1991. The sea ice drift toward to Labrador Sea can be also detected in Fig. 4.3b. The sea ice thickness displays a significant augmentation in polar region (Fig. 4.3c). As comparison, *Strat* experiment illustrates a weak sea ice dipole pattern which is not significant (Fig. 4.3d). The strengthened westerlies are consistent with the positive NAO signal for *Strat* during this month. While for *Surf* experiment, we have a remarkably increase of sea ice near southwest of Greenland, as well as strengthened south-westward wind blowing from Greenland Sea (Fig. 4.3g) and sea ice drift from Greenland Sea to

Labrador Sea (Fig. 4.3h). This phenomena suggests a wind-driven sea ice advection anomaly theory as have been discussed by many researchers, e.g. Deser et al. (2000), Hilmer and Jung (2000). The sea ice thickness endures a significant increase (Fig. 4.3i), that is reasonable from surface dimming setting of *Surf*. However, we also notice sea ice concentration increase over Barents Sea which explains to a certain degree the negative SIC index we got for Surf during January 1993.

To conclude, this subsection gives a preliminary analysis of the sea ice feedback on NAO phenomenon. It is supposed that surface cooling could also modulate the NAO phase after volcanic eruption through sea ice negative feedback. We highly recommend synoptic scale study in the future for a solid founded mechanism behind this interaction.

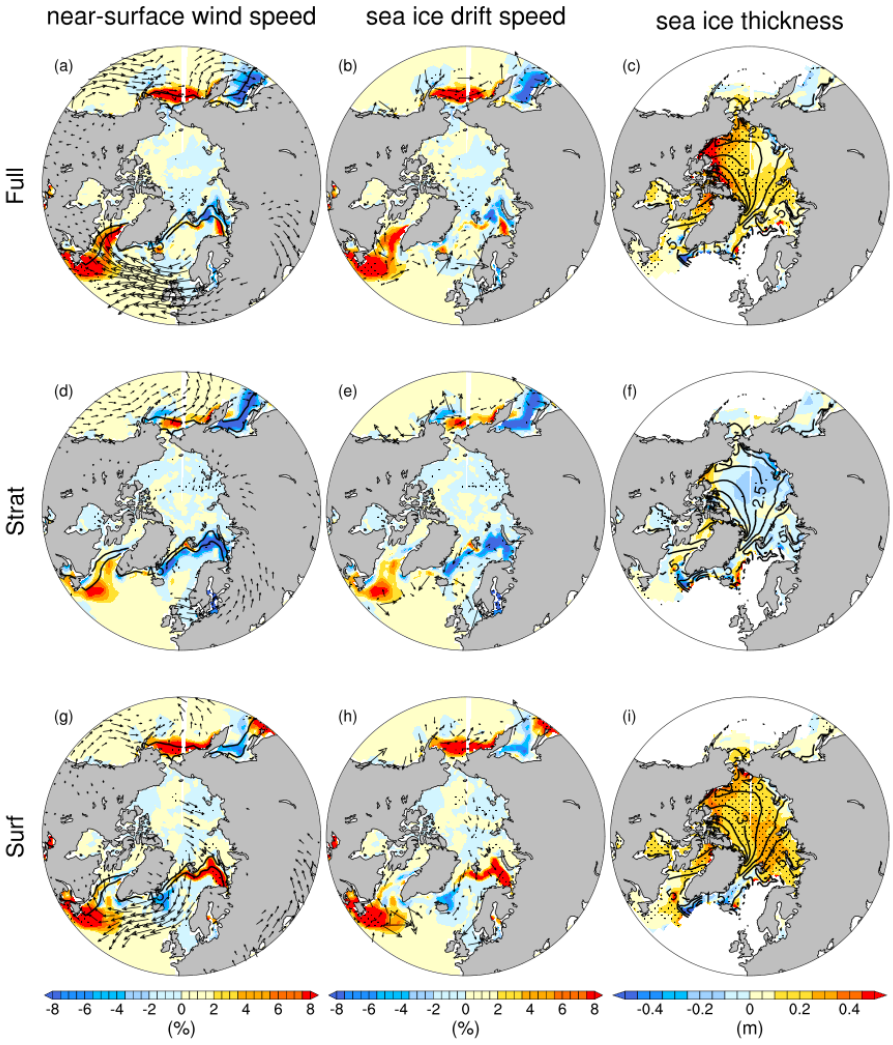

Figure 4.3: Paired anomalies of sea ice concentration (color fill in the left and middle panel) overlayed with near-surface wind vector (left) or sea ice drift speed vector (middle), and sea ice thickness (color fill in the right panel) overlayed with isolines of piControl sea ice thickness values for **a-c** *volc-pinatubo-full*, **d-f** *volc-pinatubo-strat*, **g-i** *volc-pinatubo-surf* in January 1993. The 45% and 90% of piControl sea ice concentration extent are in indicated in thin and thick black lines in the left panel.

Chapter 5

Conclusions and Perspectives

Contents

5.1 Results synthesis and discussions

In the current context of climate change, in order to be able to monitor the evolution of our climate in transition, and more generally our environment, and to be able to interpret the observed changes and attribute the probable cause(s), it is essential to distinguish the internal variability, natural forcings and anthropogenic forcing. Firstly, it is necessary to be able to rely on observation data networks during the modern instrumental period, which is generally shorter than 150 years. Secondly, perennial and multidisciplinary reconstructions make it possible to extend the observation window and provide a better characterization of the natural variability. Thirdly, numerical models are indispensable tools to not only extend the study period back to the past but also stress on the physical processes. Constructed on climate concepts and theories, modelling tools can represent the complexity of the physical processes and mechanisms at play in the Earth system, while apprehending the different spatial and temporal scales.

In this thesis, a global coupled climate system model, IPSL-CM6A-LR, is used to study the interannual climate impacts of volcanism, one of the most important natural climate forcing. For the long last millennium, three transient simulations lasting from 500 CE to 1849 CE have been applied to study the model sensitivity to different eruption conditions. For the best observed Pinatubo eruption during the industrial era, large ensemble simulations have been carried out with IPSL-CM6-LR to probe the mechanism along with comparison to instrumental observations.

The **Chapter** 3 focus on one prime question: how the eruption conditions (e.g. eruption season, latitude, strength) will alter the post-eruption winter NH climate. By testing the linearity between PNJ and eruption strength, it is found that amplitude of PNJ is linearly related to the eruption strength during the first winter following tropical eruptions. In contrast there is no linear relationship between PNJ and eruption strength for extra-tropical Northern Hemisphere eruptions.

By delicately building four volcanic composites (i.e., NHw, EQw, EQe and EQmega), the inter-composite climate response differences to volcanic forcing have been visited. It is found that NH high latitude eruptions which erupted in winter (i.e., NHw, n=30) also reduce the incoming solar radiation north of 45^{o}N, consistent with Graf et al. (1992). At the same time the sulfate aerosol absorbs the solar radiation and warms the nearby stratosphere. Because of the high eruption latitude, it pose effect directly on the meridional temperature gradient near the extratropical jet position during in-phase winter,

hence leads to strengthened PNJ and positive NAO under thermal wind balance. This result is in disagreement with several studies (e.g., Oman, 2005; Sjolte et al., 2021; Zambri et al., 2019) which suggested a negative NAO winter after extratropical eruptions.

In comparison, tropical eruptions which also erupted in winter (i.e., EQw, n=63) can hardly induce robust climate variability during in-phase winter. These winter tropical eruptions rather induce significant signals (p>99%) in strengthened PNJ and positive NAO in Y+1. While tropical eruptions which erupted in spring/summer (i.e., EQe, n=9) can induce significant positive NAO in the first winter after eruption, in consistent with studies on tropical events (e.g., Christiansen, 2008; Graf et al., 1993; Robock, 2000; Shindell et al., 2003; Stenchikov, 2002).

The distinct response to tropical eruptions in different season reveals the importance of seasonal cycle of stratospheric transport of aerosol. The volcanic aerosols injected into the stratosphere from a tropical eruption was believed to be transported to both hemispheres via Brewer-Dobson circulation and finally reach both poles. This generates larger areas being affected by aerosols with long lifetimes in the stratosphere, thus causing larger and longer-lasting climate effects (Schneider et al., 2009). While the EVA module (Toohey et al., 2016) parametrized the mixing and residual transport of aerosol in the NH to be strongest in January and weakest in July, our results have shown that tropical eruptions still need time to transport the aerosol to subpolar region. Even happening during winter with strongest residual transport, winter tropical eruptions cannot guarantee a volcanic forced NAO during in-phase winter. In other hand, the strong Brewer-Dobson circulation during winter helps the NH high latitude winter eruption to influence North Atlantic climate. When selecting out massive winter tropical eruptions (EQmega, n=21), the response is still more robust in Y+1 for NAO and PNJ. Nevertheless, we could already observe a warming over north Eurasia during in-phase winter for EQmega, which is reasonable from dynamical response caused by stronger radiative forcing of EQmega. The positive NAO can persist over two winters for specific 1257 Samalas case (due to specific forcing structure).

Results in **Chapter** 3 stress the model robustness of IPSL-CM6A-LR in simulating volcanic forced winter climate variability under different volcanic cluster. The differences in the effect of high- and low- latitude eruptions on atmospheric circulation and regional temperature provide important insights in understanding the past and future climate variability in response to volcanic forcing. Furthermore, the results have revealed some imperfections in other studies (e.g., Sjolte et al., 2021) which did not consider filter out eruption season when doing similar volcanic composite analysis. For example in the work

of Sjolte et al.(2021), they did not separate the summer NH high latitude eruptions from the winter ones. It is hence inappropriate to conclude a universal negative NAO winter after NH eruptions from their analysis.

To gain a profound understanding of the mechanism by which volcanic eruption will influence the NAO and North Atlantic-Mediterranean sector climate, large ensemble numerical simulation is indispensable in climate science. The **Chapter** 4 is devoted to study the *volc-pinatubo* experiment, an essential part of VolMIP which deals with the volcanically forced responses by state-of-art coupled climate model and with different physical processes. It has stressed the contributions of direct radiative (i.e. surface cooling) and the dynamical (i.e. stratospheric warming) response following the an idealised Pinatubo eruption on North Atlantic-Europe climate using 49-ensemble numerical modelling. It is found that IPSL-CM6A-LR simulates a robust positive NAO in the first winter in response to 1991 Pinatubo eruption, a summer tropical eruption. The second winter signal is otherwise less significant in the experiment *volc-pinatubo-full*, which indicates a rapid wave breaking in the second winter as compared with continuous two positive NAO winters in reanalysis data (Fischer et al., 2007; Graf et al., 1993; Robock, 2000; Stenchikov, 2002).

By comparing *volc-pinatubo-full*, *volc-pinatubo-strat* and *volc-pinatubo-surf*, we found that the significant positive NAO in the first volcanic winter is attributed primarily to stratospheric heating by enhancing the meridional temperature gradient and consequently the polar vortex, which is proven to be an up-to-low process. The surface cooling plays a destructive role in amplifying polar jets in *volc-pinatubo-surf*, different from Stenchikov et al. (2002, 2006) who suggested a decreased planetary wave propagation related to surface cooling. However, the nonlinear interaction between stratosphere and troposphere/surface will make a stronger polar vortex in *volc-pinatubo-full* therefore a stronger positive NAO than in *volc-pinatubo-strat*.

When checking in detail the eddy momentum and eddy heat transport, during the first volcanic winter there is stronger convergence of EP flux and more wave drugs for *volc-pinatubo-full* and *volc-pinatubo-strat* experiments from the surface to the mid-troposphere, consistent with findings of Graf et al. (2007). While an equatorward EP flux deflection in *volc-pinatubo-full* and *volc-pinatubo-strat* will aid planetary waves to propagate more toward tropical areas and influence less the polar vortex (Bittner et al., 2016). The significant divergence of EP flux was confined to the surface and low-troposphere for *volc-pinatubo-surf*. At the end of **Chapter** 4, a negative feedback from sea-ice dipole pattern to NAO is

briefly analysed using monthly data outputs. Further diagnostics based on daily outputs is recommended in the future study.

Overall, different from previous studies (e.g., Swingedouw et al., 2017; Driscoll et al., 2011) which reported a general failure of CMIP5 models to simulate robust NAO response after volcanic eruption, our results confirmed the efficiency of IPSL-CM6A-LR in simulating NAO variability in response to volcanic forcing, which can also be viewed as one cheering progress of CMIP6.

5.2 Perspectives

The results obtained within the framework of these experiments (*past1000* and *volc-pinatubo*) using IPSL-CM6A-LR offer two axes of future progressions with on the one hand possible understanding of teleconnection between other circulation components and NAO during volcanic winter, and on the other hand the comparison with other AOGCMs and paleoclimate reconstructions.

5.2.1 Teleconnection between other circulation components and NAO

Beside intrinsic characteristics (hemispheric loading, eruption season, latitude) of volcanic eruption, the simulated climatic response to individual volcanic eruptions also critically depends on the background climate, including the mean climate state, the ongoing internal climate variability and the presence of additional forcing factors such as variations in solar radiation. The teleconnection between other ocean/atmosphere circulation mode (e.g., ENSO, PNA, AMOC, monsoon, QBO) and NAO is especially an envisaging topic for us to explore whether such teleconnections will influence the volcanic forced NAO phenomenon.

A few several studies have investigated this subject. By analysing NCEP/NCAR observations, Graf et al. (2014) found that no-volcanic winter samples of strong polar vortex (and positive NAO) nearly exclusively occur during cold ENSO states, while a weak polar vortex is observed for both cold and warm ENSO. Moreover, during a warm ENSO phase, the related positive Pacific-North Atlantic Pattern (PNA) will imprint on both troposphere and stratosphere and will reflect on a coupled positive PNA/negative NAO state. However they argued divers states of ENSO after four volcanic winters that it is relevant to compare the anomalous pattern associated with strong polar vortex in volcanically-disturbed winter and in volcanically-undisturbed winters.

Relating the *volc-pinatubo* experiment, we have found rather robust warm ENSO signal in the summer 1992 following the Pinatubo eruption (Fig. A.2.1 and Fig. A.2.2 in

Appendix A.2). We are wondering if this simulated El Niño signal will project on the North Atlantic sector through planetary disturbances in the second winter after Pinatubo eruption. Hence increasing ensemble size and compositing upon different ENSO state would be important perspectives to help explore ENSO modulation with NAO during volcanic winters.

Moreover, similar ensemble experiment protocol is also expected to analyse the NH high-latitude eruption, as we have done for the tropical eruption Pinatubo. There are rising studies which stressed the potential effects of the high-latitude eruptions on global and regional climate. Toohey et al. (2019) and Yang et al. (2019) pointed out that the spatial distribution of volcanic aerosols and associated radiative forcing affects the climate impact of volcanic eruptions. Scientific fellows are paying more attention to their influences on monsoon system (Colose et al., 2016; Haywood et al., 2013; Liu et al., 2016; Pausata et al., 2015) or ENSO variations (Brad Adams et al., 2003; Khodri et al., 2017; Liu et al., 2017; Stevenson et al., 2016; Sun et al., 2019). For example, recent studies suggested that sporadic volcanic eruptions in the NH strongly influence the surface temperature gradient and cause Sahelian drought (Haywood et al., 2013) and southward movement of ITCZ (Pausata et al., 2015), while large asymmetric stratospheric aerosol loadings concentrated in the SH induce a greening of the Sahel (Haywood et al., 2013) and northward movement of ITCZ (Liu et al., 2016). However, regardless the casual link between Pacific and Atlantic through "atmospheric bridge" or other teleconnection (Brönnimann, 2007; Brönnimann et al., 2006; Fraedrich, 1994; Graf and Zanchettin, 2012; Hamilton, 1988), the ENSO-volcano studies did not extend to North Atlantic-Europe sector.

The relation between NAO and another circulation component, i.e., Quasi-Biennial Oscillation (QBO), is also a worthwhile topic to investigate considering QBO's influences on surface climates and weather predictions. Recently published by (DallaSanta et al., 2021), it is pointed out that eruptions will bias the QBO towards a westerly state, such that the QBO period response depends upon the phase at the time of eruption. From the composite study of our *past1000* experiment, we are also suggesting a easterly phase of QBO phase in the first winter after NH high-latitude eruptions may weaken the polar vortex.

In the future, we are looking forward to deepening study upon the possible teleconnection between these circulation components with NAO after onset of volcanic eruptions.

5.2.2 Multi-model comparison and proxy-model comparison

Climate models are very sophisticated, however they still have strong biases and uncertainties, which requires multi-model comparison and validation work using adapted observations, from instrumental measurements or paleo reconstructions. This is essential to then assess the level of confidence and uncertainty of future climate projections provided by these models.

In the frame of work of PMIP4/CMIP6, more stringer experimental set-ups (e.g. an identical forcing data set) and output data are implemented in the CMIP6 process, provide an improved basis for multi-model studies. Especially the improvements in volcanic forcing reconstructions (Toohey et al., 2016; Toohey and Sigl, 2017) regarding their accuracy and complexity have the potential to improve quality in comparative model-data studies.

Additionally, proxy-model comparison is also a crucial perspective related to the thesis work. The combination of instrumental observations with climatic variables deduced from carbonate natural archives resolving the annual to multi-annual scale, such as corals in marine areas or speleothems in continental areas, makes it possible to extend the observation window. beyond the instrumental period and serve as good constraints for numerical simulations. A better understanding the functioning of the Earth's climate and environmental system can be also achieved through the use of statistical tools applied to the analysis of these observation data (instrumental and proxy).

Numerous paleo reconstructions of past millennium climate are described concerning the volcanic influences, especially the sea level pressure, temperature and rainfall patterns over Euro-Mediterranean sector (e.g., B. I. Cook et al., 2016; E. R. Cook et al., 2002, 2015; Luterbacher et al., 2002, 2004; Steiger et al., 2018). From a global scale average of new regional reconstructions, Past Global Changes 2k (PAGES 2k) Consortium (Ahmed et al., 2013) found periods with strong volcanic and solar forcing combined occurring over the past millennium show significantly cooler and conditions than randomly selected periods from the last millennium. As shown in Fig. A.2.3 in **Appendix A.2**, our past millennium runs can generally simulate a consistent global mean temperature variability as PAGES2k. Some studies also contribute the transition from MCA to LIA to the volcanic forcing (e.g., *Miller et al., 2012*) Since volcanic forcing shows a detectable influence on large-scale temperature and plays an important role in explaining past cool episodes, for example, in the late 17th and early 19th centuries (parts of LIA; Hegerl et al., 2007; Jungclaus et al., 2010; Miller et al., 2012). However, based on multi-proxy reconstructions of surface temperature field, Luterbacher et al. (2004) proposed that solar forcing dominant

over volcanic eruptions by inducing a more homogeneous hemispheric-wide cooling at decadal time scales. In contrast, Bengtsson et al. (2006) emphasized the role of internal variability in pre-industrial European climate using same surface temperature reconstruction data.

E. R. Cook et al. (2015) proposed "Old World Drought Atlas" (OWDA) which is a set of year-to-year maps of tree-ring reconstructed summer wetness and dryness over Europe and the Mediterranean Basin during the Common Era (1000~2012 CE). This product is reconstructed using summer season (JJA) self-calibrating Palmer Drought Severity Index (scPDSI) (van der Schrier et al., 2013). By applying this product, Gao and Gao (2017) found different European summer hydroclimate response to tropical and Northern high latitude volcanic eruptions (Sigl et al., 2015) by super epoch analysis. A significant wetting response (at the 95% confidence level) is found for year 0 and year +1 after tropical eruptions, followed by a significant drying in year +2; while large high latitude eruptions tend to cause a drying response in western-central Europe in year +2, which shifts south-eastwards in years +3 and +4.

Recently, a new Paleo Hydrodynamics Data Assimilation (PHYDA) product developed by Steiger et al. (2018) has drawn our attention in extending the last millennium study into paleo reconstruction. This dataset combines abundant proxy time series with the physical constraints of an atmosphere-ocean climate model (the CESM-LME simulation, Otto-Bliesner et al., 2016). Using this latest proxy assimilation product, Tejedor et al. (2021) find large VEs tend to produce dry conditions over tropical Africa, Central Asia, and the Middle East; while wet conditions over much of Oceania and the South America Monsoon region. They also suggest that proxy-constrained PHYDA estimates are larger and more consistent than the response simulated by CESM last millennium ensemble simulation. However, we found distinct regional patterns between PHYDA and IPSL-CM6A-LR when we carried comparison analysis on the surface temperature anomaly during MCA and LIA, the two most important period during the last millennium using PHDA and our *past1000* experiment outputs (Fig. A.2.4 in **Appendix A.2**). Considering there is little consensus across these different records regarding the character and dominant drivers of hydroclimate variability across the basin over the last millennium, more rigorous work based on more reconstructions from paleoclimate community is awaiting us to do proxy-model comparison.

Bibliography

Ahmed, M., Anchukaitis, K. J., Asrat, A., Borgaonkar, H. P., Braida, M., Buckley, B. M., BĂźntgen, U., Chase, B. M., Christie, D. A., Cook, E. R., Curran, M. A. J., Diaz, H. F., Esper, J., Fan, Z.-X., Gaire, N. P., Ge, Q., Gergis, J., GonzĂĄlez-Rouco, J. F., Goosse, H., … PAGES 2k Consortium. (2013). Continental-scale temperature variability during the past two millennia. *Nature Geoscience*, *6*(5), 339–346. https://doi.org/10.1038/ngeo1797

Ahn, J., Brook, E. J., Schmittner, A., and Kreutz, K. (2012). Abrupt change in atmospheric CO2 during the last ice age. *Geophysical Research Letters*, *39*(18). https://doi.org/10.1029/2012GL053018

Albrecht, B. A. (1989). Aerosols, Cloud Microphysics, and Fractional Cloudiness. *Science*, *245*(4923), 1227–1230. https://doi.org/10.1126/science.245.4923.1227

Alexander, M. A., Bhatt, U. S., Walsh, J. E., Timlin, M. S., Miller, J. S., and Scott, J. D. (2004). The Atmospheric Response to Realistic Arctic Sea Ice Anomalies in an AGCM during Winter. *Journal of Climate*, *17*(5), 890–905. https://doi.org/10.1175/1520-0442(2004)017<0890:TARTRA>2.0.CO;2

Ambaum, M. H. P., Hoskins, B. J., and Stephenson, D. B. (2001). Arctic Oscillation or North Atlantic Oscillation? *Journal of Climate*, *14*(16), 3495–3507. https://doi.org/10.1175/1520-0442(2001)014<3495:AOONAO>2.0.CO;2

Ammann, C. M., Meehl, G. A., Washington, W. M., and Zender, C. S. (2003). A monthly and latitudinally varying volcanic forcing dataset in simulations of 20th century climate. *Geophysical Research Letters*, *30*(12). https://doi.org/10.1029/2003GL016875

Ammann, C. M., and Naveau, P. (2003). Statistical analysis of tropical explosive volcanism occurrences over the last 6 centuries. *Geophysical Research Letters*, *30*(5). https://doi.org/10.1029/2002GL016388

Ammann, C. M., and Naveau, P. (2010). A statistical volcanic forcing scenario generator for climate simulations. *Journal of Geophysical Research: Atmospheres*, *115*(D5). https://doi.org/10.1029/2009JD012550

Atwood, A. R., Wu, E., Frierson, D. M. W., Battisti, D. S., and Sachs, J. P. (2016). Quantifying Climate Forcings and Feedbacks over the Last Millennium in the CMIP5–PMIP3 Models*. *Journal of Climate*, *29*(3), 1161–1178. https://doi.org/10.1175/JCLI-D-15-0063.1

Aumont, O., Ethé, C., Tagliabue, A., Bopp, L., and Gehlen, M. (2015). PISCES-v2: An ocean biogeochemical model for carbon and ecosystem studies. *Geoscientific Model Development Discussions*, *8*(2), 1375–1509. https://doi.org/10.5194/gmdd-8-1375-2015

Baker, A., C. Hellstrom, J., Kelly, B. F. J., Mariethoz, G., and Trouet, V. (2015). A composite annual-resolution stalagmite record of North Atlantic climate over the last three millennia. *Scientific Reports*, *5*(1), 10307. https://doi.org/10.1038/srep10307

Baker, L. H., Shaffrey, L. C., Sutton, R. T., Weisheimer, A., and Scaife, A. A. (2018). An Intercomparison of Skill and Overconfidence/Underconfidence of the Wintertime North Atlantic Oscillation in Multimodel Seasonal Forecasts. *Geophysical Research Letters*, *45*(15), 7808–7817. https://doi.org/10.1029/2018GL078838

Barnes, E. A., Solomon, S., and Polvani, L. M. (2016). Robust Wind and Precipitation Responses to the Mount Pinatubo Eruption, as Simulated in the CMIP5 Models. *Journal of Climate*, *29*(13), 4763–4778. https://doi.org/10.1175/JCLI-D-15-0658.1

Baroni, M., Savarino, J., Cole-Dai, J., Rai, V. K., and Thiemens, M. H. (2008). Anomalous sulfur isotope compositions of volcanic sulfate over the last millennium in Antarctic ice cores. *Journal of Geophysical Research: Atmospheres*, *113*(D20). https://doi.org/10.1029/2008JD010185

Bauman, J. J., Russell, P. B., Geller, M. A., and Hamill, P. (2003). A stratospheric aerosol climatology from SAGE II and CLAES measurements: 1. Methodology. *Journal of Geophysical Research: Atmospheres*, *108*(D13). https://doi.org/10.1029/2002JD002992

Bellouin, N., Jones, A., Haywood, J., and Christopher, S. A. (2008). Updated estimate of aerosol direct radiative forcing from satellite observations and comparison against the Hadley Centre climate model. *Journal of Geophysical Research: Atmospheres*, *113*(D10). https://doi.org/10.1029/2007JD009385

Bengtsson, L., Hodges, K. I., Roeckner, E., and Brokopf, R. (2006). On the natural variability of the pre-industrial European climate. *Climate Dynamics*, *27*(7), 743–760. https://doi.org/10.1007/s00382-006-0168-y

Berger, A. L. (1978). Long-Term Variations of Daily Insolation and Quaternary Climatic Changes. *Journal of Atmospheric Sciences*, *35*(12), 2362–2367. https://doi.org/10.1175/1520-0469(1978)035<2362:LTVODI>2.0.CO;2

Berger, A., and Loutre, M. F. (1991). Insolation values for the climate of the last 10 million years. *Quaternary Science Reviews*, *10*(4), 297–317. https://doi.org/10.1016/0277-3791(91)90033-Q

Betts, R. A., Falloon, P. D., Goldewijk, K. K., and Ramankutty, N. (2007). Biogeophysical effects of land use on climate: Model simulations of radiative forcing and large-scale temperature change. *The Contribution of Agriculture to the State of Climate*, *142*(2), 216–233. https://doi.org/10.1016/j.agrformet.2006.08.021

Bittner, M., Schmidt, H., Timmreck, C., and Sienz, F. (2016). Using a large ensemble of simulations to assess the Northern Hemisphere stratospheric dynamical response to tropical volcanic eruptions and its uncertainty: LARGE ENSEMBLES FOR VOLCANIC ERUPTIONS. *Geophysical Research Letters*, *43*(17), 9324–9332. https://doi.org/10.1002/2016GL070587

Bittner, M., Timmreck, C., Schmidt, H., Toohey, M., and Krüger, K. (2016). The impact of wave- mean flow interaction on the Northern Hemisphere polar vortex after tropical volcanic eruptions. *Journal of Geophysical Research*, 17.

Bluth, G. J. S., Doiron, S. D., Schnetzler, C. C., Krueger, A. J., and Walter, L. S. (1992). Global tracking of the SO2 clouds from the June, 1991 Mount Pinatubo eruptions. *Geophysical Research Letters*, *19*(2), 151–154. https://doi.org/10.1029/91GL02792

Boucher, O., Randall, D., Artaxo, P., Bretherton, C., Feingold, G., Forster, P., Kerminen, V.-M., Liao, H., Lohman, U., Rasch, P., Satheesh, S. K., Sherwood, S., Stevens, B., and Zhang, X. Y. (2014). Clouds and Aerosols. In IPCC (Ed.), *Climate Change 2013: The Physical Science Basis: Working Group I Contribution to the Fifth Assessment Report of the Intergovernmental Panel on Climate Change* (pp. 571–658). Cambridge University Press; Cambridge Core. https://doi.org/10.1017/CBO9781107415324.016

Boucher, O., Servonnat, Jăš., Albright, A. L., Aumont, O., Balkanski, Y., Bastrikov, V., Bekki, S., Bonnet, Răš., Bony, S., Bopp, L., Braconnot, P., Brockmann, P., Cadule, P., Caubel, A., Cheruy, F., Codron, F., Cozic, A., Cugnet, D., D'Andrea, F., … Vuichard, N. (2020). Presentation and Evaluation of the IPSL-CM6A-LR Climate Model. *Journal of Advances in Modeling Earth Systems*, *12*(7), e2019MS002010. https://doi.org/10.1029/2019MS002010

Braconnot, P., Harrison, S. P., Kageyama, M., Bartlein, P. J., Masson-Delmotte, V., Abe-Ouchi, A., Otto-Bliesner, B., and Zhao, Y. (2012a). Evaluation of climate models using palaeoclimatic data. *Nature Climate Change*, *volume 2*, pages417-424(2012).

Braconnot, P., Harrison, S. P., Kageyama, M., Bartlein, P. J., Masson-Delmotte, V., Abe-Ouchi, A., Otto-Bliesner, B., and Zhao, Y. (2012b). Evaluation of climate models using palaeoclimatic data. *Nature Climate Change*, *2*(6), 417–424. https://doi.org/10.1038/nclimate1456

Brad Adams, J., Mann, M. E., and Ammann, C. M. (2003). Proxy evidence for an El Niño-like response to volcanic forcing. *Nature*, *426*(6964), 274–278. https://doi.org/10.1038/nature02101

Brohan, P., Allan, R., Freeman, E., Wheeler, D., Wilkinson, C., and Williamson, F. (2012). Constraining the temperature history of the past millennium using early instrumental observations. *Climate of the Past*, *8*(5), 1551–1563. https://doi.org/10.5194/cp-8-1551-2012

Brönnimann, S. (2007). *Impact of El Niño–Southern Oscillation on European climate*. 28.

Brönnimann, S., Xoplaki, E., Casty, C., Pauling, A., and Luterbacher, J. (2006). ENSO influence on Europe during the last centuries. *Climate Dynamics*, *28*(2–3), 181–197. https://doi.org/10.1007/s00382-006-0175-z

Brovkin, V., Loren, S., Jungclaus, J., Raddatz, T., Timmreck, C., Reick, C., Segschneider, J., and Six, K. (2010). Sensitivity of a coupled climate-carbon cycle model to large volcanic eruptions during the last millennium. *Tellus B: Chemical and Physical Meteorology*, *62*(5), 674–681. https://doi.org/10.1111/j.1600-0889.2010.00471.x

Brovkin, V., Sitch, S., Von Bloh, W., Claussen, M., Bauer, E., and Cramer, W. (2004). Role of land cover changes for atmospheric CO2 increase and climate change during the last 150 years. *Global Change Biology*, *10*(8), 1253–1266. https://doi.org/10.1111/j.1365-2486.2004.00812.x

Cassou, C., and Terray, L. (2001). Oceanic Forcing of the Wintertime Low-Frequency Atmospheric Variability in the North Atlantic European Sector: A Study with the ARPEGE Model. *Journal of Climate*, *14*(22), 4266–4291. https://doi.org/10.1175/1520-0442(2001)014<4266:OFOTWL>2.0.CO;2

Cassou, C., Terray, L., Hurrell, J. W., and Deser, C. (2004). North Atlantic Winter Climate Regimes: Spatial Asymmetry, Stationarity with Time, and Oceanic Forcing. *Journal of Climate*, *17*(5), 1055–1068. https://doi.org/10.1175/1520-0442(2004)017<1055:NAWCRS>2.0.CO;2

Charlton-Perez, A. J., Baldwin, M. P., Birner, T., Black, R. X., Butler, A. H., Calvo, N., Davis, N. A., Gerber, E. P., Gillett, N., Hardiman, S., Kim, J., Krüger, K., Lee, Y.-Y., Manzini, E., McDaniel, B. A., Polvani, L., Reichler, T., Shaw, T. A., Sigmond, M., … Watanabe, S. (2013). On the lack of stratospheric dynamical variability in low-top versions of the CMIP5 models: STRATOSPHERE IN

CMIP5 MODELS. *Journal of Geophysical Research: Atmospheres*, *118*(6), 2494–2505. https://doi.org/10.1002/jgrd.50125

Chen, K., Ning, L., Liu, Z., Liu, J., Yan, M., Sun, W., Yuan, L., Lv, G., Li, L., Jin, C., and Shi, Z. (2020). One Drought and One Volcanic Eruption Influenced the History of China: The Late Ming Dynasty Mega-drought. *Geophysical Research Letters*, *47*(16). https://doi.org/10.1029/2020GL088124

Chree, C. (1913). III. Some phenomena of sunspots and of terrestrial magnetism at Kew Observatory. *Philosophical Transactions of the Royal Society of London. Series A, Containing Papers of a Mathematical or Physical Character*, *212*(484–496), 75–116. https://doi.org/10.1098/rsta.1913.0003

Chree, C. (1914). VI. Some phenomena of sunspots and of terrestrial magnetism.-Part II. *Philosophical Transactions of the Royal Society of London. Series A, Containing Papers of a Mathematical or Physical Character*, *213*(497–508), 245–277. https://doi.org/10.1098/rsta.1914.0006

Christiansen, B. (2008a). Volcanic Eruptions, Large-Scale Modes in the Northern Hemisphere, and the El Niño-Southern Oscillation. *Journal of Climate*, *21*(5), 910–922. https://doi.org/10.1175/2007JCLI1657.1

Christiansen, B. (2008b). Volcanic Eruptions, Large-Scale Modes in the Northern Hemisphere, and the El Niño–Southern Oscillation. *Journal of Climate*, *21*(5), 910–922. https://doi.org/10.1175/2007JCLI1657.1

Cole-Dai, J., Ferris, D., Lanciki, A., Savarino, J., Baroni, Măš., and Thiemens, M. H. (2009). Cold decade (AD 1810-1819) caused by Tambora (1815) and another (1809) stratospheric volcanic eruption. *Geophysical Research Letters*, *36*(22). https://doi.org/10.1029/2009GL040882

Colose, C. M., LeGrande, A. N., and Vuille, M. (2016). Hemispherically asymmetric volcanic forcing of tropical hydroclimate during the last millennium. *Earth System Dynamics*, *7*(3), 681–696. https://doi.org/10.5194/esd-7-681-2016

Compo, G. P., Whitaker, J. S., Sardeshmukh, P. D., Matsui, N., Allan, R. J., Yin, X., Gleason, B. E., Vose, R. S., Rutledge, G., Bessemoulin, P., BrĂśnnimann, S., Brunet, M., Crouthamel, R. I., Grant, A. N., Groisman, P. Y., Jones, P. D., Kruk, M. C., Kruger, A. C., Marshall, G. J., … Worley, S. J. (2011). The Twentieth Century Reanalysis Project. *Quarterly Journal of the Royal Meteorological Society*, *137*(654), 1–28. https://doi.org/10.1002/qj.776

Cook, B. I., Anchukaitis, K. J., Touchan, R., Meko, D. M., and Cook, E. R. (2016). Spatiotemporal drought variability in the Mediterranean over the last 900 years. *Journal of Geophysical Research: Atmospheres*, *121*(5), 2060–2074. https://doi.org/10.1002/2015JD023929

Cook, E. R., D'Arrigo, R. D., and Mann, M. E. (2002). A Well-Verified, Multiproxy Reconstruction of the Winter North Atlantic Oscillation Index since A.D. 1400. *JOURNAL OF CLIMATE*, *15*, 11.

Cook, E. R., Kushnir, Y., Smerdon, J. E., Williams, A. P., Anchukaitis, K. J., and Wahl, E. R. (2019). A Euro-Mediterranean tree-ring reconstruction of the winter NAO index since 910 C.E. *Climate Dynamics*, *53*(3–4), 1567–1580. https://doi.org/10.1007/s00382-019-04696-2

Cook, E. R., Seager, R., Kushnir, Y., Briffa, K. R., Bu ntgen, U., Frank, D., Krusic, P. J., Tegel, W., van der Schrier, G., Andreu-Hayles, L., Baillie, M., Baittinger, C., Bleicher, N., Bonde, N., Brown, D., Carrer, M., Cooper, R., Cufar, K., Dittmar, C., … Zang, C. (2015). Old World megadroughts and pluvials during the Common Era. *Science Advances*, *1*(10), e1500561–e1500561. https://doi.org/10.1126/sciadv.1500561

Crowley, T. J., and Unterman, M. B. (2013). Technical details concerning development of a 1200 yr proxy index for global volcanism. *Earth System Science Data*, *5*(1), 187–197. https://doi.org/10.5194/essd-5-187-2013

Crowley, T. J., Zielinski, G., Vinther, B., Udisti, R., Kreutz, K., Cole-Dai, J., and Castellano, E. (2008). Volcanism and the Little Ice Age. *PAGES News*, *16*(2), 22–23. https://doi.org/10.22498/pages.16.2.22

DallaSanta, K., Orbe, C., Rind, D., Nazarenko, L., and Jonas, J. (2021). Response of the Quasi- Biennial Oscillation to Historical Volcanic Eruptions. *Geophysical Research Letters*, *48*(20). https://doi.org/10.1029/2021GL095412

D'Arrigo, R., Seager, R., Smerdon, J. E., LeGrande, A. N., and Cook, E. R. (2011). The anomalous winter of 1783-1784: Was the Laki eruption or an analog of the 2009-2010 winter to blame? *Geophysical Research Letters*, *38*(5). https://doi.org/10.1029/2011GL046696

Delaygue, G., and Bard, E. (2011). An Antarctic view of Beryllium-10 and solar activity for the past millennium. *Climate Dynamics*, *36*(11), 2201–2218. https://doi.org/10.1007/s00382-010-0795-1

Deligne, N. I., Coles, S. G., and Sparks, R. S. J. (2010). Recurrence rates of large explosive volcanic eruptions. *Journal of Geophysical Research: Solid Earth*, *115*(B6). https://doi.org/10.1029/2009JB006554

Denman, K., Brasseur, G., Chidthaisong, A., Ciais, P., Cox, P., Dickinson, R., Haugustaine, D., Heinze, C., Holland, E., Jacob, D., Lohmann, U., S., R., Silva Dias, P., Wofsy, S., and Zhang, X. (2007). Couplings Between Changes in the Climate System and Biogeochemistry. In *Climate Change 2007:*

The Physical Science Basis: Contribution of Working Group I to the Fourth Assessment Report of the Intergovernmental Panel on Climate Change (Vol. 2007, pp. 499–587).

Deser, C. (2000). On the teleconnectivity of the "Arctic Oscillation." *Geophysical Research Letters*, *27*(6), 779–782. https://doi.org/10.1029/1999GL010945

Deser, C., Magnusdottir, G., Saravanan, R., and Phillips, A. (2004). The Effects of North Atlantic SST and Sea Ice Anomalies on the Winter Circulation in CCM3. Part II: Direct and Indirect Components of the Response. *Journal of Climate*, *17*(5), 877–889. https://doi.org/10.1175/1520-0442(2004)017<0877:TEONAS>2.0.CO;2

Deser, C., Tomas, R. A., and Peng, S. (2007). The Transient Atmospheric Circulation Response to North Atlantic SST and Sea Ice Anomalies. *Journal of Climate*, *20*(18), 4751–4767. https://doi.org/10.1175/JCLI4278.1

Deser, C., Walsh, J. E., and Timlin, M. S. (2000). Arctic Sea Ice Variability in the Context of Recent Atmospheric Circulation Trends. *Journal of Climate*, *13*(3), 617–633. https://doi.org/10.1175/1520-0442(2000)013<0617:ASIVIT>2.0.CO;2

Domeisen, D. I. V. (2019). Estimating the Frequency of Sudden Stratospheric Warming Events From Surface Observations of the North Atlantic Oscillation. *Journal of Geophysical Research: Atmospheres*, *124*(6), 3180–3194. https://doi.org/10.1029/2018JD030077

Driscoll, S., Bozzo, A., Gray, L. J., Robock, A., and Stenchikov, G. (2012). Coupled Model Intercomparison Project 5 (CMIP5) simulations of climate following volcanic eruptions: VOLCANIC IMPACTS IN THE CMIP5 MODELS. *Journal of Geophysical Research: Atmospheres*, *117*(D17), n/a-n/a. https://doi.org/10.1029/2012JD017607

Dufresne, J.-L., Foujols, M.-A., Denvil, S., Caubel, A., Marti, O., Aumont, O., Balkanski, Y., Bekki, S., Bellenger, H., Benshila, R., Bony, S., Bopp, L., Braconnot, P., Brockmann, P., Cadule, P., Cheruy, F., Codron, F., Cozic, A., Cugnet, D., … Vuichard, N. (2013). Climate change projections using the IPSL-CM5 Earth System Model: From CMIP3 to CMIP5. *Climate Dynamics*, *40*(9–10), 2123–2165. https://doi.org/10.1007/s00382-012-1636-1

Dunstone, N., Smith, D., Scaife, A., Hermanson, L., Eade, R., Robinson, N., Andrews, M., and Knight, J. (2016). Skilful predictions of the winter North Atlantic Oscillation one year ahead. *Nature Geoscience*, *9*(11), 809–814. https://doi.org/10.1038/ngeo2824

Eade, R., Smith, D., Scaife, A., Wallace, E., Dunstone, N., Hermanson, L., and Robinson, N. (2014). Do seasonal-to-decadal climate predictions underestimate the predictability of the real world? *Geophysical Research Letters*, *41*(15), 5620–5628. https://doi.org/10.1002/2014GL061146

Efron, B., and Tibshirani, R. (1994). *An introduction to the bootstrap*. Chapman & Hall.

English, J. M., Toon, O. B., and Mills, M. J. (2013). Microphysical simulations of large volcanic eruptions: Pinatubo and Toba. *Journal of Geophysical Research: Atmospheres*, *118*(4), 1880–1895. https://doi.org/10.1002/jgrd.50196

Eyring, V., Bony, S., Meehl, G. A., Senior, C. A., Stevens, B., Stouffer, R. J., and Taylor, K. E. (2016). Overview of the Coupled Model Intercomparison Project Phase 6 (CMIP6) experimental design and organization. *Geoscientific Model Development*, *9*(5), 1937–1958. https://doi.org/10.5194/gmd-9-1937-2016

Eyring, V., Cionni, I., Bodeker, G. E., Charlton-Perez, A. J., Kinnison, D. E., Scinocca, J. F., Waugh, D. W., Akiyoshi, H., Bekki, S., Chipperfield, M. P., Dameris, M., Dhomse, S., Frith, S. M., Garny, H., Gettelman, A., Kubin, A., Langematz, U., Mancini, E., Marchand, M., … Yamashita, Y. (2010). Multi-model assessment of stratospheric ozone return dates and ozone recovery in CCMVal-2 models. *Atmospheric Chemistry and Physics*, *10*(19), 9451–9472. https://doi.org/10.5194/acp-10-9451-2010

Faust, J. C., Fabian, K., Milzer, G., Giraudeau, J., and Knies, J. (2016). Norwegian fjord sediments reveal NAO related winter temperature and precipitation changes of the past 2800 years. *Earth and Planetary Science Letters*, *435*, 84–93. https://doi.org/10.1016/j.epsl.2015.12.003

Feldstein, S. B., and Franzke, C. (2006). Are the North Atlantic Oscillation and the Northern Annular Mode Distinguishable? *Journal of the Atmospheric Sciences*, *63*(11), 2915–2930. https://doi.org/10.1175/JAS3798.1

Fischer, E. M., Luterbacher, J., Zorita, E., Tett, S. F. B., Casty, C., and Wanner, H. (2007). European climate response to tropical volcanic eruptions over the last half millennium: CLIMATE RESPONSE TO VOLCANIC ERUPTIONS. *Geophysical Research Letters*, *34*(5). https://doi.org/10.1029/2006GL027992

Forster, P., Ramaswamy, V., Artaxo, P., Berntsen, T., Betts, R., Fahey, D., Haywood, J., Lean, J., Lowe, D., Myhre, G., Nganga, J., Prinn, R., Raga, G., Schulz, M., Dorland, R., Bodeker, G., Boucher, O., Collins, W., Conway, T., and Whorf, T. (2007). *Changes in Atmospheric Constituents and in Radiative Forcing*.

Fraedrich, K. (1994). *An ENSO impact on Europe?* 13.

Frölicher, T. L., Joos, F., and Raible, C. C. (2011). Sensitivity of atmospheric CO_2 and climate to explosive volcanic eruptions. *Biogeosciences*, *8*(8), 2317–2339. https://doi.org/10.5194/bg-8-2317-2011

Gaillard, M.-J., Sugita, S., Mazier, F., Trondman, A.-K., Broström, A., Hickler, T., Kaplan, J. O., Kjellström, E., Kokfelt, U., Kuneš, P., Lemmen, C., Miller, P., Olofsson, J., Poska, A., Rundgren, M., Smith, B., Strandberg, G., Fyfe, R., Nielsen, A. B., … Seppä, H. (2010). Holocene land-cover reconstructions for studies on land cover-climate feedbacks. *Climate of the Past*, *6*(4), 483–499. https://doi.org/10.5194/cp-6-483-2010

Gao, C., Ludlow, F., Matthews, J. A., Stine, A. R., Robock, A., Pan, Y., Breen, R., Nolan, B., and Sigl, M. (2021). Volcanic climate impacts can act as ultimate and proximate causes of Chinese dynastic collapse. *Communications Earth & Environment*, *2*(1), 234. https://doi.org/10.1038/s43247-021-00284-7

Gao, C., Robock, A., and Ammann, C. (2008). Volcanic forcing of climate over the past 1500 years: An improved ice core-based index for climate models. *Journal of Geophysical Research*, *113*(D23). https://doi.org/10.1029/2008JD010239

Gao, C., Robock, A., and Ammann, C. (2012). Correction to "Volcanic forcing of climate over the past 1500 years: An improved ice core-based index for climate models." *Journal of Geophysical Research: Atmospheres*, *117*(D16). https://doi.org/10.1029/2012JD018052

Gao, Y., and Gao, C. (2017). European hydroclimate response to volcanic eruptions over the past nine centuries. *International Journal of Climatology*, *37*(11), 4146–4157. https://doi.org/10.1002/joc.5054

Gerber, S., Joos, F., Brügger, P., Stocker, T., Mann, M., Sitch, S., and Scholze, M. (2003). Constraining temperature variations over the last millennium by comparing simulated and observed atmospheric CO2. *Climate Dynamics*, *20*(2), 281–299. https://doi.org/10.1007/s00382-002-0270-8

Giorgetta, M. A., Jungclaus, J., Reick, C. H., Legutke, S., Bader, Jă., BĂśttinger, M., Brovkin, V., Crueger, T., Esch, M., Fieg, K., Glushak, K., Gayler, V., Haak, H., Hollweg, H.-D., Ilyina, T., Kinne, S., Kornblueh, L., Matei, D., Mauritsen, T., … Stevens, B. (2013). Climate and carbon cycle changes from 1850 to 2100 in MPI-ESM simulations for the Coupled Model Intercomparison Project phase 5. *Journal of Advances in Modeling Earth Systems*, *5*(3), 572–597. https://doi.org/10.1002/jame.20038

Goosse, H., Arzel, O., Luterbacher, J., Mann, M. E., Renssen, H., Riedwyl, N., Timmermann, A., Xoplaki, E., and Wanner, H. (2006). The origin of the European "Medieval Warm Period." *Clim. Past*, 15.

Graf, H.-F. (1992). Arctic radiation deficit and climate variability. *Climate Dynamics*, *7*(1), 19–28. https://doi.org/10.1007/BF00204818

Graf, H.-F., Kirchner, I., Robock, A., and Schult, I. (1993). Pinatubo eruption winter climate effects: Model versus observations. *Climate Dynamics*, *9*(2), 81–93. https://doi.org/10.1007/BF00210011

Graf, H.-F., and Zanchettin, D. (2012). Central Pacific El Niño, the "subtropical bridge," and Eurasian climate: TWO EL NIÑO TYPES AND EURASIAN CLIMATE. *Journal of Geophysical Research: Atmospheres*, *117*(D1), n/a-n/a. https://doi.org/10.1029/2011JD016493

Graf, H.-F., Zanchettin, D., Timmreck, C., and Bittner, M. (2014). Observational constraints on the tropospheric and near-surface winter signature of the Northern Hemisphere stratospheric polar vortex. *Climate Dynamics*, *43*(12), 3245–3266. https://doi.org/10.1007/s00382-014-2101-0

Gregory, J. M. (2010). Long-term effect of volcanic forcing on ocean heat content. *Geophysical Research Letters*, *37*(22). https://doi.org/10.1029/2010GL045507

Guillet, S., Corona, C., Stoffel, M., Khodri, M., Lavigne, F., Ortega, P., Eckert, N., Sielenou, P. D., Daux, V., Churakova (Sidorova), O. V., Davi, N., Edouard, J.-L., Zhang, Y., Luckman, B. H., Myglan, V. S., Guiot, J., Beniston, M., Masson-Delmotte, V., and Oppenheimer, C. (2017). Climate response to the Samalas volcanic eruption in 1257 revealed by proxy records. *Nature Geoscience*, *10*(2), 123–128. https://doi.org/10.1038/ngeo2875

Guo, S., Bluth, G. J. S., Rose, W. I., Watson, I. M., and Prata, A. J. (2004). Re-evaluation of SO2 release of the 15 June 1991 Pinatubo eruption using ultraviolet and infrared satellite sensors. *Geochemistry, Geophysics, Geosystems*, *5*(4). https://doi.org/10.1029/2003GC000654

Gusev, A. A. (2008). Temporal structure of the global sequence of volcanic eruptions: Order clustering and intermittent discharge rate. *Physics of the Earth and Planetary Interiors*, *166*(3), 203–218. https://doi.org/10.1016/j.pepi.2008.01.004

Hamilton, K. (1988). A detailed examination of the extratropical response to Tropical El Niño/Southern Oscillation events. *Journal of Climatology*, *8*(1), 67–86. https://doi.org/10.1002/joc.3370080107

Hartmann, D. L., Klein Tank, A. M. G., Rusticucci, M., Alexander, L., Brönnimann, S., Charabi, Y., Dentener, F., Dlugokencky, E. J., Easterling, D., Kaplan, A., Soden, B., Thorne, P., Wild, M., and Zhai, P. (2014). *Observations: Atmosphere and Surface* (Cambridge University Press, pp. 159–254). https://www.cambridge.org/core/books/climate-change-2013-the-physical-science-basis/observations-atmosphere-and-surface/61A8F156E8720E337BC2B161B005F0B8

Haug, G. H., Günther, D., Peterson, L. C., Sigman, D. M., Hughen, K. A., and Aeschlimann, B. (2003). Climate and the Collapse of Maya Civilization. *Science*, *299*(5613), 1731–1735. https://doi.org/10.1126/science.1080444

Hauglustaine, D. A., Balkanski, Y., and Schulz, M. (2014). A global model simulation of present and future nitrate aerosols and their direct radiative forcing of climate. *Atmospheric Chemistry and Physics*, *14*(20), 11031–11063. https://doi.org/10.5194/acp-14-11031-2014

Haywood, A. M., Dowsett, H. J., Dolan, A. M., Rowley, D., Abe-Ouchi, A., Otto-Bliesner, B., Chandler, M. A., Hunter, S. J., Lunt, D. J., Pound, M., and Salzmann, U. (2016). The Pliocene Model Intercomparison Project (PlioMIP) Phase 2: Scientific objectives and experimental design. *Climate of the Past*, *12*(3), 663–675. https://doi.org/10.5194/cp-12-663-2016

Haywood, J. M., Jones, A., Bellouin, N., and Stephenson, D. (2013). Asymmetric forcing from stratospheric aerosols impacts Sahelian rainfall. *Nature Climate Change*, *3*(7), 660–665. https://doi.org/10.1038/nclimate1857

Hegerl, G. C., Crowley, T. J., Hyde, W. T., and Frame, D. J. (2006). Climate sensitivity constrained by temperature reconstructions over the past seven centuries. *Nature*, *440*(7087), 1029–1032. https://doi.org/10.1038/nature04679

Hegerl, G., Luterbacher, J., González-Rouco, F., Tett, S. F. B., Crowley, T., and Xoplaki, E. (2011). Influence of human and natural forcing on European seasonal temperatures. *Nature Geoscience*, *4*(2), 99–103. https://doi.org/10.1038/ngeo1057

Hegerl, G., Zwiers, F. W., Braconnot, P., Gillett, N. P., Luo, Y., Marengo Orsini, J. A., Nicholls, N., Penner, J. E., and Stott, P. A. (2007). Understanding and attributing climate change. In *Climate Change 2007: The Physical Science Basis. Contribution of Working Group I to the Fourth Assessment Report of the IPCC. Cambridge, United Kingdom Cambridge University Press* (pp. 669–670). Cambridge University Press.

Helama, S., Fauria, M. M., MielikÄ¤inen, K., Timonen, M., and Eronen, M. (2010). Sub-Milankovitch solar forcing of past climates: Mid and late Holocene perspectives. *GSA Bulletin*, *122*(11–12), 1981–1988. https://doi.org/10.1130/B30088.1

Hermanson, L., Bilbao, R., Dunstone, N., Ménégoz, M., Ortega, P., Pohlmann, H., Robson, J. I., Smith, D. M., Strand, G., Timmreck, C., Yeager, S., and Danabasoglu, G. (2020). Robust Multiyear Climate Impacts of Volcanic Eruptions in Decadal Prediction Systems. *Journal of Geophysical Research: Atmospheres*, *125*(9). https://doi.org/10.1029/2019JD031739

Hernández, A., Sánchez-López, G., Pla-Rabes, S., Comas-Bru, L., Parnell, A., Cahill, N., Geyer, A., Trigo, R. M., and Giralt, S. (2020). *NAO proxy-based reconstruction from Iberian Peninsula (-150 to 2010 CE)*. PANGAEA. https://doi.org/10.1594/PANGAEA.921916

Hilmer, M., and Jung, T. (2000). Evidence for a recent change in the link between the North Atlantic Oscillation and Arctic Sea ice export. *Geophysical Research Letters*, *27*(7), 989–992. https://doi.org/10.1029/1999GL010944

Hourdin, F., Rio, C., Grandpeix, J.-Y., Madeleine, J.-B., Cheruy, F., Rochetin, N., Jam, A., Musat, I., Idelkadi, A., Fairhead, L., Foujols, M.-A., Mellul, L., Traore, A.-K., Dufresne, J.-L., Boucher, O., Lefebvre, M.-P., Millour, E., Vignon, E., Jouhaud, J., … Ghattas, J. (2020). LMDZ6A: The Atmospheric Component of the IPSL Climate Model With Improved and Better Tuned Physics. *Journal of Advances in Modeling Earth Systems*, *12*(7), e2019MS001892. https://doi.org/10.1029/2019MS001892

Hurrell, J. W. (1995). Decadal Trends in the North Atlantic Oscillation: Regional Temperatures and Precipitation. *Science*, *269*(5224), 676–679. https://doi.org/10.1126/science.269.5224.676

Hurrell, J. W., and Deser, C. (2009). North Atlantic climate variability: The role of the North Atlantic Oscillation. *Journal of Marine Systems*, *78*(1), 28–41. https://doi.org/10.1016/j.jmarsys.2008.11.026

Hurrell, J. W., Holland, M. M., Gent, P. R., Ghan, S., Kay, J. E., Kushner, P. J., Lamarque, J.-F., Large, W. G., Lawrence, D., Lindsay, K., Lipscomb, W. H., Long, M. C., Mahowald, N., Marsh, D. R., Neale, R. B., Rasch, P., Vavrus, S., Vertenstein, M., Bader, D., … Marshall, S. (2013). The Community Earth System Model: A Framework for Collaborative Research. *Bulletin of the American Meteorological Society*, 130204122247009. https://doi.org/10.1175/BAMS-D-12-00121

Hurrell, J. W., Kushnir, Y., Ottersen, G., and Visbeck, M. (2003). An overview of the North Atlantic Oscillation. In J. W. Hurrell, Y. Kushnir, G. Ottersen, and M. Visbeck (Eds.), *Geophysical Monograph Series* (Vol. 134, pp. 1–35). American Geophysical Union. https://doi.org/10.1029/134GM01

Hurtt, G. C., Chini, L., Sahajpal, R., Frolking, S., Bodirsky, B. L., Calvin, K., Doelman, J. C., Fisk, J., Fujimori, S., Klein Goldewijk, K., Hasegawa, T., Havlik, P., Heinimann, A., Humpenöder, F., Jungclaus, J., Kaplan, J. O., Kennedy, J., Krisztin, T., Lawrence, D., … Zhang, X. (2020). Harmonization of global land use change and management for the period 850–2100 (LUH2) for

CMIP6. *Geoscientific Model Development*, *13*(11), 5425–5464. https://doi.org/10.5194/gmd-13-5425-2020

Iles, C. E., Hegerl, G. C., Schurer, A. P., and Zhang, X. (2013). The effect of volcanic eruptions on global precipitation. *Journal of Geophysical Research: Atmospheres*, *118*(16), 8770–8786. https://doi.org/10.1002/jgrd.50678

Jansen, E., Overpeck, J., Briffa, K. R., Duplessy, J.-C., Joos, F., Masson-Delmotte, V., Olago, D., Otto-Bliesner, B., Peltier, W. R., Rahmstorf, S., Ramesh, R., Raynaud, D., Rind, D., Solomina, O., Villalba, R., and Zhang, D. (2007). *Palaeoclimate. In: Climate Change 2007: The Physical Science Basis. Contribution of Working Group I to the Fourth Assessment Report of the IPCC* (Vols. 499–587, pp. 434–497). Cambridge University Press.

Jones, C. D., and Cox, P. M. (2001). Modeling the volcanic signal in the atmospheric CO2 record. *Global Biogeochemical Cycles*, *15*(2), 453–465. https://doi.org/10.1029/2000GB001281

Jones, P. D., Harpham, C., and Vinther, B. M. (2014). Winter-responding proxy temperature reconstructions and the North Atlantic Oscillation: WINTER-RESPONDING PROXIES AND THE NAO. *Journal of Geophysical Research: Atmospheres*, *119*(11), 6497–6505. https://doi.org/10.1002/2014JD021561

Jones, P. D., Jonsson, T., and Wheeler, D. (1997). Extension to the North Atlantic oscillation using early instrumental pressure observations from Gibraltar and south-west Iceland. *International Journal of Climatology*, *17*(13), 1433–1450. https://doi.org/10.1002/(SICI)1097-0088(19971115)17:13<1433::AID-JOC203>3.0.CO;2-P

Joshi, M. M., and Jones, G. S. (2009). The climatic effects of the direct injection of water vapour into the stratosphere by large volcanic eruptions. *Atmospheric Chemistry and Physics*, *9*(16), 6109–6118. https://doi.org/10.5194/acp-9-6109-2009

Jungclaus, J. H., Bard, E., Baroni, M., Braconnot, P., Cao, J., Chini, L. P., Egorova, T., Evans, M., González-Rouco, J. F., Goosse, H., Hurtt, G. C., Joos, F., Kaplan, J. O., Khodri, M., Klein Goldewijk, K., Krivova, N., LeGrande, A. N., Lorenz, S. J., Luterbacher, J., … Zorita, E. (2017). The PMIP4 contribution to CMIP6 – Part 3: The last millennium, scientific objective, and experimental design for the PMIP4 past1000 simulations. *Geoscientific Model Development*, *10*(11), 4005–4033. https://doi.org/10.5194/gmd-10-4005-2017

Jungclaus, J. H., Lorenz, S. J., Timmreck, C., Reick, C. H., Brovkin, V., Six, K., Segschneider, J., Giorgetta, M. A., Crowley, T. J., Pongratz, J., Krivova, N. A., Vieira, L. E., Solanki, S. K., Klocke, D., Botzet, M., Esch, M., Gayler, V., Haak, H., Raddatz, T. J., … Marotzke, J. (2010). Climate and carbon-cycle variability over the last millennium. *Climate of the Past*, *6*(5), 723–737. https://doi.org/10.5194/cp-6-723-2010

Kageyama, M., Albani, S., Braconnot, P., Harrison, S. P., Hopcroft, P. O., Ivanovic, R. F., Lambert, F., Marti, O., Peltier, W. R., Peterschmitt, J.-Y., Roche, D. M., Tarasov, L., Zhang, X., Brady, E. C., Haywood, A. M., LeGrande, A. N., Lunt, D. J., Mahowald, N. M., Mikolajewicz, U., … Zheng, W. (2017). The PMIP4 contribution to CMIP6 – Part 4: Scientific objectives and experimental design of the PMIP4-CMIP6 Last Glacial Maximum experiments and PMIP4 sensitivity experiments. *Geoscientific Model Development*, *10*(11), 4035–4055. https://doi.org/10.5194/gmd-10-4035-2017

Kaplan, J. O., Krumhardt, K. M., Ellis, E. C., Ruddiman, W. F., Lemmen, C., and Goldewijk, K. K. (2011). Holocene carbon emissions as a result of anthropogenic land cover change. *The Holocene*, *21*(5), 775–791. https://doi.org/10.1177/0959683610386983

Khodri, M., Izumo, T., Vialard, J., Janicot, S., Cassou, C., Lengaigne, M., Mignot, J., Gastineau, G., Guilyardi, E., Lebas, N., Robock, A., and McPhaden, M. J. (2017). Tropical explosive volcanic eruptions can trigger El Niño by cooling tropical Africa. *Nature Communications*, *8*(1). https://doi.org/10.1038/s41467-017-00755-6

Kirchner, I., Stenchikov, G., Graf, H.-F., Robock, A., and AntuÃąa-Marrero, J. C. (1999). Climate model simulation of winter warming and summer cooling following the 1991 Mount Pinatubo volcanic eruption. *Journal of Geophysical Research*, *1041*, 19039–19056. https://doi.org/10.1029/1999JD900213

Kleinschmitt, C., Boucher, O., Bekki, S., Lott, F., and Platt, U. (2017). The Sectional Stratospheric Sulfate Aerosol module (S3A-v1) within the LMDZ general circulation model: Description and evaluation against stratospheric aerosol observations. *Geoscientific Model Development*, *10*(9), 3359–3378. https://doi.org/10.5194/gmd-10-3359-2017

Kravitz, B., and Robock, A. (2011). Climate effects of high-latitude volcanic eruptions: Role of the time of year. *Journal of Geophysical Research*, *116*(D1), D01105. https://doi.org/10.1029/2010JD014448

Krinner, G., Viovy, N., de Noblet-Ducoudré, N., Ogée, J., Polcher, J., Friedlingstein, P., Ciais, P., Sitch, S., and Prentice, I. C. (2005). A dynamic global vegetation model for studies of the coupled atmosphere-biosphere system. *Global Biogeochemical Cycles*, *19*(1). https://doi.org/10.1029/2003GB002199

Krivova, N. A., Vieira, L. E. A., and Solanki, S. K. (2010). Reconstruction of solar spectral irradiance since the Maunder minimum: SOLAR SPECTRAL IRRADIANCE SINCE 1610. *Journal of Geophysical Research: Space Physics*, *115*(A12), n/a-n/a. https://doi.org/10.1029/2010JA015431

Labitzke, K., and McCormick, M. P. (1992). Stratospheric temperature increases due to Pinatubo aerosols. *Geophysical Research Letters*, *19*(2), 207–210. https://doi.org/10.1029/91GL02940

Lanciki, A., Cole-Dai, J., Thiemens, M. H., and Savarino, J. (2012). Sulfur isotope evidence of little or no stratospheric impact by the 1783 Laki volcanic eruption. *Geophysical Research Letters*, *39*(1). https://doi.org/10.1029/2011GL050075

Laskar, J., Robutel, P., Joutel, F., Gastineau, M., Correia, A. C. M., and Levrard, B. (2004). A long-term numerical solution for the insolation quantities ofÂ theÂ Earth. *A&A*, *428*(1), 261–285. https://doi.org/10.1051/0004-6361:20041335

Lawrence, D. M., Hurtt, G. C., Arneth, A., Brovkin, V., Calvin, K. V., Jones, A. D., Jones, C. D., Lawrence, P. J., de Noblet-Ducoudré, N., Pongratz, J., Seneviratne, S. I., and Shevliakova, E. (2016). The Land Use Model Intercomparison Project (LUMIP) contribution to CMIP6: Rationale and experimental design. *Geoscientific Model Development*, *9*(9), 2973–2998. https://doi.org/10.5194/gmd-9-2973-2016

Lean, J. L., White, O. R., and Skumanich, A. (1995). On the solar ultraviolet spectral irradiance during the Maunder Minimum. *Global Biogeochemical Cycles*, *9*(2), 171–182. https://doi.org/10.1029/95GB00159

Legras, B., Mestre, O., Bard, E., and Yiou, P. (2010). A critical look at solar-climate relationships from long temperature series. *Climate of the Past*, *6*(6), 745–758. https://doi.org/10.5194/cp-6-745-2010

Liou, K.-N., and Ou, S.-C. (1989). The role of cloud microphysical processes in climate: An assessment from a one-dimensional perspective. *Journal of Geophysical Research: Atmospheres*, *94*(D6), 8599–8607. https://doi.org/10.1029/JD094iD06p08599

Liu, F., Chai, J., Wang, B., Liu, J., Zhang, X., and Wang, Z. (2016). Global monsoon precipitation responses to large volcanic eruptions. *Scientific Reports*, *6*(1). https://doi.org/10.1038/srep24331

Liu, F., Li, J., Wang, B., Liu, J., Li, T., Huang, G., and Wang, Z. (2017). Divergent El Niño responses to volcanic eruptions at different latitudes over the past millennium. *Climate Dynamics*. https://doi.org/10.1007/s00382-017-3846-z

Liu, X., Easter, R. C., Ghan, S. J., Zaveri, R., Rasch, P., Shi, X., Lamarque, J.-F., Gettelman, A., Morrison, H., Vitt, F., Conley, A., Park, S., Neale, R., Hannay, C., Ekman, A. M. L., Hess, P., Mahowald, N., Collins, W., Iacono, M. J., … Mitchell, D. (2012). Toward a minimal representation of aerosols in climate models: Description and evaluation in the Community Atmosphere Model CAM5. *Geoscientific Model Development*, *5*(3), 709–739. https://doi.org/10.5194/gmd-5-709-2012

Lurton, T., Balkanski, Y., Bastrikov, V., Bekki, S., Bopp, L., Braconnot, P., Brockmann, P., Cadule, P., Contoux, C., Cozic, A., Cugnet, D., Dufresne, J., Éthé, C., Foujols, M., Ghattas, J., Hauglustaine, D., Hu, R., Kageyama, M., Khodri, M., … Boucher, O. (2020). Implementation of the CMIP6 Forcing Data in the IPSL- CM6A- LR Model. *Journal of Advances in Modeling Earth Systems*, *12*(4). https://doi.org/10.1029/2019MS001940

Luterbacher, J., Dietrich, D., Xoplaki, E., Grosjean, M., and Wanner, H. (2004). European Seasonal and Annual Temperature Variability, Trends, and Extremes Since 1500. *Science*, *303*(5663), 1499–1503. https://doi.org/10.1126/science.1093877

Luterbacher, J., Xoplaki, E., Dietrich, D., Rickli, R., Jacobeit, J., Beck, C., Gyalistras, D., Schmutz, C., and Wanner, H. (2002). Reconstruction of sea level pressure fields over the Eastern North Atlantic and Europe back to 1500. *Climate Dynamics*, *18*(7), 545–561. https://doi.org/10.1007/s00382-001-0196-6

MacFarling Meure, C., Etheridge, D., Trudinger, C., Steele, P., Langenfelds, R., van Ommen, T., Smith, A., and Elkins, J. (2006). Law Dome CO2, CH4 and N2O ice core records extended to 2000 years BP. *Geophysical Research Letters*, *33*(14). https://doi.org/10.1029/2006GL026152

Madec, G., Bourdallé-Badie, R., Pierre-Antoine Bouttier, Bricaud, C., Bruciaferri, D., Calvert, D., Chanut, J., Clementi, E., Coward, A., Delrosso, D., Éthé, C., Flavoni, S., Graham, T., Harle, J., Iovino, D., Lea, D., Lévy, C., Lovato, T., Martin, N., … Vancoppenolle, M. (2017). *NEMO ocean engine*. https://doi.org/10.5281/ZENODO.1472492

Magnusdottir, G., Deser, C., and Saravanan, R. (2004). The Effects of North Atlantic SST and Sea Ice Anomalies on the Winter Circulation in CCM3. Part I: Main Features and Storm Track Characteristics of the Response. *Journal of Climate*, *17*(5), 857–876. https://doi.org/10.1175/1520-0442(2004)017<0857:TEONAS>2.0.CO;2

Maher, N., McGregor, S., England, M. H., and Gupta, A. S. (2015). Effects of volcanism on tropical variability. *Geophysical Research Letters*, *42*(14), 6024–6033. https://doi.org/10.1002/2015GL064751

Malavelle, F. F., Haywood, J. M., Jones, A., Gettelman, A., Clarisse, L., Bauduin, S., Allan, R. P., Karset, I. H. H., KristjÄĄnsson, Jă. E., Oreopoulos, L., Cho, N., Lee, D., Bellouin, N., Boucher, O., Grosvenor, D. P., Carslaw, K. S., Dhomse, S., Mann, G. W., Schmidt, A., … Thordarson, T. (2017). Strong

constraints on aerosol-cloud interactions from volcanic eruptions. *Nature*, *546*(7659), 485–491. https://doi.org/10.1038/nature22974

Manning, J. G., Ludlow, F., Stine, A. R., Boos, W. R., Sigl, M., and Marlon, J. R. (2017). Volcanic suppression of Nile summer flooding triggers revolt and constrains interstate conflict in ancient Egypt. *Nature Communications*, *8*(1), 900. https://doi.org/10.1038/s41467-017-00957-y

Marchand, M., Keckhut, P., Lefebvre, S., Claud, C., Cugnet, D., Hauchecorne, A., LefÄ¨vre, F., Lefebvre, M.-P., Jumelet, J., Lott, F., Hourdin, F., Thuillier, G., Poulain, V., Bossay, S., Lemennais, P., David, C., and Bekki, S. (2012). Dynamical amplification of the stratospheric solar response simulated with the Chemistry-Climate Model LMDz-Reprobus. *Atmospheric Coupling Processes in the Sun-Earth System*, *75–76*, 147–160. https://doi.org/10.1016/j.jastp.2011.11.008

Marsh, D. R., Mills, M. J., Kinnison, D. E., Lamarque, J.-F., Calvo, N., and Polvani, L. M. (2013). Climate Change from 1850 to 2005 Simulated in CESM1(WACCM). *Journal of Climate*, *26*(19), 7372–7391. https://doi.org/10.1175/JCLI-D-12-00558.1

Marshall, J., Kushnir, Y., Battisti, D., Chang, P., Czaja, A., Dickson, R., Hurrell, J., McCartney, M., Saravanan, R., and Visbeck, M. (2001). North Atlantic climate variability: Phenomena, impacts and mechanisms. *International Journal of Climatology*, *21*(15), 1863–1898. https://doi.org/10.1002/joc.693

Masson-Delmotte, V., Schulz, M., Abe-Ouchi, A., Beer, J., Ganopolski, A., González Rouco, J. F., Jansen, E., Lambeck, K., Luterbacher, J., Naish, T. R., Osborn, T., Otto-Bliesner, B. L., Quinn, T. M., Ramesh, R., Rojas, M., Shao, X., and Timmermann, A. (2013). Information from Paleoclimate Archives. In IPCC (Ed.), *Climate Change 2013—The Physical Science Basis: Working Group I Contribution to the Fifth Assessment Report of the Intergovernmental Panel on Climate Change*. Cambridge University Press. https://doi.org/10.1017/CBO9781107415324.013

McCormick, M. P., and Veiga, R. E. (1992). SAGE II measurements of early Pinatubo aerosols. *Geophysical Research Letters*, *19*(2), 155–158. https://doi.org/10.1029/91GL02790

Meinshausen, M., Vogel, E., Nauels, A., Lorbacher, K., Meinshausen, N., Etheridge, D. M., Fraser, P. J., Montzka, S. A., Rayner, P. J., Trudinger, C. M., Krummel, P. B., Beyerle, U., Canadell, J. G., Daniel, J. S., Enting, I. G., Law, R. M., Lunder, C. R., O'Doherty, S., Prinn, R. G., … Weiss, R. (2017). Historical greenhouse gas concentrations for climate modelling (CMIP6). *Geoscientific Model Development*, *10*(5), 2057–2116. https://doi.org/10.5194/gmd-10-2057-2017

Mellado-Cano, J., Barriopedro, D., García-Herrera, R., Trigo, R. M., and Hernández, A. (2019). Examining the North Atlantic Oscillation, East Atlantic Pattern, and Jet Variability since 1685. *Journal of Climate*, *32*(19), 6285–6298. https://doi.org/10.1175/JCLI-D-19-0135.1

Meurdesoif, Y., Caubel, A., Lacroix, R., Dérouillat, J., and Nguyen, M. H. (2016). *XIOS_tutorial*. Retrieved from http://forge.ipsl.jussieu.fr/ioserver/raw-attachment/wiki/WikiStart/XIOS-tutorial.pdf

Miller, G. H., GeirsdÃłttir, Ã., Zhong, Y., Larsen, D. J., Otto-Bliesner, B. L., Holland, M. M., Bailey, D. A., Refsnider, K. A., Lehman, S. J., Southon, J. R., Anderson, C., BjÃśrnsson, H., and Thordarson, T. (2012). Abrupt onset of the Little Ice Age triggered by volcanism and sustained by sea-ice/ocean feedbacks. *Geophysical Research Letters*, *39*(2). https://doi.org/10.1029/2011GL050168

Mills, M. J., Schmidt, A., Easter, R., Solomon, S., Kinnison, D. E., Ghan, S. J., Neely III, R. R., Marsh, D. R., Conley, A., Bardeen, C. G., and Gettelman, A. (2016). Global volcanic aerosol properties derived from emissions, 1990-2014, using CESM1(WACCM). *Journal of Geophysical Research: Atmospheres*, *121*(5), 2332–2348. https://doi.org/10.1002/2015JD024290

Mills, M. J., Toon, O. B., Turco, R. P., Kinnison, D. E., and Garcia, R. R. (2008). Massive global ozone loss predicted following regional nuclear conflict. *Proceedings of the National Academy of Sciences*, *105*(14), 5307. https://doi.org/10.1073/pnas.0710058105

Mitchell, L. E., Brook, E. J., Sowers, T., McConnell, J. R., and Taylor, K. (2011). Multidecadal variability of atmospheric methane, 1000-1800 C.E. *Journal of Geophysical Research: Biogeosciences*, *116*(G2). https://doi.org/10.1029/2010JG001441

Moore, J. C., Beaudon, E., Kang, S., Divine, D., Isaksson, E., Pohjola, V. A., and van de Wal, R. S. W. (2012). Statistical extraction of volcanic sulphate from nonpolar ice cores. *Journal of Geophysical Research: Atmospheres*, *117*(D3). https://doi.org/10.1029/2011JD016592

Morice, C. P., Kennedy, J. J., Rayner, N. A., and Jones, P. D. (2012). Quantifying uncertainties in global and regional temperature change using an ensemble of observational estimates: The HadCRUT4 data set. *Journal of Geophysical Research: Atmospheres*, *117*(D8). https://doi.org/10.1029/2011JD017187

Muscheler, R., Joos, F., Beer, J., Müller, S. A., Vonmoos, M., and Snowball, I. (2007). Solar activity during the last 1000yr inferred from radionuclide records. *Quaternary Science Reviews*, *26*(1), 82–97. https://doi.org/10.1016/j.quascirev.2006.07.012

Myhre, G., Berglen, T. F., Johnsrud, M., Hoyle, C. R., Berntsen, T. K., Christopher, S. A., Fahey, D. W., Isaksen, I. S. A., Jones, T. A., Kahn, R. A., Loeb, N., Quinn, P., Remer, L., Schwarz, J. P., and Yttri,

K. E. (2009). Modelled radiative forcing of the direct aerosol effect with multi-observation evaluation. *Atmospheric Chemistry and Physics*, *9*(4), 1365–1392. https://doi.org/10.5194/acp-9-1365-2009

Myhre, G., Samset, B. H., Schulz, M., Balkanski, Y., Bauer, S., Berntsen, T. K., Bian, H., Bellouin, N., Chin, M., Diehl, T., Easter, R. C., Feichter, J., Ghan, S. J., Hauglustaine, D., Iversen, T., Kinne, S., Kirkevåg, A., Lamarque, J.-F., Lin, G., … Zhou, C. (2013). Radiative forcing of the direct aerosol effect from AeroCom Phase II simulations. *Atmospheric Chemistry and Physics*, *13*(4), 1853–1877. https://doi.org/10.5194/acp-13-1853-2013

Myhre, G., Shindell, D., Bréon, F.-M., Collins, W., Fuglestvedt, J., Huang, J., Lamarque, J.-F., D. Lee, B., Mendoza, B., Nakajima, T., Robock, A., Stephens, G., Takemura, T., and Zhang, H. (2014). Anthropogenic and Natural Radiative Forcing. In IPCC (Ed.), *Climate Change 2013—The Physical Science Basis: Working Group I Contribution to the Fifth Assessment Report of the Intergovernmental Panel on Climate Change* (pp. 659–740). Cambridge University Press; Cambridge Core. https://doi.org/10.1017/CBO9781107415324.018

Oman, L., Robock, A., Stenchikov, G., Schmidt, G. A., and Ruedy, R. (2005). Climatic response to high-latitude volcanic eruptions. *Journal of Geophysical Research*, *110*(D13), D13103. https://doi.org/10.1029/2004JD005487

O'Reilly, C. H., Zanna, L., and Woollings, T. (2019). Assessing External and Internal Sources of Atlantic Multidecadal Variability Using Models, Proxy Data, and Early Instrumental Indices. *Journal of Climate*, *32*(22), 7727–7745. https://doi.org/10.1175/JCLI-D-19-0177.1

Ortega, P., Lehner, F., Swingedouw, D., Masson-Delmotte, V., Raible, C. C., Casado, M., and Yiou, P. (2015). A model-tested North Atlantic Oscillation reconstruction for the past millennium. *Nature*, *523*(7558), 71–74. https://doi.org/10.1038/nature14518

Otterå, O. H., Bentsen, M., Drange, H., and Suo, L. (2010). External forcing as a metronome for Atlantic multidecadal variability. *Nature Geoscience*, *3*, 688–694. https://doi.org/10.1038/ngeo955

Otto-Bliesner, B. L., Braconnot, P., Harrison, S. P., Lunt, D. J., Abe-Ouchi, A., Albani, S., Bartlein, P. J., Capron, E., Carlson, A. E., Dutton, A., Fischer, H., Goelzer, H., Govin, A., Haywood, A., Joos, F., LeGrande, A. N., Lipscomb, W. H., Lohmann, G., Mahowald, N., … Zhang, Q. (2017). The PMIP4 contribution to CMIP6 – Part 2: Two interglacials, scientific objective and experimental design for Holocene and Last Interglacial simulations. *Geoscientific Model Development*, *10*(11), 3979–4003. https://doi.org/10.5194/gmd-10-3979-2017

Otto-Bliesner, B. L., Brady, E. C., Fasullo, J., Jahn, A., Landrum, L., Stevenson, S., Rosenbloom, N., Mai, A., and Strand, G. (2016). Climate Variability and Change since 850 CE: An Ensemble Approach with the Community Earth System Model. *Bulletin of the American Meteorological Society*, *97*(5), 735–754. https://doi.org/10.1175/BAMS-D-14-00233.1

Owens, M. J., Lockwood, M., Hawkins, E., Usoskin, I., Jones, G. S., Barnard, L., Schurer, A., and Fasullo, J. (2017). The Maunder minimum and the Little Ice Age: An update from recent reconstructions and climate simulations. *J. Space Weather Space Clim.*, *7*. https://doi.org/10.1051/swsc/2017034

Ozdogan, M., Robock, A., and Kucharik, C. (2012). Impacts of a nuclear war in South Asia on soybean and maize production in the Midwest United States. *Climatic Change*, *116*. https://doi.org/10.1007/s10584-012-0518-1

Pausata, F. S. R., Chafik, L., Caballero, R., and Battisti, D. S. (2015). Impacts of high-latitude volcanic eruptions on ENSO and AMOC. *Proceedings of the National Academy of Sciences*, *112*(45), 13784–13788. https://doi.org/10.1073/pnas.1509153112

Pausata, F. S. R., Zanchettin Davide, Karamperidou Christina, Caballero Rodrigo, and Battisti David S. (2020). ITCZ shift and extratropical teleconnections drive ENSO response to volcanic eruptions. *Science Advances*, *6*(23). https://doi.org/10.1126/sciadv.aaz5006

Pincus, R., and Baker, M. B. (1994). Effect of precipitation on the albedo susceptibility of clouds in the marine boundary layer. *Nature*, *372*(6503), 250–252. https://doi.org/10.1038/372250a0

Plazzotta, M., Séférian, R., Douville, H., Kravitz, B., and Tjiputra, J. (2018). Land Surface Cooling Induced by Sulfate Geoengineering Constrained by Major Volcanic Eruptions. *Geophysical Research Letters*, *45*(11), 5663–5671. https://doi.org/10.1029/2018GL077583

Plummer, C. T., Curran, M. A. J., van Ommen, T. D., Rasmussen, S. O., Moy, A. D., Vance, T. R., Clausen, H. B., Vinther, B. M., and Mayewski, P. A. (2012). An independently dated 2000-yr volcanic record from Law Dome, East Antarctica, including a new perspective on the dating of the 1450s CE eruption of Kuwae, Vanuatu. *Climate of the Past*, *8*(6), 1929–1940. https://doi.org/10.5194/cp-8-1929-2012

Polvani, L. M., Banerjee, A., and Schmidt, A. (2019). Northern Hemisphere continental winter warming following the 1991 Mt.\ Pinatubo eruption: Reconciling models and observations. *Atmospheric Chemistry and Physics*, *19*(9), 6351–6366. https://doi.org/10.5194/acp-19-6351-2019

Predybaylo, E., Stenchikov, G., Wittenberg, A. T., and Osipov, S. (2020). El Niño/Southern Oscillation response to low-latitude volcanic eruptions depends on ocean pre-conditions and eruption timing. *Communications Earth & Environment*, *1*(1), 12. https://doi.org/10.1038/s43247-020-0013-y

Rasch, P. J., Tilmes, S., Turco, R. P., Robock, A., Oman, L., Chen, C.-C. (Jack), Stenchikov, G. L., and Garcia, R. R. (2008). An overview of geoengineering of climate using stratospheric sulphate aerosols. *Philosophical Transactions of the Royal Society A: Mathematical, Physical and Engineering Sciences*, *366*(1882), 4007–4037. https://doi.org/10.1098/rsta.2008.0131

Rayner, N. A., Parker, D. E., Horton, E. B., Folland, C. K., Alexander, L. V., Rowell, D. P., Kent, E. C., and Kaplan, A. (2003). Global analyses of sea surface temperature, sea ice, and night marine air temperature since the late nineteenth century. *Journal of Geophysical Research: Atmospheres*, *108*(D14). https://doi.org/10.1029/2002JD002670

Read, W. G., Froidevaux, L., and Waters, J. W. (1993). Microwave limb sounder measurement of stratospheric SO2 from the Mt. Pinatubo Volcano. *Geophysical Research Letters*, *20*(12), 1299–1302. https://doi.org/10.1029/93GL00831

Rieger, L. A., Bourassa, A. E., and Degenstein, D. A. (2015). Merging the OSIRIS and SAGE II stratospheric aerosol records. *Journal of Geophysical Research: Atmospheres*, *120*(17), 8890–8904. https://doi.org/10.1002/2015JD023133

Robock, A. (2000). Volcanic Eruptions and Climate. *REVIEWSOF GEOPHYSICS*, 29.

Robock, A., and Mao, J. (1992). Winter warming from large volcanic eruptions. *Geophysical Research Letters*, *19*(24), 2405–2408. https://doi.org/10.1029/92GL02627

Robock, A., and Mao, J. (1995). The Volcanic Signal in Surface Temperature Observations. *Journal of Climate*, *8*(5), 1086–1103. https://doi.org/10.1175/1520-0442(1995)008<1086:TVSIST>2.0.CO;2

Robock, A., Oman, L., and Stenchikov, G. (2007). Nuclear winter revisited with a modern climate model and current nuclear arsenals: Still catastrophic consequences. *Journal of Geophysical Research*, *112*. https://doi.org/10.1029/2006JD008235

Robock, A., Oman, L., Stenchikov, G. L., Toon, O. B., Bardeen, C., and Turco, R. P. (2007). Climatic consequences of regional nuclear conflicts. *Atmospheric Chemistry and Physics*, *7*(8), 2003–2012. https://doi.org/10.5194/acp-7-2003-2007

Rogers, J. C. (1984). The Association between the North Atlantic Oscillation and the Southern Oscillation in the Northern Hemisphere. *Monthly Weather Review*, *112*(10), 1999–2015. https://doi.org/10.1175/1520-0493(1984)112<1999:TABTNA>2.0.CO;2

Rousset, C., Vancoppenolle, M., Madec, G., Fichefet, T., Flavoni, S., Barthélemy, A., Benshila, R., Chanut, J., Levy, C., Masson, S., and Vivier, F. (2015). The Louvain-La-Neuve sea ice model LIM3.6: Global and regional capabilities. *Geoscientific Model Development*, *8*(10), 2991–3005. https://doi.org/10.5194/gmd-8-2991-2015

Russell, P. B., Livingston, J. M., Pueschel, R. F., Bauman, J. J., Pollack, J. B., Brooks, S. L., Hamill, P., Thomason, L. W., Stowe, L. L., Deshler, T., Dutton, E. G., and Bergstrom, R. W. (1996). Global to microscale evolution of the Pinatubo volcanic aerosol derived from diverse measurements and analyses. *Journal of Geophysical Research: Atmospheres*, *101*(D13), 18745–18763. https://doi.org/10.1029/96JD01162

Santer, B. D., Bonfils, C., Painter, J. F., Zelinka, M. D., Mears, C., Solomon, S., Schmidt, G. A., Fyfe, J. C., Cole, J. N. S., Nazarenko, L., Taylor, K. E., and Wentz, F. J. (2014). Volcanic contribution to decadal changes in tropospheric temperature. *Nature Geoscience*, *7*(3), 185–189. https://doi.org/10.1038/ngeo2098

Sato, M., Hansen, J. E., McCormick, M. P., and Pollack, J. B. (1993). Stratospheric aerosol optical depths, 1850–1990. *Journal of Geophysical Research*, *98*(D12), 22987. https://doi.org/10.1029/93JD02553

Scaife, A. A., Karpechko, A. Yu., Baldwin, M. P., Brookshaw, A., Butler, A. H., Eade, R., Gordon, M., MacLachlan, C., Martin, N., Dunstone, N., and Smith, D. (2016). Seasonal winter forecasts and the stratosphere. *Atmospheric Science Letters*, *17*(1), 51–56. https://doi.org/10.1002/asl.598

Scaife, A. A., and Smith, D. (2018). A signal-to-noise paradox in climate science. *Npj Climate and Atmospheric Science*, *1*(1), 28. https://doi.org/10.1038/s41612-018-0038-4

Schmidt, A., Thordarson, T., Oman, L. D., Robock, A., and Self, S. (2012). Climatic impact of the long-lasting 1783 Laki eruption: Inapplicability of mass-independent sulfur isotopic composition measurements. *Journal of Geophysical Research: Atmospheres*, *117*(D23). https://doi.org/10.1029/2012JD018414

Schmidt, G. A., Jungclaus, J. H., Ammann, C. M., Bard, E., Braconnot, P., Crowley, T. J., Delaygue, G., Joos, F., Krivova, N. A., Muscheler, R., Otto-Bliesner, B. L., Pongratz, J., Shindell, D. T., Solanki, S. K., Steinhilber, F., and Vieira, L. E. A. (2011). Climate forcing reconstructions for use in PMIP simulations of the last millennium (v1.0). *Geoscientific Model Development*, *4*(1), 33–45. https://doi.org/10.5194/gmd-4-33-2011

Schneider, D. P., Ammann, C. M., Otto-Bliesner, B. L., and Kaufman, D. S. (2009). Climate response to large, high-latitude and low-latitude volcanic eruptions in the Community Climate System Model. *Journal of Geophysical Research*, *114*(D15). https://doi.org/10.1029/2008JD011222

Schurer, A. P., Hegerl, G. C., Mann, M. E., Tett, S. F. B., and Phipps, S. J. (2013). Separating Forced from Chaotic Climate Variability over the Past Millennium. *Journal of Climate*, *26*(18), 6954–6973. https://doi.org/10.1175/JCLI-D-12-00826.1

Shindell, D. T., Schmidt, G. A., Mann, M. E., and Faluvegi, G. (2004). Dynamic winter climate response to large tropical volcanic eruptions since 1600. *Journal of Geophysical Research: Atmospheres*, *109*(D5). https://doi.org/10.1029/2003JD004151

Shindell, D. T., Schmidt, G. A., Miller, R. L., and Mann, M. E. (2003). Volcanic and Solar Forcing of Climate Change during the Preindustrial Era. *Journal of Climate*, *16*(24), 4094–4107. https://doi.org/10.1175/1520-0442(2003)016<4094:VASFOC>2.0.CO;2

Siegenthaler, U., Stocker, T., Monnin, E., Lüthi, D., Schwander, J., Stauffer, B., Raynaud, D., Barnola, J.-M., Fischer, H., Masson-Delmotte, V., and Jouzel, J. (2005). *Stable Carbon Cycle-Climate Relationship During the Late Pleistocene*.

Sigl, M., McConnell, J. R., Layman, L., Maselli, O., McGwire, K., Pasteris, D., Dahl-Jensen, D., Steffensen, J. P., Vinther, B., Edwards, R., Mulvaney, R., and Kipfstuhl, S. (2013). A new bipolar ice core record of volcanism from WAIS Divide and NEEM and implications for climate forcing of the last 2000 years: A 2000YR BIPOLAR VOLCANO RECORD. *Journal of Geophysical Research: Atmospheres*, *118*(3), 1151–1169. https://doi.org/10.1029/2012JD018603

Sigl, M., Winstrup, M., McConnell, J. R., Welten, K. C., Plunkett, G., Ludlow, F., Büntgen, U., Caffee, M., Chellman, N., Dahl-Jensen, D., Fischer, H., Kipfstuhl, S., Kostick, C., Maselli, O. J., Mekhaldi, F., Mulvaney, R., Muscheler, R., Pasteris, D. R., Pilcher, J. R., … Woodruff, T. E. (2015). Timing and climate forcing of volcanic eruptions for the past 2,500 years. *Nature*, *523*(7562), 543–549. https://doi.org/10.1038/nature14565

Sjolte, J., Adolphi, F., Guðlaugsdòttir, H., and Muscheler, R. (2021). Major Differences in Regional Climate Impact Between High- and Low- Latitude Volcanic Eruptions. *Geophysical Research Letters*, *48*(8). https://doi.org/10.1029/2020GL092017

Sjolte, J., Sturm, C., Adolphi, F., Vinther, B. M., Werner, M., Lohmann, G., and Muscheler, R. (2018). Solar and volcanic forcing of North Atlantic climate inferred from a process-based reconstruction. *Climate of the Past*, *14*(8), 1179–1194. https://doi.org/10.5194/cp-14-1179-2018

Steiger, N. J., Smerdon, J. E., Cook, E. R., and Cook, B. I. (2018). A reconstruction of global hydroclimate and dynamical variables over the Common Era. *Scientific Data*, *5*(1), 180086. https://doi.org/10.1038/sdata.2018.86

Steinhilber, F., Beer, J., and Fröhlich, C. (2009). Total solar irradiance during the Holocene. *Geophysical Research Letters*, *36*(19). https://doi.org/10.1029/2009GL040142

Stenchikov, G., Delworth, T. L., Ramaswamy, V., Stouffer, R. J., Wittenberg, A., and Zeng, F. (2009). Volcanic signals in oceans. *Journal of Geophysical Research: Atmospheres*, *114*(D16). https://doi.org/10.1029/2008JD011673

Stenchikov, G., Hamilton, K., Robock, A., Ramaswamy, V., and Schwarzkopf, M. (2004). Arctic Oscillation response to the 1991 Pinatubo eruption in the SKYHI general circulation model with a realistic Quasi-Biennial Oscillation. *Journal of Geophysical Research*, *109*. https://doi.org/10.1029/2003JD003699

Stenchikov, G., Hamilton, K., Stouffer, R. J., Robock, A., Ramaswamy, V., Santer, B., and Graf, H.-F. (2006). Arctic Oscillation response to volcanic eruptions in the IPCC AR4 climate models. *Journal of Geophysical Research*, *111*(D7), D07107. https://doi.org/10.1029/2005JD006286

Stenchikov, G., Robock, A., Ramaswamy, V., Schwarzkopf, M. D., Hamilton, K., and Ramachandran, S. (2002). Arctic Oscillation response to the 1991 Mount Pinatubo eruption: Effects of volcanic aerosols and ozone depletion. *Journal of Geophysical Research*, *107*(D24), 4803. https://doi.org/10.1029/2002JD002090

Stephenson, D. B., Pavan, V., Collins, M., Junge, M. M., Quadrelli, R., and Participating CMIP2 Modelling Groups. (2006). North Atlantic Oscillation response to transient greenhouse gas forcing and the impact on European winter climate: A CMIP2 multi-model assessment. *Climate Dynamics*, *27*(4), 401–420. https://doi.org/10.1007/s00382-006-0140-x

Stevenson, S., Fasullo, J. T., Otto-Bliesner, B. L., Tomas, R. A., and Gao, C. (2017). Role of eruption season in reconciling model and proxy responses to tropical volcanism. *Proceedings of the National Academy of Sciences*, *114*(8), 1822–1826. https://doi.org/10.1073/pnas.1612505114

Stevenson, S., Otto-Bliesner, B., Fasullo, J., and Brady, E. (2016). "El Niño Like" Hydroclimate Responses to Last Millennium Volcanic Eruptions. *Journal of Climate*, *29*(8), 2907–2921. https://doi.org/10.1175/JCLI-D-15-0239.1

Stommel, H. M., and Stommel, E. (1983). *Volcano weather: The story of 1816, the year without a summer* (Seven Seas Press).

Stommel, H., and Stommel, E. (1979). The Year without a Summer. *Scientific American*, *240*(6), 176–187. JSTOR.

Stothers, R. B. (1996). Major optical depth perturbations to the stratosphere from volcanic eruptions: Pyrheliometric period, 188Q 1960. *Journal of Geophysical Research*, *101*, 3901–3920.

Stothers, R. B. (1997). Stratospheric aerosol clouds due to very large volcanic eruptions of the early twentieth century: Effective particle sizes and conversion from pyrheliometric to visual optical depth. *Journal of Geophysical Research: Atmospheres*, *102*(D5), 6143–6151. https://doi.org/10.1029/96JD03985

Stothers, R. B. (2001). Major optical depth perturbations to the stratosphere from volcanic eruptions: Stellar extinction period, 1961-1978. *Journal of Geophysical Research: Atmospheres*, *106*(D3), 2993–3003. https://doi.org/10.1029/2000JD900652

Stothers, R. B. (2007). Three centuries of observation of stratospheric transparency. *Climatic Change*, *83*(4), 515–521. https://doi.org/10.1007/s10584-007-9238-3

Strong, C., Magnusdottir, G., and Stern, H. (2009). Observed Feedback between Winter Sea Ice and the North Atlantic Oscillation. *Journal of Climate*, *22*(22), 6021–6032. https://doi.org/10.1175/2009JCLI3100.1

Su, W., Loeb, N. G., Schuster, G. L., Chin, M., and Rose, F. G. (2013). Global all-sky shortwave direct radiative forcing of anthropogenic aerosols from combined satellite observations and GOCART simulations. *Journal of Geophysical Research: Atmospheres*, *118*(2), 655–669. https://doi.org/10.1029/2012JD018294

Sun, W., Wang, B., Liu, J., Chen, D., Gao, C., Ning, L., and Chen, L. (2019). How Northern High-Latitude Volcanic Eruptions in Different Seasons Affect ENSO. *Journal of Climate*, *32*(11), 3245–3262. https://doi.org/10.1175/JCLI-D-18-0290.1

Swingedouw, D., Mignot, J., Ortega, P., Khodri, M., Menegoz, M., Cassou, C., and Hanquiez, V. (2017). Impact of explosive volcanic eruptions on the main climate variability modes. *Global and Planetary Change*, *150*, 24–45. https://doi.org/10.1016/j.gloplacha.2017.01.006

Tejedor, E., Steiger, N. J., Smerdon, J. E., Serrano-Notivoli, R., and Vuille, M. (2021). Global hydroclimatic response to tropical volcanic eruptions over the last millennium. *Proceedings of the National Academy of Sciences*, *118*(12), e2019145118. https://doi.org/10.1073/pnas.2019145118

Thomason, L. W., Ernest, N., Millán, L., Rieger, L., Bourassa, A., Vernier, J.-P., Manney, G., Luo, B., Arfeuille, F., and Peter, T. (2018). A global space-based stratospheric aerosol climatology: 1979–2016. *Earth System Science Data*, *10*(1), 469–492. https://doi.org/10.5194/essd-10-469-2018

Thompson, D. W. J., and Wallace, J. M. (1998). The Arctic oscillation signature in the wintertime geopotential height and temperature fields. *Geophysical Research Letters*, *25*(9), 1297–1300. https://doi.org/10.1029/98GL00950

Thompson, D. W. J., and Wallace, J. M. (2000). Annular Modes in the Extratropical Circulation. Part I: Month-to-Month Variability. *Journal of Climate*, *13*(5), 1000–1016. https://doi.org/10.1175/1520-0442(2000)013<1000:AMITEC>2.0.CO;2

Timmreck, C. (2012). Modeling the climatic effects of large explosive volcanic eruptions. *WIREs Climate Change*, *3*(6), 545–564. https://doi.org/10.1002/wcc.192

Timmreck, C., Lorenz, S. J., Crowley, T. J., Kinne, S., Raddatz, T. J., Thomas, M. A., and Jungclaus, J. H. (2009). Limited temperature response to the very large AD 1258 volcanic eruption. *Geophysical Research Letters*, *36*(21). https://doi.org/10.1029/2009GL040083

Toohey, M., KrÄźger, K., Schmidt, H., Timmreck, C., Sigl, M., Stoffel, M., and Wilson, R. (2019). Disproportionately strong climate forcing from extratropical explosive volcanic eruptions. *Nature Geoscience*, *12*(2), 100–107. https://doi.org/10.1038/s41561-018-0286-2

Toohey, M., Krüger, K., Bittner, M., Timmreck, C., and Schmidt, H. (2014). The impact of volcanic aerosol on the Northern Hemisphere stratospheric polar vortex: Mechanisms and sensitivity to forcing structure. *Atmospheric Chemistry and Physics*, *14*(23), 13063–13079. https://doi.org/10.5194/acp-14-13063-2014

Toohey, M., Krüger, K., Niemeier, U., and Timmreck, C. (2011). The influence of eruption season on the global aerosol evolution and radiative impact of tropical volcanic eruptions. *Atmospheric Chemistry and Physics*, *11*(23), 12351–12367. https://doi.org/10.5194/acp-11-12351-2011

Toohey, M., and Sigl, M. (2017). Volcanic stratospheric sulfur injections and aerosol optical depth from 500 BCE to 1900 CE. *Earth System Science Data*, *9*(2), 809–831. https://doi.org/10.5194/essd-9-809-2017

Toohey, M., Stevens, B., Schmidt, H., and Timmreck, C. (2016). Easy Volcanic Aerosol (EVA v1.0): An idealized forcing generator for climate simulations. *Geoscientific Model Development*, *9*(11), 4049–4070. https://doi.org/10.5194/gmd-9-4049-2016

Toon, O., Robock, A., and Turco, R. (2008). Environmental consequences of nuclear war. *Physics Today*, *61*, 37–42. https://doi.org/10.1063/1.3047679

Trudinger, C. M., Etheridge, D. M., Rayner, P. J., Enting, I. G., Sturrock, G. A., and Langenfelds, R. L. (2002). Reconstructing atmospheric histories from measurements of air composition in firn. *Journal of Geophysical Research: Atmospheres*, *107*(D24), ACH 15-1. https://doi.org/10.1029/2002JD002545

Twomey, S. (1977). The Influence of Pollution on the Shortwave Albedo of Clouds. *Journal of Atmospheric Sciences*, *34*(7), 1149–1152. https://doi.org/10.1175/1520-0469(1977)034<1149:TIOPOT>2.0.CO;2

van der Schrier, G., Barichivich, J., Briffa, K. R., and Jones, P. D. (2013). A scPDSI-based global data set of dry and wet spells for 1901-2009. *Journal of Geophysical Research: Atmospheres*, *118*(10), 4025–4048. https://doi.org/10.1002/jgrd.50355

Vancoppenolle, M., Fichefet, T., Goosse, H., Bouillon, S., Madec, G., and Maqueda, M. A. M. (2009). Simulating the mass balance and salinity of Arctic and Antarctic sea ice. 1. Model description and validation. *Ocean Modelling*, *27*(1), 33–53. https://doi.org/10.1016/j.ocemod.2008.10.005

Vernier, J.-P., Thomason, L. W., and Kar, J. (2011). CALIPSO detection of an Asian tropopause aerosol layer. *Geophysical Research Letters*, *38*(7). https://doi.org/10.1029/2010GL046614

Vieira, L. E. A., Solanki, S. K., Krivova, N. A., and Usoskin, I. (2011). Evolution of the solar irradiance during the Holocene. *A&A*, *531*. https://doi.org/10.1051/0004-6361/201015843

Wang, Y.-M., Lean, J. L., and Sheeley, Jr., N. R. (2005). Modeling the Sun's Magnetic Field and Irradiance since 1713. *The Astrophysical Journal*, *625*(1), 522–538. https://doi.org/10.1086/429689

Wei, L., Mosley-Thompson, E., Gabrielli, P., Thompson, L. G., and Barbante, C. (2008). Synchronous deposition of volcanic ash and sulfate aerosols over Greenland in 1783 from the Laki eruption (Iceland). *Geophysical Research Letters*, *35*(16). https://doi.org/10.1029/2008GL035117

Xia, L., and Robock, A. (2013). Impacts of a nuclear war in South Asia on rice production in Mainland China. *Climatic Change*, *116*(2), 357–372. https://doi.org/10.1007/s10584-012-0475-8

Yang, W., Vecchi, G. A., Fueglistaler, S., Horowitz, L. W., Luet, D. J., MuĂąoz, Ă. G., Paynter, D., and Underwood, S. (2019). Climate Impacts From Large Volcanic Eruptions in a High-Resolution Climate Model: The Importance of Forcing Structure. *Geophysical Research Letters*, *46*(13), 7690–7699. https://doi.org/10.1029/2019GL082367

Zambri, B., LeGrande, A. N., Robock, A., and Slawinska, J. (2017). Northern Hemisphere winter warming and summer monsoon reduction after volcanic eruptions over the last millennium. *Journal of Geophysical Research: Atmospheres*, *122*(15), 7971–7989. https://doi.org/10.1002/2017JD026728

Zambri, B., and Robock, A. (2016). Winter warming and summer monsoon reduction after volcanic eruptions in Coupled Model Intercomparison Project 5 (CMIP5) simulations. *Geophysical Research Letters*, *43*(20), 10,920-10,928. https://doi.org/10.1002/2016GL070460

Zambri, B., Robock, A., Mills, M. J., and Schmidt, A. (2019a). Modeling the 1783–1784 Laki Eruption in Iceland: 1. Aerosol Evolution and Global Stratospheric Circulation Impacts. *Journal of Geophysical Research*, 20.

Zambri, B., Robock, A., Mills, M. J., and Schmidt, A. (2019b). Modeling the 1783–1784 Laki Eruption in Iceland: 2. Climate Impacts. *Journal of Geophysical Research: Atmospheres*, *124*(13), 6770–6790. https://doi.org/10.1029/2018JD029554

Zanchettin, D., Khodri, M., Timmreck, C., Toohey, M., Schmidt, A., Gerber, E. P., Hegerl, G., Robock, A., Pausata, F. S. R., Ball, W. T., Bauer, S. E., Bekki, S., Dhomse, S. S., LeGrande, A. N., Mann, G. W., Marshall, L., Mills, M., Marchand, M., Niemeier, U., … Tummon, F. (2016). The Model Intercomparison Project on the climatic response toVolcanic forcing (VolMIP): Experimental design and forcing input data for CMIP6. *Geoscientific Model Development*, *9*(8), 2701–2719. https://doi.org/10.5194/gmd-9-2701-2016

Zanchettin, D., Rubino, A., Matei, D., Bothe, O., and Jungclaus, J. H. (2013). Multidecadal-to-centennial SST variability in the MPI-ESM simulation ensemble for the last millennium. *Climate Dynamics*, *40*(5–6), 1301–1318. https://doi.org/10.1007/s00382-012-1361-9

Zanchettin, D., Timmreck, C., Bothe, O., Lorenz, S. J., Hegerl, G., Graf, H.-F., Luterbacher, J., and Jungclaus, J. H. (2013). Delayed winter warming: A robust decadal response to strong tropical volcanic eruptions? *Geophysical Research Letters*, *40*(1), 204–209. https://doi.org/10.1029/2012GL054403

Zelenski, M., Taran, Y., and Galle, B. (2015). High emission rate of sulfuric acid from Bezymianny volcano, Kamchatka. *Geophysical Research Letters*, *42*(17), 7005–7013. https://doi.org/10.1002/2015GL065340

Zelinka, M. D., Myers, T. A., McCoy, D. T., Po-Chedley, S., Caldwell, P. M., Ceppi, P., Klein, S. A., and Taylor, K. E. (2020). Causes of Higher Climate Sensitivity in CMIP6 Models. *Geophysical Research Letters*, *47*(1), e2019GL085782. https://doi.org/10.1029/2019GL085782

Zhang, D. D., Jim, C. Y., Lin, G. C.-S., He, Y.-Q., Wang, J. J., and Lee, H. F. (2006). Climatic Change, Wars and Dynastic Cycles in China Over the Last Millennium. *Climatic Change*, *76*(3–4), 459–477. https://doi.org/10.1007/s10584-005-9024-z

Zhong, Y., Miller, G. H., Otto-Bliesner, B. L., Holland, M. M., Bailey, D. A., Schneider, D. P., and Geirsdottir, A. (2011). Centennial-scale climate change from decadally-paced explosive volcanism: A coupled sea ice-ocean mechanism. *Climate Dynamics*, *37*(11), 2373–2387. https://doi.org/10.1007/s00382-010-0967-z

Zhuo, Z., Gao, C., and Pan, Y. (2014). Proxy evidence for China's monsoon precipitation response to volcanic aerosols over the past seven centuries: Volcanic effect on China's Precipitation. *Journal of Geophysical Research: Atmospheres*, *119*(11), 6638–6652. https://doi.org/10.1002/2013JD021061

Zhuo, Z., Kirchner, I., Pfahl, S., and Cubasch, U. (2021). Climate impact of volcanic eruptions: The sensitivity to eruption season and latitude in MPI-ESM ensemble experiments. *Atmospheric Chemistry and Physics Discussions*, *2021*, 1–26. https://doi.org/10.5194/acp-2021-260

Zuo, M., Man, W., and Zhou, T. (2021). Dependence of global monsoon response to volcanic eruptions on the background oceanic states. *Journal of Climate*, 1–53. https://doi.org/10.1175/JCLI-D-20-0891.1

Appendix A – Supplementary figures and tables

A.1 – Chapter 2

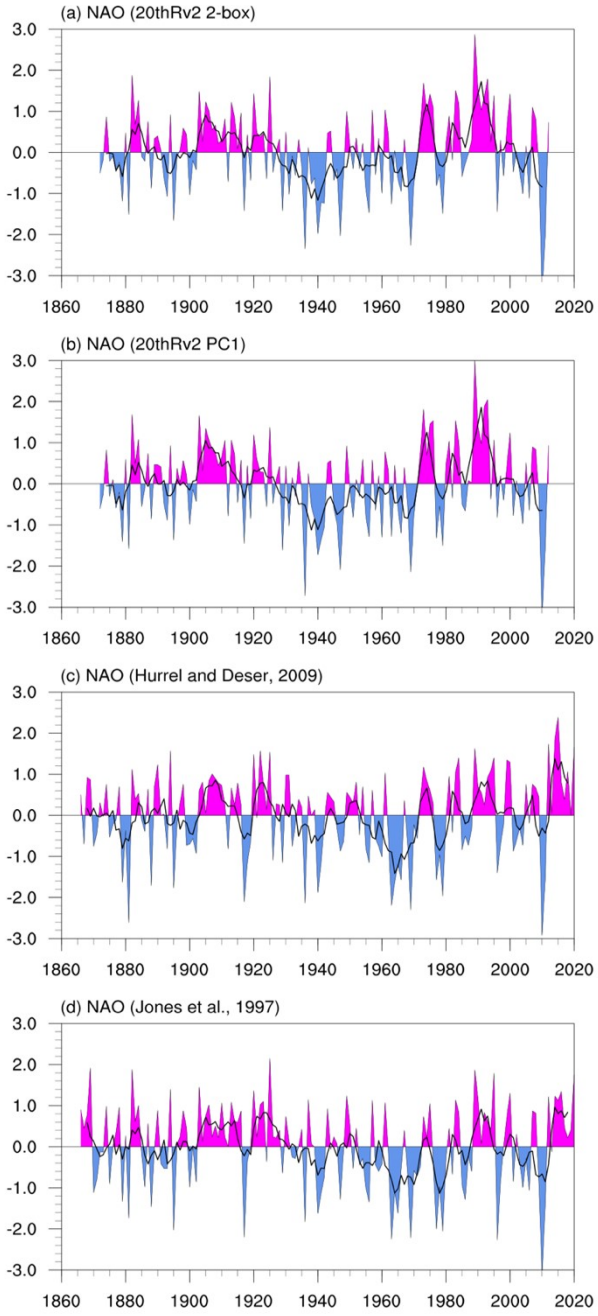

Figure A.1.1: (a) The 2-box NAO index and **(b)** PC1 NAO index calculated from 30-yrs running anomalies of sea level pressure in *20thRv2* dataset (Compo et al., 2011) over period 1871-2011, sharing a central correlation of 0.97. The station-based instrumental NAO index updated in **(c)** Hurrell (1995) and in **(d)** Jones et al. (1997) over their common period 1865-2019, sharing a central correlation of 0.86. The thick black lines represent the indices smoothed to remover the fluctuations with period less than 5 years. The indicated year corresponds to the January of the winter season (e.g, 1872 is the winter of 1871/1872).

Table A.1.1: Summary of 8 observed intense volcanic eruptions in tropics and northern extratropic.

Volcanic event	Eruption time	Location	Country	Strength (VEI)
Krakatau	May 1883	6º S, 165º E	Indonesia	6
Santa Maria	October 1902	14º N, 91º W	Guatemala	6
Agung	February 1963	8º S, 115º E	Indonesia	5
El Chichón	March 1982	17º N, 99º W	Mexico	5
Pinatubo	June 1991	15º N, 120º E	Philippines	6
Ksudach	March 1907	52º N, 157º E	Russia	5
Katmai/Novorupta	June 1912	58º N, 155º W	United States	6
Bezymianny	October 1955	56º N, 160º E	Russia	5

Table A.1.2: Summary of 11 large tropical volcanic eruptions used in Ortega et al. (2015) for NAO reconstruction.

Volcanic event	Country	Final selected date	Date from CEA (2013)	Date from GRA (2008)	Date from Sigl et al., (2014)
Unknown	Indonesia	1229	1229	1227	1229
Samalas	Indonesia	1257*	1258	1258	1257
Unknown	Indonesia	1285	1286	1284	1285
Huaynaputina	Peru	1600+	1600	1600	1600
Parker	Philippines	1640+	1641	1641	1641
Serua	Indonesia	1693+	1696	1693	1694
Unknown	-	1809	1809	1809	1809
Tambora	Indonesia	1815+	1816	1815	1815
Cosiguina	Nicaragua	1835+	1835	1835	1834
Krakatau	Indonesia	1883+	1884	1883	1884
Agung	Indonesia	1963+	1964	1963	1963

* Date recently constrained using local deposits and historical records.
+ Date extracted from historical observations.

A.2 – Chapter 5

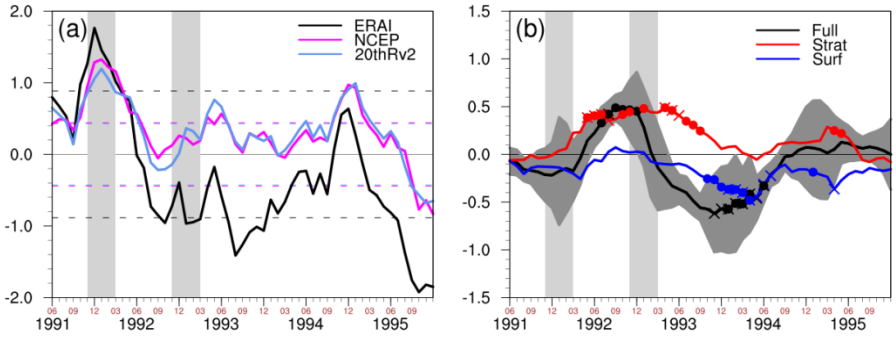

Figure A.2.1: Time series of Niño3.4 index from June 1991 to December 1994 based on sea surface temperature from **a** Reanalysis data, **b** Simulated *volc-pinatubo* ensemble runs. Small dots indicate respectively that at least 2/3 of ensemble members have anomalies of the same sign. Crosses indicate ensemble mean anomalies are significant compared to piControl at 90% level according to the student t-test.

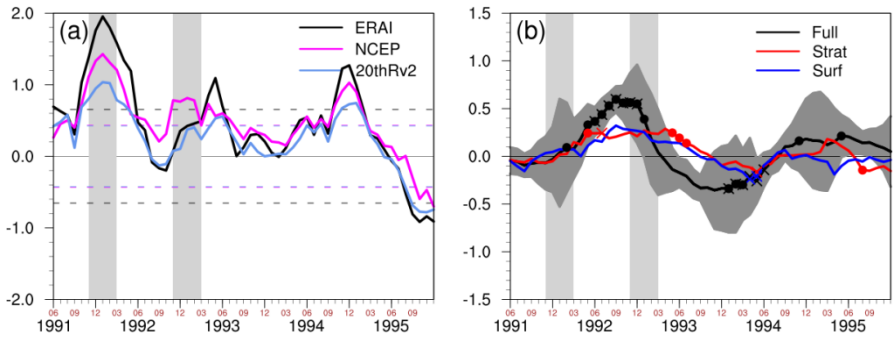

Figure A.2.2: Time series of RSST Niño3.4 index from June 1991 to December 1994 based on relative sea surface temperature (RSST, obtained by removing the tropical Pacific mean between 20°S and 20°N from SST) from **a** Reanalysis data, **b** Simulated *volc-pinatubo* ensemble runs. Small dots indicate respectively that at least 2/3 of ensemble members have anomalies of the same sign. Crosses indicate ensemble mean anomalies are significant compared to piControl at 90% level according to the student t-test.

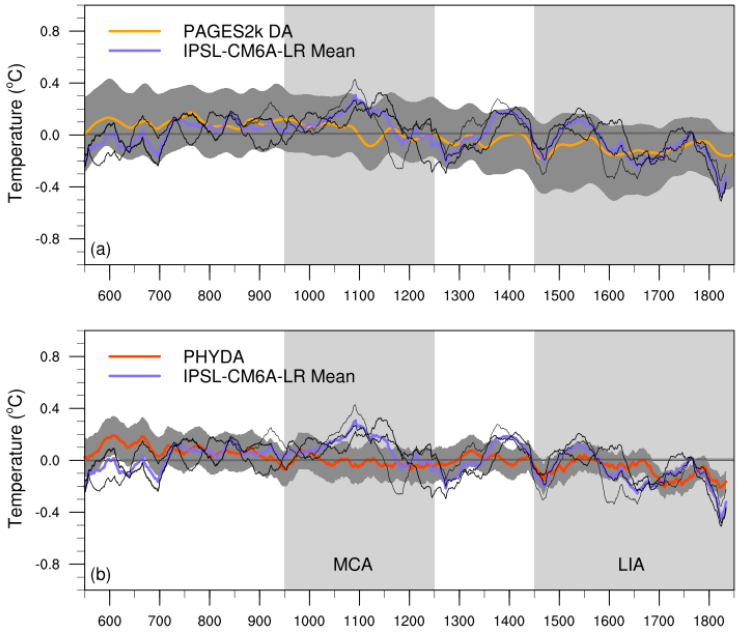

Figure A.2.3: Global mean surface temperature anomalies relevant to the 500~1849 CE reference period of **a)** PAGES-2k Data Assimilation product (orange line), **b)** PHYDA reconstruction (red line, Steiger et al., 2018), and IPSL-CM6A-LR *past1000* runs mean (purple lines in two panels). The IPSL-CM6A-LR *past1000* r1, r2 and r4 runs are shown in black thin lines. The grey shades correspond respectively to 5-95th percentile of PAGES-2k and mean ± 1sd of PHYDA

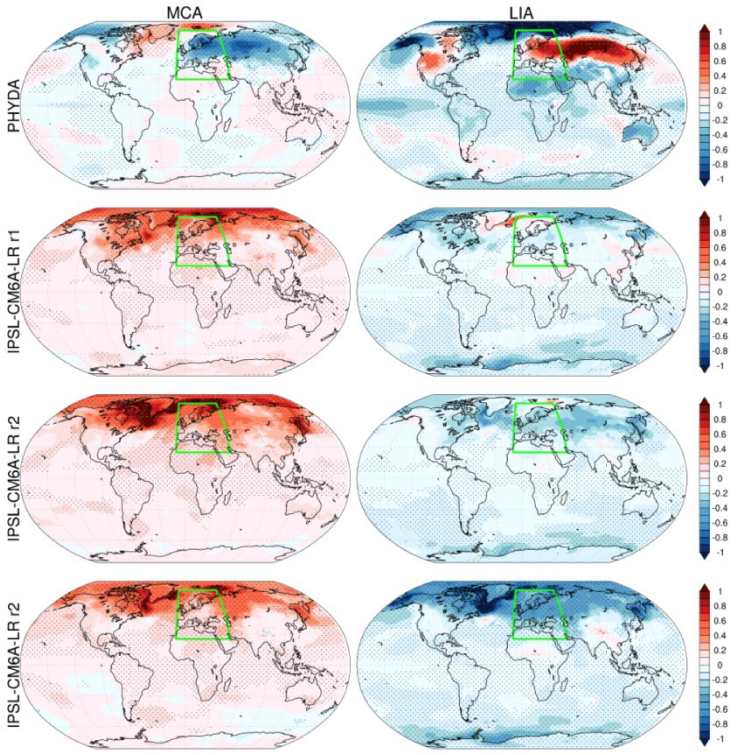

Figure A.2.4: Spatial surface temperature anomalies relevant to the 500~1849 CE means during periods associated with MCA (950~1249 CE, left panel) and LIA (1250~ 1849, right panel). From top to low are respectively PHYDA reconstruction (Steiger et al., 2018), IPSL-CM6A-LR *past1000* r1, r2 and r4 simulation results. Green contours denotes the Euro-Mediterranean region (25°N~75°N, 10°W~50°E). Significant values at 95% confidences level using student t-test are stippled.

Appendix B – Key meteorology dynamics

B.1 – Thermal wind balance

The *thermal wind* is not a "real" wind, but is defined as a vector difference between the geostrophic wind at upper layer and a lower later (Holton & Hakim, 2013). The concept of "thermal wind" serves use to link the vertical wind shear and horizontal gradient of temperature.

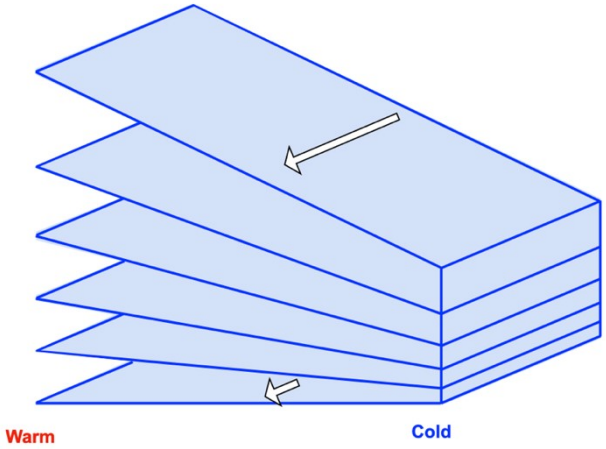

Figure B.1.1: Schematic diagram to explain "thermal wind".

For example we can notice from the diagram above that sharper tilt of pressure surfaces, which associated with strong geopotential gradient, consequently will be associated with stronger wind speed under geostrophic balance. While the bottom surface with lighter tilt pressure surface we will have much weaker geostrophic wind speed. Systematically, on the right hand side when we have cold air, the distance between geopotential surfaces is much smaller due to less space occupied by cold air, while in the left warm regions the layer thickness is much larger since warmer fluid takes larger volume consequently pushes up the geopotential height surfaces. Because it is accumulated with altitude, we could see warmer layers have stronger tilts in the upper levels. Such changes of horizontal gradients of pressure related with temperature then lead to vertical wind shear, which is explicitly described by "thermal wind". In the following we will explicitly recall the theoretical dynamic equations to help understand thermal wind.

(1) Layer thickness and temperature

Letting p, T, ρ, and α ($\equiv 1/\rho$) denote pressure, temperature, density and specific volume respectively, we can express the equation of state for dry air as:

$$p\alpha = RT \quad \text{or} \quad p = \rho RT \tag{B1.1}$$

where R is the gas constant for dry air ($R = 287\ \mathrm{J \cdot kg^{-1} \cdot K^{-1}}$).

In other hand, the *hydrostatic balance* provides an excellent approximation for the vertical dependence of the pressure field in the real atmosphere, which is depicted by:

$$\frac{dp}{dz} = -\rho g \tag{B1.2}$$

Integrating (B1.2) from a height z to the top of the atmosphere, we get:

$$p(z) = \int_{z}^{\infty} \rho g dz \tag{B1.3}$$

Noting from definition of geopotential that $d\Phi = gdz$ and from equation of state for dry air (B1.1), we can express the hydrostatic equation in the form:

$$gdz = d\Phi = -\left(\frac{RT}{p}\right)dp = -RTd(\ln p) \tag{B1.4}$$

Therefore, the variation in geopotential with respect to pressure depends only on temperature. Integration of (B1.4) in the vertical field yields a form of the *hypsometric equation*:

$$\Phi(z_2) - \Phi(z_1) = g_0(Z_2 - Z_1) = R\int_{p_2}^{p_1} Td(\ln p) \tag{B1.5}$$

Here $Z \equiv \Phi(z)/g_0$ is the *geopotential height*. If we write the equation (B1.5) in terms of Z, we get another form of the *hypsometric equation*:

$$Z_T = Z_2 - Z_1 = \frac{R}{g_0}\int_{p_2}^{p_1} Td(\ln p) \tag{B1.6}$$

where Z_T is the *thickness* of the atmospheric layer between the pressure surfaces p_2 and p_1. If we define a layer mean temperature $\bar{T}$:

$$\bar{T} = \left[\int_{p_2}^{p_1} Td(\ln p)\right]\left[\int_{p_2}^{p_1} d(\ln p)\right]^{-1} \tag{B1.7}$$

and a layer mean scale height $H \equiv R\bar{T}/g_0$, we get from Eq. (B1.6) that:

$$Z_T = \frac{R\bar{T}}{g_0}\ln\left(\frac{p_1}{p_2}\right) = H\ln\left(\frac{p_1}{p_2}\right) \tag{B1.8}$$

Hence, the thickness of a layer bounded by isobaric surfaces is proportional to the mean temperature of the layer. In a word, if the atmosphere is cold, it will tend to produce smaller geopotential thickness corresponding to a thinner layer, while higher temperature will tend to favour expansion of air mass and lead to a thicker layer. That is also why we observe in Figure B.1.1 that pressure decreases more rapidly (thinner isobaric layers) in cold levels than in warm levels (wider isobaric layers).

(2) Thermal wind balance and thermal wind

Based on hydrostatic equilibrium, the geostrophic wind must have vertical shear in presence of a horizontal temperature gradient. In an in isobaric system, the geostrophic wind is defined as:

$$f\boldsymbol{V}_g = \boldsymbol{k} \times \nabla_p \Phi \tag{B1.9}$$

Or in component form ($\boldsymbol{V}_g = u_g\boldsymbol{i} + v_g\boldsymbol{j}$) :

$$u_g = -\frac{1}{f\rho}\frac{\partial p}{\partial y} = -\frac{1}{f}\frac{\partial \Phi}{\partial y} \tag{B1.10}$$

$$v_g = \frac{1}{f\rho}\frac{\partial p}{\partial x} = \frac{1}{f}\frac{\partial \Phi}{\partial x} \tag{B1.11}$$

Hence in the North Hemisphere (where Coriolis parameter $f > 0$), the geostrophic wind is directed along the positive x axis (i.e. westerly) if the slope of the isobaric surface $\frac{\partial \Phi}{\partial y}$ is negative, as shown by Figure B1.2. Furthermore, the geostrophic wind directed along the positive x axis that increases with height requires the isobaric surface with respect to y axis must be steeper (i.e. more negative) with height.

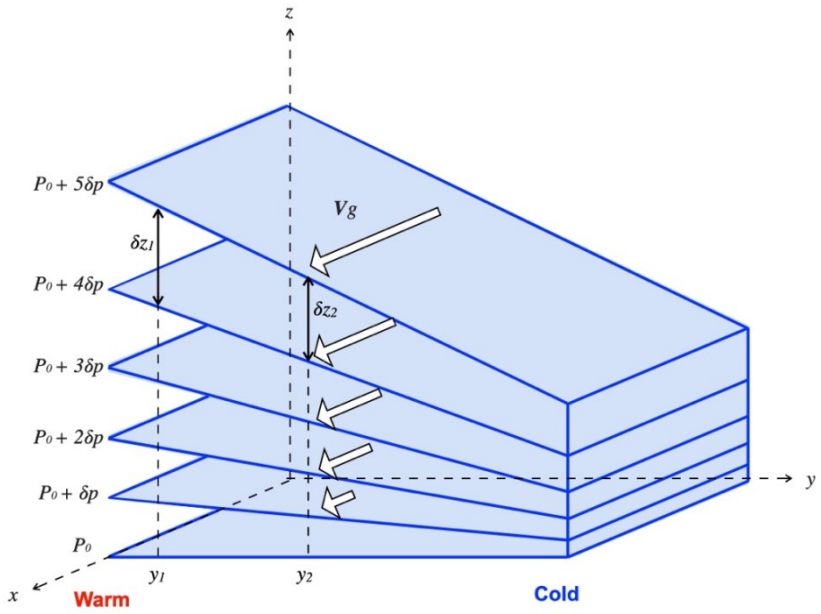

Figure B.1.2: Relationship between vertical wind shear of the geostrophic wind and horizontal thickness gradients. (Note that δp<0.)

According to the *hypsometric equation* (B1.6), the thickness δz, corresponding to a (positive) pressure interval δp is:

$$\delta z \approx \frac{R\bar{T}}{g}\delta \ln p \tag{B1.12}$$

The thickness of the layer δz between two isobaric surfaces is proportional to the mean temperature in the layer, $\bar{T}$. In Figure B.1.2, the mean temperature T_1 for the column denoted δz_1, must be higher than the mean temperature T_2 for the column denoted δz_2. Hence, an increase with height of a (negative) y axis directed pressure gradient must be associated with a negative y axis directed temperature gradient.

Differentiating Eq. (B1.10) and (B1.11) with respect to pressure, and applying Eq. (B1.4) which gives $d\Phi/dp = -RT/p$, we obtain:

$$p\frac{\partial u_g}{\partial p} = \frac{\partial u_g}{\partial \ln p} = \frac{R}{f}(\frac{\partial T}{\partial y})_p \tag{B1.13}$$

$$p\frac{\partial v_g}{\partial p} = \frac{\partial v_g}{\partial \ln p} = -\frac{R}{f}(\frac{\partial T}{\partial x})_p \tag{B1.14}$$

or in vectorial form:

$$f\frac{\partial \boldsymbol{V}_g}{\partial \ln p} = -\frac{R}{f}\boldsymbol{k} \times \nabla_p \mathrm{T} \tag{B1.15}$$

Equation (B1.15) is the *thermal wind balance* equation that we often referred. Applying this in Figure B.1.2, we can see that since $(\frac{\partial T}{\partial y})_p < 0$, $\frac{\partial u_g}{\partial p}$ is then negative, which means with increase of altitude (pressure decreasing), the geopotential wind directed along positive *x* axis will get stronger.

To note that the *thermal wind relationship* does not actually describe the *thermal wind*, but rather the vertical shear of geostrophic wind field (i.e., the rate of change of the geopotential wind with respect to *lnp*). In order to obtain the expression of the thermal wind, which is defined as the vector difference between geostrophic winds at two layers, we need to integrate the equation (B1.15) vertically from pressure level p_0 to level p_1 ($p_1 < p_0$). Designating the thermal wind vector by $\boldsymbol{V}_T$, we have:

$$\boldsymbol{V}_T \equiv \boldsymbol{V}_g(p_1) - \boldsymbol{V}_g(p_0) = -\frac{R}{f}\int_{\boldsymbol{p_0}}^{\boldsymbol{p_1}} \left(\boldsymbol{k} \times \nabla_p T\right) d\,\ln p \tag{B1.16}$$

If we define again a layer mean temperature $\bar{T}$ between pressure p_0 and p_1, we can also get the *x* and *y* component of the thermal wind:

$$u_T = -\frac{R}{f}\left(\frac{\partial \bar{T}}{\partial y}\right)_p \ln\left(\frac{p_0}{p_1}\right) \tag{B1.17}$$

$$v_T = \frac{R}{f}\left(\frac{\partial \bar{T}}{\partial x}\right)_p \ln\left(\frac{p_0}{p_1}\right) \tag{B1.18}$$

(3) An example

Following above theoretical argumentation, an example will help us gain a more concrete idea on thermal wind balance. As demonstrated below in Figure B.1.3a&c, the zonal temperature average in North Hemisphere winter has such a pattern: i) in the lower troposphere, due to orbital inclination the temperature decrease from equator to North Pole, indicating a negative temperature gradient in the *y* axis, $\left(\frac{\partial \bar{T}}{\partial y}\right)_p < 0$; ii) in the upper troposphere, the temperature has a minima above equator and it increase northward which indicates a positive temperature gradient in the *y* axis, $\left(\frac{\partial \bar{T}}{\partial y}\right)_p > 0$; iii) nevertheless from stratosphere, the temperature will again decrease from equator to North Pole,

$\left(\frac{\partial \bar{T}}{\partial y}\right)_p < 0$. The three white lines in Figure B.1.3a&c indicate three different position example to describe the meridional temperature gradient evolution from troposphere to stratosphere.

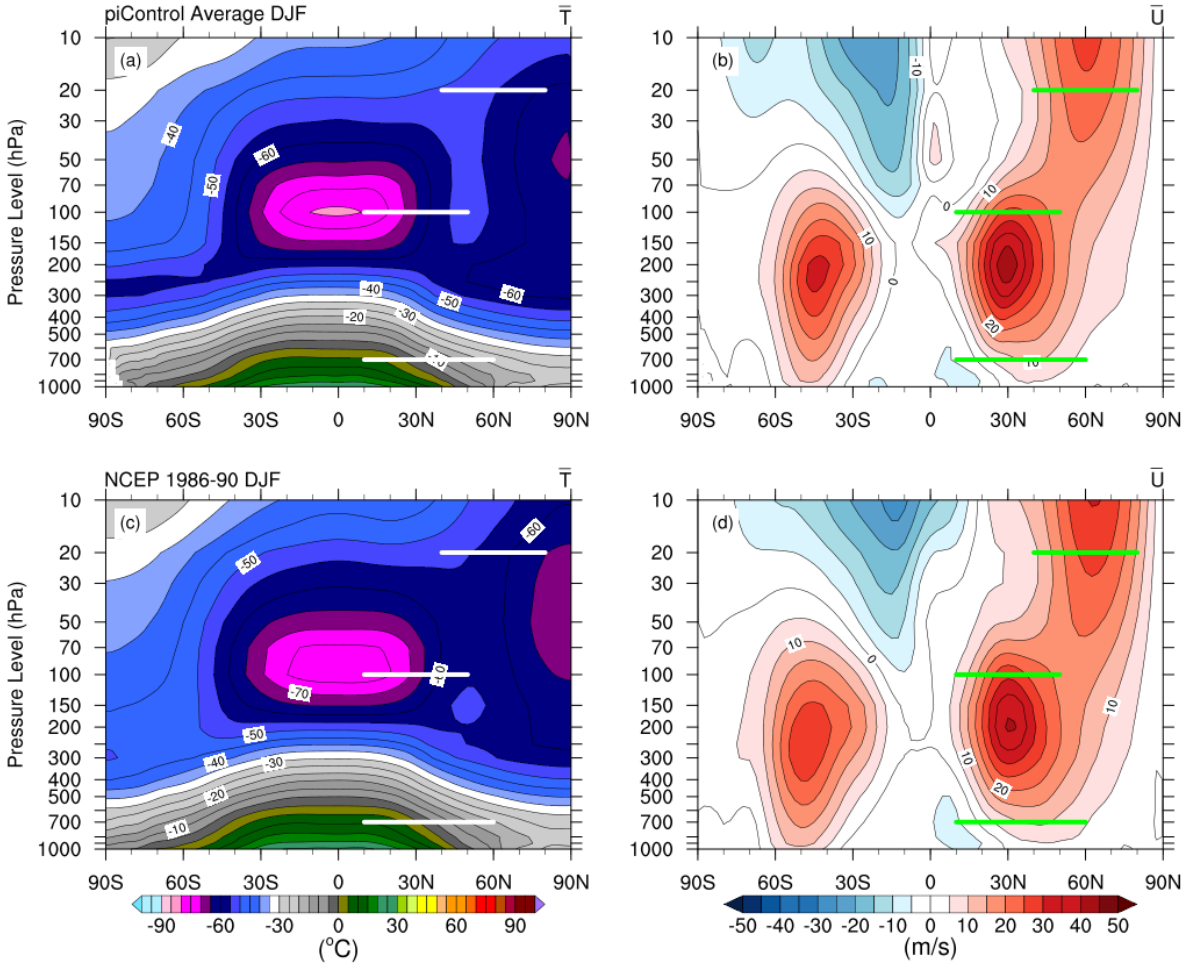

Figure B.1.3: Latitude-pressure height cross section of zonal averaged temperature (left panel) and zonal wind velocity (right panel) in winter (DJF mean). The data are coming from IPSL-CM6A-LR model *piControl* run for 500 winters' average (upper panel) and NCEP/NCAR Reanalysis dataset for 1986-1990 winters' average (lower panel) respectively.

From lower to upper levels, we resumed the signs of meridional temperature gradient and zonal wind shear in Table B.1 based on *thermal wind balance* equation (B1.13):

Table B.1: Signs of $(\partial \bar{T}/\partial y)_p$, $\partial \bar{u}_g/\partial p$ and $\partial \bar{u}_g/\partial z$ in three representative levels.

Layer (hPa)	$(\partial \bar{T}/\partial y)_p$	$\partial \bar{u}_g/\partial p$	$\partial \bar{u}_g/\partial z$
700	-	-	+
100	+	+	-
20	-	-	+

Thus in the North Hemisphere from surface to stratosphere, we have the geostrophic wind speed increases through the lower level of the troposphere until it hits tropopause and begins to decrease, while in the stratosphere, it will increase again. This evolution can be clearly seen in Figure B.1.3b&d with green lines indicating the corresponding positions we discusses in Table B.1. In fact, along the two green lines in the bottom we have increase of zonal winds with altitude from surface

through troposphere, that is also where we find the tropospheric jet or mid-latitude westerlies associated with atmosphere. To identify the location of jets in the North Hemisphere, we can also turn to $\frac{\partial \bar{u}_g}{\partial p}$ to locate the region where we have an augmentation of zonal winds in the lower level, and the region where we have a decline of zonal wind in the upper level. For instance, the region between these two green lines in Figure B.1.3b&d then suggest the position of westerly jets.

The above diagnose can also be seen in Figure B.1.4 where the temperature gradients $\left(\frac{\partial \bar{T}}{\partial y}\right)$ are shown with overlaying the wind shear $\left(\frac{\partial \bar{u}_g}{\partial p}\right)$.

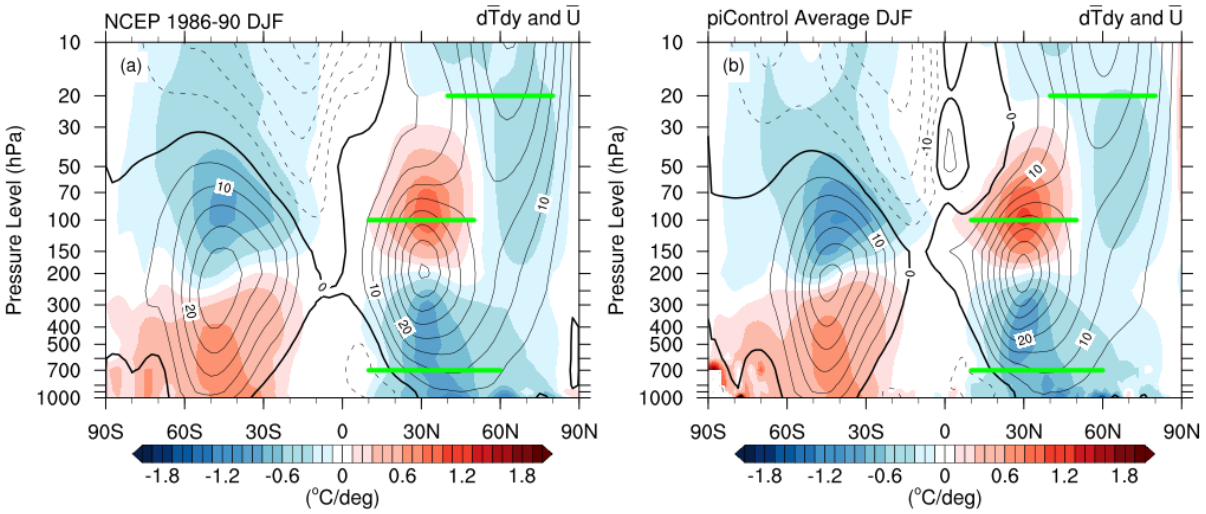

Figure B.1.4: Latitude-pressure height cross section of zonal averaged temperature gradient (color shading) and zonal wind velocity (contours) in winter (DJF mean). The data are coming from and NCEP/NCAR Reanalysis dataset for 1986-1990 winters' average (left panel) and IPSL-CM6A-LR model *piControl* run (right panel) respectively.

References

James R. Holton, Gregory J. Hakim, Chapter 3 - Elementary Applications of the Basic Equations, An Introduction to Dynamic Meteorology (Fifth Edition), Academic Press, 2013, Pages 67-93, ISBN 9780123848666, https://doi.org/10.1016/B978-0-12-384866-6.00003-9.

B.2 – Eliassen-Palm flux

The *Eliassen-Palm flux* (EP flux) is a vector defined in the meridional (y, z) plane with $\boldsymbol{F} \equiv \boldsymbol{j}F_y + \boldsymbol{k}F_z$, representing the eddy fluxes of momentum and heat respectively in meridional and vertical components. EP flux vector and its convergence ($\nabla \cdot \boldsymbol{F}$) have been considered powerful tools in evaluating the eddy forcing of zonal-mean flows and in diagnosing the propagation of transient planetary wave activity. Hereafter we will explicitly recall the theoretical dynamic equations to help understand EP flux.

(1) Background: the zonally averaged circulation

A complete understanding of the physical basis for the general circulation requires an explanation for the zonally averaged circulation, the longitudinally and time-varying components. It proves useful to isolate those processes that maintain the zonal-mean flow (i.e., the flow in the averaged along latitude circles). Then we are allowed to split the flow fields into zonal mean and longitudinally dependent eddy components. Hence analysis of the zonally averaged circulation involves study of the interaction of longitudinally varying disturbance (referred to as *eddies* and denoted by primed variables) with the longitudinally averaged flow (referred to as *mean flow* and denoted by overbars). For instance, a variable A is expresses in the form $A = \overline{A} + A'$. Such sort of average is also called a *Eulerian Mean*, as it is evaluated at fixed latitude, height and time.

In the log-pressure system, the vertical coordinate is defined as $z \equiv -H\ln(p/p_s)$, where is the standard reference pressure (usually taken 1000 hPa) and $H = RT_s/g$ is the standard scale height with T_s indicating the global standard average temperature. The x and y components of the momentum equations, the hydrostatic approximation, the continuity equation, and thermodynamic energy equation can be written as below:

$$\frac{Du}{Dt} - fv + \frac{\partial \Phi}{\partial x} = X \tag{B2.1}$$

$$\frac{Dv}{Dt} + fu + \frac{\partial \Phi}{\partial y} = Y \tag{B2.2}$$

$$\frac{\partial \Phi}{\partial z} = \frac{RT}{H} \tag{B2.3}$$

$$\frac{\partial u}{\partial x} + \frac{\partial v}{\partial y} + \frac{1}{\rho_0}\frac{\partial(\rho_0 w)}{\partial z} = 0 \tag{B2.4}$$

$$\frac{DT}{Dt} + \frac{\kappa T}{H}w = \frac{J}{c_p} \tag{B2.5}$$

where

$$\frac{D}{Dt} \equiv \frac{\partial}{\partial t} + u\frac{\partial}{\partial x} + v\frac{\partial}{\partial y} + w\frac{\partial}{\partial z}$$

$$\kappa = R/c_p$$

and X and Y designate the zonal and meridional components of drag sue to small-scale eddies.

Starting from this set of equations we will obtain the conventional form of *Eulerian mean equations* by taking zonal averages of equations (B2.1) through (B2.5). Therefore for quasi-geostrophic motions on the midlatitude β plane (i.e., the Coriolis parameter varies linearly with latitude, $f = f_0 + \beta y$):

$$\frac{\partial \overline{u}}{\partial t} - f_0 \overline{v} = -\frac{\partial\left(\overline{u'v'}\right)}{\partial y} + \overline{X} \qquad (B3.6)$$

$$f_0 \overline{u} = -\frac{\partial \overline{\Phi}}{\partial y} \qquad (B2.7)$$

$$\frac{\partial \overline{\Phi}}{\partial z} = \frac{R\overline{T}}{H} \qquad (B2.8)$$

$$\frac{\partial \overline{v}}{\partial y} + \frac{1}{\rho_0}\frac{\partial(\rho_0 \overline{w})}{\partial z} = 0 \qquad (B2.9)$$

$$\frac{\partial \overline{T}}{\partial t} + \frac{N^2 H}{R}\overline{w} = -\frac{\partial\left(\overline{v'T'}\right)}{\partial y} + \frac{\overline{J}}{c_p} \qquad (B2.10)$$

where N is the buoyancy frequency defined by

$$N^2 = \frac{R}{H}\left(\frac{\kappa T_0}{H} + \frac{\mathrm{d}T_0}{\mathrm{d}z}\right)$$

Combining (B2.7) with the hydrostatic approximation (B2.3) we can also give the thermal wind relation:

$$f_0 \frac{\partial \overline{u}}{\partial z} = -\frac{R}{H}\frac{\partial\left(\overline{T}\right)}{\partial y} \qquad (B2.11)$$

In fact, for steady-state mean flow conditions, the $(\overline{u}, \overline{w})$ circulation must just balance the eddy forcing plus the diabatic heating so that the balances in (B2.6) and (B2.10) are as follows:

- Coriolis forcing $(f_0\overline{v})$ ≈ divergence of eddy momentum fluxes $(\partial(\overline{u'v'})/\partial y)$
- Adiabatic cooling $(N^2 H\overline{w}/R)$ ≈ diabatic heating $(\overline{J}/c_p)$ plus convergence of the eddy heat flux $(-\partial(\overline{v'T'})/\partial y)$

Note that the mean meridional mass circulation is non-divergent in the meridional plane, the Eulerian meridional circulation can be represented in terms of a meridional mass transport streamfunction $(\overline{\chi})$, which identically satisfies the continuity equation (B2.9) by letting:

$$\rho_0 \overline{v} = -\frac{\partial \overline{\chi}}{\partial z}\,; \qquad \rho_0 \overline{w} = -\frac{\partial \overline{\chi}}{\partial y} \qquad (B2.12)$$

where $\overline{\chi} > 0$ for clockwise meridional circulation and $\overline{\chi} < 0$ for anticlockwise meridional circulation.

The diagnostic equation for is thereby derived by first taking

$$f_0 \frac{\partial}{\partial z}(B3.6) = -\frac{R}{H}\frac{\partial}{\partial y}(B3.10) \qquad (B2.13)$$

and then using thermal wind relation (B2.11) to eliminate the time derivatives and (B2.12) to express the mean meridional circulation in term of $\overline{\chi}$.

The resulting elliptic equation has the form:

$$\frac{\partial^2\overline{\chi}}{\partial y^2}+\frac{f_0^2}{N^2}\rho_0\frac{\partial}{\partial z}\left(\frac{1}{\rho_0}\frac{\partial\overline{\chi}}{\partial z}\right) = \frac{\rho_0}{N^2}\left[\frac{\boldsymbol{\partial}}{\boldsymbol{\partial y}}\left(\frac{\kappa\bar{J}}{H}-\frac{R}{H}\frac{\boldsymbol{\partial}}{\boldsymbol{\partial y}}\left(\overline{v'T'}\right)\right)-f_0\left(\frac{\boldsymbol{\partial^2}}{\boldsymbol{\partial z\partial y}}\left(\overline{u'v'}\right)-\frac{\boldsymbol{\partial}\overline{X}}{\boldsymbol{\partial z}}\right)\right] \quad \text{(B2.14)}$$

Equation (B2.14) can be used to qualitatively diagnose the mean meridional circulation. Since $\overline{\chi}$ must vanish on the boundaries, it can be represented by a double Fourier series in y and z. Therefore the elliptic operator on the left side of (B2.14) is approximately proportional to $-\overline{\chi}$, and (B2.14) states qualitatively that:

$$\overline{\chi}\propto-\frac{\boldsymbol{\partial}}{\boldsymbol{\partial y}}(\text{diabatic heating})+\frac{\boldsymbol{\partial^2}}{\boldsymbol{\partial y^2}}(\text{large scale eddy heat flux}) + \frac{\boldsymbol{\partial^2}}{\boldsymbol{\partial z\partial y}}(\text{large scale eddy momentum flux})+\frac{\boldsymbol{\partial}\overline{X}}{\boldsymbol{\partial z}}(\text{zonal drag force})$$

In the North Hemisphere winter, diabatic heating decreases for increase y. Thus the first term on the right is positive and tends to force a mean meridional cell with $\overline{\chi} > 0$. This is also referred to as a *thermally direct cell*, as warm air is rising in tropics and cold air is sinking in the high latitudes.

While the poleward eddy heat fluxes due to both transient synoptic-scale eddies and stationary planetary waves tend to transfer heat poleward in the extratropical Northern Hemisphere, producing a maximum poleward hear flux $\overline{v'T'}$ in the lower troposphere around 50ºN. While $\overline{\chi}$ is proportional to the second derivative ($\frac{\boldsymbol{\partial^2}}{\boldsymbol{\partial y^2}}$) of $\overline{v'T'}$, which should be negative where $\overline{v'T'} > 0$, so the term of eddy heat flux will tend to produce a mean meridional cell with $\overline{\chi} < 0$ centered in the lower troposphere at midlatitudes. Thus, the eddy heat flux tends to drive an *indirect* meridional circulation.

The third term is proportional to the vertical gradient of the horizontal eddy momentum flux convergence. However it can be shown that this term is proportional to the vertical derivation of the meridional vorticity flux

$$-\frac{\partial^2}{\partial z\partial y}\left(\overline{u'v'}\right)=+\frac{\partial}{\partial z}\left(\overline{v'\zeta'}\right)$$

where $\zeta'=\frac{\partial v'}{\partial x}-\frac{\partial u'}{\partial y}$ is the eddy relative vorticity.

In the Northern Hemisphere troposphere poleward of the core the jet stream, $\overline{u'v'}$ tends to be poleward and to reach its maximum near the tropopause at around 30ºN (core of the mean jet stream). Thus for this momentum configuration, we will have $\partial^2\left(\overline{u'v'}\right)/\partial y\partial z < 0$ in the midlatitude troposphere, thus again drives an *indirect* mean meridional cell with $\overline{\chi} < 0$. From (B2.6) it is also clear that the Coriolis force of this induced indirect meridional circulation is required, otherwise the vertical shear of the mean zonal wind would be increased such that the thermal wind balance would be destroyed.

Thus, the combined eddy heat flux and the eddy momentum flux distributions tend to drive indirect mean meridional cells.

(2) The Transformed Eulerian Mean and EP flux

Andrews and McIntyre (1976) introduced a more direct view of transport processes in the meridional plane by noting the fact that in (B2.10) there tends to be a strong convergence heat flux convergence and adiabatic cooling. They built up the *Transformed Eulerian Mean* (TEM) formulation by defining the residual circulation $(\overline{v}^*, \overline{w}^*)$ as follows:

$$\overline{v}^* = \overline{v} - \frac{1}{\rho_0}\frac{R}{H}\frac{\partial}{\partial z}\left(\frac{\rho_0 \overline{v'T'}}{N^2}\right) \tag{B2.15a}$$

$$\overline{w}^* = \overline{w} + \frac{R}{H}\frac{\partial}{\partial y}\left(\frac{\overline{v'T'}}{N^2}\right) \tag{B2.15b}$$

The residual vertical velocity defined in this manner clearly represents the part of the mean vertical velocity with a contribution to adiabatic temperature change that is not cancelled by the eddy heat flux divergence.

Substituting from (B2.15) into (B2.6) and (B2.10) to eliminate $(\overline{u}, \overline{w})$ yields the TEM equations:

$$\frac{\partial \overline{u}}{\partial t} - f_0 \overline{v}^* = +\frac{1}{\rho_0}\nabla \cdot \boldsymbol{F} + \overline{X} \tag{B2.16}$$

$$\frac{\partial \overline{T}}{\partial t} + \frac{N^2 H}{R}\overline{w}^* = +\frac{\overline{J}}{c_p} \tag{B2.17}$$

where $\boldsymbol{F} \equiv \boldsymbol{j}F_y + \boldsymbol{k}F_z$, the *Eliassen-Palm flux* (EP flux) for large quasi-geostrophic eddies has the components

$$F_y = -\rho_0 \overline{u'v'}, \qquad F_z = \rho_0 f_0 R \frac{\overline{v'T'}}{N^2 H} \tag{B2.18}$$

The TEM equations clearly demonstrates that the eddy heat and momentum fluxes do not act separately to drive changes in the zonal-mean circulation, but only in the combination given by the divergence of the EP flux ($\nabla \cdot \boldsymbol{F}$). To facilitate interpret, the eddy forcing of zonal-mean flow can be displayed conveniently by mapping the field of $\boldsymbol{F}$ by arrows and contouring the isolines of its divergence ($\nabla \cdot \boldsymbol{F}$). When EP flux vector points upward, the meridional heat flux dominates; when the EP flux vector points in the meridional direction, the meridional flux of zonal momentum dominates. In the midlatitude of Northern Hemisphere, usually dynamical acceleration of westerlies takes place at lower levels when $\nabla \cdot \boldsymbol{F} > 0$ (divergent), whilst a deceleration near the tropopause in the mid-latitude and on the southern flank of the subtropical jet will occur with $\nabla \cdot \boldsymbol{F} < 0$ (convergent).

The mean global EP flux and its divergence pattern for a Northern Hemisphere winter is shown in Figure B.2.1 based on NCEP/NCAR Reanalysis data (take the average from 1986-1990 DJF for example) and IPSL-CM6A-LR piControl run. The monthly (daily) data are applied to calculate related covariance to represent the stationary (transient) planetary waves.

As can be seen in Figure B.2.1a&b, both reanalysis and model data show that the stationary waves have two major branches of EP flux (one equatorward and one upward) from the extratropical troposphere and two major zones of convergences (one in subtropical upper troposphere and one in

subpolar stratosphere), consistent with Li et al. (2011). During North Hemisphere winter, in most of the extratropical troposphere the EP flux divergent is convergent (negative) so that stationary eddies exert a westward zonal force on the atmosphere. It will lead to intense deceleration of mean zonal wind and the poleward residual mean meridional flow in the stratosphere. The results are consistent with Li et al. (2007) that stationary wave propagation has important role in modulating the stratospheric polar vortex regimes.

While for the transient waves (Figure B.2.1b&c), there are also two major branches of propagation, and compared to stationary waves, we find that transient waves propagate less from the troposphere to the stratosphere, but that more wave activity is excited in the subpolar troposphere and propagated to the subtropical troposphere (one major convergent zone in the mid-troposphere).

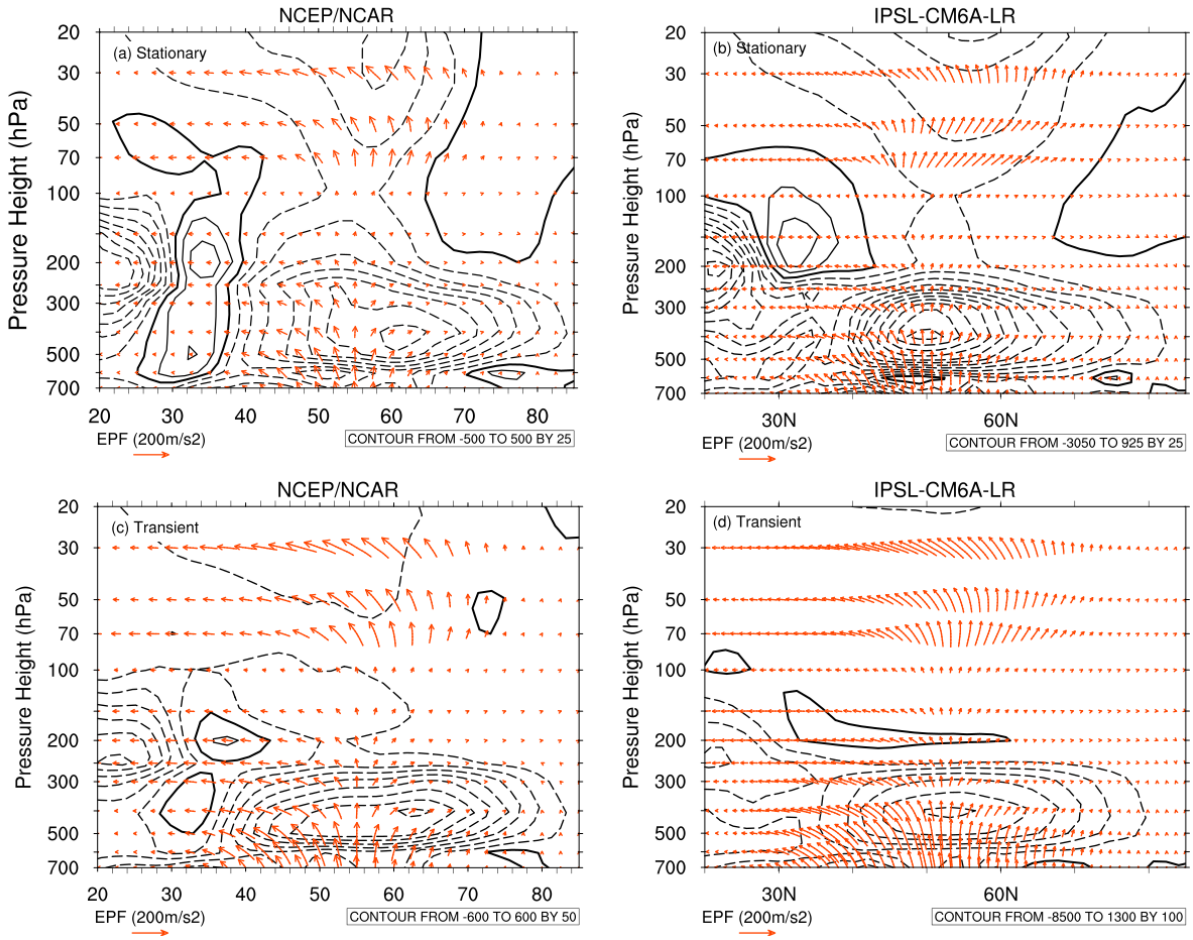

Figure B.2.1: Eliassen-Palm flux vector (arrows, units: m/s^2) and divergence (divided by the standard density ρ_0, blue and red contours for negative and positive values respectively, units: m s^{-2}) for Northern Hemisphere winter (here DJF 1960/61). Monthly (upper panel) and daily (lower panel) data from NCEP/NCAR Reanalysis dataset (left panel) and IPSL-CM6A-LR piControl run (right panel) are used in the calculation metrics.

It is suggested by Li et al. (2011) that both stationary waves and transient waves contribute to the maintenance of the observed stratospheric polar vortex regimes in NH winter, but in different pathways. For strong vortex regimes, stationary waves will exert strong westerly forcing in the subpolar stratosphere (their Figure 2b and 5b). Unlike the stationary waves, the transient waves

provide more eddy heat flux in the subpolar stratosphere in strong vortex regime (their Figure 4b and 5c).

(3) EP flux and residual meridional circulation

Following defining the residual circulation ($\overline{v}^*, \overline{w}^*$), we can also better understand the residual mean meridional circulation by defining a residual streamfunction:

$$\overline{\chi}^* = \overline{\chi} + \rho_0 \frac{R}{H}\frac{\overline{v'T'}}{N^2} = \overline{\chi} + \rho_0 \frac{\overline{v'\theta'}}{d\theta/dz} \tag{B2.19}$$

It can be shown by direct substitution into (B2.12) and (B2.14) that

$$\rho_0 \overline{v}^* = -\frac{\partial \overline{\chi}^*}{\partial z}\,; \qquad \rho_0 \overline{w}^* = -\frac{\partial \overline{\chi}^*}{\partial y} \tag{B2.20}$$

and

$$\frac{\partial^2 \overline{\chi}^*}{\partial y^2} + \frac{f_0^2}{N^2}\rho_0 \frac{\partial}{\partial z}\left(\frac{1}{\rho_0}\frac{\partial \overline{\chi}^*}{\partial z}\right) = \frac{\rho_0}{N^2}\left[\frac{\boldsymbol{\partial}}{\boldsymbol{\partial y}}\left(\frac{\kappa \bar{J}}{H}\right) + f_0 \frac{\boldsymbol{\partial}}{\boldsymbol{\partial z}}\left(\frac{1}{\rho_0}\nabla \cdot \boldsymbol{F} + \overline{X}\right)\right] \tag{B2.21}$$

Similar to the analysis of conventional Eulerian Mean streamfunction, we will have

$$-\overline{\chi}^* \propto \frac{\boldsymbol{\partial}}{\boldsymbol{\partial y}}(\text{diabatic heating}) + \frac{\boldsymbol{\partial}}{\boldsymbol{\partial z}}(\text{EP flux}) + \frac{\boldsymbol{\partial}\overline{X}}{\boldsymbol{\partial z}}(\text{zonal drag force})$$

If neglecting zonal force drag $\overline{X}$, the diabatic heating and EP flux contribute to the residual circulation. In the Northern Hemisphere troposphere, the source term on the right of (B2.21) are generally negative, which implies $\overline{\chi}^*$ itself is negative in the Northern Hemisphere so that the residual meridional circulation consists of a single thermally direct overturing in Northern Hemisphere While for Southern Hemisphere the overturning is in reverse direction.

Recalling (B2.17), the residual mean vertical motion for time-averaged conditions is proportional to the diabatic heating. It approximately represents the *diabatic circulation* in the meridional plane. Hence , $\overline{w}^*$ approximates the mean motion of air parcels which rise or sink due to diabatically heating or cooling.

(4) The zonal-mean potential vorticity and EP flux

Further insights into the nature of the extratropical zonal-mean circulation can be obtained by zonally averaging the quasi-geostrophic potential vorticity (QG PV) equation in log-pressure coordinate system

$$\left(\frac{\partial}{\partial t} - \boldsymbol{V_g} \cdot \nabla_h\right) q = \frac{D_g q}{Dt} = 0 \tag{B2.22}$$

where $q \equiv \frac{1}{f_0}\nabla^2 \Phi + f + \frac{f_0}{\rho_0}\frac{\partial}{\partial z}\left(\frac{\rho_0}{N^2}\frac{\partial \Phi}{\partial z}\right)$

to obtain the zonal-mean PV equation

$$\frac{\partial}{\partial t}\overline{q} + \frac{\partial}{\partial y}\overline{q'v'} = 0 \tag{B2.23}$$

where the zonal-mean PV is

$$\overline{q} = \frac{1}{f_0}\frac{\partial^2\overline{\Phi}}{\partial y^2} + f_0 + \beta y + \frac{f_0}{\rho_0}\frac{\partial}{\partial z}\left(\frac{\rho_0}{N^2}\frac{\partial\overline{\Phi}}{\partial z}\right) \tag{B2.24}$$

and the eddy potential vorticity is

$$q' = \frac{1}{f_0}\left(\frac{\partial^2\Phi'}{\partial x^2} + \frac{\partial^2\Phi'}{\partial y^2}\right) + \frac{f_0}{\rho_0}\frac{\partial}{\partial z}\left(\frac{\rho_0}{N^2}\frac{\partial\Phi'}{\partial z}\right) \tag{B2.25}$$

The quantity $\overline{q'v'}$ on the right in (B2.22) is the divergence of the meridional flux of potential vorticity. According to (B2.22), for adiabatic quasi-geostrophic flow, the mean distribution of potential vorticity can be changes only if there is nonzero flux of eddy potential vorticity. Thus, eddy-driven mean flow accelerations require a nonzero potential vorticity fluxes.

It can be further proven that the potential vorticity flux is related to the eddy momentum and heat fluxes such that

$$\overline{q'v'} = -\frac{\partial\overline{u'v'}}{\partial y} + \frac{f_0}{\rho_0}\frac{\partial}{\partial z}\left(\frac{\rho_0}{N^2}\overline{\frac{\partial\Phi'}{\partial z}v'}\right) \tag{B2.26}$$

Comparing (B2.26) and (B2.18), we see that the potential flux is proportional to the divergence of the EP flux vector:

$$\overline{q'v'} = \frac{1}{\rho_0}\nabla\cdot\boldsymbol{F} \tag{B2.27}$$

Thus, it is not the eddy momentum flux $\overline{u'v'}$ or heat flux $\overline{\frac{\partial\Phi'}{\partial z}v'}$ that drives net change in the mean flow distribution, but rather the combination given by the potential vorticity flux $\overline{q'v'}$. And recalling the horizontal zonal-mean momentum equation in (B2.16), the contribution of large-scale motion to the zonal force equals the QG PV.

References

Andrews, D. G. and McIntyre, M. E.: Planetary Waves in Horizontal and Vertical Shear: The Generalized Eliassen- Palm Relation and the Mean Zonal Acceleration, J. At- mos. Sci., 1976, 33, 2031–2048, https://doi.org/10.1175/1520-0469(1976)033<2031:PWIHAV>2.0.CO;2.

Graf, H.-F., Li, C., and Giorgetta, M. A. (2007). Volcanic effects on climate: Revisiting the mechanisms. Atmos. Chem. Phys., 10.

James R. Holton, Gregory J. Hakim, Chapter 10 - The General Circulation, An Introduction to Dynamic Meteorology (Fifth Edition), Academic Press, 2013, Pages 67-93, ISBN 9780123848666, https://doi.org/10.1016/B978-0-12-384866-6.00003-9.

James R. Holton, Gregory J. Hakim, Chapter 12 - The Middle Atmosphere Dynamics, An Introduction to Dynamic Meteorology (Fifth Edition), Academic Press, 2013, Pages 67-93, ISBN 9780123848666, https://doi.org/10.1016/B978-0-12-384866-6.00003-9.

Li, Q., Graf, H.-F., and Cui, X. (2011). The role of stationary and transient planetary waves in the maintenance of stratospheric polar vortex regimes in Northern Hemisphere winter. Advances in Atmospheric Sciences, 28(1), 187–194. https://doi.org/10.1007/s00376-010-9163-7.

Li, C., Graf, H. F., and Giorgetta, M. A. (2007). Stationary planetary wave propagation in Northern Hemisphere winter – climatological analysis of the refractive index. Atmos. Chem. Phys., 18.

Appendix C – Résumé détaillé en français

Les forçages naturels liés à l'activité solaire et volcanique sont prépondérants devant les forçages anthropiques pendant le dernier millénaire précédant le XIXème siècle. Dans cette thèse, mes travaux sont consacrés à l'étude d'un des forçages naturels le plus important, dit "volcanique", ainsi qu'à la variabilité climatique dans le bassin Atlantique Nord-Méditerranéen lors du dernier millénaire (500-1849 CE) en utilisant le modèle IPSL-CM6A-LR et des archives d'observations.

Le chapitre **1** présente le contexte de la thèse puis les motivations, les objectifs et sa structure.

Dans la première partie du chapitre **2**, je présente les facteurs externes climatiques au dernier millénaire. Ensuite, j'ai choisi de développer plus particulièrement le volet qui a nécessité/demandé le plus d'investissement : les effets radiatifs des éruptions volcaniques sur le système terrestre et l'étude de son impact climatique dans le secteur ciblé, notamment par ses influences sur l'Oscillation Nord Atlantiques (ONA). Je rappelle brièvement l'état des connaissances sur les défis autour de l'étude volcanique et l'ONA : (i) la manque d'échantillons volcaniques dans la période instrumentale ; (ii) les incertitudes des modélisations ; (iii) la compréhension du mécanisme qui intervient entre les éruptions volcaniques et l'ONA. Puis dans ce chapitre je présente deux programmes d'intercomparaison dans la cadre de CMIP6 qui a spécialement attiré notre attention pour répondre à ces défis. L'un est la phase 4 du Projet d'Intercomparaison des Modélisations Paléoclimatiques (en anglais, PMIP4), tandis que l'autre est le Projet d'Intercomparaison des Modèles de Forçages Volcaniques (VolMIP). Par la suite, je présente notre modèle IPSL-CM6A-LR et les reconstructions volcaniques paléoclimatiques et historiques (plus précisément, Mt. Pinatubo) ainsi que ses implications dans le modèle pour la simulation paléoclimatique (c.-à-d., past1000, l'expérimentation clé du PMIP4) et la simulation Pinatubo (c.-à-d., volc-pinatubo, le protocole central du VolMIP).

Le chapitre **3** présente surtout le travail de validation de IPSL-CM6A-LR pour simuler l'ONA à l'aide de comparaison des signaux climatiques hivernaux comprenant quatre catégories d'éruptions volcaniques différentes en utilisant la simulation past1000 du PMIP4. Ces quatre catégories se divisent selon la latitude d'éruption (tropical ou haute latitude de l'Hémisphère Nord), la saison d'éruption (hiver ou printemps/été), et l'intensité d'éruption.

Le chapitre **4** décrit ensuite mes travaux sur le mécanisme auquel lie le volcanisme et l'ONA à travers trois exercices (volc-pinatubo-full, volc-pinatubo-strat, volc-pinatubo-surf) du VolMIP par notre modèle IPSL-CM6A-LR et de comparaisons avec divers jeux d'observations instrumentales. Ce chapitre est présenté comme une publication à soumettre dans le journal *Earth System Dynamics* (ESD) Issue Spécial du VolMIP d'ici la soutenance.

Enfin, le chapitre **5** conclut la thèse avec la synthèse de conclusions et les perspectives. Les figures et tableaux supplémentaires sont joints dans l'annexe **A**. Les connaissances requises sur la

météorologie dynamique sont attachées dans l'annexe **B**. Le résumé détaillé en français est dans l'annexe **C**.

Chapitre 2 (Volcanisme et la variabilité climatique)

Le dernier millénaire est une période dont on dispose d'enregistrements paléoclimatiques ou d'informations historiques relativement précises. Ces informations témoignent d'une variabilité importante du climat, aux échelles de temps interannuelle, décennale et séculaire, et qui permettent de caractériser le temps de retour d'événements météorologiques rares (fortes tempêtes, vagues de chaleur ou de froid, les éruptions volcaniques, etc). Enfin, elles posent la question des conséquences de cette variabilité du climat sur les sociétés humaines et leur adaptation. Cette période permet donc de caractériser la variabilité « naturelle » du climat.

Trois types de forçages externes d'origine naturelle ont agi et vont continuer d'agir sur le climat à l'avenir (Khodri et al., 2015) : (i) les variations lentes de la répartition de l'énergie solaire incidente du fait des modifications graduelles des caractéristiques de l'orbite de la Terre autour du Soleil (forçage dit « astronomique ») ; (ii) les variations de l'activité du Soleil et donc l'intensité et les caractéristiques du flux radiatif solaire incident ; (iii) la formation de particules sulfatées dans l'atmosphère du fait de l'activité volcanique (point privilégié de cette thèse). Au cours du dernier millénaire, le rejet d'aérosols et de gaz à effet de serre par les activités humaines, et les changements d'usage des sols (déforestations, cultures, urbanisation), ont aussi commencé à agir sur le climat. Ces forçages dit anthropiques sont néanmoins faibles et régionalement limités avant le 19ème siècle et le début de l'ère industrielle.

Le forçage volcanique est d'une grande importance pour le climat sous divers aspects, principalement via quatre mécanismes (Forster et al., 2007) : (i) l'interaction aérosol-rayonnement ; (ii) le chauffage différentiel (vertical ou horizontal) pouvant produire des gradients thermiques dans l'atmosphère et provoquer des changements dans la circulation atmosphérique ; (iii) les éruptions volcaniques en interaction avec d'autres modes de circulation et oscillations, tels qu'El Niño-Oscillation Australe (ENSO), l'Oscillation Atlantique Multidécennale (AMO) et l'ONA ; (iv) les aérosols volcaniques pouvant modifier les conditions de la chimie atmosphérique et induire un appauvrissement de la couche d'ozone avec pour conséquence une réduction de l'absorption stratosphérique du rayonnement solaire.

Les éruptions volcaniques qui ont un impact sur le climat sont surtout celles dont la colonne éruptive projette des quantités considérables de gaz riches en soufre suffisamment haut en altitude pour atteindre la stratosphère. Une fois dans la stratosphère, les gaz volcaniques sont transformés par réaction chimique en particules fines d'aérosols sulfatés qui vont ensuite être transportés vers les pôles en quelques mois par la circulation Brewer-Dobson (BDC) avant de retomber à la surface. Ce sont ces aérosols sulfatés dans la stratosphère qui vont perturber le rayonnement solaire incident. En effet, en raison de leur composition et leur taille, premièrement ces aérosols réfléchissent le

rayonnement solaire (principalement des ondes courtes dans l'ultraviolet et le visible) et diminuent le rayonnement solaire net atteint en surface de Terre. Cet effet est traduit par une augmentation de l'albédo de la Terre et un refroidissement net des températures à la surface de la Terre pendant les deux premières années suivant l'éruption. Deuxièmement, ces aérosols sulfatés dans la stratosphère absorbent une partie du rayonnement infrarouge solaire et terrestre (ondes longues) alors qu'un réchauffement est conduit dans la basse stratosphère. Ces deux effets - le refroidissement de surface et le réchauffement de la stratosphère - sont les deux effets radiatifs principaux liés aux éruptions volcaniques.

Bien qu'un consensus s'accorde sur le fait que les aérosols volcaniques produisent un refroidissement à la surface de la Terre (en raison de la réduction du rayonnement atteint en surface), l'hiver suivant plusieurs grandes éruptions tropicales a été plus chaud et plus humide que la moyenne climatologique sur l'Amérique du Nord et l'Eurasie du Nord (par exemple l'hiver après l'éruption du 1991 Pinatubo). Ce phénomène est observé à la fois dans les températures de la basse troposphère, dérivées par satellite, et dans les observations synoptiques de surface. En comparaison, pendant ce temps, des anomalies négatives de températures et de précipitations ont été observées principalement sur la Méditerranée orientale et sur la partie nord-est de l'Amérique du Nord.

Ce mode d'anomalie hivernale ressemble à une phase positive typique d'ONA, de sorte que des questions se posent quant à (i) si cette anomalie est simplement due à une variabilité interne (Polvani et al., 2019), ou produite par un processus déterministe en raison de l'éruption volcanique (la réduction des ondes courtes ou autres) ; (ii) si cette anomalie est une réponse privilégiée pour les éruptions tropicales, ou reproductible (opposant) pour les éruptions volcaniques extratropicales. Ainsi, les relations dynamiques entre l'éruption volcanique et le modèle de circulation atmosphérique en hiver boréal continuent d'attirer l'attention des communautés scientifiques.

Par la suite, j'ai analysé le climat d'hiver à partir des archives d'observation (HadCRU, Morice et al., 2012; et 20thRv2, Compo et al., 2011) pour cinq éruptions tropicales (Krakatau en mai 1883, Santa María en octobre 1902, Agung en février 1963, El Chichón en mars 1907 et Pinatubo en juin 1991) et trois éruptions haute-latitude de l'Hémisphère Nord (Ksudach en mars 1907, Katmai ou Novarupta en juin 1912, Bezymianny en octobre 1955). Toutes ces éruptions rejettent abondamment de soufre dans la stratosphère (Bluth et al., 1992; Stothers, 1996, 1997, 2001; Zelenski et al., 2015, etc). En conséquence, une baisse de la température globale à la surface est observée après le déclenchement des cinq éruptions tropicales. Le refroidissement maximal a lieu généralement la deuxième année après les éruptions. Les éruptions extratropicales n'ont néanmoins pas montré d'effets de refroidissement comparatif comme leurs homologues tropicales, en partie à cause de la durée de vie plus courte de leurs émissions et donc de leurs impacts.

Afin d'explorer dans les observations la relation entre des éruptions avec l'ONA, les séries chronologiques de l'indice ONA et le climat à la surface du premier hiver suivant les mêmes cinq éruptions tropicales et trois éruptions NH extratropicales sont présentés. Il faut noter que le calcul de

l'indice ONA se fonde sur la méthode de Stephenson et al. (2016) où nous appliquons deux « boîtes » pour la pression au niveau de la mer (SLP). En pratique, deux grandes régions longitude-latitude ont été prises dans la région subtropicale de l'Atlantique Nord et sud de l'Europe (20°–55°N, 90°W–60°E) et depuis la région subpolaire de l'Atlantique Nord et nord de l'Europe (55°–90°N, 90°W–60°E). Ensuite, l'indice ONA est défini comme la différence entre la moyenne SLP de décembre-février (DJF) moyennée spatialement sur ces deux « boîtes ».

Les séries chronologiques dans le graphique à barres (Fig. 2.7) montrent qu'à l'exception des éruptions de l'Agung de 1963 et du Bezymianny de 1955, toutes les autres éruptions ont un indice ONA positif au cours du premier hiver volcanique, dépassant l'écart type de l'indice ONA hivernal de toute la période historique 1871-2011. Leur moyenne d'ensemble montre également un indice ONA positif au cours du premier hiver, bien que le signal d'ensemble ne dépasse pas un écart type. Le signal de l'indice ONA en deuxième hiver volcanique est moins cohérent parmi les huit éruptions. Par rapport au climat à la surface en premier hiver, généralement, toutes les éruptions, à l'exception de l'Agung en 1963 et de la Bezymianny en 1955 qui ont éclaté après une année à ONA fortement négative, ont montré une caractéristique positive de l'ONA avec un schéma en dents de scie d'anomalies SLP entre les régions subpolaire et subtropicale de l'Atlantique Nord, conformément à ce qui a été rapporté dans Christiansen (2008). Le continent de l'Eurasie du Nord, en particulier la région scandinave, connaît un hiver plus chaud et plus humide accompagné de vents d'ouest plus forts soufflant du sud du Groenland au nord de l'Europe pour les éruptions tropicales et une éruption extratropicale (dit, 1912 Katmai/Novarupta).

Robock et Mao (1992) ont déjà attribué le signal ONA aux éruptions volcaniques, inspirés par le signal ONA fortement positif observé au cours des hivers suivant l'éruption du Mt. Pinatubo. Néanmoins, il convient de rappeler que l'observation réelle n'est qu'« une réalisation du monde réel » et que la variabilité naturelle de l'ONA est impossible à ignorer et difficile à éliminer. Les échantillons d'observation limités nous interdisent cependant toujours de tirer des conclusions plausibles entre l'ONA et les éruptions volcaniques surtout en raison de la nature bruyante de la variabilité interne du climat. En outre, par rapport aux signaux de réchauffement hivernal prononcés des éruptions tropicales, le signal observé pour les éruptions extratropicales semble plutôt ambigu parmi les trois événements listés. On pense qu'une analyse complète de l'observation et du multi-proxy combinée à des simulations de modèle permet de mieux comprendre la signification et le mécanisme de la réponse de l'ONA après les éruptions volcaniques.

Tout au long d'études scientifiques sur le rôle et l'impact de volcanisme sur l'ONA et donc sur la variabilité climatique dans l'Atlantique Nord-Méditerranée, j'ai distingué/discerné trois défis (ci-dessous) qu'il faut résoudre sur la base de l'état des connaissances :

(1) Le manque des échantillons volcaniques dans la période instrumentale.

Comme cela a été introduit précédemment, les événements volcaniques observés pendant l'ère industrielle sont très limités, ce qui constitue le premier défi de l'étude des volcans-NAO.

Pour surmonter le défi de la rareté des événements volcaniques dans l'ère instrumentale, des événements volcaniques du dernier millénaire, qui sont beaucoup plus importants que ceux du XXe siècle, ont été étudiés soit à l'aide de modèles climatiques (par exemple, Stevenson et al., 2016, 2017, 2018 ; Colose et al., 2016 ; Zanchettin et al., 2013, 2016) soit par des enregistrements proxy (par exemple, Trouet et al., 2009 ; D'Arrigo et al., 2009 ; Schneider et al., 2017 ; Esper et al., 2015 ; Cook et al., 2019 ; Pinto et Raible, 2012 ; Ortega et al., 2015) avec des méthodes statistiques appropriées pour analyser la signification du signal.

Par exemple, Ortega et al. (2015) ont présenté une reconstruction annuelle de l'ONA pour l'ensemble du dernier millénaire sur la base de 48 enregistrements proxy résolus annuellement et répartis dans l'océan Atlantique. Leur reconstruction révèle également une empreinte ONA positive significative un an après de fortes éruptions volcaniques tropicales, ce qui est cohérent avec les résultats de simulation et les observations satellitaires pour l'éruption du Mt. Pinatubo. Dans le même temps, l'estimation du rôle du volcanisme explosif nécessite un grand nombre de données proxy climatiques avec une bonne distribution spatiale. Alors que le nombre d'enregistrements appropriés diminue en remontant dans le temps, une grande incertitude subsiste également dans l'estimation de la variabilité climatique et la reconstruction des facteurs de forçage, en particulier avant ~1600 (Schneider et al., 2009).

De l'autre côté, les modèles couplés des systèmes climatiques sont des outils particulièrement utiles. En effet, certains modèles ont simulé avec succès l'effet majeur de refroidissement de surface observé suite aux grandes éruptions volcaniques alors que les informations provenant d'observations/ données proxy étaient parfois restreintes. Le Projet d'Intercomparaison des Modélisations Paléoclimatiques (dit an anglais, PMIP) est un effort important de la communauté climatique internationale pour comprendre de manière représentative les réponses du système climatique à différents forçages climatiques liés aux états climatiques du passé (avant la période actuelle et historique). Le protocole de base de PMIP3/CMIP5 promeut l'expérience past1000 en se concentrant sur les variations climatiques du dernier millénaire. Un objectif important de past1000 est d'étudier les réponses climatiques au forçage volcanique avec des longues simulations transitoires. Le défi de l'insuffisance des événements volcaniques peut également être largement résolu en étudiant les simulations past1000.

(2) Les incertitudes des modélisations.

Les études de modélisation n'aboutissent pas aux mêmes conclusions. D'une part, certaines simulations (eg, Graf et al., 1993 ; Kirchner et al., 1999 ; Shindell et al., 2004 ; Stenchikov, 2002 ; Stenchikov et al., 2004) arrivent à simuler le climat hivernal post-éruption lié à l'ONA positive; d'autre part, il existe également des simulations indiquant un échec ou une inefficacité du modèle à reproduire la phase positive de l'ONA après les plus grandes éruptions volcaniques (par exemple, Braconnot et al., 2012 ; Driscoll et al., 2012 ; Stenchikov et al., 2006 ; Swingedouw et al., 2017, Zambri et al., 2017). Swingedouw et al. (2017) a également trouvé que la version précédente du

modèle IPSL, dit IPSL-CM5A-LR, ne parvient pas à reproduire un signal robust de l'ONA. Par conséquent, nous concluons que le deuxième défi important dans l'étude du volcan-ONA est de surmonter les incertitudes de la modélisation.

(3) La compréhension du mécanisme qui intervient entre les éruptions volcaniques et l'ONA.

La compréhension univoque du mécanisme qui relie les éruptions volcaniques et l'ONA représente le défi le plus important de l'étude du volcan-ONA. À partir de la littérature scientifique, nous concluons trois théories principales permettant d'expliquer le mécanisme derrière le phénomène ONA lié aux éruptions tropicales :

i) « Mécanisme de gradient stratosphérique de type I » par l'excitation de modes de variabilité moyenne zonale inhérents tels qu'un fort vortex polaire ou NAO après le réchauffement de la stratosphère volcanique. Ce processus Top-Down est notamment représenté par Robock et al. (2000) et Raible et al. (2016).

ii) « Mécanisme de gradient stratosphérique de type II » par la réflexion renforcée des ondes planétaires qui se réfléchit éventuellement sur la NAO après le réchauffement de la stratosphère volcanique, ce qui ne ressemble pas à la variabilité inhérente de la circulation. Ce processus Top-Down est représenté par Graf et al. (2007, 2014) et Bittner et al. (2016).

iii) « Mécanisme du gradient troposphérique » par la diminution de l'énergie moyenne zonale et de l'amplitude des ondes planétaires troposphériques après le refroidissement de la surface sous l'influence des forçages radiatifs volcaniques. Ce processus Down-Top est représenté par Stenchikov et al. (2002).

Il est donc suggéré qu'une compréhension et une représentation correctes du mécanisme physique sont essentielles dans l'étude de modélisation pour acquérir des connaissances complètes sur les variabilités climatiques dues aux volcans tropicaux et extratropicaux.

Pour répondre à ces défis, deux programmes du projet CMIP6 ont plus particulièrement attiré notre attention.

Le premier est la phase 4 du Projet d'Intercomparaison des Modélisations Paléoclimatiques (PMIP4) qui a montré plusieurs progrès en comparaison avec l'ancien PMIP3. Les progrès comprennent, par exemple, une résolution spatiale plus élevée pour les modèles, une amélioration des reconstructions de forçage (eVolv2k, Toohey et Sigl, 2017), la proposition du module standard Easy Volcanic Aerosol (EVA, Toohey et al., 2016) et des configurations expérimentales plus strictes. Avec les mises-à-jour faites dans PMIP4/CMIP6, nous nous continuerons concentrer sur son expérience « past1000 » (premier travail de thèse, voir chapitre **3**) tourné dans IPSL-CM6A-LR pour étudier l'efficacité du modèle dans la simulation des impacts climatiques des éruptions volcaniques au cours du dernier millénaire avec une claire stratification (en fonction de la latitude, la saison, l'intensité d'éruption).

Le deuxième est le Projet d'Intercomparaison des Modèles de Forçages Volcaniques (VolMIP). Le VolMIP a défini un protocole standard pour des expériences de perturbation volcanique idéalisées

afin d'améliorer la comparabilité des résultats entre différents modèles climatiques permettant ainsi de diminuer les incertitudes liés à la modélisation. Parmi les nombreuses expériences de perturbation volcanique idéalisées du VolMIP, le cœur d'expériences (« volc-pinatubo ») se concentre sur l'évaluation de l'incertitude et des différences inter-modèles dans la réponse climatique saisonnière à interannuelle à une éruption de type Pinatubo idéalisée en 1991 (surtout dans l'expérience « volc-pinatubo-full »). Les expériences « volc-pinatubo » comprennent également deux simulations de sensibilité importantes, à savoir « volc-pinatubo-strat » et « volc-pinatubo-surf ». Plus précisément, « volc-pinatubo-surf » spécifie une perturbation prescrite du flux d'ondes courtes pour imiter l'atténuation du rayonnement solaire par les aérosols volcaniques, et donc le refroidissement de la surface. De même, « volc-pinatubo-strat » spécifie une perturbation prescrite des taux de chauffage radiatif totaux (ondes longues et ondes courtes), cherchant à réproduire l'impact local des aérosols volcaniques. Ces expériences contribuent ainsi à élucider les mécanismes par lesquels le forçage volcanique conduit à des changements dans la circulation atmosphérique : le refroidissement de surface et le réchauffement stratosphérique (deuxième travail de thèse, voir chapitre **4**).

Par la suite je présente l'implication de forçage volcanique paléo pour past1000 et de forçage volcanique historique pour Pinatubo.

Notre modèle IPSL-CM6A-LR a adopté le méthode *prescrit* pour simuler le volcanisme, ce qui se différencie le méthode *pronostique* où le cycle de vie de soufre (rejeter-réaction chimique-nucléation-condensation-coagulation-distribution-dépôt) est modélisé. Dans le méthode *prescrit*, on simule directement les paramètres physiques radiatifs de l'aérosol de sulfate stratosphérique volcanique (e.g., l'extinction de l'aérosol, la profondeur optique de l'aérosol, l'albédo de diffusion unique et le facteur d'asymétrie de diffusion, rayons effectifs). Dans le cas du modèle IPSL-CM6A-LR, il s'agit de simuler la profondeur optique de l'aérosol ainsi que son rayon effectif.

Pour la simulation past1000 du projet PMIP4, l'archive de eVolv2k développé par Toohey et Sigl. (2017) ainsi que l'outil Easy Volcanic Aerosols (EVA) (Toohey et al., 2016) sont recommandés. Le module EVA convertit les dépôts de sulfate d'eVolv2k en ensembles de données de propriétés optiques, dans la thèse ceci est abrégé EVA(2k) afin de symboliser la relation entre le module EVA et eVolv2k. La Figure 2.14 montre la distribution latitude-temps de la profondeur moyenne zonale des aérosols stratosphériques (issue des informations supplémentaires de Toohey et al., 2016).

Pour la simulation du 1991 Pinatubo, l'expérience « volc-pinatubo-full » utilise l'ensemble de données d'aérosols stratosphériques CMIP6 (GloSSAC version 3 par Thomason et al., 2018), conformément à l'expérience historique CMIP6. La Figure 2.15 montre la distribution de la profondeur optique moyenne zonale des aérosols stratosphériques à 0,55 µm observée et simulée sur la période 1991-1994 lors de l'éruption du Pinatubo. Globalement, l'ensemble de données CMIP6 AOD ont une bonne cohérence avec les données d'observation (SAGE II, Bauman et al., 2003; Sato

et al., 1993) en termes de distribution spatiale et d'évolution temporelle, tout en comblant les lacunes présentes dans les données SAGE-II.

Chapitre 3 (Past1000)

Dans ce chapitre, j'ai interrogé la performance du modèle IPSL-CM6A-LR dans la simulation past1000 à reproduire les anomalies climatiques hivernales. J'ai axé mon étude sur les éruptions de différentes latitudes, saisons d'éruption et magnitudes à une échelle de temps interannuelle dans le secteur ciblé en utilisant la méthode « clustering » ou « composite » (Chree, 1913, 1914). Les trois runs (dit r1, r2, r4, de 500 à 1849) de la simulation past1000 sont traités comme des membres d'ensemble. La simulation CMIP6-DECK « piControl » (c.-à-d. contrôle préindustriel sans forçage volcanique, de 1850 à 3049) décrivant des conditions climatiques préindustrielles non perturbées (Eyring et al., 2016) est également utilisée pour aider à estimer la significativité statistique par la méthode Mont-Carlo Bootstrapping (Efron et Tibshirani, 1994). En pratique, je ré-échantillonne les données de « piControl » aléatoirement et génère une donnée « pseudo-échantillon ». À partir de la fonction de distribution de probabilité (PDF) de ces données de « pseudo-échantillon », nous pourrions estimer la signification statistique d'un signal de past1000.

Pour réduire efficacement la tendance à long terme ou la variabilité à basse fréquence, nous adoptons une stratégie de « running anomalies » pour en déduire les anomalies pertinentes. C'est-à-dire que nous appliquons une fenêtre continue de 30 ans (360 mois) pour chaque année individuelle, afin d'établir sa climatologie (par exemple, les périodes 500~529, 501~530, …, 1819~1848). La fenêtre de climatologie précède toujours l'année réelle, sauf pour les 30 premières années au début de la série temporelle où la climatologie est juste établie à partir de ces 30 années. Une fois la climatologie définie, on peut obtenir des anomalies comme un écart par rapport à la climatologie. Cette procédure est appliquée individuellement à r1, r2, r4 et « piControl » pour les variables climatiques.

Clusters volcaniques

Pour acquérir une catégorisation logique, je commence par filtrer une centaine d'éruptions volcaniques pendant 500-1849 en Hémisphère Nord extratropical (NH), équatorial (EQ) et Hémisphère Sud extratropical (SH) selon leurs latitudes et saisons d'éruption, qui a résulté 57 NH événements (dont 52 éruptions en hiver), 35 EQ événements (dont 31 éruptions en hiver), 16 SH événements (tous en hiver) (Fig. 3.4 et Table 3.1). Cette catégorisation préliminaire est obtenue par la comparaison entre les moyennes des profondeurs optiques des aérosols à 0.55 μm dans trois bandes de latitudes, c.-à-d. 30°N ~ 60°N, 15°S ~ 15°N, et 30°S ~ 60°S. Pour simplifier, ces indices sont abrégés en AOD550_3060n, AOD550_15sn, AOD550_3060s.

Néanmoins ces 108 éruptions n'ont pas toutes été utilisées dans l'analyse de « composite ». Toutes les éruptions SH sont très petites avec leurs AOD550_3060s inférieurs à 0,1, et n'ont donc

pas été considérées dans l'analyse suivante. La réflexion suivante concerne l'existence d'un linéarité dans l'amplitude de l'éruption forçant/induisant un tourbillon polaire renforcé. Par conséquent, nous retirons les indices PNJ (pour Polar Night Jet, définis comme la moyenne zonale d'anomalies des vents zonaux à 65°N au niveau de pression 50 hPa) pour tous les hivers en-phase ainsi les premiers hivers d'éruptions hivernales, et pour les premiers hivers des autres éruptions non-hivernales pour r1, r2 et r4. Ensuite, les PNJ sont tracés en fonction des intensités d'éruptions (c.-à-d. le pic AOD550_3060n pour les événements NH, le pic AOD550_15sn pour les événements EQ). Les diagrammes de nuages des points (Fig. 3.5) et les courbes de régressions peuvent servir d'expériences de sensibilité pour tester la linéarité existants dans NH VEs ou EQ VEs pour induire une forte PNJ in-situ détectable.

Les résultats révèlent qu'il y a linéarité entre PNJ et l'amplitude d'éruptions pour les éruptions tropicales. Un vortex polaire plus fort est détecté au cours du premier hiver suivant une éruption tropicale estivale ou hivernale, avec des amplitudes de réponses des jets nocturnes polaires qui sont linéairement lié à la force d'éruption. Aucune relation linéaire avec la magnitude de l'éruption n'est identifiée pour les événements extratropicaux de l'hémisphère Nord.

Selon le processus ci-dessus, nous proposons l'intensité d'éruption comme autre critère pour une catégorisation propre et efficace. Nous utilisons 0,11 comme seuil de sélection pour les éruptions NH ou EQ hivernales (NHw, EQw), et 0,4 comme seuil pour les gigantesques éruptions EQ hivernales (EQmega). Les trois grands événements volcaniques EQ des autres saisons sont regroupés dans une seule catégorie, nomée EQe. Les événements NH des autres saisons ne sont pas pris en compte. De ce fait, nous avons rétabli quatre catégories volcaniques finales, avec NHw (n=10x3=30), EQw (n=21x3=63), EQmega (n=7x3=21), EQe (n=3x3=9), voir table 3.2. Les événements sont triplés car nous possédons trois runs millénaires et nous les considérons comme ensemble. Les quatre « clusters » sont utilisés pour calculer les signaux moyens de chaque classe volcanique.

Il est à noter que différents nombres d'hivers ont été utilisés dans la méthode « bootstrapping » pour chaque « cluster » volcanique.. Par exemple, la composite HNw ne comporte que 30 évènements au total, alors que nous calculée en moyennant 10 000 fois de chacun 30 années d'hiver au hasard provenant de la période totale (1200 ans) du piControl. Ensuite la fonction de distribution de probabilité (PDF en anglais) des 10 000moyens est calculée pour piControl. Si le signal moyen du composite volcanique dépasse l'intervalle de confiance (i.c.) du 5e au 95e percentile des PDF du piControl, nous supposons que le signal est significatif à 95 % i.c.

PNJ et ONA

Le premier résultat sur l'indice PNJ et l'indice ONA des quatre « composites » volcaniques à partir de l'expérience past1000 est présenté dans la figure 3.9. Les pics significatifs indiquent un écart par rapport à la ligne de base climatique du piControl et sont considérés comme d'origine volcanique.

Pour le composite NHw (Fig. 3.9a-b), une forte augmentation significative (>99 % i.c.) de la PNJ et de l'ONA positive est observée à l'année 0, qui est l'hiver en-phase. Le PNJ est suivi d'une autre augmentation dans l'année 1 (premier hiver post-éruption) mais la positivité de l'ONA n'a pas franchi le test de signification dans l'année 1. Les autres années ne possèdent pas de signal significatif.

Pour le composite EQw (Fig. 3.9c-d), les pics significatifs pour le PNJ et l'ONA n'apparaissent pas pendant l'hiver en-phase d'éruption, mais plutôt au cours du premier hiver (Y+1). Nous supposons une distribution différente du transport des aérosols et des effets radiatifs entre NHw et EQw conduisant à une année de décalage distincte.

Si nous sélectionnons les méga éruptions d'EQw, nous voyons alors une autre histoire. Pour le composite EQmega (Fig. 3.9e-f), de l'année d'hiver en-phase à l'année 2, nous observons un signal PNJ significatif (> 95% i.c.). Mais le signal le plus fort pour l'augmentation du PNJ a toujours lieu durant le premier hiver (Y+1). L'ONA positive est également forte au cours de l'année 1, bien qu'elle franchisse à peine la ligne significative du piControl.

Pour les éruptions EQe, la taille du composite est n = 9 , y compris l'éruption de Samalas qui est la plus forte. L'importante augmentation significative de la PNJ et de l'ONA est observée à la fois durant le premier et le deuxième hiver. Cependant, en considérant la distribution des aérosols de Samalas (la ligne de dépassement dans le panneau central de la figure 3.4), qui subit en fait deux pics pendant l'éruption, cela peut rendre le signal PNJ et ONA du deuxième hiver moins fiable pour le cluster EQe.

Climat d'hiver après l'éruption

Pour avoir plus de détail sur le climat dans la région Atlantique Nord-Méditerranée, les cartes d'anomalies d'hiver (pression au niveau de la mer, température à la surface, précipitation, hauteur géopotentielle au niveau de pression 50 hPa) pour trois clusters volcaniques hivernaux (NHw, EQw, EQmega) sont présentés dans la figure 3.10, 12, 14.

Dans l'hiver 0 (en-phase) , pour NHw, un régime chaud et humide est présent sur l'Eurasie du Nord, tandis que des anomalies négatives de température sont présentes sur l'Amérique du Nord. La Méditerranée rencontre un hiver plus chaud et plus humide dans le bassin d'ouest contrairement à un hiver plus froid et plus sec dans le bassin d'est. Les anomalies de température et de précipitations peuvent s'expliquer par l'advection anormale de masses d'air associées à la circulation atmosphérique liée à l'ONA positive. Nous observons des vents d'ouest renforcés soufflant du détroit de Davis vers la Scandinavie qui sont des anomalies de circulation typiques résultant d'un dipôle de l'anomalie de pression au niveau de la mer sur l'Atlantique Nord-Europe. Le vortex polaire est également renforcé. Toutes les preuves indiquent un hiver en-phase a l'ONA positive pour le cluster volcanique NHw.

Cependant, pour le cluster EQw, nous ne capturons pas la phase positive de l'ONA. Néanmoins, lors du filtrage des éruptions hivernales équatoriales massives, le cluster EQmega

pourrait révéler des signaux positifs de l'ONA avec d'importantes anomalies de température positives sur la mer de Barents et une partie du nord de la Russie et un vortex polaire approfondi.

Dans l'hiver +1 après l'éruption, tous les clusters (NHw, EQw, EQe et EQmega) ont une augmentation de la hauteur géopotentielle au niveau de pression de 50 mb. Cependant, les anomalies climatiques de surface ne se projettent pas sur une phase de l'ONA positive pour le cluster NHw, seules les éruptions équatoriales (EQw, EQe et EQmega) rencontrent un climat de type ONA positive avec un mode dipolaire de pression au niveau de la mer. Il dévoile une question qui est de savoir dans quelle mesure un vortex polaire renforcé sera corrélé avec une ONA positive.

Dans l'hiver +2, l'ONA positive n'est pas capturée pour NHw ni pour EQw. Seul EQe montre un réchauffement marginal sur la Scandinavie alors qu'il se refroidit partout ailleurs dans le globe. Cependant, pour des raisons de assez petite taille d'échantillon (N = 9) et de distribution irrégulière d'aérosols susmentionnée de Samalas avec deux pics dans AOD550_15sn, nous ne pouvons pas affirmer que le signal de l'ONA positive au cours du deuxième hiver volcanique est valable pour tous les événements équatoriaux printemps-été. Des expériences sur de grands ensembles de membres sont nécessaires pour effectuer un diagnostic plus approfondi. Il révèle aussi que le cluster EQmega est incapable de produire un signal de l'ONA positive dans hiver +2, à l'exception d'un faible effet sur la hauteur géopotentielle polaire.

Gradient méridional de la température

Nous revenons au mécanisme proposé pour un renforcement des vents zonaux stratosphériques qui est le gradient de température méridional amélioré.

Nous traçons les gradients de température méridionaux superposés aux anomalies de vent zonal pour quatre clusters volcaniques dans la Fig. 3.16. En se référant au bilan du vent thermique introduit dans l'annexe **B.1** pour la moyenne zonale du vent zonal perturbé et de la température perturbée dans une échelle quasi-géostrophique (petit nombre de Rossby), nous avons:

$$f\frac{\partial \bar{u}}{\partial z} = -\frac{R}{H}\frac{\partial \bar{T}}{\partial y}$$

où la barre supérieure indique la moyenne zonale, u et T sont la moyenne d'ensemble des anomalies de vent zonal et de température dans chaque cluster volcanique.

Par conséquent, le gradient de température méridional est crucial pour déterminer le cisaillement vertical du vent.

Pour le cluster NHw en hiver en-phase, nous avons pu observer un gradient de température méridional négatif cohérent avec le cisaillement positif du vent de 20 mb à 1000 mb, ce qui indique que l'éruption de NHw sera capable d'induire un gradient de température suffisamment négatif une fois éclaté en hiver à 45ºN. Nous relions cette rapidité à l'emplacement des événements volcaniques NHw, qui est 45ºN en défaut selon EVA(2k) (Toohey et al., 2016). En résultat, le forçage radiatif des aérosols de sulfate agira directement sur le jet NH et mènera une ONA positive, ce qui contredit

d'autres études (Oman, 2005; Sjolte et al., 2021 ; Zambri et al., 2019b) suggérant par ailleurs un hiver accompagné d'une ONA négative.

D'un autre côté pour les éruptions équatoriales, le gradient de température méridional reste largement inchangé sur les latitudes moyennes à élevées pendant l'hiver en-phase. Cette particularité peut être expliquée par le décalage de transport des aérosols de la stratosphère équatoriale à la zone des hautes latitudes, ce qui explique l'échec du cluster EQw à produire une tourbillon polaire plus forte. Cependant, si l'on retire les éruptions les plus fortes, la charge massive d'aérosols est supposée être capable de forcer un fort vortex polaire, et concurremment une NAO positive, ce qui est le cas d'EQmega.

Le bilan du vent thermique basé sur la circulation quasi-géostrophique ne s'applique pas à l'atmosphère tropicale qui peut également moduler le vortex polaire par oscillation quasi-biennale (QBO en anglais). Au cours du premier hiver après l'éruption, le cluster NHw rencontre une oscillation quasi-biennale (une phase QBO à l'est) assez différente de celle des autres catégories d'éruptions hivernales (une phase QBO à l'ouest). Holton et Tan (1980) ont proposé une caractéristique intrigante de l'hémisphère nord (NH) selon laquelle un vortex polaire plus fort existe lorsque le QBO dans la basse stratosphère (50 hPa) est dans sa phase ouest (QBOw), et, inversement, un vortex polaire plus faible existe lorsque le QBO est dans sa phase est (QBOe). Un tel phénomène, également connu sous le nom d'effet Holton-Tan (THE), est également confirmé par White et al. (2015), associant la QBOe à une propagation accrue des ondes vers les pôles, conduisant à une meilleure convergence des ondes planétaires et à une croissance des ondes aux hautes latitudes et contribuant à un vortex polaire plus faible. En ceci, nous suggérons que l'affaiblissement du signal PNJ au cours du premier hiver pour NHw est le résultat d'un changement de phase QBO, qui est finalement lié au modèle de chauffage diabatique stratosphérique différent des éruptions NH par rapport aux éruptions EQ. Nous prévoyons d'effectuer un travail approfondi dans l'étude de la dynamique derrière l'effet de modulation QBO pour les éruptions à différentes latitudes.

Conclusions

En conclusion, dans la simulation past1000, notre modèle IPSL-CM6A-LR a pu simuler clairement un hiver avec une ONA positive plutôt robuste et des jets nocturnes polaires renforcés, qui sont forcés in-situ par le forçage volcanique. La significativité du signal est sensible à la latitude, à la saison et à l'intensité de l'éruption, puisque tous ces facteurs sont importants pour décider de la distribution des aérosols de sulfate volcanique et du gradient de température atmosphérique méridional qui en résulte.

Ce travail est d'une grande importance puisque le volcanisme stratosphérique explosif représente un forçage radiatif naturel essentiel. Comprendre dans quelle mesure la variabilité climatique observée à l'échelle saisonnière et décennale est une réponse au forçage radiatif naturel et anthropique, par opposition à la variabilité interne, est un défi fondamental pour les modèles

climatiques qui visent à prédire les variations climatiques futures (Shindell et al. ., 2003 ; Stenchikov, 2002).

Chapitre 4 (Pinatubo)

L'objectif de ce chapitre est d'étudier le mécanisme par lesquels différentes composantes radiatives du forçage volcanique dans l'atmosphère peuvent avoir un impact sur le comportement de l'ONA et le climat dans l'Atlantique Nord-Méditerranée. Pour cela, ce chapitre porte sur une étude de cas de l'éruption du Pinatubo en juin 1991 utilisant le modèle IPSL-CM6A-LR et des archives d'observation.

L'ensemble de l'étude contenue dans ce chapitre par, à l'exception de la discussion sur glace de mer, est présenté sous forme de publication en vue d'une soumission à la sortie spéciale du VolMIP du journal *Earth System Dynamics*.

Une grande partie de nos connaissances climatiques est basée sur la comparaison d'observations avec des simulations à partir de modèles climatiques et sur notre compréhension physique des phénomènes identifiés. Les effets radiatifs volcaniques sont principalement la réflexion du rayonnement solaire à ondes courtes (provoquant le refroidissement de la surface) et l'absorption du rayonnement terrestre ou solaire à ondes longues (provoquant le réchauffement de la stratosphère). Nous allons d'abord évaluer et discuter de la capacité de l'IPSL-CM6A-LR à reproduire la variabilité climatique et la variation de l'ONA après l'éruption du Pinatubo de 1991. Nous utilisons l'expérience VolMIP « volc-pinatubo-full » sous forçage radiatif volcanique complet et comparons les résultats des modes avec les données d'observation (20thCv2, Compo et al., 2011; ERAI, Dee et al., 2011; NCEP, Kalnay et al., 1996).

IPSL-CM6A-LR permet de séparer les effets dominants des ondes courtes (refroidissement de surface) et des ondes longues (réchauffement stratosphérique) des aérosols volcaniques. Ainsi, dans un deuxième temps, nous comparons les climats entre les trois expériences « volc-pinatubo-full », « volc-pinatubo-strat », « volc-pinatubo-surf ». Démêler le rôle relatif du refroidissement de surface et du réchauffement stratosphérique sur le climat d'hiver moyen, l'ONA, le vortex polaire et les turbulences dans le bassin Atlantique Nord-Méditerranée est d'une grande importance car cela améliorera notre compréhension de la sensibilité du climat aux différents forçages radiatifs.

Protocole d'expérimentation

La simulation de base, « volc-pinatubo-full », utilise à la fois des flux radiatifs à ondes courtes et à ondes longues avec des aérosols volcaniques (représentant toutes les interférences des aérosols volcaniques, Thomason et al., 2018) pour mettre à jour la tendance de la température. Alors que les expériences de sensibilité « volc-pinatubo-strat » et « volc-pinatubo-surf » ont été respectivement conçues pour représenter uniquement, soit, les perturbations des aérosols volcaniques par rapport aux taux de chauffage radiatif totaux (ondes longues et proche infrarouge) (« volc-pinatubo-strat »), soit

les perturbations à le flux d'ondes courtes de surface (« volc-pinatubo-surf »). Chaque simulation a 25 membres individuels.

Dans « volc-pinatubo-strat », le deuxième appel au code radiatif est utilisé pour diagnostiquer les perturbations 3D des flux solaire proche infrarouge (en anglais, NIR) et terrestre sortant des ondes longues (en anglais, LW), qui sont ensuite transmises au modèle à chaque pas de temps de transfert radiatif, au-dessus des flux de ciel clair en ondes courtes (SWcs) de surface calculés lors du premier appel (sans aérosols stratosphériques). Cette procédure permet de prendre en compte les taux de chauffage radiatif des aérosols volcaniques tout en gardant les flux SW descendants en surface sans aérosols (Fig. 3a). Dans « volc-pinatubo-surf », le deuxième appel au code radiatif est utilisé pour diagnostiquer les flux SWs de surface qui sont transmis au modèle à chaque pas de temps de transfert radiatif ainsi que le premier appel les flux 3D sans aérosols (Fig. 3b) . Cette procédure permet de ne prendre en compte que la réduction du SW de surface due à l'augmentation de l'albédo planétaire par les aérosols volcaniques (et non les rétroactions climatiques).

Méthode

Pour les jeux de données d'observation et de réanalyse, les anomalies sont calculées en supprimant les moyennes sur 5 ans précédant l'éruption du Pinatubo, c'est-à-dire 1986-1990. Pour les simulations, toutes les anomalies sont calculées en supprimant le cycle saisonnier moyen de piControl. Lorsque les moyennes d'ensemble de chaque expérience volcanique (c'est-à-dire Full, Strat, Surf) sont comparées à la simulation de référence, un test « Student » a été effectué avec le nombre de degrés de liberté correspondant au nombre total de membres (25 +25= 50) moins un. Ce test a été appliqué soit à chaque point géographique, soit pour une moyenne de surface, avec l'intervalle de confiance égal 90 %.

Deux principaux indices climatiques sont aussi utilisés dans notre étude pour suivre les comportements climatiques des simulations. Ils sont généralement calculés au niveau de chaque membre individuel, mais s'expriment souvent sous forme de moyenne d'ensemble pour chaque expérimentation. Comme présenté précédemment, le premier indice est l'indice de l'ONA qui est calculé à base de Stephenson et al. (2016) en considérant la pression au niveau de la mer à l'intérieur de deux zones (pour rappel, l'une est délimitée par les coordonnées 20°–55°N, 90°W–60°E, l'autre par 55°–90°N, 90°W–60°E). Ensuite, l'indice ONA est défini comme la différence entre la moyenne SLP moyennée spatialement sur ces deux « boîtes » pour chaque mois.

Le deuxième indice est l'indice mensuel de vortex polaire (PV) dont le calcul s'appuie sur la méthode de Graf et al. (2014) mais en considérant directement l'anomalie de hauteur géopotentielle moyenne au niveau 50 hPa dans la région subpolaire (au nord de 65°N). Plus le PV est négatif, plus les tourbillons polaires sont intenses.

Le gradient de température méridional a été obtenu à partir des anomalies de température moyenne zonale pour les simulations Full, Strat, Surf et de piControl. Le calcul a été fait avec une méthode de différences finies à chaque degré de latitude.

Pour quantifier la propagation des ondes planétaires dans différentes conditions de forçage externe, nous calculons le flux Eliassen-Palm (flux EP) sur la base des équations de la moyenne eulérienne transformée pour les tourbillons quasi-géostrophiques (Holton et Hakim, 2013) :

Les champs mensuels de température et de vent ont été utilisés pour calculer le flux EP hivernal et sa divergence dans chaque simulation. Ceci permet de représenter l'activité des ondes planétaires stationnaires, un élément important pour le contrôle du transport de chaleur turbulente de la basse troposphère à la haute stratosphère dans les régions subtropicales et subpolaires (Graf et al., 2007, Li et al., 2011). Une présentation détaillée sur le flux EP est dans l'annexe **B.2**.

Résultats

En résultat, dans l'expérience Full le modèle IPSL-CM6A-LR simule une ONA positive robuste au cours du premier hiver et une ONA négative bruyante au cours du deuxième hiver en réponse à l'éruption du Pinatubo de 1991. Ces résultats indiquent une décomposition rapide des modes au cours du deuxième hiver en simulation par rapport aux deux hivers à ONA positives observés dans les données de réanalyse (Graf et al., 1993 ; Robock, 2000 ; Stenchikov et al., 2002 ; Fischer et al., 2007).

D'après nos expériences de simulation, l'ONA significativement positive au cours du premier hiver volcanique est principalement attribuée au réchauffement stratosphérique en augmentant le gradient de température méridional et par conséquent le vortex polaire, qui s'est avéré être un processus allant de haut en bas (Top-down). Pendant le premier hiver volcanique, une convergence plus forte du flux EP et un effondrement du mode d'onde se produisent pour les expériences Full et Strat de la surface jusqu'à la troposphère, conformément aux conclusions de Graf et al. (2007). Une déviation du flux EP vers l'équateur dans Full et Strat aidera les ondes planétaires à se propager davantage vers les zones tropicales et à moins influencer le vortex polaire (Bittner et al., 2016). La divergence significative du flux EP était confinée à la surface et à la basse troposphère pour la simulation Surf.

Le refroidissement superficiel joue un rôle destructeur en amplifiant les jets polaires lorsqu'il est seul dans la scène. Alors que l'interaction non linéaire entre la stratosphère et la troposphère/surface induit un vortex polaire plus fort dans l'expérience Full, ce qui explique une ONA positive plus visible que pour l'expérience Strat.

Pendant le deuxième hiver volcanique, le signal ONA est plus bruyant avec une tendance au NAO négatif dans la simulation Full. Nous suggérons une influence de surface par un feed-back négatif de glace de mer (Alexander et al., 2004 ; Deser et al., 2004, 2007 ; Magnusdottir et al., 2004 ; Strong et al., 2009). D'autres analyses sur l'ONA et la glace de mer sont attendues

Il est également intéressant de constater que notre expérience Full a simulé des forts événements El Niño durant l'hiver 1992/93 (Fig. A.2.2 dans l'annexe **A.2**). Strong et al. (1986) ont montré que les aérosols volcaniques perturbent la circulation des cellules de Hadley sous les tropiques, ce qui réduit les alizés et déclenche un El Niño. Il est également suggéré par de nombreux chercheurs qu'El Niño augmentera les chances d'avoir une ONA négative en construisant un pont subtropical pour la propagation des ondes planétaires par phase positive de la téléconnexion Pacifique-Amérique du Nord (PNA) (Taguchi et Hartmann, 2006 ; Graf et Zanchettin, 2012 ; Graf et al., 2015) . Les résultats associés à nos simulations Pinatubo seront bientôt disponibles dans les prochains travaux de Khodri M. (2022). L'ONA négative simulée au cours du deuxième hiver volcanique serait donc le produit de l'effet combiné du transport accru des ondes planétaires vers les pôles et de la téléconnexion subtropicale d'El Niño.

Conclusions

Nos résultats mettent en évidence le rôle dominant du réchauffement de la stratosphère sur la formation de ONA positive dans le secteur Atlantique Nord-Méditerranée après l'éruption du Pinatubo. Or, on simule une NAO négative (avec du bruit) dans l'expérience Full pendant le deuxième hiver, contrairement aux observations/réanalyses. Ceci ne peut pas être attribué directement à un seul effet de forçage radiatif (réchauffement stratosphérique ou refroidissement de surface). Cela est probablement dû aux impacts indirects, soit, par feed-back de la glace de mer sur la propagation ascendante des ondes planétaires, soit par les incertitudes issues de la modélisation. Ceci sera vérifié dans les futurs travaux. L'influence des déplacements et des distorsions des vortex stratosphériques sur le climat de surface est également un sujet d'étude essentiel afin de mieux comprendre les impacts des vortex stratosphériques sur le climat de surface de la Terre. En outre, l'analyse des données à l'échelle synoptique est également nécessaire pour évaluer les contributions des turbulences transitoires dans la modulation du vortex polaire.

Chapitre 5 (Synthèse de conclusions et les perspectives)

Dans cette thèse, un modèle couplé du système climatique global, IPSL-CM6A-LR, est utilisé pour étudier les impacts climatiques interannuels du volcanisme, l'un des forçages climatiques naturels les plus importants. Au cours du dernier millénaire, trois simulations transitoires d'une durée de 500 EC à 1849 EC ont été appliquées pour étudier la sensibilité du modèle à différentes conditions d'éruption. Pour l'éruption du Pinatubo, la mieux observée à l'ère industrielle, des simulations de grands ensembles ont été réalisées avec le modèle IPSL-CM6-LR pour sonder les mécanismes physiques liés à ces événements et comparer les simulations aux observations instrumentales. Nous avons prêté une attention particulière au secteur géographique Atlantique Nord-Méditerranée.

Les résultats du chapitre **3** soulignent la robustesse du modèle d'IPSL-CM6A-LR dans la simulation de la variabilité volcanique forcée du climat hivernal sous différents amas volcaniques.

Les différences dans l'effet des éruptions des hautes et des basses latitudes sur la circulation atmosphérique et la température régionale fournissent des informations importantes pour comprendre les variabilités climatiques passées et futures en réponse au forçage volcanique. De plus, les résultats ont révélé certaines imperfections dans d'autres études (par exemple, Sjolte et al., 2021) qui n'ont pas pris en compte la saison des éruptions lors de l'analyse de composites volcaniques similaires. Par exemple, dans les travaux de Sjolte et al. (2021), les éruptions estivales de haute latitude NH n'ont pas été séparées de celles hivernales. Il est donc inapproprié de conclure à un hiver NAO négatif universel après les éruptions NH à partir de leur analyse.

Contrairement aux études précédentes (par exemple, Swingedouw et al., 2017 ; Driscoll et al., 2011) qui ont signalé un échec général des modèles CMIP5 pour simuler une réponse NAO robuste après une éruption volcanique, nos résultats ont confirmé l'efficacité de l'IPSL-CM6A- LR dans la simulation de la variabilité de la ONA en réponse au forçage volcanique, qui peut également être considérée comme un progrès encourageant de CMIP6.

Pour acquérir une compréhension approfondie du mécanisme par lequel l'éruption volcanique influencera le climat de la NAO et du secteur Atlantique Nord-Méditerranée, la simulation numérique de grands ensembles est indispensable en climatologie. Le chapitre **4** est consacré à l'étude de l'expérience volc-pinatubo, une partie essentielle de VolMIP qui traite des réponses volcaniques forcées par un modèle climatique couplé et avec différents processus physiques. Il a souligné les contributions de la réponse radiative directe (c.-à-d. le refroidissement de surface) et dynamique (c.-à-d. le réchauffement stratosphérique) à la suite d'une éruption du Pinatubo idéalisée sur le climat Atlantique Nord-Méditerranée en utilisant la modélisation numérique de grands ensembles.

On constate que IPSL-CM6A-LR simule une ONA positive robuste au cours du premier hiver en réponse à l'éruption du Pinatubo de 1991, une éruption tropicale estivale. Le signal du deuxième hiver est par ailleurs moins significatif dans l'expérience « volc-pinatubo-full », ce qui indique un déferlement rapide des vagues au cours du deuxième hiver par rapport à deux hivers ONA positifs continus dans les données de réanalyse (Fischer et al., 2007; Graf et al. , 1993 ; Robock, 2000 ; Stenchikov, 2002).

En comparant « volc-pinatubo-full », « volc-pinatubo-strat » et « volc-pinatubo-surf », nous avons constaté que l'ONA significativement positive au cours du premier hiver volcanique est attribuée principalement au réchauffement stratosphérique en augmentant le gradient de température méridional et par conséquent le vortex polaire, qui s'est avéré être un processus de haut en bas. Le refroidissement de surface joue un rôle destructeur dans l'amplification des jets polaires dans le « volc-pinatubo-surf », différemment de Stenchikov et al. (2002, 2006) qui ont suggéré une diminution de la propagation des ondes planétaires liée au refroidissement de la surface. Cependant, l'interaction non linéaire entre la stratosphère et la troposphère/surface fera un vortex polaire plus fort dans « volc-pinatubo-full » donc une ONA positive plus forte que dans « volc-pinatubo-strat ».

Lors de la vérification en détail du transport des ondes planétaires, au cours du premier hiver volcanique, il y a une convergence plus forte du flux EP et plus d'effets décélérations pour les expériences « volc-pinatubo-full » et « volc-pinatubo-strat » de la surface à la troposphère, en accord avec les conclusions de Graf et al. (2007). Alors qu'une déviation du flux EP vers l'équateur dans « volc-pinatubo-full » et « volc-pinatubo-strat » aidera les ondes planétaires à se propager davantage vers les zones tropicales et à moins influencer le vortex polaire (Bittner et al., 2016). La divergence significative du flux EP était confinée à la surface et à la basse troposphère pour « volc-pinatubo-surf ». À la fin du chapitre **4**, une rétroaction négative du mode dipolaire de la glace de mer à l'ONA est brièvement analysée à l'aide de sorties de données mensuelles. D'autres diagnostics basés sur les sorties quotidiennes sont recommandés dans une future étude.

Les résultats obtenus dans le cadre de ces expériences par IPSL-CM6A-LR pour VolMIP et PMIP4 ouvrent sur deux axes d'amélioration pour les études futures : d'une part une compréhension possible de la téléconnection entre d'autres composantes de la circulation (par exemple, ENSO, PNA, AMOC, mousson, QBO) et l'ONA pendant l'hiver volcanique, et d'autre part, la comparaison avec d'autres AOGCMs de nouvelles générations et des nouvelles archives paléoclimatiques.

Étude de la variabilité climatique et le rôle du volcanisme dans le secteur Atlantique Nord-Méditerranée au dernier millénaire

Résumé : La thèse vise à étudier le rôle du volcanisme ainsi ses impacts sur la variabilité climatique hivernale (spécialement l'ONA) dans le secteur Atlantique Nord-Méditerranée à l'échelle interannuelle. La première partie est consacrée à la caractérisation du signal d'ONA en hivers à la suite d'éruptions volcaniques stratosphériques grâce à trois simulations transitoires du dernier millénaire (500-1849 CE) par IPSL-CM6A-LR dans le cadre de PMIP4. La robustesse et la sensibilité de réponse liée à la latitude, la saison et la magnitude des éruptions sont ainsi explorées. La deuxième partie étend plus loin pour décrypter le mécanisme concernant différentes composantes radiatives du forçage volcanique (le refroidissement de la surface et le réchauffement du stratosphère). Le travail est axé sur trois 25-membres ensembles de simulation par IPSL-CM6A-LR suivant le protocole VolMIP sur l'éruption tropicale Mt. Pinatubo (Philippines, juin 1991), la meilleure observée. Les expériences de sensibilité indiquent que la signature d'ONA positive de surface dans nos expériences de modèle est principalement attribuée au réchauffement dans la basse stratosphère tropicale qui génère des vents zonaux subtropicaux plus forts à travers le bilan de vent thermique et accélère le vortex polaire. Les propagations d'ondes planétaires stationnaires jouent également des effets de modulations indispensables.

Mots clés : volcanisme ; dernier millénaire ; variabilité climatique ; ONA; IPSL-CM6A-LR

Study of the climate variability and the role of volcanism in the North Atlantic-Mediterranean sector during the last millennium

Abstract : The PhD work aims at studying the role of volcanism in influencing winter climate variability (especially, NAO) over the North Atlantic-Mediterranean sector at inter-annual scale. The first part is devoted to characterizing the simulated NAO signal in winters following stratospheric volcanic eruptions using three long transient simulations of the past millennium (500-1849 CE) by IPSL-CM6A-LR in the frame of PMIP4. The robustness and sensitivity of the response related to the latitude, season and strength of the eruptions are also explored. The second part extends further to decrypt the physical mechanism regarding different components of volcanic radiative forcing (the surface cooling and stratospheric warming). The work focuses on three 25-members ensemble simulations by IPSL-CM6A-LR following the VolMIP protocol for the well observed Mt. Pinatubo tropical eruption (Philippines, June 1991). Sensitivity experiments indicate that the surface positive NAO signature in our model experiments is primarily attributable to heating in the lower tropical stratosphere which generates stronger subtropical zonal winds through the thermal wind balance and accelerates the polar vortex. Stationary planetary wave propagations are also playing indispensable modulations effects.

Keywords : volcanism; last millennium; climate variability; NAO; IPSL-CM6A-LR